In Vitro Studies of Dermally Absorbed Cu(II) Tripeptide Complexes as Potential Anti-Inflammatory Drugs.

A dissertation submitted to the

University of Cape Town

In fulfilment of the requirements for the degree of

MASTER OF SCIENCE

By

Giselle M. Vicatos

Supervisor:

Prof. Graham E. Jackson

Department of Chemistry
University of Cape Town
Rondebosch 7701
South Africa

January 2016

Acknowledgements

- I wish to thank my supervisor, Professor Graham Jackson, for his guidance and support throughout this dissertation.

- I also wish to thank the following people for their constant advice and help throughout this dissertation:

    Ahmed Hammouda

    Fatin Elmagbari

    Mamohale Mohajane

Plagiarism Declaration

I, Giselle Vicatos, declare that "*In Vitro* Studies of Dermally Absorbed Cu(II) Tripeptide Complexes as Potential Anti-Inflammatory Drugs" is my own unaided work both in concept and execution and that all sources that I have used and quoted have been indicated and acknowledged by means of complete and clear references. This thesis is submitted for the Master of Science (MSc) degree to the Department of Chemistry at the Faculty of Science at the University of Cape Town. It has not been submitted before for any degree or any examination at the University of Cape or any other university.

Signed by candidate

January 2016

Abstract

Copper(II) complexes have anti-inflammatory properties which can alleviate the symptoms of rheumatoid arthritis (RA) and thus control the progression of the disease. In this study two tripeptides, namely sarcosyl-L-leucyl-phenylalanine (Sar-Leu-Phe) and glycyl-L-leucyl-phenylalanine (Gly-Leu-Phe) were studied as potential chelators, which would increase the bioavailability of copper(II) through dermal absorption.

Glass electrode potentiometry was used to measure the solution thermodynamics of copper(II), nickel(II) and zinc(II) with Gly-Leu-Phe and Sar-Leu-Phe, at 25 ± 0.01 °C and an ionic strength of 0.15 M (NaCl). The terminal amine of both tripeptides was found to have the same basicity, but the methyl group on the terminal amine decreased the stability constants of the copper(II) ligand species by 0.38 to 1.67 log units. It increased the stability constants of the zinc(II) ligand species by 0.13 to 1.07 log units and it also increased the stability constant of the NiL_2H_{-1} species by 1.3 to 1.4 log units, while not affecting the NiL species.

The solution structures of the complexes were determined spectroscopically using Ultraviolet-visible spectrophotometry, Infrared spectroscopy and ^{1}H NMR spectroscopy. The copper(II) complexes tend more towards a square planar geometry, rather than the expected tetragonally distorted octahedral geometry. All the nickel(II) species, were square planar, except for the ML species, which was octahedral. The ligand coordinated to the metal ion via an amine-N, two amide-Ns, two carbonyl-Os and a carboxyl-O. The postulated coordination modes were validated using quantum mechanical calculations.

Two methods were used to study percutaneous skin absorption, namely octanol/water partition coefficients and Franz cell permeation. The partition coefficient values were found to be negative over a pH range from 2-10 and specifically, -1.79 ± 0.01 and -1.72 ± 0.01 for Cu-Gly-Leu-Phe and Cu-Sar-Leu-Phe respectively at a physiological pH of 7.4. These values are relatively high for copper(II) complexes, but the negative values indicate that all the species are hydrophilic. The membrane permeability of copper(II) increased when complexed to either of the tripeptides in comparison to copper(II) chloride.

The stability of the copper(II) complexes of Gly-Leu-Phe and Sar-Leu-Phe, and their ability to promote membrane permeability, warrant their testing as dermally absorbable, anti-inflammatory drugs.

Abbreviations

RA	- Rheumatoid arthritis
HSA	- Human Serum Albumin
KHP	- Potassium hydrogen phthalate
Gly-Leu-Phe	- Glycyl-L-leucyl-phenylalanine
Sar-Leu-Phe	- Sarcosyl-L-leucyl-phenylalanine
Gly-His-Lys	- Glycyl-L-histidyl-L-lysine
Sar-His-Lys	- Sarcosyl-L-histidyl-L-lysine
Sar-Lys-His	- Sarcosyl-L-lysyl-L-histidine
Sar-His-His	- Sarcosyl-L-histidyl-L-histidine
Sar-Lys-Lys	- Sarcosyl-L-lysyl-L-lysine
Sar-Gly-His	- Sarcosyl-L-glycyl-L-histidine
Gly-Gly-Gly	- Triglycine
Gly-Gly	- Glycyl-glycine
Gly-Phe	- Glycyl-L-phenylalanine
Gly-Leu	- Glycyl-L-leucine
Gly-His	- Glycyl-L-histidine
Sar-Gly	- Sarcosyl-glycine
Sar-Leu	- Sarcosyl-L-leucine
Sar-Phe	- Sarcosyl-L-phenylalanine
Sar-His	- Sarcosyl-L-histidine
Gly	- Glycine
Sar	- Sarcosine
Leu	- Leucine
Phe	- Phenylalanine
ESTA	- Equilibrium Simulations for Titration Analysis
UV-Vis	- Ultraviolet-visible spectroscopy
IR	- Infrared spectroscopy
DFT	- Density Functional Theory
ECCLES	- Evaluation of Constituent Concentrations in Large Equilibrium Systems
P.M.I	- Plasma Mobilizing Index
T_2	- Transverse relaxation time
R_f^H	- Hamilton R-factor

R^{H}_{lim}	- Hamilton R-factor limit
n-bar	- The formation function
Z_H-bar	- The protonation function
Z_M-bar	- The metal formation function
Q_M-bar	- The deprotonation function
Log *K*	- Logarithm of equilibrium constants
log β_{pqr}	- Logarithm of the overall stability constant
n_T	- The number of titrations
n_P	- The number of titration points
λ_{max}	- Maximum wavelength
ε	- The extinction coefficient
log $P_{oct/aq}$	- Octanol/water partition coefficient
J	- Steady state flux
K_p	- The permeability coefficient

List of Figures

Figure 1.1: Progression of inflammation and degeneration in rheumatoid arthritis.

Figure 1.2: Structure of cageL which has a large lipophilic cage moiety attached to an amino/amido ligand.

Figure 1.3: The binding sites for copper(II) in Human Serum Albumin (HSA) .

Figure 1.4: P.M.I as a function of Log_{10} [L] for the metal ligand complexes.

Figure 1.5: Structure of the tripeptides, Gly-Leu-Phe and Sar-Leu-Phe.

Figure 3.1: Graphs which represent typical Z_H-bar, Z_M-bar and Q_M-bar curves.

Figure 3.2: Example of how to calculate log *K* values from potentiometric species using stability constants.

Figure 3.3: Z_H-bar as a function of pH for the protonation of Gly-Leu-Phe at 25 ^oC in 0.15 $mol.dm^{-3}$ of NaCl.

Figure 3.4: Protonation species distribution curve for Gly-Leu-Phe at 25 ^oC in 0.15 $mol.dm^{-3}$ of NaCl.

Figure 3.5: Z_H-bar as a function of pH for the protonation of Sar-Leu-Phe at 25 ^oC in 0.15 $mol.dm^{-3}$ of NaCl.

Figure 3.6: Protonation species distribution curve for Sar-Leu-Phe at 25 ^oC in 0.15 $mol.dm^{-3}$ of NaCl.

Figure 3.7: Z_M-bar as a function of pH for the 1:3 and 1:4 complexation of copper(II) and Gly-Leu-Phe at 25 ^oC in 0.15 mol dm^{-3} NaCl.

Figure 3.8: Q_M-bar as a function of pH for the 1:3 and 1:4 complexation of copper(II) and Gly-Leu-Phe at 25 ^oC in 0.15 $mol.dm^{-3}$ NaCl.

Figure 3.9: Protonation species distribution curve for copper(II) and Gly-Leu-Phe (1:4 ratio) at 25 ^oC in 0.15 $mol.dm^{-3}$ of NaCl.

Figure 3.10: Z_M-bar as a function of pH for the 1:3 and 1:4 complexation of copper(II) and Sar-Leu-Phe at 25 ^oC in 0.15 $mol.dm^{-3}$ NaCl.

Figure 3.11: Q_M-bar as a function of pH for the 1:3 and 1:4 complexation of copper(II) and Sar-Leu-Phe at 25 ^oC in 0.15 $mol.dm^{-3}$ NaCl.

Figure 3.13: Model 1 of Z_M-bar as a function of pH for the 1:3 and 1:4 complexation of nickel(II) and Gly-Leu-Phe at 25 ^oC in 0.15 $mol.dm^{-3}$ NaCl.

Figure 3.14: Model 2 of Z_M-bar as a function of pH for the 1:3 and 1:4 complexation of

nickel(II) and Gly-Leu-Phe at 25 ºC in 0.15 mol.dm^{-3} NaCl.

Figure 3.15: Model 1 of Q_M-bar as a function of pH for the 1:3 and 1:4 complexation of nickel(II) and Gly-Leu-Phe at 25 ºC in 0.15 mol.dm^{-3} NaCl.

Figure 3.16: Model 2 of Q_M-bar as a function of pH for the 1:3 and 1:4 complexation of nickel(II) and Gly-Leu-Phe at 25 ºC in 0.15 mol.dm^{-3} NaCl.

Figure 3.17: Model 1 of the protonation species distribution curve for nickel(II) and Gly-Leu-Phe (1:4 ratio) at 25 ºC in 0.15 mol.dm^{-3} of NaCl.

Figure 3.18: Model 2 of the protonation species distribution curve for nickel(II) and Gly-Leu-Phe (1:4 ratio) at 25 ºC in 0.15 mol.dm^{-3} of NaCl.

Figure 3.19: Model 1 of Z_M-bar as a function of pH for the 1:3 and 1:4 complexation of nickel(II) and Sar-Leu-Phe at 25 ºC in 0.15 mol.dm^{-3} NaCl.

Figure 3.20: Model 2 of Z_M-bar as a function of pH for the 1:3 and 1:4 complexation of nickel(II) and Sar-Leu-Phe at 25 ºC in 0.15 mol.dm^{-3} NaCl.

Figure 3.21: Model 1 of Q_M-bar as a function of pH for the 1:3 and 1:4 complexation of nickel(II) and Sar-Leu-Phe at 25 ºC in 0.15 mol.dm^{-3} NaCl.

Figure 3.22: Model 2 of Q_M-bar as a function of pH for the 1:3 and 1:4 complexation of nickel(II) and Sar-Leu-Phe at 25 ºC in 0.15 mol.dm^{-3} NaCl.

Figure 3.23: Model 1 of the protonation species distribution curve for nickel(II) and Sar-Leu-Phe (1:4 ratio) at 25 ºC in 0.15 mol.dm^{-3} of NaCl.

Figure 3.24: Model 2 of the protonation species distribution curve for nickel(II) and Sar-Leu-Phe (1:4 ratio) at 25 ºC in 0.15 mol.dm^{-3} of NaCl.

Figure 3.25: Z_M-bar as a function of pH for the 1:3 and 1:4 complexation of zinc(II) and Gly-Leu-Phe at 25 ºC in 0.15 mol.dm^{-3} NaCl.

Figure 3.26: Q_M-bar as a function of pH for the 1:3 and 1:4 complexation of zinc(II) and Gly-Leu-Phe at 25 ºC in 0.15 mol.dm^{-3} NaCl.

Figure 3.27: Protonation species distribution curve for zinc(II) and Gly-Leu-Phe (1:4 ratio) at 25 ºC in 0.15 mol.dm^{-3} of NaCl.

Figure 3.28: Z_M-bar as a function of pH for the 1:3 and 1:4 complexation of zinc(II) and Sar-Leu-Phe at 25 ºC in 0.15 mol.dm^{-3} NaCl.

Figure 3.29: Q_M-bar as a function of pH for the 1:3 and 1:4 complexation of zinc(II) and Sar-Leu-Phe at 25 ºC in 0.15 mol.dm^{-3} NaCl.

Figure 3.30: Protonation species distribution curve for zinc(II) and Sar-Leu-Phe (1:4 ratio) at 25 ºC in 0.15 mol.dm^{-3} of NaCl.

Figure 4.1: Electronic spectra for solutions containing 7.63 x10^{-4} mol.dm^{-3} of copper(II) and 0.0025 mol.dm^{-3} of Gly-Leu-Phe.

Figure 4.2: Electronic spectra for solutions containing 7.04 x 10^{-4} mol.dm^{-3} of copper(II) and 0.0025 mol.dm^{-3} of Sar-Leu-Phe.

Figure 4.3: Calculated species absorption spectra for the copper(II) and Gly-Leu-Phe complexes as a function of wavelength.

Figure 4.4: Calculated species absorption spectra for the copper(II) and Sar-Leu-Phe complexes as a function of wavelength.

Figure 4.5: Electronic spectra for solutions containing 0.0009 mol.dm^{-3} of nickel(II) and 0.0036 mol.dm^{-3} of Gly-Leu-Phe.

Figure 4.6: Electronic spectra for solutions containing 0.0009 mol.dm^{-3} of nickel(II) and 0.0037 mol.dm^{-3} of Sar-Leu-Phe.

Figure 4.7: Calculated species absorption spectra of Model 1 for the nickel(II) and Gly-Leu-Phe complexes as a function of wavelength.

Figure 4.8: Calculated species absorption spectra of Model 2 for the nickel(II) and Gly-Leu-Phe complexes as a function of wavelength.

Figure 4.9: Calculated species absorption spectra of Model 1 for the nickel(II) and Sar-Leu-Phe complexes as a function of wavelength.

Figure 4.10: Calculated species absorption spectra of Model 2 for the nickel(II) and Sar-Leu-Phe complexes as a function of wavelength.

Figure 4.11: Section of the infrared spectrum for Gly-Leu-Phe and Cu-Gly-Leu-Phe with the pH values of 5.0, 6.0, 7.6 and 9.6 in D_2O at 25 °C.

Figure 4.12: Section of the infrared spectrum for Sar-Leu-Phe and Cu-Sar-Leu-Phe with the pH values of 4.5, 6.0, 8.0 and 11.0 in D_2O at 25 °C.

Figure 4.13: Illustration of the possible binding sites for copper(II) onto the Gly-Leu-Phe ligand. Sar-Leu-Phe has the same binding sites.

Figure 4.14: A: ^1H NMR spectra of Gly-Leu-Phe at increasing pH values from 2-11. B: The proton assignments.

Figure 4.15: A: ^1H NMR spectra of Sar-Leu-Phe at increasing pH values from 2-11. B: The proton assignments.

Figure 4.16: The change in Gly-Leu-Phe ^1H chemical shift as a function of pH.

Figure 4.17: The change in Sar-Leu-Phe ^1H chemical shift as a function of pH.

Figure 4.18: A: ^1H NMR spectra of the titration of Gly-Leu-Phe with copper(II) at a pH of

5.33 in D_2O. B: The proton assignments for Gly-Leu-Phe.

Figure 4.19: A: ^1H NMR spectra of the titration of Gly-Leu-Phe with copper(II) at a pH of 6.16 in D_2O. B: The proton assignments for Gly-Leu-Phe.

Figure 4.20: A: ^1H NMR spectra of the titration of Gly-Leu-Phe with copper(II) at a pH of 7.62 in D_2O. B: The proton assignments for Gly-Leu-Phe.

Figure 4.21: A: ^1H NMR spectra of the titration of Gly-Leu-Phe with copper(II) at a pH of 9.63 in D_2O. B: The proton assignments for Gly-Leu-Phe.

Figure 4.22: A: ^1H NMR spectra of the titration of Sar-Leu-Phe with copper(II) at a pH of 4.61 in D_2O. B: The proton assignments for Sar-Leu-Phe.

Figure 4.23: A: ^1H NMR spectra of the titration of Sar-Leu-Phe with copper(II) at a pH of 6.22 in D_2O. B: The proton assignments for Sar-Leu-Phe.

Figure 4.24: A: ^1H NMR spectra of the titration of Sar-Leu-Phe with copper(II) at a pH of 8.22 in D_2O. B: The proton assignments for Sar-Leu-Phe.

Figure 4.25: A: ^1H NMR spectra of the titration of Sar-Leu-Phe with copper(II) at a pH of 10.16 in D_2O. B: The proton assignments for Sar-Leu-Phe.

Figure 4.26: Possible metal ligand coordination modes for the ML species of Cu-Gly-Leu-Phe at a pH of 5.33.

Figure 4.27: Possible metal ligand coordination modes for the MLH_{-1} species of Cu-Gly-Leu-Phe at a pH of 6.16.

Figure 4.28: Possible metal ligand coordination modes for the ML_2H_{-1} species of Cu-Gly-Leu-Phe at a pH of 7.62.

Figure 4.29: Possible metal ligand coordination modes for the ML species of Cu-Sar-Leu-Phe at a pH of 4.61.

Figure 4.30: Possible metal ligand coordination modes for the MLH_{-1} species of Cu-Sar-Leu-Phe at a pH of 6.22.

Figure 4.31: i: Gaussian 09 side view, ii: Gaussian 09 top down view and iii: a line drawing of coordination mode **a** from the ML species in Cu-Gly-Leu-Phe, which has a ground state energy of -7,864,187.52 kJ/mol.

Figure 4.32: i: Gaussian 09 side view, ii: Gaussian 09 top down view and iii: a line drawing of coordination mode **b** from the ML species in Cu-Gly-Leu-Phe, which has a ground state energy of -7,663,766.02 kJ/mol.

Figure 4.33: i: Gaussian 09 side view, ii: Gaussian 09 top down view and iii: a line

drawing of coordination mode **a** from the MLH_{-1} species in Cu-Gly-Leu-Phe, which has a ground state energy of -7,863,208.27 kJ/mol.

Figure 4.34: i: Gaussian 09 side view, ii: Gaussian 09 top down view and iii: a line drawing of coordination mode **b** from the MLH_{-1} species in Cu-Gly-Leu-Phe, which has a ground state energy of -7,863,142.37 kJ/mol.

Figure 4.35: i: Gaussian 09 side view, ii: Gaussian 09 top down view and iii: a line drawing of coordination mode **c** from the MLH_{-1} species in Cu-Gly-Leu-Phe, which has a ground state energy of -7,863,055.34 kJ/mol.

Figure 4.36: i: Gaussian 09 side view, ii: Gaussian 09 top down view and iii: a line drawing of coordination mode **d** from the MLH_{-1} species in Cu-Gly-Leu-Phe, which has a ground state energy of -7,662,718.67 kJ/mol.

Figure 4.37: i: Gaussian 09 side view, ii: Gaussian 09 top down view and iii: a line drawing of coordination mode **a** from the ML_2H_{-1} species in Cu-Gly-Leu-Phe, which has a ground state energy of -10,614,276.27 kJ/mol.

Figure 4.38: i: Gaussian 09 side view, ii: Gaussian 09 top down view and iii: a line drawing of coordination mode **b** from the ML_2H_{-1} species in Cu-Gly-Leu-Phe, which has a ground state energy of -10,619,800.63 kJ/mol.

Figure 4.39: i: Gaussian 09 side view, ii: Gaussian 09 top down view and iii: a line drawing of coordination mode **a** from the MLH_{-2} species in Cu-Gly-Leu-Phe, which has a ground state energy of -7,861,342.53 kJ/mol.

Figure 4.40: i: Gaussian 09 side view, ii: Gaussian 09 top down view and iii: a line drawing of coordination mode **b** from the MLH_{-2} species in Cu-Gly-Leu-Phe, which has a ground state energy of -7,660,922.49 kJ/mol.

Figure 4.41: i: Gaussian 09 side view, ii: Gaussian 09 top down view and iii: a line drawing of coordination mode **a** from the ML species in Cu-Sar-Leu-Phe, which has a ground state energy of -8,166,964.67 kJ/mol.

Figure 4.42: i: Gaussian 09 side view, ii: Gaussian 09 top down view and iii: a line drawing of coordination mode **b** from the ML species in Cu-Sar-Leu-Phe, which has a ground state energy of -8,167,557.10 kJ/mol.

Figure 4.43: i: Gaussian 09 side view, ii: Gaussian 09 top down view and iii: a line drawing of coordination mode **c** from the ML species in Cu-Sar-Leu-Phe, which has a ground state energy of -7,967,259.42 kJ/mol.

Figure 4.44: i: Gaussian 09 side view, ii: Gaussian 09 top down view and iii: a line

drawing of coordination mode **d** from the ML species in Cu-Sar-Leu-Phe, which has a ground state energy of -7,766,840.08 kJ/mol.

Figure 4.45: i: Gaussian 09 side view, ii: Gaussian 09 top down view and iii: a line drawing of coordination mode **a** from the MLH_{-1} species in Cu-Sar-Leu-Phe, which has a ground state energy of -7,966,126.71 kJ/mol.

Figure 4.46: i: Gaussian 09 side view, ii: Gaussian 09 top down view and iii: a line drawing of coordination mode **b** from the MLH_{-1} species in Cu-Sar-Leu-Phe, which has a ground state energy of -7,966,277.78 kJ/mol.

Figure 4.47: Gaussian 09 side view, ii: a line drawing of coordination mode **a** from the ML_2H_{-1} species in Cu-Sar-Leu-Phe, which has a ground state energy of -10,824,337.87 kJ/mol.

Figure 4.48: i: Gaussian 09 side view, ii: Gaussian 09 top down view and iii: a line drawing of coordination mode **a** from the MLH_{-2} species in Cu-Sar-Leu-Phe, which has a ground state energy of -7,964,717.81 kJ/mol.

Figure 4.49: i: Gaussian 09 side view and ii: a line drawing of coordination mode **b** from the MLH_{-2} species in Cu-Sar-Leu-Phe, which has a ground state energy of -7,964,678.07 kJ/mol.

Figure 4.50: i: Gaussian 09 side view, ii: Gaussian 09 top down view and iii: a line drawing of coordination mode **c** from the MLH_{-2} species in Cu-Sar-Leu-Phe, which has a ground state energy of -7,763,994.47 kJ/mol.

Figure 5.1: Illustration of the stratum corneum.

Figure 5.2: Flow diagram depicting the method outlined for determining the partition coefficients.

Figure 5.3: Protonation species distribution curve for Cu-Gly-Leu-Phe at 25 ^{o}C in 0.15 $mol.dm^{-3}$ of NaCl overlaid with the partition coefficient values of Cu-Gly-Leu-Phe (1:4) over a pH range from 2-10.

Figure 5.4: Protonation species distribution curve for Cu-Sar-Leu-Phe at 25 ^{o}C in 0.15 $mol.dm^{-3}$ of NaCl overlaid with the partition coefficient values of Cu-Sar-Leu-Phe (1:4) over a pH range from 2-10.

Figure 5.5: A modified Franz cell.

Figure 5.6: Graphical representation of the copper(II) concentration in the receiver phase of the Franz cell plotted against time after the copper(II) complexes at a pH of 7.4 and copper(II) chloride at a pH of 4.2 diffused through the Cerasome

9005 lipid membrane.

Figure 5.7: Gradient of the linear region in an accumulative absorption-time curve of copper(II) concentration in the receiver phase for Cu-Gly-Leu-Phe, Cu-Sar-Leu-Phe and $CuCl_2.2H_2O$.

Figure 5.8: Graphical representation of the steady state flux for Cu-Gly-Leu-Phe, Cu-Sar-Leu-Phe and $CuCl_2.2H_2O$ after diffusion through the Cerasome 9005 lipid membrane has taken place.

Figure 5.9: Graphical representation of the permeability coefficient for Cu-Gly-Leu-Phe, Cu-Sar-Leu-Phe and $CuCl_2.2H_2O$.

Figure 6.1: Log P.M.I curves for copper(II), nickel(II) and zinc(II) with Gly-Leu-Phe and plotted against –log[Gly-Leu-Phe].

Figure 6.2: Log P.M.I curves for copper(II), nickel(II) and zinc(II) with Sar-Leu-Phe and plotted against –log[Sar-Leu-Phe].

Figure 7.1: The resultant ratios of Cu-Gly-Leu-Phe and Cu-Sar-Leu-Phe with copper(II) tripeptide complexes from literature, by calculating the difference in permeability coefficients of the copper(II) complex and copper(II) chloride from the same studies.

Figure 7.2: Visual observation of Cu-Gly-Leu-Phe as the pH increases in increments of 1 from left to right from a pH of 2-10.

Figure 7.3: Visual observation of Cu-Sar-Leu-Phe as the pH increases in increments of 1 from left to right from a pH of 2-10.

Figure 7.4: Copper(II) plasma mobilising index for, [555-N] and [H(555)-N], found in Zvimba *et al.* and Cu-Gly-Leu-Phe and Cu-Sar-Leu-Phe.

List of Tables

Table 3.1: Stability constants (log β_{pqr}) and logarithms for Gly-Leu-Phe at 25 ^{o}C and 0.15 mol.dm^{-3} NaCl.

Table 3.2: Stability constants (log β_{pqr}) and logarithms for Sar-Leu-Phe at 25 ^{o}C and 0.15 mol.dm^{-3} NaCl.

Table 3.3**:** Stability constants (log β_{pqr}) and logarithms for the 1:4 complexation between copper(II) and Gly-Leu-Phe at 25 ^{o}C and 0.15 mol.dm^{-3} NaCl.

Table 3.4: Stability constants (log β_{pqr}) and logarithms for the 1:4 complexation between copper(II) and Sar-Leu-Phe at 25 ^{o}C and 0.15 mol.dm^{-3} NaCl.

Table 3.5: Model 1 and Model 2 of the stability constants (log β_{pqr}) and logarithms for the 1:4 complexation between nickel(II) and Gly-Leu-Phe at 25 ^{o}C and 0.15 mol.dm^{-3} NaCl.

Table 3.6: Model 1 and Model 2 for the stability constants (log β_{pqr}) and logarithms for the 1:4 complexation between nickel(II) and Sar-Leu-Phe at 25 ^{o}C and 0.15 mol.dm^{-3} NaCl.

Table 3.7: Stability constants (log β_{pqr}) and logarithms for the 1:4 complexation between zinc(II) and Gly-Leu-Phe at 25 ^{o}C and 0.15 mol.dm^{-3} NaCl.

Table 3.8: Stability constants (log β_{pqr}) and logarithms for the 1:4 complexation between zinc(II) and Sar-Leu-Phe at 25 ^{o}C and 0.15 mol.dm^{-3} NaCl.

Table 3.9: Protonation constants for the ligands, Gly-Leu-Phe and Sar-Leu-Phe, as well as literature values for diglycine (Gly-Gly) and triglycine (Gly-Gly-Gly).

Table 3.10: Stability constants for the complexes formed between the two ligands, Gly-Leu-Phe and Sar-Leu-Phe and the metals, Cu(II), Ni(II) and Zn(II), as well as the literature values for diglycine (Gly-Gly), triglycine (Gly-Gly-Gly), glycyl-L-phenylalanine (Gly-Phe) and sarcosyl-L-phenylalanine (Sar-Phe).

Table 3.11: Comparison between dipeptides from literature and the tripeptides, Gly-Leu-Phe and Sar-Leu-Phe.

Table 4.1: Relevant electron donor groups and their corresponding contribution to the ligand field.

Table 4.2: Maximum wavelengths corresponding to the molar absorption coefficients of individual complex species of copper(II) and Gly-Leu-Phe.

Table 4.3: Maximum wavelengths corresponding to the molar absorption coefficients of

individual complex species of copper(II) and Sar-Leu-Phe.

Table 4.4: Maximum wavelengths corresponding to the molar absorption coefficients of individual complex species for Model 1 and Model 2 of nickel(II) and Gly-Leu-Phe.

Table 4.5: Maximum wavelengths corresponding to the molar absorption coefficients of individual complex species for Model 1 and Model 2 of nickel(II) and Sar-Leu-Phe.

Table 4.6: Proposed coordinations of the nickel(II) species for the two ligands Gly-Leu-Phe and Sar-Leu-Phe, as well as the observed wavelengths of each species.

Table 4.7: Proposed coordination modes for the species of Cu-Gly-Leu-Phe with their relative energies with respect to a particular coordination mode, geometries, ring sizes, bond lengths and bite angles.

Table 4.8: Proposed coordination modes for the species of Cu-Sar-Leu-Phe with their relative energies with respect to a particular coordination mode, geometries, ring sizes, bond lengths and bite angles.

Table 5.1: Comparison of the partition coefficient values at a pH of 7.4 between dipeptides from literaure and the tripeptides, Gly-Leu-Phe and Sar-Leu-Phe.

Table 5.2: Comparison of the partition coefficient values at pH 7.4 between the tripeptides from literature and the tripeptides, Gly-Ley-Phe and Sar-Leu-Phe.

Table 5.3: Measured copper (II) concentration in the receiver phase of the Franz cell as a function of time after the copper (II) complexes at a pH of 7.4 diffused through a Cerasome 9005 lipid membrane.

Table 5.4: Measured copper (II) concentration in the receiver phase of the Franz cell as a function of time after copper (II) chloride at a pH of 4.2 diffused through a Cerasome 9005 lipid membrane.

Table 5.5: Steady state flux, J, and permeability coefficient, K_p, of Cu-Gly-Leu-Phe, Cu-Sar-Leu-Phe and $CuCl_2.2H_2O$ after diffusion through the Cerasome 9005 lipid membrane has taken place.

Table 5.6: A comparison between the permeability of Cu-Gly-Leu-Phe and Cu-Sar-Leu-Phe with the copper(II) tripeptide complexes investigated in the study by Mazurowska and Mojski and by Hammouda, by calculating the difference in permeability coefficients of the copper(II) complex and copper(II) chloride from the same studies and comparing the resultant ratios.

Table 7.1: A summary of the results from each structure determining technique that was used to determine the coordination mode of each species.

Table of Contents

1 Introduction....21
References....28
2 Aim and Objectives....29
3 Potentiometric Titrations....30
3.1 Introduction....30
3.2 Experimental....35
3.2.1 Solution preparations....35
3.2.2 Potentiometric titrations....35
3.2.3 Data analysis....36
3.3 Results....37
3.3.1 Protonation of Gly-Leu-Phe and Sar-Leu-Phe....37
3.3.1(a) Protonation of Gly-Leu-Phe....38
3.3.1(b) Protonation of Sar-Leu-Phe....40
3.3.2 Copper(II) complexation of Gly-Leu-Phe and Sar-Leu-Phe....43
3.3.2(a) Cu-Gly-Leu-Phe....43
3.3.2(b) Cu-Sar-Leu-Phe....47
3.3.3 Nickel(II) complexation of Gly-Leu-Phe and Sar-Leu-Phe....51
3.3.3(a) Ni-Gly-Leu-Phe....51
3.3.3(b) Ni-Sar-Leu-Phe....56
3.3.4 Zinc(II) complexation of Gly-Leu-Phe and Sar-Leu-Phe....62
3.3.4(a) Zn-Gly-Leu-Phe....62
3.3.4(b) Zn-Sar-Leu-Phe....65
3.4 Discussion....69
3.5 Conclusion....74
References....75
4 Structural Studies....77
4.1 Ultraviolet-Visible (UV-Vis) Spectrophotometry....77
4.1.1 Introduction....77
4.1.2 Experimental....81
4.1.3 Results....82
4.1.3(a) Copper(II) complexes....82

4.1.3(b) Nickel(II) complexes 88
4.1.4 Discussion 93
4.1.4(a) Copper(II) complexes 93
4.1.4(b) Nickel(II) complexes 94
4.1.5 Conclusion 97
References 98
4.2 Infrared (IR) Spectroscopy 100
4.2.1 Introduction 100
4.2.2 Experimental 101
4.2.3 Results 102
4.2.4 Discussion 104
4.2.4(a) Gly-Leu-Phe 104
4.2.4(b) Sar-Leu-Phe 105
4.2.5 Conclusion 107
References 108
4.3 ^{1}H NMR Spectroscopy 109
4.3.1 Introduction 109
4.3.2 Experimental 111
4.3.3 Results 112
4.4.3(a) Protonation of Gly-Leu-Phe and Sar-Leu-Phe 112
4.3.3(b) Titration of Gly-Leu-Phe and Sar-Leu-Phe with copper(II) 117
4.3.3(b.i) Cu-Gly-Leu-Phe 117
4.3.3(b.ii) Cu-Sar-Leu-Phe 125
4.3.4 Discussion 132
4.3.5 Conclusion 141
References 142
4.4 Molecular Modelling 144
4.4.1 Introduction 144
4.4.2 Experimental 149
4.4.3 Results 150
4.4.3(a) Cu-Gly-Leu-Phe 150
4.4.3(b) Cu-Sar-Leu-Phe 161
4.4.4 Discussion 173

4.4.4(a) Cu-Gly-Leu-Phe 180
4.4.4(a.i) ML coordination modes 180
4.4.4(a.ii) MLH_{-1} coordination modes 180
4.4.4(a.iii) ML_2H_{-1} coordination modes 181
4.4.4(a.iv) MLH_{-2} coordination modes 181
4.4.4(b) Cu-Sar-Leu-Phe 182
4.4.4(b.i) ML coordination modes 182
4.4.4(b.ii) MLH_{-1} coordination modes 182
4.4.4(b.iii) ML_2H_{-1} coordination modes 183
4.4.4(b.iv) MLH_{-2} coordination modes 183
4.4.5 Conclusion 184
References 185
5 Dermal Absorption 188
5.1 Introduction 188
5.2 Octanol/Water Partition Coefficient 191
5.2.1 Flask Shake method 191
5.2.2Experimental 192
5.2.3 Results 194
5.2.4 Discussion 197
5.2.5 Conclusion 200
5.3 Modified Franz cell: Permeability Coefficient 201
5.3.1 Franz cell diffusion method 201
5.3.2 Experimental 203
5.3.3 Results 205
5.3.4 Discussion 211
5.3.4(a) Physiochemical properties 211
5.3.4(a.i) Molecular size 211
5.3.4(a.ii) Compound ionisation 212
5.3.4(a.iii) Hydrogen bonding 212
5.3.4(a.iv) Solubility 213
5.3.5 Conclusion 216
References 217
6 Blood Plasma Model 220

6.1 Introduction 220
6.2 Experimental 222
6.3 Results 223
6.4 Discussion 225
6.5 Conclusion 226
References 227
7 General Concluding Remarks 228
References 237
Appendix 238

1 Introduction

Rheumatoid arthritis (RA) is a chronic, inflammatory, auto-immune disease which affects connective tissue. The disease first appears in the knuckle joints as slight swelling, accompanied by pain and stiffness and as the disease progresses, the swelling increases and the joint progressively degenerates.[1,2] Inflammation and degeneration also occur in other articular and related structures of the body as the disease progresses and this leads to immobility and ultimately death.[2] The progression of inflammation and degeneration can be seen in Figure 1.1 below. RA affects 1-5% of the world's population and is mainly prevalent in the elderly and is more common amongst women.[1,3] RA occurs when the immune system stops functioning in the way it should and instead starts attacking connective tissue, which results in inflammation and degeneration of joints.[3] The exact cause of the disease is not known and at present there is no cure. However, it can be controlled with immunosuppressive drugs and the symptoms can be treated with anti-inflammatory drugs.[1,3]

Figure 1.1: Progression of inflammation and degeneration in rheumatoid arthritis.[4]

Copper(II) complexes have been used as early as 1941 as a treatment for RA and other connective tissue diseases due to copper's anti-inflammatory properties. Copper bangles have also been used as a treatment for RA for centuries, where sweat solubilises and stimulates dermal absorption of copper into the blood stream.[3,5] During RA, serum copper(II) levels are elevated and this leads to the hypothesis that endogenous copper(II) could have a protective function in chronic inflammatory conditions. This has resulted in the design of ligands which would form a complex with copper(II) and result in the increase of copper(II)'s

bioavailability. However, the homeostasis of other endogenous metal ions has to remain undisrupted.[5]

Copper is an essential element for all living organisms as it is required for reproduction, haemoglobin synthesis, bone formation and many other biological processes. The oxidation states for biologically active copper are (I), (II) and (III) and are transported in the body to specific sites as copper complexes. The body obtains copper from dietary sources such as animal liver, shellfish, nuts, dried fruit, and also chocolate.[3,6]

There are a few possible mechanisms for the anti-inflammatory property of copper.[1] These mechanisms include the ability of copper to induce the activity of lysyl oxidase, which is a copper dependant enzyme that repairs tissue damaged from inflammation.[7] Another mechanism of copper is the modulation of prostaglandin synthesis, where copper decreases the amount of a prostaglandin that promotes inflammation by vasodilation.[8] Copper also induces the activity of superoxide dismutase, which is an enzyme that mutates the superoxide anion to oxygen and hydrogen peroxide and therefore stops the property of the superoxide anion from initiating inflammation.[9] Copper can stabilize the lysosomal membrane by making it less permeable to synovial fluid and therefore inhibiting contact between the synovial fluid and cartilage. The synovial fluid contains lysosomal enzymes, which destroy cartilage and therefore the stabilisation of the lysosomal membrane prevents degeneration of cartilage.[10] Copper is also involved in the modulation of the physiological effects of histamine, since the enzyme diamine oxidase which has a role in regulating histamine is dependent on copper.[3]

The effective use of copper as a treatment for the inflammation of RA, has resulted in the search for copper(II) complexes which enhance oral and/or dermal absorption of copper(II).[1] The focus was to design a ligand that will form a complex with copper(II) and increase its bioavailability, but at the same time not disrupt the homeostasis of the other endogenous metal ions. For this, the ligand would need to have primarily nitrogen donor groups which could increase the selectivity of copper(II). It would also have to form a strong chelation with copper(II), but not so strong that the copper(II) cannot be released to exert its anti-inflammatory property and instead get excreted along with the ligand. In order to release copper(II) *in vivo*, the complex needs to be kinetically labile. For dermal absorption the complex also has to be lipophilic, but not too lipophilic or it gets trapped in the skin.[5]

These criteria led Jackson *et al.* to the design of polyamine ligands, namely 3,6,9,12-tetra-azatetradecanedioate (ttda) and 3,6,9-triazatetradecanedioate (dtda), which are dicarboxylic acids and therefore form formally neutral complexes with copper(II).[11,12] However, these drugs were found to be such good chelators of copper(II) that they were not able to release the copper(II) at the active site. Instead they were excreted intact through urine as opposed to the usual excretory pathway of copper(II), which is via the bile and through the liver. This is due to their hydrophilic nature, even though the neutral charge should have made them more lipophilic in nature. Therefore these ligands were too stable and too hydrophilic.[5,11-13] In order to bury the charge within the complex, Jackson *et al.,* used amino/amido ligands.[1] These ligands were found to be more lipophilic and selective, but because the amide needed to deprotonate before complexation could take place, the complexes were only formed at a high pH.[1] To improve the lipophilicity, a study by Odisitse *et al.* attached a pentacyclo-undecane cage (adamantine) derivative onto the amino/amido ligands, since the cage moiety is largely lipophilic in nature.[5] The resulting ligand was 3,5-diaminodiamido-4-oxahexacyclo[5.4.1.02,6.03,10.05,9.08,11]dodecane (cageL) and can be seen in Figure 1.2 below.

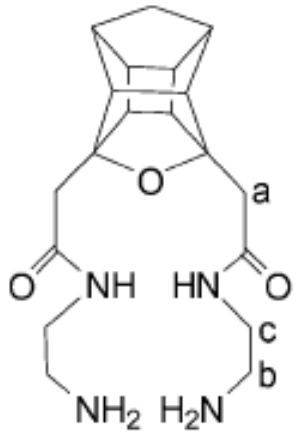

cageL

Figure 1.2: Structure of cageL which has a large lipophilic cage moiety attached to an amino/amido ligand.[5]

However, the study showed that the complex was largely hydrophilic and this could have been due to the overall charge of the complexes, the presence of water molecules or hydrogen bonding. The cage also increased the stability which was presumed to be due to the correct pre-formed structure for metal binding. Through dermal absorption studies, more activity was retained, instead of being excreted through the urine.[5]

In vivo, copper(II) is transported by proteins. The most effective copper(II) transport protein is human serum albumin (HSA), where the copper(II) is reversibly bound to the peptide C-terminus.[14] The main binding sites on HSA for copper(II) are the amine and amide N-donors. These N-donor groups are more selective for copper(II) than the other metals *in vivo*. However, this results in a very stable complex and thus less bioavailability.[14,15] An illustration for the binding sites of copper(II) to HSA can be seen below in Figure 1.3.

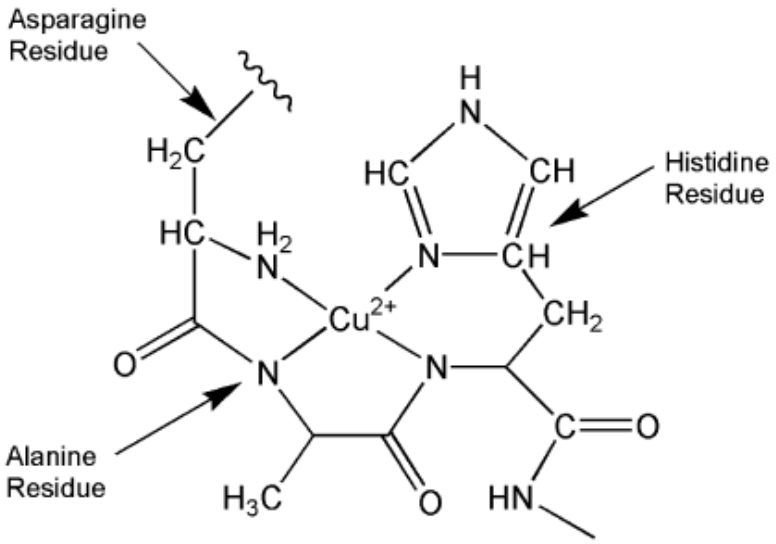

Figure 1.3: The binding sites for copper(II) in Human Serum Albumin (HSA) .[16]

Therefore, studies then led to the design of peptides which would resemble the structure of HSA. Peptides are good chelators of copper(II), but cannot be used as oral drugs because of their rapid metabolism in the stomach. However, they can be used to promote dermal absorption of copper(II). This led to the studies on increasing the bioavailable pool of copper(II) *in vivo* through dermal absorption.

There are two methods of increasing the bioavailable pool of copper(II) *in vivo* via dermal absorption. One way is to design a ligand that will form a complex with copper(II) and

undergo dermal absorption, from where it can release copper(II) into the blood plasma. The other way is for the ligand to release copper(II) ions from endogenous sources like serum albumin.

Mohajane focused on the design of a ligand, which could increase the bioavailable pool of copper(II) *in vivo* via dermal absorption.[15] These ligands were four glycine dipeptides, namely glycyl-glycine (Gly-Gly), glycyl-L-phenylalanine (Gly-Phe), glycyl-L-leucine (Gly-Leu) and glycyl-L-histidine (Gly-His) and four sarcosine dipeptides, namely sarcosyl-glycine (Sar-Gly), sarcosyl-L-leucine (Sar-Leu), sarcosyl-L-phenylalanine (Sar-Phe) and sarcosyl-L-histidine (Sar-His) which formed complexes with copper(II). The sarcosine dipeptides were expected to be more lipophilic than the glycine dipeptides, because the added methyl group on the N-terminal of the sarcosine amino acid has been reported to increase the lipophilicity of complexes compared to the non-methylated analogues.[15,17] However, the N-methyl substituent should not affect the stability of the complex, since this could affect the transport of copper(II). It was found that the N-methylated substituent did increase the lipophilicity of the complex, but did not affect the stability. However, the lipophilic values were not high enough to indicate that an efficient dermal absorption could take place. The dipeptides with the highest lipophilicities were Gly-Leu and Sar-Leu. The mobilising index (P.M.I), which measures the ability of the ligand to move a metal that is bound to a protein to a low molecular weight form, was also studied to determine if these dipeptides can release copper(II) from endogenous reserves.[15,18] It was found that the dipeptides had a low mobilising capacity and that unrealistically high concentrations of the ligand were needed in order to achieve a 10-fold increase in low molecular weight molecules.[15] The dipeptides with the highest mobilising capacity were Gly-Leu and Gly-Phe. The mobilising capacities of the dipeptides can be seen in Figure 1.4 as a function of the ligand concentration.

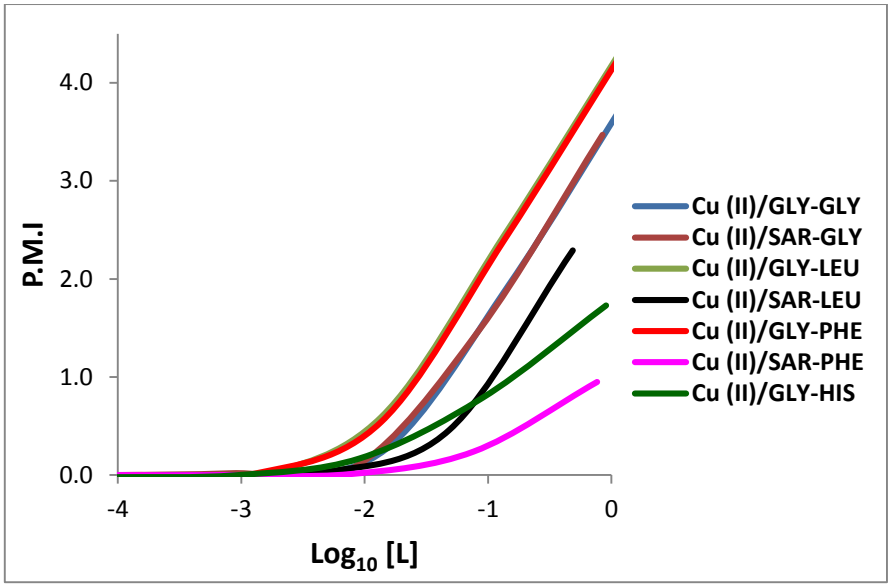

Figure 1.4: P.M.I as a function of Log_{10} [L] for the metal ligand complexes.[15]

These stability, lipophilic and mobility results led to the suggestion that tripeptides with the amino acids, leucine (Leu) and phenylalanine (Phe) should be added to either a glycine (Gly) or a sarcosine (Sar) amino acid. The two tripeptides should then undergo the same experimental methods to see if the results compare to the dipeptides.

Thus the ligands glycyl-L-leucyl-phenylalanine (Gly-Leu-Phe) and sarcosyl-L-leucyl-phenylalanine (Sar-Leu-Phe) were used to form complexes with copper(II). Tripeptides will have an increased coordination with copper(II) and therefore they should increase the stability and hence mobility of the complex. The added methyl group from the sarcosine amino acid should increase the lipophilicity of the complex. However, since it increases the electron density on the N-terminal of sarcosine and therefore increases the electron donation between the ligand and the copper(II), it could also increase the bond strength and hence the stability of the complex.

The design of the ligands has the following active binding sites for copper(II): one amine N-donor, two amide-N donors, two carbonyl-O donors and one carboxylate O-donor. The N-donor atoms will make the ligands more selective for copper(II) over the high concentrations of other metal ions in the blood plasma. The O-donor groups are weaker than the N-donor groups and thus will decrease the stability of the complex compared to Cu(II)-HSA, since HSA has four N-donor groups. This should therefore improve the bioavailability of the complexes. The two structures of the ligands can be seen below in Figure 1.5.

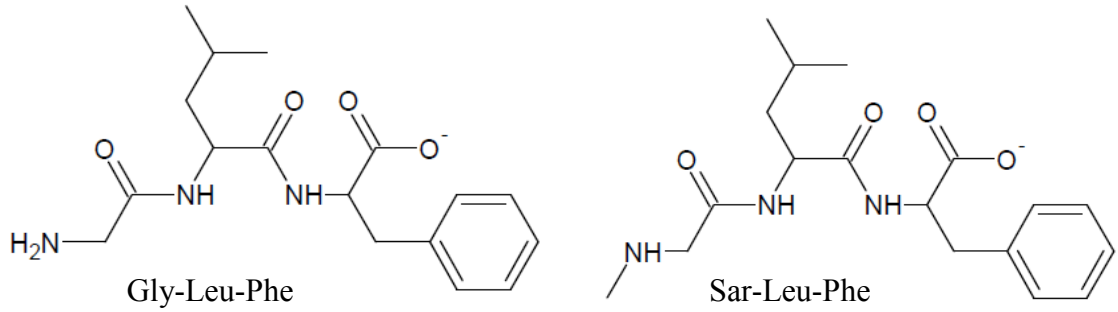

Figure 1.5: Structure of the tripeptides, Gly-Leu-Phe and Sar-Leu-Phe.

The resulting copper(II) tripeptide complexes must be stable enough to be formed at a near neutral pH, but also able to release copper *in vivo.* In addition they must be lipophilic enough to undergo dermal absorption. At the same time the tripeptides must not disrupt the homeostasis of the other endogenous metal ions. An added advantage would be if the complexes have high mobilising capacities so that they can release endogenous copper(II) into the blood plasma or have anti-inflammatory properties themselves. The resultant increase in bioavailable copper(II) *in vivo* will thus help to treat the symptoms of rheumatoid arthritis.

References

1. G. E. Jackson, L. Gama-M, A. Voye and M. J. Kelly, *J. Inorg. Biochem.*, 2000, **79**, 147-152.
2. E. T. Nomkoko, G. E. Jackson and B. S. Nakani, *J. Chem. Soc. Dalton Trans.*, 2004, 1432-1440.
3. S. Odisitse, MSc Thesis, University of Cape Town, 2003.
4. Bodybuilidng.com, http://www.bodybuilding.com/fun/manage_rheumatoid_arthritis.htm, (accessed December 2015).
5. S. Odisitse, G. E. Jackson, T. Govender, H. G. Kruger and A. Singh, *J. Chem. Soc. Dalton Trans.*, 2007, 1140–1149.
6. H. T. Delves, *Biological role of copper, Ciba Foundation Symposium 79*, Excerpta Medica, Amsterdam, 1980, pp. 5-22.
7. E.D. Harris, *Proc. Nat. Acad. Sci. USA.*, 1976, **73**, 371-374.
8. B.B. Vargaftig, Y. Trainer and M. Chignard, *Europ. J. Pharmacol.*, 1976, **33**, 19.
9. M.L. Salin and J.M. McCord, *Science 18*, 1974, 529.
10. J. Chayen, L. Bitensky, R. G. Butcher and L.W. Poulter, *Nature 222*, 1969, 281-282.
11. G. E. Jackson and M. J. Kelly, *J. Chem. Soc. Dalton Trans*., 1989, 2429-2433.
12. G. E. Jackson and M. J. Kelly, *J. Chem. Soc. Dalton Trans*., 1990, 1889-1893.
13. G. E. Jackson, *Handbook of Metal-Ligand Interactions in Biological Fluids, Bioinorganic Chemistry*, ed. G. Berthon, M. Dekker, Inc., New York, 1995, vol. 2, pp. 1228.
14. L. Perrone, E. Mothes, M. Vignes, A. S. Mockel, C. Figueroa, M. C. Miquel, M. L. Maddelein and P. Faller, *ChemBioChem*., 2010, **11**, 110-118.
15. M. Mohajane, PhD Thesis, University of Cape Town, 2013.
16. J. N. Zvimba and G. E. Jackson, *Polyhedron,* 2007, **26**, 2395-2404.
17. T. Uhlmann, V. L. Geoghegan, B. Thomas, G. Ridlova, D. C. Trudgian and O. Acuto, *Mol. Cell proteomics*, 2012, 1489-1498.
18. S. Odisitse and G. E. Jackson, *Polyhedron*, 2008, **27**, 453-464.

2 Aim and Objectives

The aim of this study was to develop a ligand that could increase the bioavailable pool of copper(II) *in vivo.* The ligand will bring about an increase through dermal absorption and consequently the release of copper(II) ions into the blood plasma, without disrupting the homeostasis of endogenous metal ions. A secondary aim is for the copper(II) ligand complex to have anti-inflammatory activity itself and have sufficient mobilising capacity to release copper(II) from endogenous sources.

In order to achieve this aim the following objectives were set:

1. Through a survey of the literature, to decide on two ligands which are most likely to satisfy the aims.
2. To measure the stability of these two ligands with H^{+}, Cu^{2+}, Ni^{2+}, and Zn^{2+}, using glass electrode potentiometry.
3. To measure the lipophilicities of the metal ligand complexes using octanol/water partition coefficients.
4. To measure dermal absorption using an artificial membrane in a modified Franz cell.
5. To determine the plasma mobilising capacities using ECCLES (Evaluation of Constituent Concentrations in Large Equilibrium Systems).
6. To determine the structure of the metal ligand complexes using Ultraviolet-visible spectroscopy, Infrared spectroscopy and ^{1}H NMR.
7. To evaluate the structure of the species formed in solution using molecular mechanics.

3 Potentiometric Titrations

3.1 Introduction

Glass Electrode Potentiometry is used to measure the equilibrium of metal complexes in a solution containing metal ions, ligands and protons. It achieves this by responding to hydrogen activity.[1-4]

A generalised equilibrium reaction can be seen below in the Equation 1, where M, L and H represent metal ions, ligands and protons respectively and *p*, *q*, and *r* represent the stoichiometric components in the complex.

$$pM + qL + rH \rightleftharpoons M_pL_qH_r \quad (1)$$

When *r* = -1n, where n is the number of protons, it represents the amount of protons that have been dissociated from the ligand. When r = +1n, it represents the number of protons that have been added to the ligand. The stability constants of the ligands can then be determined even if the concentration of metal ions is low.[1,5] The equilibrium/stability constant for the equilibrium reaction can then be represented by the symbol β_{pqr}, where

$$\beta_{pqr} = \frac{[M_pL_qH_r]}{[M]^p[L]^q[H]^r} \quad (2)$$

$[M_pL_qH_r]$ is the concentration of the metal ligand complex and $[M]^p$, $[L]^q$ and $[H]^r$ are the concentrations of free metal, free ligand and free hydrogen ions respectively.

The stability constants can also be considered as the accumulative stability constant, since the product of the individual stepwise formation constants gives the overall stability constant.[6,7] An example can be seen below in the stepwise formation of a general metal-ligand equilibrium formation, where K represents the individual stepwise formation constants.[8-13]

$$M + L \rightleftharpoons ML \qquad K_{ML} = \frac{[ML]}{[M][L]} \tag{3}$$

$$ML + L \rightleftharpoons ML_2 \qquad K_{ML2} = \frac{[ML_2]}{[ML][L]} \tag{4}$$

$$ML_{n-1} + L \rightleftharpoons ML_n \qquad K_{MLn} = \frac{[ML_n]}{[ML_{n-1}][L]} \tag{5}$$

Therefore,

$$\beta_{ML} = K_{ML} = \frac{[ML]}{[M][L]} \tag{6}$$

$$\beta_{ML2} = K_{ML} K_{ML2} = \frac{[ML_2]}{[ML][L]^2} \tag{7}$$

$$\beta_{MLn} = K_{ML} K_{ML2} \ldots\ldots K_{MLn} = \frac{[ML_n]}{[ML_{n-1}][L]^n} \tag{8}$$

If protons are dissociated or added to a complex, then the log of an individual stepwise stability constant will also represent the pK_a value.[14,15] This is due to the definition for pK_a, which can be seen below:

$$LH \rightleftharpoons L + H \tag{9}$$

$$K_a = \frac{[L][H]}{[LH]} \tag{10}$$

$$pK_a = - \log K_a = - \log \frac{[L][H]}{[LH]} \quad (11)$$

Since, the definition of K for this equilibrium will be:

$$K = \frac{[LH]}{[L][H]} \quad (12)$$

Therefore,

$$\text{Log } K = - \log K_a = pK_a \quad (13)$$

The potentiometric data were analysed using Equilibrium Simulations for Titration Analysis (ESTA). In this study ESTA needs to calculate the formation function, Z-bar, and the deprotonation function, Q-bar, using the tasks ZBAR and QBAR respectively. ESTA also calculates the optimization of titration parameters and species distribution using the tasks OBJE and SPEC respectively. ESTA also calculates the Hamilton R-factor (R_f^H) and compares it with its limit (R_{lim}^H). R_{lim}^H is based on the error in the number of variable and analytical data and it is the lowest possible R value.[16-19]

Z-bar can be defined as the average number of ligands bound per metal ion and Q-bar can be defined as the number of protons displaced from the ligand due to complexation. Q-bar is calculated with *n*-bar, which measures the average number of protons that would be bound to a ligand before complexation takes place. Both functions are also defined for a simple stepwise complexation. These functions are useful graphical representations of data and can also be used to estimate equilibrium constants at the half-bar value, which is taken at the midpoint of a slope. In addition deviations from the graph can indicate the formation of hydroxo species.[16-19]

Mohajane has formulated graphs representing how the plot lines of each Z-bar and Q-bar graph look after the loss and addition of protons onto ligands in the presence and absence of metal ions.[14] This can be seen in Figure 3.1 below.

A representative Z_H-bar curve can be seen in Figure 3.1A, where two protons have dissociated from a ligand, since Z_H-bar levels off twice, once at Z_H-bar = 1 and the other at Z_H-bar = 2. The Z_H-bar graphs also estimate the pK_a values, since the pK_a values correspond to the pH at the half-bar value. In Figure 3.1A this is log K_{LH} = 7.8 and log K_{LH2} = 3.4.[14]

A representation of a Z_M-bar curve can be seen in Figure 3.1B, where Z_M-bar is plotted against pL (-log[L]). The curve levels at 1 which shows the most predominant complex type is ML. If the complex type is not ML_n (n = 1, 2, 3…n), then Z_M-bar fails, which can be seen in Figure 3.1C. The twisting of plot lines indicates the formation of a hydroxo group. The black plot line first levels off at 1 and then curls back at low pL values, which indicates the formation of a MLH_{-1} type complex. The pink plot line curls without levelling off, which indicates that at low pH values the hydroxo group starts to form. Therefore depending on the graph type that is obtained, the type of copper(II) ligand complex can be predicted.[14]

A representation of a Q_M-bar can be seen in Figure 3.1D, where Q_M-bar has been plotted against pH and is presented as a blue plot line. The n-bar plot line, which is in pink, levels off at 1, which shows that one proton has dissociated from the ligand. At pH 3.9 the n-bar and the Q_M-bar intersect. The intersection indicates that the proton on the ligand has dissociated due to the ligand forming a complex with the metal ion and therefore the type of complex is ML. Q_M-bar = 2 indicates that the ligand has lost two protons and the complex type is MLH_{-1}. The n-bar and the Q_M-bar plot lines are parallel between pH 6.4 to 8.9, which indicates that protons are no longer being displaced by the metal ion. The curving of the Q_M-bar plot line at pH 8.9 indicates the formation of a hydroxo group.[14]

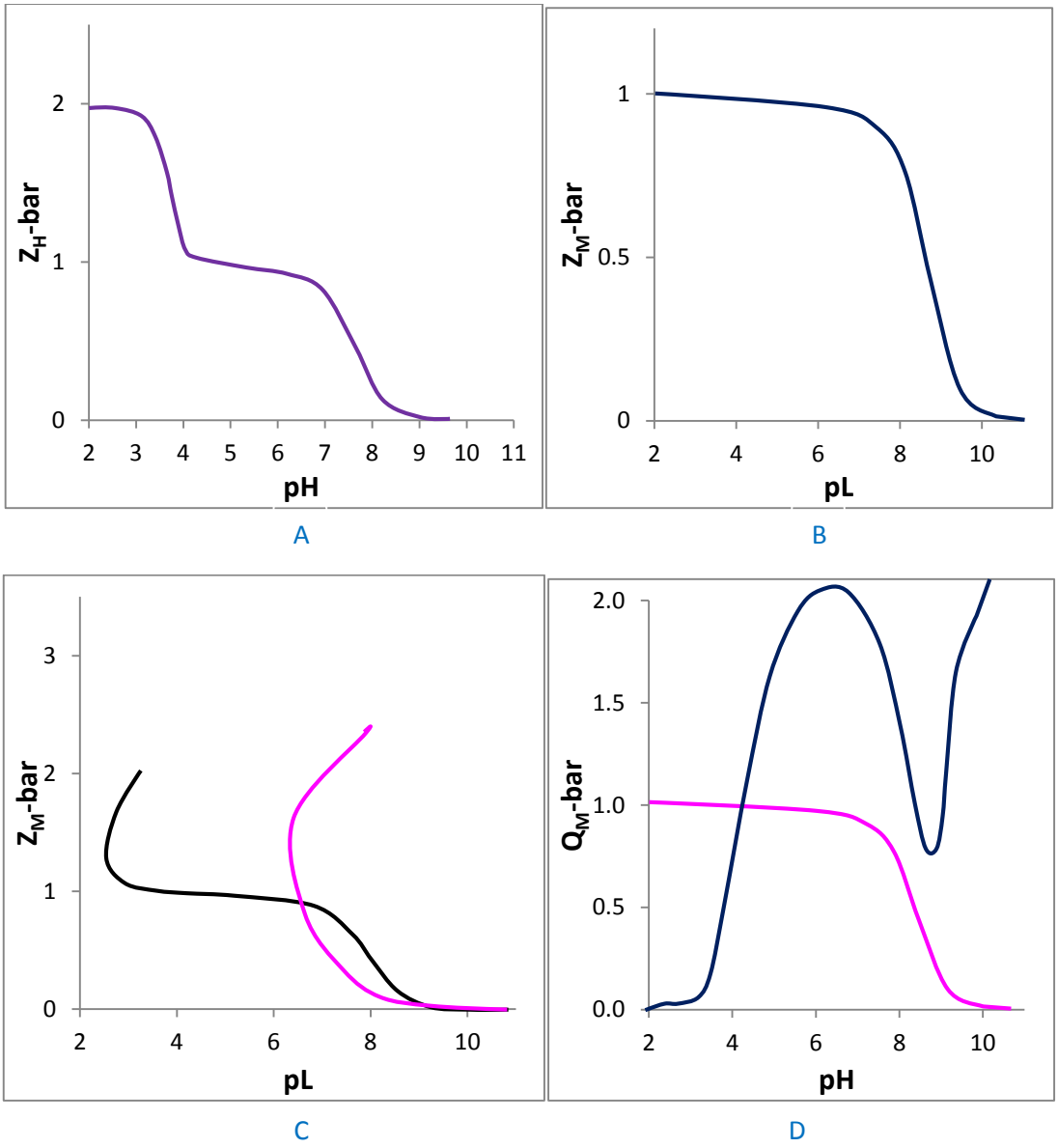

Figure 3.1: Graphs which represent typical Z_H-bar, Z_M-bar and Q_M-bar curves.[14]

3.2 Experimental

3.2.1 Solution preparations

The ligands which were used, namely Gly-Leu-Phe and Sar-Leu-Phe, were purchased from GL Biochem (Shanghai) Ltd. Other reagents were commercially available and of analytical grade.

All potentiometric titration solutions were prepared using boiled miliQ-water to remove carbon dioxide. The method can be found in Vogel.[20] Human blood is 0.15 M in NaCl and therefore the background electrolyte of the titration solutions was prepared with NaCl so that the ionic strength is 0.15 mol.dm^{-3}.

Hydrochloric acid solution (0.01 M) was prepared in background electrolyte and standardised against NaOH. Sodium hydroxide solution (0.1 M) was prepared in background electrolyte and under nitrogen to remove carbon dioxide. The solution was then standardised against potassium hydrogen phthalate (KHP).

The ligand solutions namely Gly-Leu-Phe (0.001 M) and Sar-Leu-Phe (0.001 M) were prepared by dissolving weighed samples into standardised hydrochloric acid and background electrolyte solution.

Metal solutions (0.001 M) were prepared from $CuCl_2 \cdot 2H_2O$, $NiCl_2 \cdot 6H_2O$ and $ZnCl_2$, following the method outlined in Vogel.[20] Background electrolyte solution was added to give the required ionic strength of 0.15 mol.dm^{-3} and these metal solutions were standardised using EDTA.

3.2.2 Potentiometric titrations

Potentiometric titrations were performed using a Metrohm Dosimat 665 piston burette and a Radiometer PHM 84 research pH meter which were interconnected and controlled by a computer. A Ω Metrohm glass electrode and an Ag/AgCl reference electrode were connected to the pH meter and used to measure the electrode potentials. These potentials were examined

with an 848 Titrino plus autotitrator. A double walled titration vessel was used for these electrodes to measure the pH of a solution. The titration vessel was kept at a constant temperature of 25 ± 0.1 °C by a Haake thermostat bath, which circulated water in between the double wall of the titration vessel. A capillary tip from a Metrohm Dosimat 665 piston burette delivered the titrant to the titrated solution. The electromotive force (emf) and the amount of titrant that was added to the titrated solution at each titration point were monitored by a Pascal program. All titrations were performed under nitrogen gas. Throughout the titration the titrated solution was stirred with a magnetic bar.

The glass electrode was calibrated using three different buffer solutions with pH's of 4, 7 and 9. The Nernstian slope of this pH range was found to be 55.45. The standard electrode potential (E°) and the dissociation constant of water (pK_w) were calculated using strong acid-strong base titrations (HCl/NaOH). The value of E° was 389.6 mV and the value of pK_w was 13.73.

For the protonation titrations, a volume of 10 cm^3 for Gly-Leu-Phe and Sar-Leu-Phe was added to the titration vessel and titrated against NaOH over a pH range from 2-11. For the metal ligand titrations, a volume of 10 cm^3 for each ligand was added into the titration vessel and different metal to ligand ratios were set up and titrated against NaOH over a pH range from 2-11. A back titration was not performed, because the endpoint of the titration was easily identified.

3.2.3 Data analysis

The potentiometric titration data was analysed using ESTA suite of programs. From the protonation titration, the concentration of each ligand was first determined using the Gran method.[21]

The data was entered into an ESTA file that calculates the electrode parameters, protonation and stability constants. The resulting protonation and stability constants were refined using the task OBJE. From the protonation constants, the tasks ZBAR and SPEC were used to calculate the Z_H-bar and species distribution graphs respectively. From the stability constants,

the tasks ZBAR, QBAR and SPEC were used to calculate the Z_M-bar, Q_M-bar and species distribution graphs respectively.

3.3 Results

In each of the potentiometric titrations, log *K* values for the species are calculated. An example of how to calculate a log *K* value for the MLH_{-1} species of copper(II) glycine can be seen in Figure 3.2. The stability constant for the species that is about to lose a proton, is subtracted from the stability constant of the species which has lost a proton.

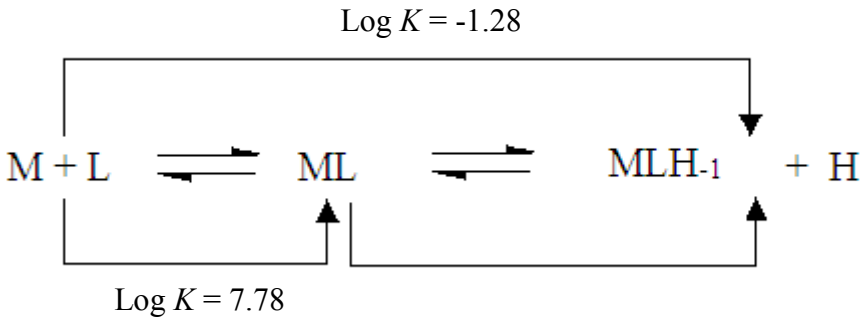

$$\text{Log } K_{MLH\text{-}1} = -1.28 - 7.78 = -9.06$$

Figure 3.2: Example of how to calculate log *K* values from potentiometric species using stability constants.

3.3.1 Protonation of Gly-Leu-Phe and Sar-Leu-Phe

Gly-Leu-Phe and Sar-Leu-Phe are zwitterions in aqueous solutions and therefore have two available sites for protonation, which are the carboxyl and amine groups. The amine group is basic and therefore gets protonated when the pH is lower than the pK_a value. The carboxyl group is an acid and therefore is deprotonated when the pH is higher than the pK_a value. For Gly-Leu-Phe, the carboxyl group is from phenylalanine and the amine group is from glycine, which goes from a (NH_2) state to a (NH_3^+). For Sar-Leu-Phe, the carboxyl group is also from phenylalanine and the amine group is from sarcosine, which goes from a (NH) state to a

(NH_2^+) state. Therefore the amine and carboxyl groups of Gly-Leu-Phe and Sar-Leu-Phe will become protonated and deprotonated at the same pH values.[22,23]

3.3.1(a) Protonation of Gly-Leu-Phe

The protonation constants for Gly-Leu-Phe were determined in a pH range from 2-11, using ESTA suite of programs. The pH range could only be measured from 2-11, since a higher or a lower pH would result in a non-linear electrode response. The protonation function, Z_H-bar, should verify that as the pH of the solution is lowered, the ligand should become protonated, first at the amine group and then at the carboxyl group. The Z_H-bar for Gly-Leu-Phe can be seen in Figure 3.3 below. The Z_H-bar curve starts at a value of zero and therefore indicates that the ligand is completely deprotonated at the corresponding pH value of 9.6. It then rises to a value of 1 and then levels off. This indicates that the ligand is protonated with one proton and therefore has changed from an L-form to an LH-form. The high pH of this protonation indicates that it is the amine group that is protonated. Between the pH values of about 7.8 to 3.7, Z_H-bar remains around the value of 1, which indicates that the L-form and the LH-form are in equilibrium. Z_H-bar then rises again to a value of 1.8 from the pH value of about 3.7 to 2.3. This shows that the ligand is able to accept another proton to become LH_2, but in order for the complete protonation of all the ligands to occur, lower pH values are needed. The low pH values indicate that it is the carboxyl group that is protonated.[22,23]

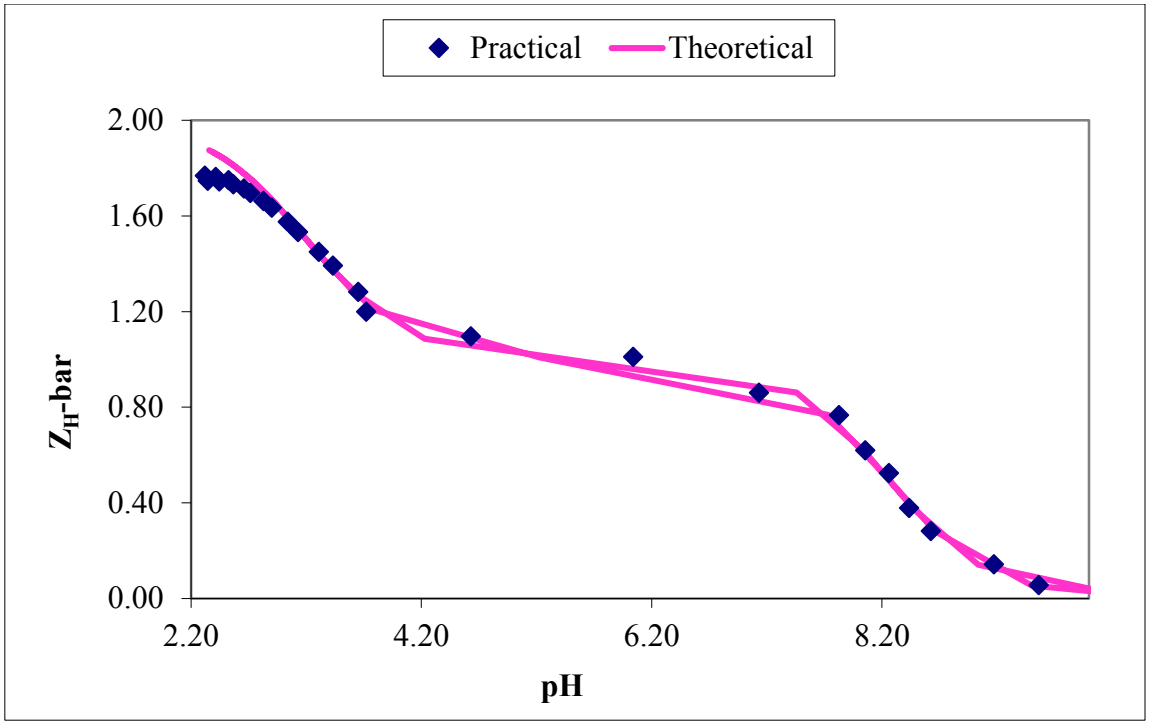

Figure 3.3: Z_H-bar as a function of pH for the protonation of Gly-Leu-Phe at 25 °C in 0.15 mol.dm^{-3} of NaCl.

The estimated log K_{ML} and log K_{ML2} values are 8.3 and 3.1 respectively. These estimated values correspond to the calculated values, which can be seen in Table 3.1 and therefore this verifies that as the pH is decreased, Gly-Leu-Phe becomes protonated to an LH form and then to an LH_2 form. The protonation constants and logarithms can also be seen in Table 3.1 below.

Table 3.1: Stability constants (log β_{pqr}) and logarithms for Gly-Leu-Phe at 25 °C and 0.15 mol.dm^{-3} NaCl.

Std is the standard deviation; R_f^H is the Hamilton R-factor and R_{lim}^H is its limit; n_T is the number of titrations and (n_P) is the number of titration points; p, q, r are the stoichiometric coefficients of a complex with a general formula of $M_pL_qH_r$; L stands for the ligand and H stands for a hydrogen atom.

Ligand	p	q	r	log β_{pqr}	Log K	std	Rf^H	R_{lim}^H	$n_T(n_p)$
LH	0	1	1	8.25	8.25	0.03			
LH_2	0	1	2	11.46	3.21	0.08	0.01	0.01	2(32)

The species distribution of Gly-Leu-Phe can be seen in Figure 3.4, and is shown as a function of pH. In the pH range from about 4.7 to 6.7 the distribution shows that all of the ligand is protonated with one proton. Above the cross-over point between L and LH at a pH of about 8.9, the dominant species becomes the L species. The graph also shows that the LH_2 species started forming at a pH of about 4.6. However LH_2 does not have 100% dominance in this pH scale, since the carboxyl group only starts becoming protonated at a pH of 3.8. These pH ranges and percentage distributions for the LH and LH_2 species therefore correspond to the Z_H-bar function in Figure 3.3.

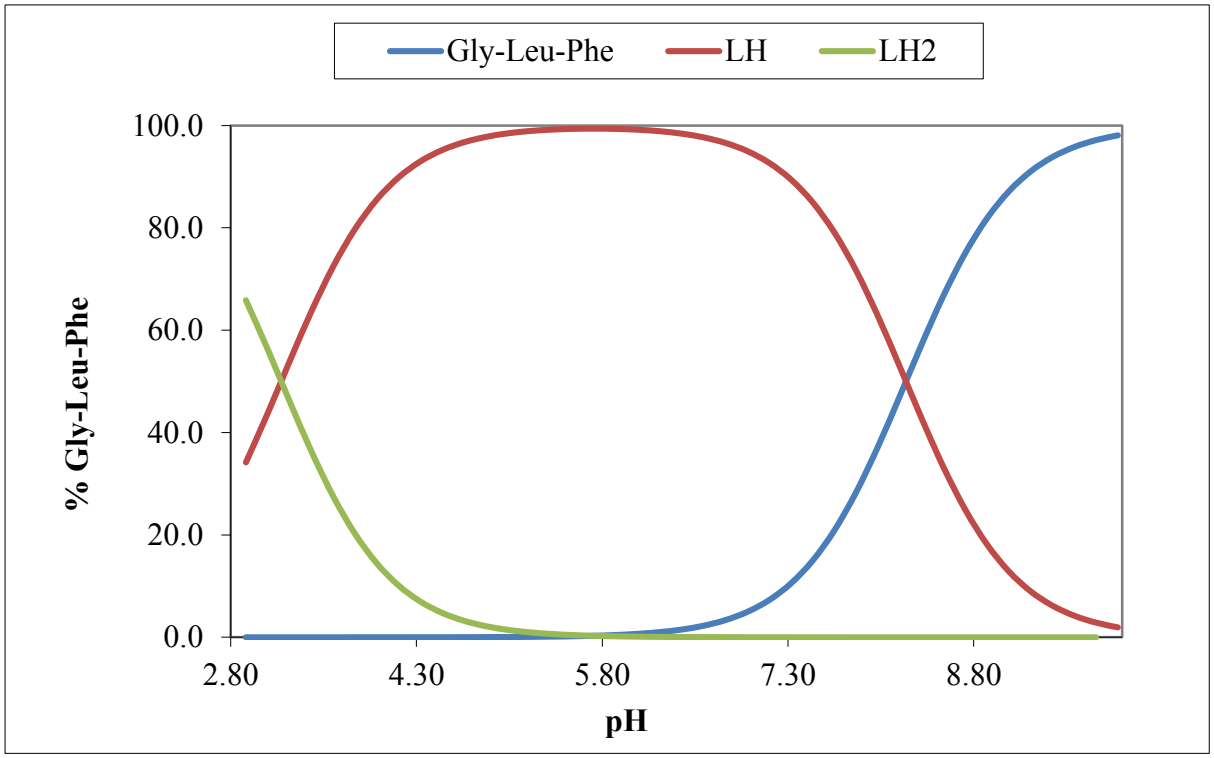

Figure 3.4: Protonation species distribution curve for Gly-Leu-Phe at 25 ^{o}C in 0.15 mol.dm^{-3} of NaCl.

3.3.1(b) Protonation of Sar-Leu-Phe

Similarly the protonation constants for Sar-Leu-Phe were determined in a pH range from 2-11, using ESTA suite of programs.

The same analysis can be made for the Z_H-bar of Sar-Leu-Phe, which can be seen in Figure 3.5. It is also completely deprotonated at a pH of 10.1 and then rises and levels off at a value of 1, indicating the formation of the LH form. The high pH value indicates that it is the amine

group which is becoming protonated. From a pH of 7.3 to 4.3 an equilibrium between the L and LH form, is established. At a pH of 4.3 the curve rises to a value of 1.5, which indicates that the LH_2 species is forming. Had the pH values been lower, complete protonation would have occurred.

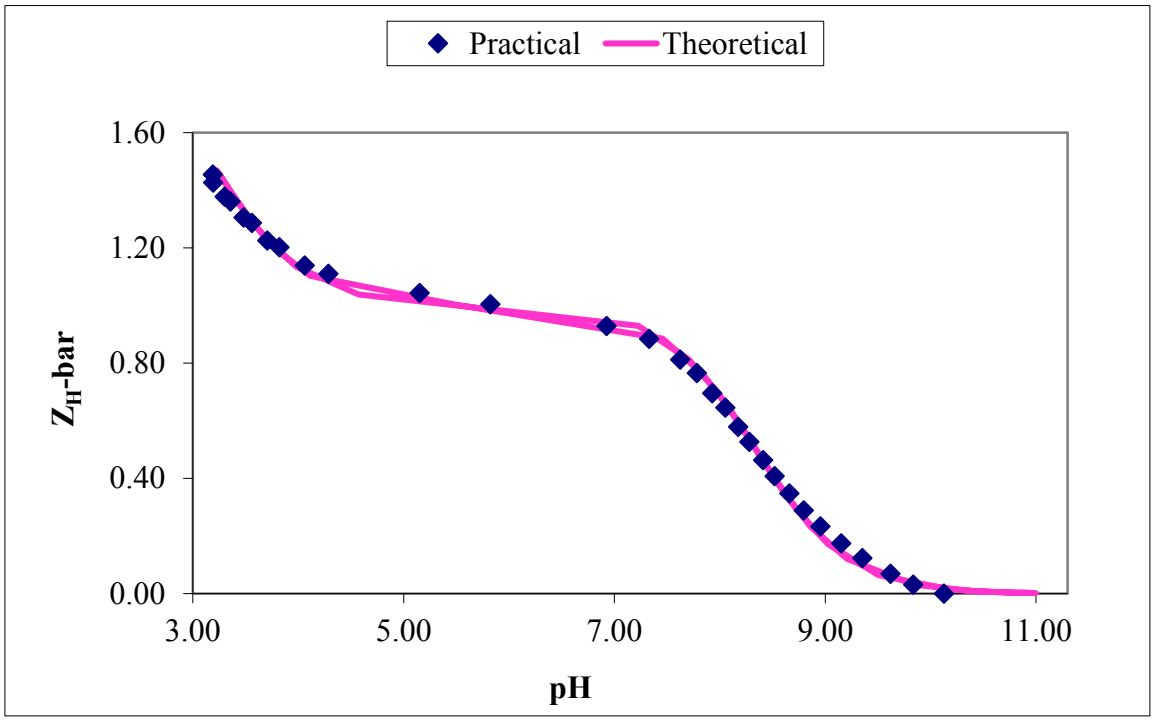

Figure 3.5: Z_H-bar as a function of pH for the protonation of Sar-Leu-Phe at 25 °C in 0.15 mol.dm^{-3} of NaCl.

The approximated log K_{ML} and log K_{ML2} values are estimated to be 8.3 and 3.2. Therefore comparing these estimated values with the calculated values, it verifies that as the pH is decreased, Sar-Leu-Phe becomes protonated to an LH and then to an LH_2 form. The calculated log K values, as well as the protonation constants and logarithms, can be seen in Table 3.2 below.

Table 3.2: Stability constants (log β_{pqr}) and logarithms for Sar-Leu-Phe at 25 °C and 0.15 mol.dm^{-3} NaCl.

Std is the standard deviation; R_f^H is the Hamilton R-factor and R_{lim}^H is its limit; n_T is the number of titrations and (n_P) is the number of titration points; p, q, r are the stoichiometric coefficients of a complex with a general formula of $M_pL_qH_r$; L stands for the ligand and H stands for a hydrogen atom.

Ligand	*p*	*q*	*r*	log β_{pqr}	Log *K*	std	Rf^H	$R_{lim}{}^H$	$n_T(n_p)$
LH	0	1	1	8.34	8.34	0.01			
LH_2	0	1	2	11.52	3.18	0.03	0.01	0.01	2(78)

The species distribution of Sar-Leu-Phe can be seen in Figure 3.6 below. Similarly in the pH range from about 4.9 to 6.6 the distribution shows that all of the ligand is protonated with one proton. At a pH of 8.4, the dominant species becomes the L species and at a pH of 3.1 the LH_2 species started forming. These pH ranges and percentage distributions for the LH and LH_2 species therefore correspond to the Z_H-bar function in Figure 3.5.

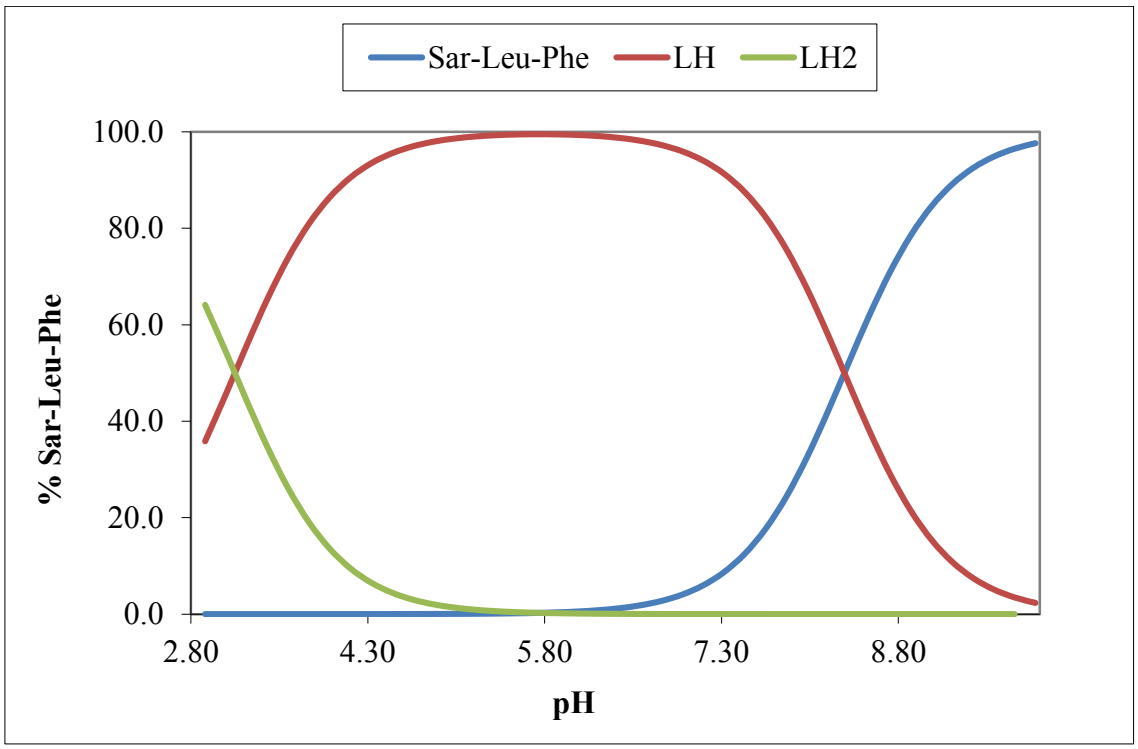

Figure 3.6: Protonation species distribution curve for Sar-Leu-Phe at 25 °C in 0.15 mol.dm^{-3} of NaCl.

Both the Gly-Leu-Phe and Sar-Leu-Phe protonation functions have a good agreement between the theoretical and experimental curves, since they overlap. This, as well as the low standard deviations of the log β_{pqr} values and the low Hamilton R factors, indicates that the model used for the protonation of Gly-Leu-Phe and Sar-Leu-Phe is a valid model.

3.3.2 Copper(II) complexation of Gly-Leu-Phe and Sar-Leu-Phe

The stability constants (log β_{pqr}) for the copper(II) Gly-Leu-Phe and Sar-Leu-Phe complexation of both a 1:3 and a 1:4 copper(II) ligand ratio, were found using ESTA suite of programs and used to determine Z_M-bar, Q_M-bar and the species distribution functions. Ligand to metal ratios of 1:2 could not be analysed, because precipitation occurred at high pH levels.

3.3.2(a) Cu-Gly-Leu-Phe

The complex formation function, Z_M-bar, can be seen in Figure 3.7 below. Both the 1:3 and 1:4 Z_M-bar curves curl backwards at low pL values without first levelling off. This indicates that the formation of the hydroxo species (MLH_{-1}, MLH_{-2} and ML_2H_{-1}) start to form at middling pH values and overlap the formation of the ML species, which also forms between low and middling pH values. The different metal to ligand ratios are superimposable up to the point where the curves indicate the formation of the hydroxo species. Therefore this verifies that the complexation is a simple stepwise complexation and no polynuclear species are present. The 1:4 curve is the curve with the lower pL values, since the higher ligand ratio requires more NaOH to reach the end point.

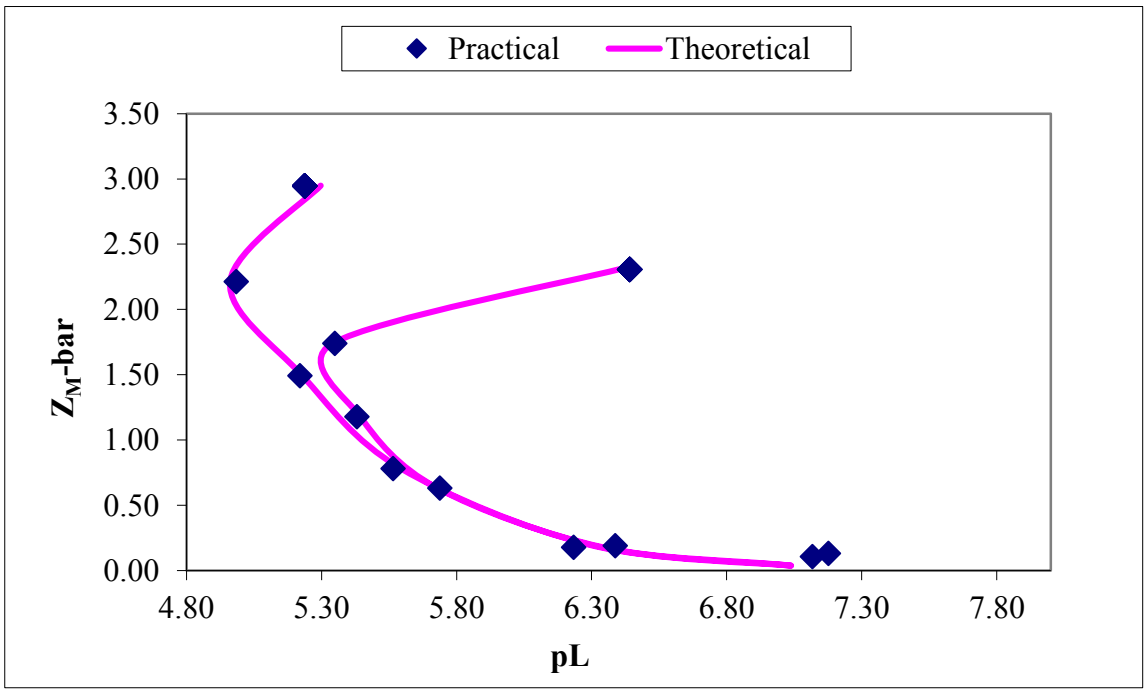

Figure 3.7: Z_M-bar as a function of pH for the 1:3 and 1:4 complexation of copper(II) and Gly-Leu-Phe at 25 ^oC in 0.15 mol.dm^{-3} NaCl. For clarity not all data points are displayed.

There is a good agreement between the theoretical and experimental functions, since the two curves overlap one another. Therefore this verifies that the potentiometic titration was performed accurately**.** The low standard deviations of the log β_{pqr} values and the low Hamilton R factors verify the validity of the model. The stability constants and the logarithms, as well as the log *K* values of the copper(II) Gly-Leu-Phe complexation, can be seen in Table 3.3.

Table 3.3**:** Stability constants (log β_{pqr}) and logarithms for the 1:4 complexation between copper(II) and Gly-Leu-Phe at 25 ^oC and 0.15 mol.dm^{-3} NaCl.

Std is the standard deviation; R_f^H is the Hamilton R-factor and R_{lim}^H is its limit; n_T is the number of titrations and (n_P) is the number of titration points; *p*, *q*, *r* are the stoichiometric coefficients of a complex with a general formula of $M_pL_qH_r$; L stands for the ligand and H stands for a hydrogen atom.

Ligand	*p*	*q*	*r*	log β_{pqr}	log *K*	std	Rf	R_{lim}	$n_T(n_p)$
ML	1	1	0	5.63	5.63	0.07			
MLH_{-1}	1	1	-1	-0.14	-5.77	0.05	0.01	0.01	2(24)
MLH_{-2}	1	1	-2	-7.02	-6.88	0.12			
ML_2H_{-1}	1	2	-1	4.02	-	0.07			

CuOH is formed when $Cu(H_2O)$ loses a proton and therefore the pK_a of CuOH will represent the equilibrium of the dissociated proton.[24] If the pK_a values of the hydroxo species are similar to the pK_a of CuOH, then the dissociated proton in the complex is due to the loss of hydrogen from the water molecule and not the amide group.

The pK_a for the deprotonation of $Cu(H_2O)$ to CuOH is -7.70.[25] Therefore, since the pK_a from ML to MLH_{-1} is -5.77, the loss of a proton is from the amide and not from water. The pK_a from MLH_{-1} to MLH_{-2} has a value of -6.88 and therefore the loss of the second proton is also from the amide and not from water. Therefore, since there are no similar values between the pK_a of the CuOH system and the hydroxo species, the dissociated protons are from the amide

groups and not from a bound water molecule. The ML_2H_{-1} group cannot be compared, because there is no ML_2 pK_a value with which to compare it.

The deprotonation function, Q_M-bar can be seen in Figure 3.8 below. The n-bar plot line levels off at a value of 1 and at a pH of 4.4 to 7.2, which indicates the formation of the LH species. The n-bar plot and the Q_M-bar intersect at a pH of 5.3 and therefore at this pH the ML complex is present. The Q_M-bar then rises above the n-bar plot line and reaches a value of 2.5. This indicates that a total of two to three protons are dissociated to form hydroxo groups due to the complexation with copper(II). Between the pH values of 7.3 and 9.1, the n-bar and Q_M-bar plot lines are parallel, which indicates that protons are no longer being dissociated from the ligand in that pH range. The Q_M-bar plot lines level out from a pH of 9.1, which indicate the formation of other hydroxo groups. There is a good agreement between the theoretical and experimental functions. This, as well as the overlap between 1:3 and 1:4 copper(II) ligand ratios, verifies the accuracy of the experimental technique.

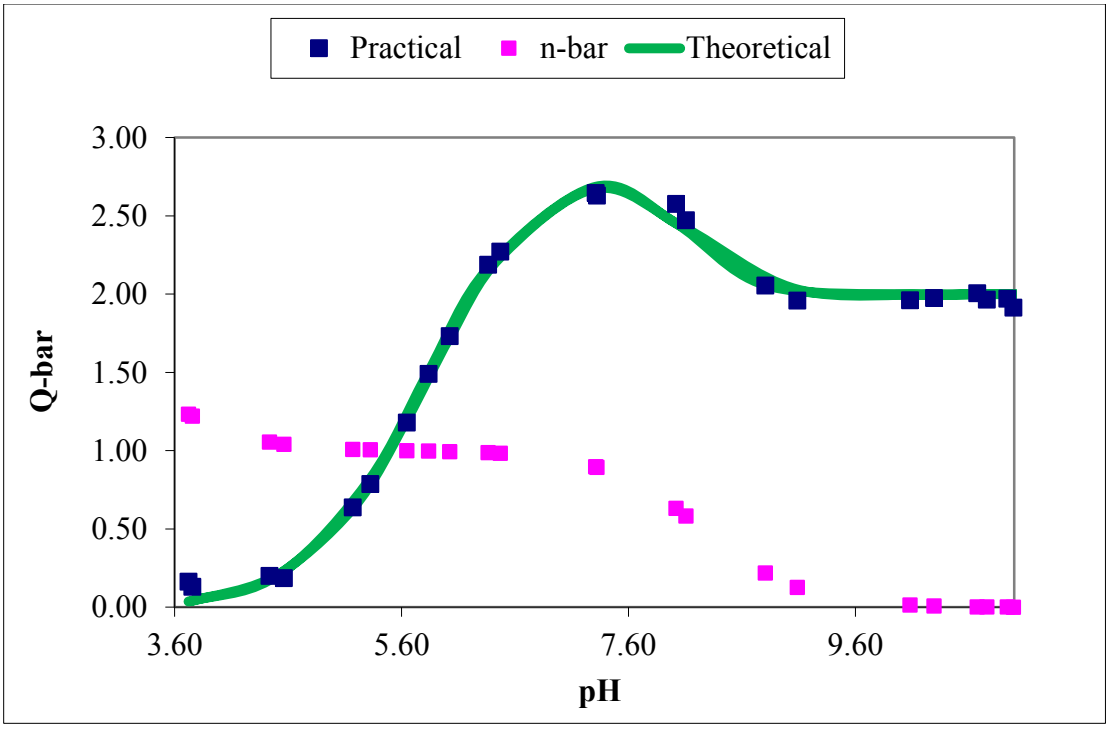

Figure 3.8: Q_M-bar as a function of pH for the 1:3 and 1:4 complexation of copper(II) and Gly-Leu-Phe at 25 ^oC in 0.15 mol.dm^{-3} NaCl.

The species distribution for the copper(II) Gly-Leu-Phe system can be seen in Figure 3.9 below. The distribution shows that the complexation of the ML species is in the pH range

from approximately 3.4 to 6.9 and that the formation of the MLH_{-1} species starts at a pH of approximately 4.2. The MLH_{-1} species is shown to start forming before the ML species could reach 100% dominance. The graph also shows that at a pH of approximately 5.5, both the ML_2H_{-1} and the MLH_{-2} species form. The presence of the ML_2H_{-1} species ends just after the analysed pH scale, while the MLH_{-2} species is still reaching a maximum dominance as the analysed pH scale ends. This species distribution graph shows that the hydroxo species associated with the levelling of the Q_M-bar curve at a pH of 9.9 is due to the formation of the MLH_{-2} species. The other hydroxo species, MLH_{-1} and ML_2H_{-1} are formed while the ML species is still forming and therefore overlap the ML formation curve, which can be seen in both the Z_M-bar and the Q_M-bar functions. Therefore this species distribution curve corresponds to the Z_M-bar and the Q_M-bar functions.

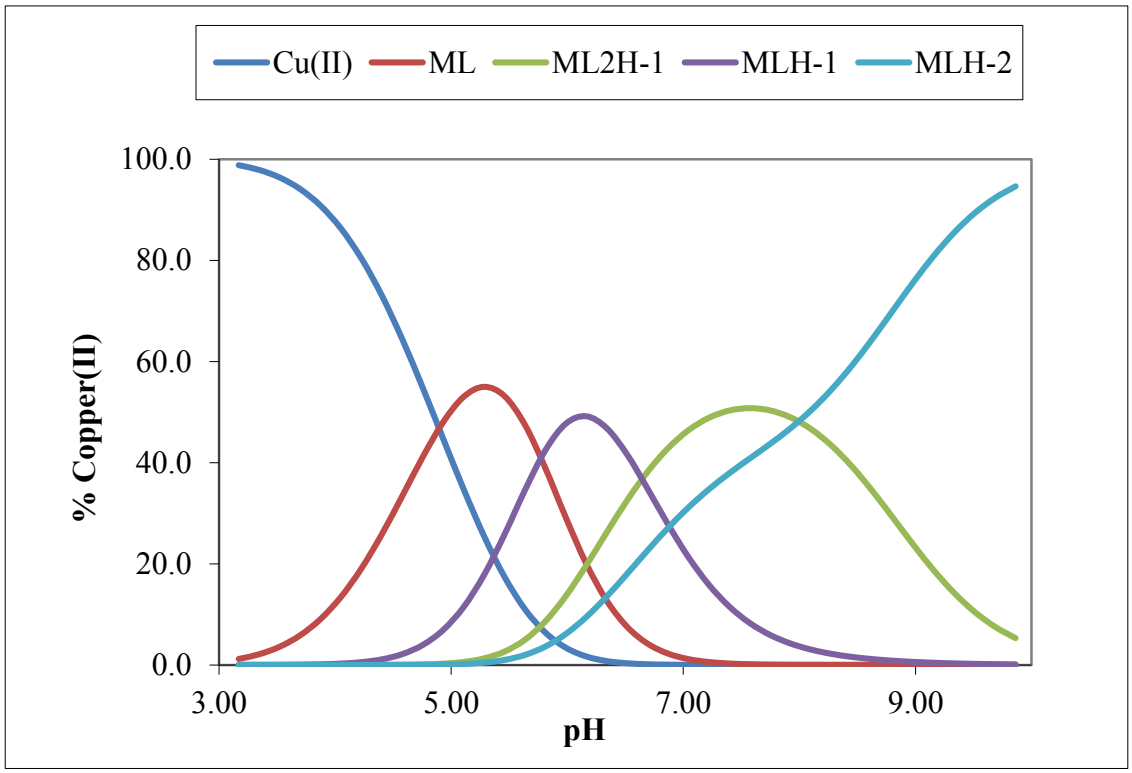

Figure 3.9: Protonation species distribution curve for copper(II) and Gly-Leu-Phe (1:4 ratio) at 25 ^{o}C in 0.15 mol.dm^{-3} of NaCl.

3.3.2(b) Cu-Sar-Leu-Phe

The complex formation function, Z_M-bar, which can be seen in Figure 3.10 below, has a good agreement between the theoretical and experimental functions. Both the 1:3 and 1:4 metal to ligand ratios are superimposable in this graph which verify that the complexation is a simple stepwise complexation.[26] The Z_M-bar function rises to a value of 2 at a pH of 5.0, and then appears to start levelling off before it curls upwards. This indicates that two ligands are bound to the copper(II) ion. Since one of the hydroxo species has two ligands bound to it, the levelling off at 2 indicates that the ML_2H_{-1} species formed, even though ML_2H_{-1} is a hydroxo species and hydroxo species do not usually level off in a Z_M-bar curve. The curling upwards indicates the formation of the other hydroxo species. However, since the Z_M-bar curve only starts to level off, it indicates that the ML_2H_{-1} species almost reaches a maximum dominance. The estimated log *K* value for the ML_2H_{-1} species is 5.1.

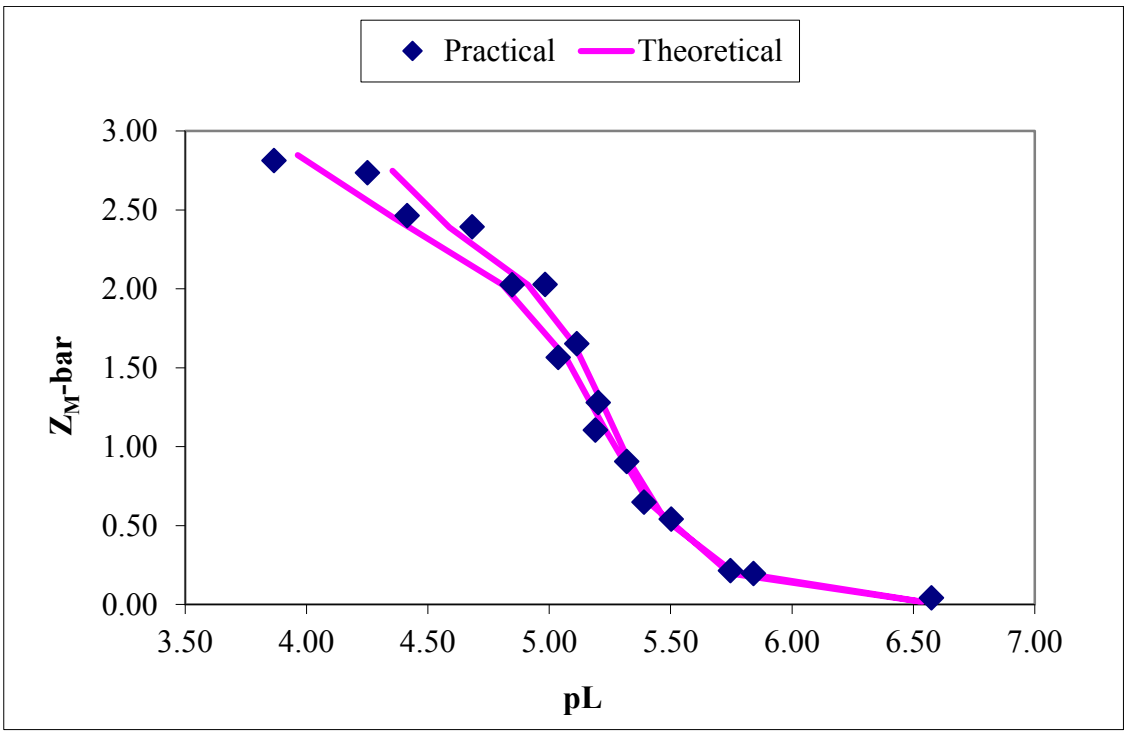

Figure 3.10: Z_M-bar as a function of pH for the 1:3 and 1:4 complexation of copper(II) and Sar-Leu-Phe at 25 °C in 0.15 mol.dm^{-3} NaCl.

The stability constants and the logarithms of the copper(II) Sar-Leu-Phe complexation can be seen in Table 3.4. The low standard deviations of the log β_{pqr} values and the low Hamilton R factors verify the validity of the model.

Table 3.4: Stability constants (log β_{pqr}) and logarithms for the 1:4 complexation between copper(II) and Sar-Leu-Phe at 25 ^{o}C and 0.15 mol.dm^{-3} NaCl.

Std is the standard deviation; R_f^H is the Hamilton R-factor and R_{lim}^H its limit; n_T is the number of titrations and (n_P) is the number of titration points; *p*, *q*, *r* are the stoichiometric coefficients of a complex with a general formula of $M_pL_qH_r$; L stands for the ligand and H stands for a hydrogen atom.

Ligand	*p*	*q*	*r*	log β_{pqr}	log *K*	Std	Rf	R_{lim}	$n_T(n_p)$
ML	1	1	0	4.72	4.72	0.13			
MLH_{-1}	1	1	-1	-0.52	-5.24	0.03	0.02	0.02	2(35)
MLH_{-2}	1	1	-2	-8.69	-8.17	0.07			
ML_2H_{-1}	1	2	-1	3.45	-	0.05			

As has been previously stated, the pK_a from Cu(H_2O) to CuOH was found to be -7.70.[25] Therefore the pK_a from ML to MLH_{-1}, with a value of -5.24, is due to the loss of a proton from the amide and not from water. The pK_a from MLH_{-1} to MLH_{-2} has a value of -8.17 and therefore the second proton could be lost from either the amide or from water.

The deprotonation function, Q_M-bar, which can be seen in Figure 3.11 below, has a good agreement between the theoretical and experimental functions. The 1:3 and 1:4 copper(II) ligand ratios also overlap one another, which verify the accuracy of the titration technique. The n-bar plot line levels off at a value of 1 and at a pH of 4.3 to 7.7, which indicates the formation of the LH species. The n-bar plot and the Q_M-bar curve intersect at a pH of 5.3 and therefore at this pH the ML complex is present. The Q_M-bar curve then rises above the n-bar plot line and reaches a value of 2.5. Similarly to the Q_M-bar curve of Cu-Gly-Leu-Phe, this indicates that a total of two to three protons are dissociated to form hydroxo groups due to the complexation with copper(II). Between the pH values of 7.5 and 9.0, the n-bar and the Q_M-bar plot lines are parallel, which indicates that protons are no longer being dissociated from the ligand in that pH range. The Q_M-bar plot lines increase from a pH of 9.0, which indicate the formation of other hydroxo groups.

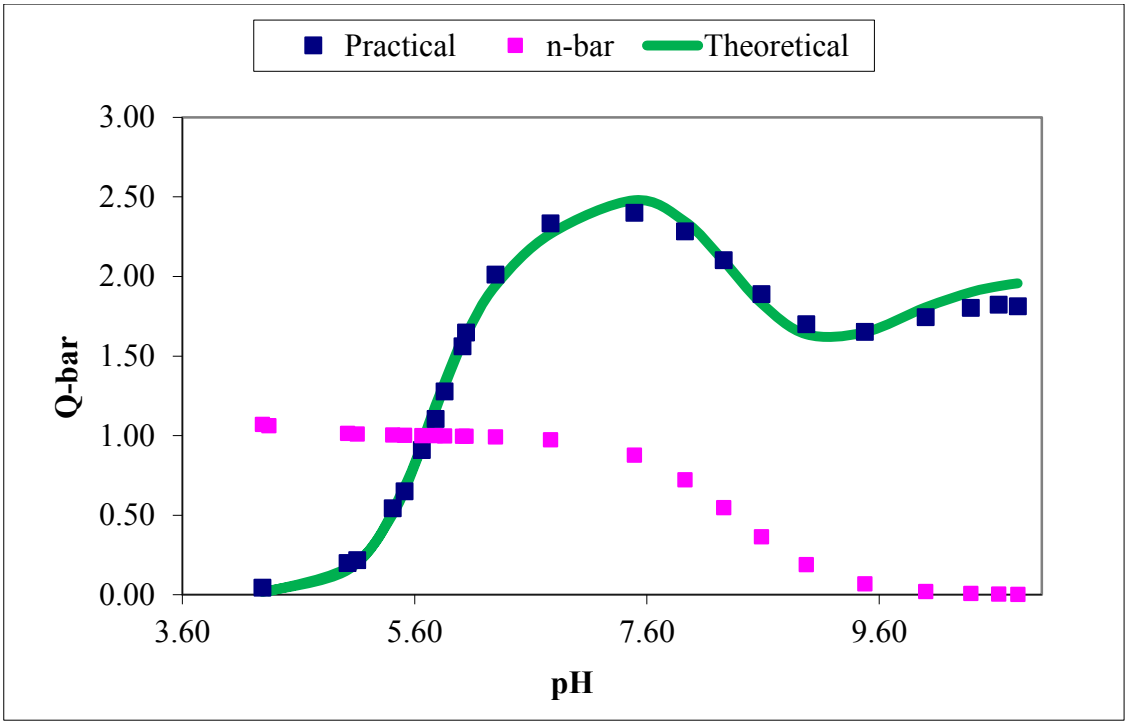

Figure 3.11: Q_M-bar as a function of pH for the 1:3 and 1:4 complexation of copper(II) and Sar-Leu-Phe at 25 ^oC in 0.15 $mol.dm^{-3}$ NaCl.

The species distribution for the copper(II) Sar-Leu-Phe system can be seen in Figure 3.12 below. The distribution shows that the complexation of the ML species is at a pH of 3.7 to 6.7 and that the formation of the MLH_{-1} species is at a pH of 4.6 to 9.9. The graph also shows that the ML_2H_{-1} and the MLH_{-2} species form at a pH of about 5.3 and 6.2 respectively and both end beyond the analysed pH scale. The formation of the MLH_{-1} species dominates over the ML species before the ML species can reach maximum dominance. This species distribution graph shows that the hydroxo species associated with the increase of the Q_M-bar curve at a pH of 9.0 is due to the formation of the MLH_{-2} species. The other hydroxo species, MLH_{-1} and ML_2H_{-1} are formed while the ML species is still forming. Therefore this species distribution curve corresponds to the Z_M-bar and the Q_M-bar functions.

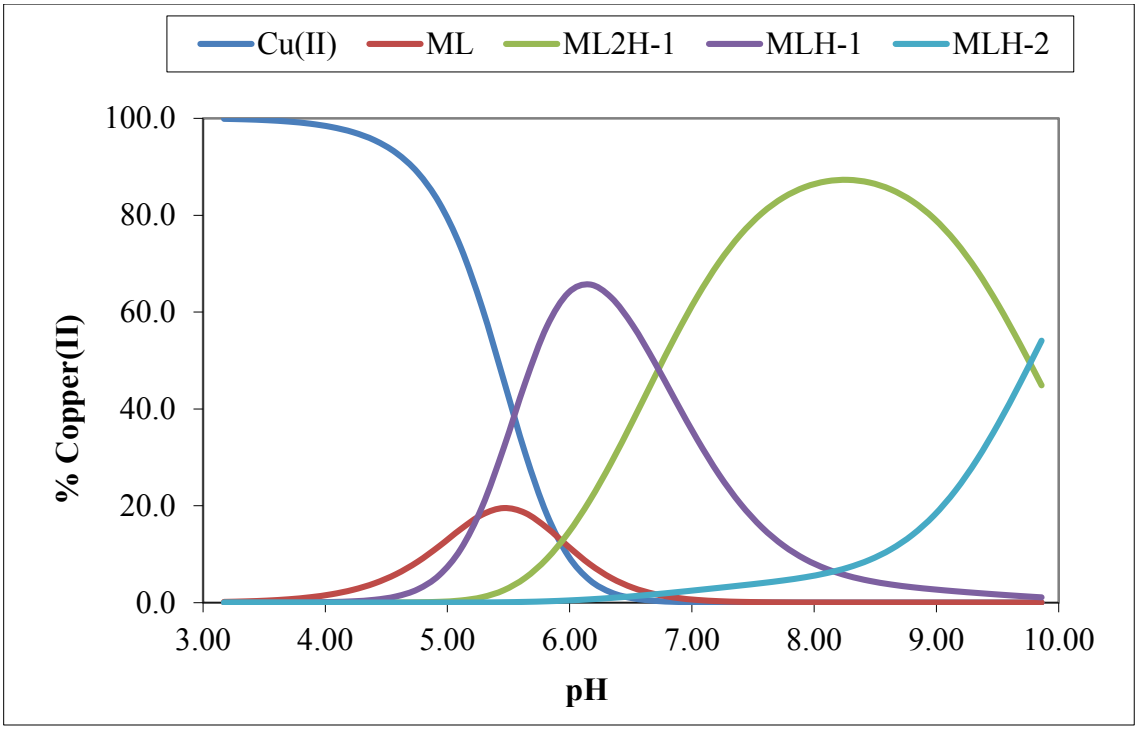

Figure 3.12: Protonation species distribution curve for copper(II) and Sar-Leu-Phe (1:4 ratio) at 25 ^{o}C in 0.15 mol.dm^{-3} of NaCl.

3.3.3 Nickel(II) complexation of Gly-Leu-Phe and Sar-Leu-Phe

The stability constants (log β_{pqr}) of a nickel(II) Gly-Leu-Phe and a nickel(II) Sar-Leu-Phe complexation of both a 1:3 and a 1:4 nickel(II) ligand ratio, were found using ESTA suite of programs and used to determine Z_M-bar, Q_M-bar and the species distribution functions. These metal ligand ratios were chosen in order to be consistent with the copper(II) ligand ratios.

3.3.3(a) Ni-Gly-Leu-Phe

The complex formation function, Z_M-bar, for Model 1 and Model 2 of nickel(II) and Gly-Leu-Phe can be seen below in Figure 3.13 and Figure 3.14 respectively. Both models have a relatively good agreement between the theoretical and experimental functions. Both the Z_M-bar models level off at a value of 1 and then twist backwards at very low pL values. The levelling off at a value of 1 indicates that the ML species is dominant and is the only species present for a particular pH range. The twisting back indicates that at very high pH values, the hydroxo species start to form. The estimated log K_{ML} value for both Model 1 and Model 2 is 4.6, which corresponds to the calculated value.

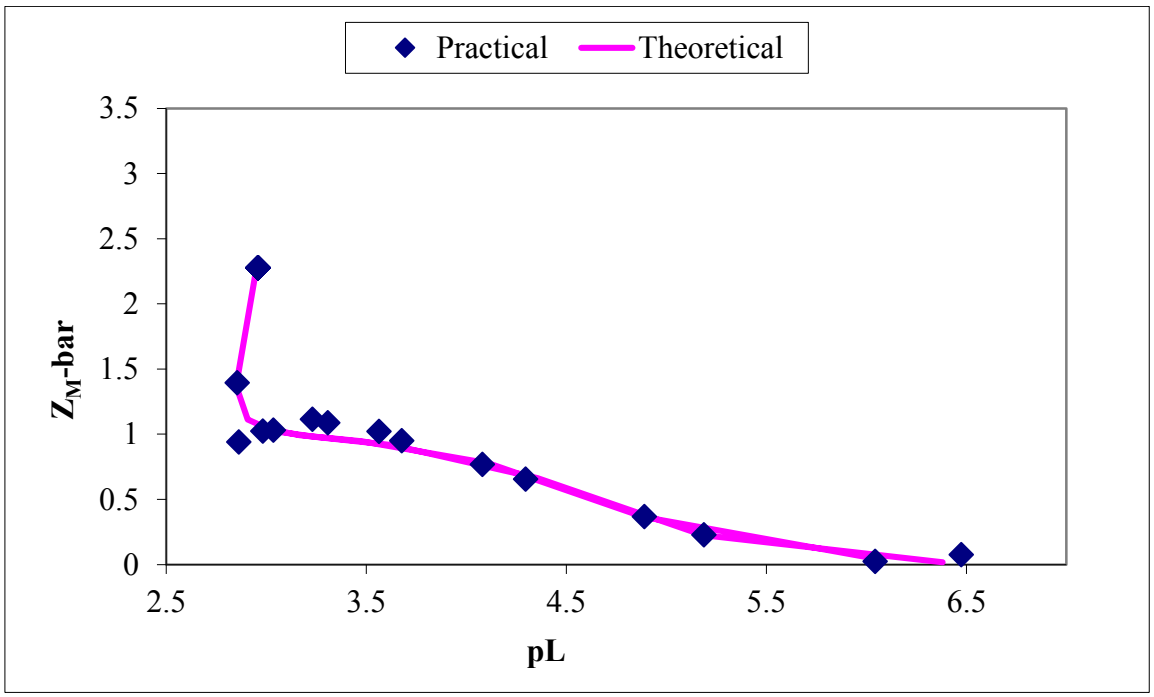

Figure 3.13: Model 1 of Z_M-bar as a function of pH for the 1:3 and 1:4 complexation of nickel(II) and Gly-Leu-Phe at 25 °C in 0.15 mol.dm^{-3} NaCl.

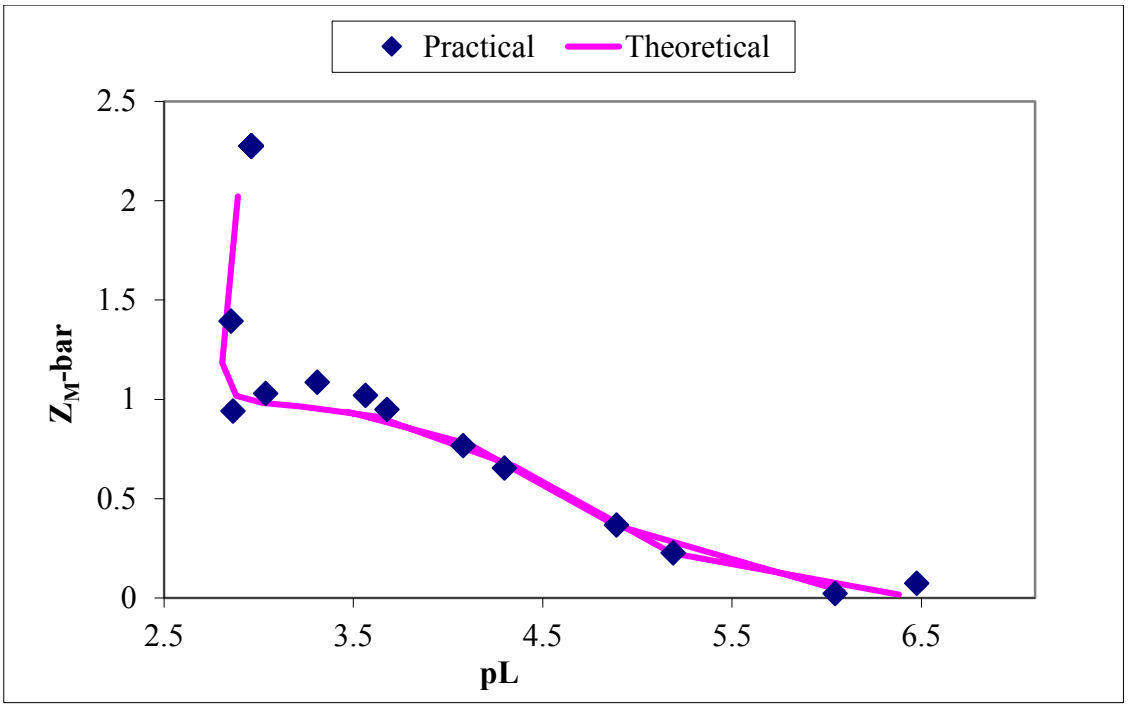

Figure 3.14: Model 2 of Z_M-bar as a function of pH for the 1:3 and 1:4 complexation of nickel(II) and Gly-Leu-Phe at 25 °C in 0.15 mol.dm^{-3} NaCl.

The low standard deviations of the log β values and low Hamilton R factors verify the validity of the model. The stability constants and the logarithms of the nickel(II) Gly-Leu-Phe complexation can be seen in Table 3.5 below.

Table 3.5: Model 1 and Model 2 of the stability constants (log β_{pqr}) and logarithms for the 1:4 complexation between nickel(II) and Gly-Leu-Phe at 25 °C and 0.15 mol.dm^{-3} NaCl.

Std is the standard deviation; R_f^H is the Hamilton R-factor and R_{lim}^H its limit; n_T is the number of titrations and (n_P) is the number of titration points; *p*, *q*, *r* are the stoichiometric coefficients of a complex with a general formula of $M_pL_qH_r$; L stands for the ligand and H stands for a hydrogen atom.

Model	Complex form	*p*	*q*	*r*	log β_{pqr}	log *K*	std	Rf	R_{lim}	$n_T(n_p)$
1	ML MLH_{-1} ML_2H_{-2}	1 1 1	1 1 2	0 -1 -2	4.65 -4.95 -11.34	4.65 -9.60 -	0.06 0.10 0.08	0.02	0.02	2(32)
2	ML ML_2H_{-1} ML_2H_{-2}	1 1 1	1 2 2	0 -1 -2	4.66 -2.27 -11.32	4.66 - -9.05	0.06 0.10 0.08	0.02	0.02	2(32)

The pK_a from Ni(H_2O) to NiOH is -9.86.[25] Therefore, since the pK_a from ML to MLH_{-1}, is -9.60, the loss of the proton is due to water and not from the amide. As mentioned previously, the hydroxo species that have L2 cannot be compared.

The deprotonation function, Q_M-bar, for Model 1 and Model 2, can be seen in Figure 3.15 and Figure 3.16 respectively. Model 1 has a good agreement between the theoretical and experimental functions, while Model 2 has a relatively good agreement, which slightly deviates at a pH of 9.7. The n-bar plot line in both models level off at a value of 1, which indicates the formation of the LH species. The Q_M-bar plot line rises to a value of 1 in both models, which indicates that a maximum of one proton is dissociated from the ligand as a result of complexation. This maximum value is also the point where the n-bar plot and the Q_M-bar curve of both models intersect. This is at a pH of about 7.2 and therefore at this pH the ML complex is present. Between the pH values of 7.2 and 8.4 the n-bar and Q_M-bar plot lines are parallel in both models, which indicate that protons are no longer being dissociated from the ligands. The function in both models then curves upwards from a pH of 8.5, which indicates the formation of hydroxo groups.

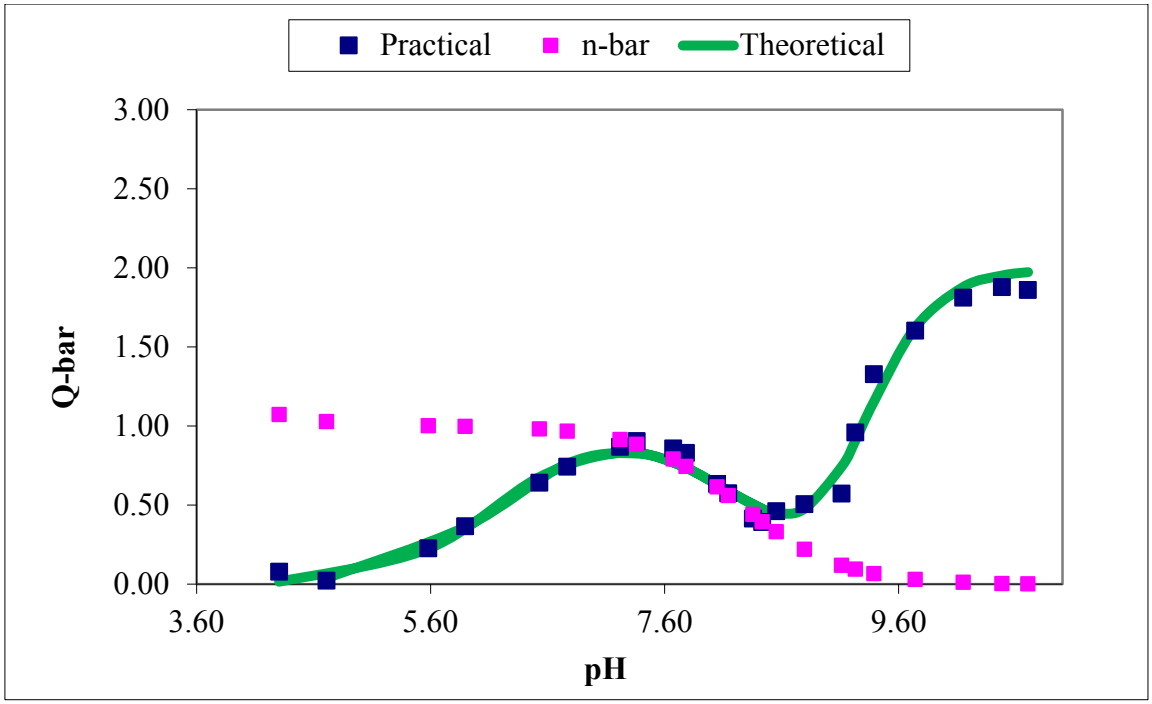

Figure 3.15: Model 1 of Q_M-bar as a function of pH for the 1:3 and 1:4 complexation of nickel(II) and Gly-Leu-Phe at 25 ^oC in 0.15 $mol.dm^{-3}$ NaCl.

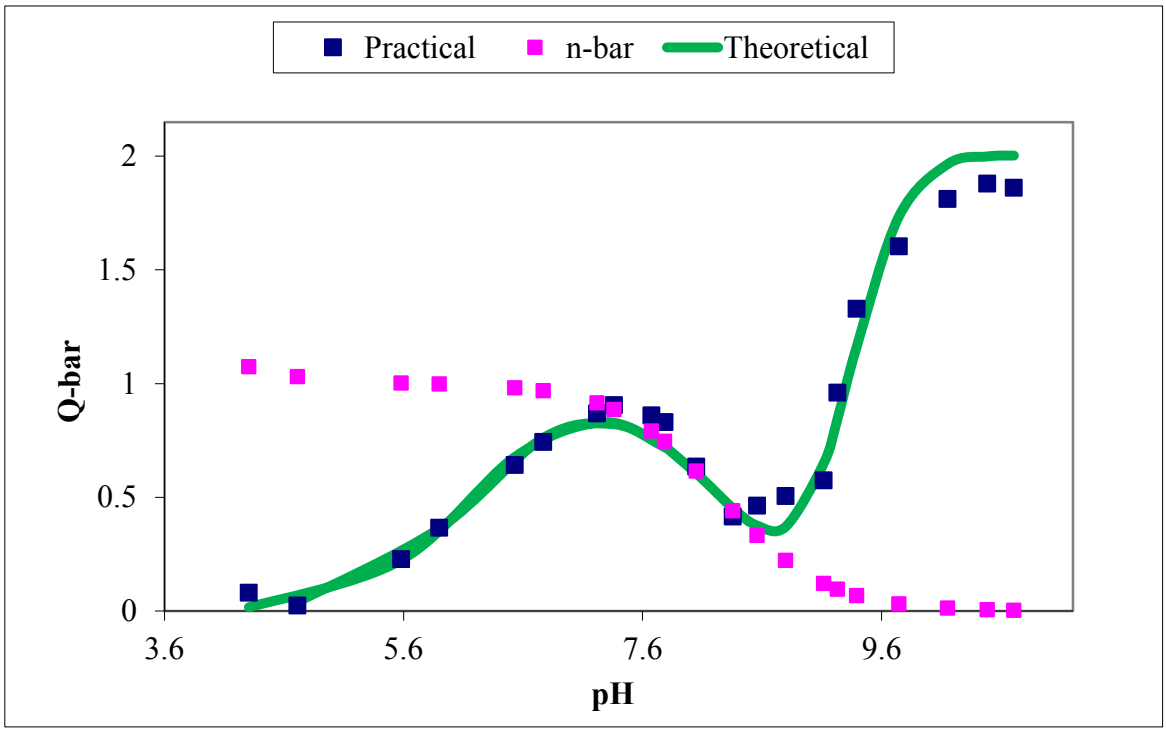

Figure 3.16: Model 2 of Q_M-bar as a function of pH for the 1:3 and 1:4 complexation of nickel(II) and Gly-Leu-Phe at 25 ^oC in 0.15 $mol.dm^{-3}$ NaCl.

The species distribution for Model 1 and Model 2 of the nickel(II) Gly-Leu-Phe system can be seen in Figure 3.17 and Figure 3.18 respectively. In both models the distribution shows that the complexation of the ML species is present at the pH of about 3.5 to 9.9. The formation of the hydroxo species MLH_{-1} and MLH_{-2} in Model 1 and the hydroxo species ML_2H_{-1} and ML_2H_{-2} in Model 2 all start at a pH value of about 8.1. This species distribution graph therefore corresponds to the Z_M-bar and the Q_M-bar functions, since it shows that the ML species becomes 100% dominant in both models and that there is a correspondence with pH ranges. It also shows that the MLH_{-2} species in Model 1 dominates over the MLH_{-1} species and the ML_2H_{-2} species in Model 2 dominates over the ML_2H_{-1} species.

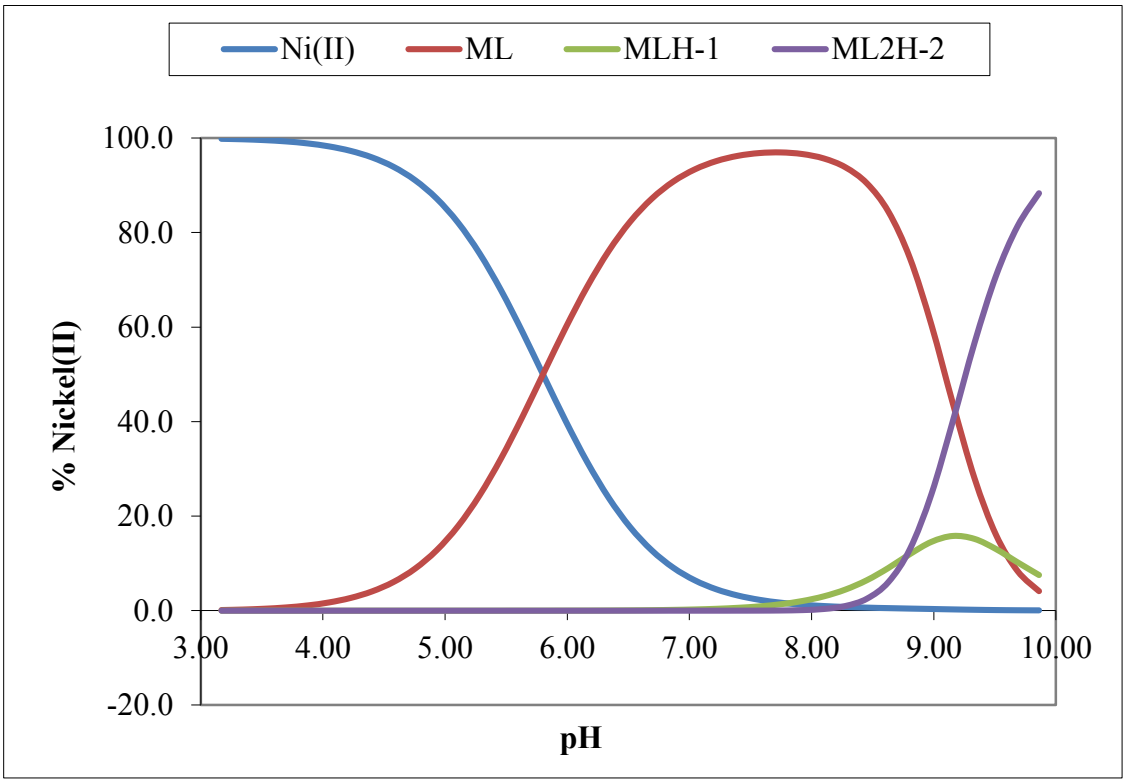

Figure 3.17: Model 1 of the protonation species distribution curve for nickel(II) and Gly-Leu-Phe (1:4 ratio) at 25 ^{o}C in 0.15 mol.dm^{-3} of NaCl.

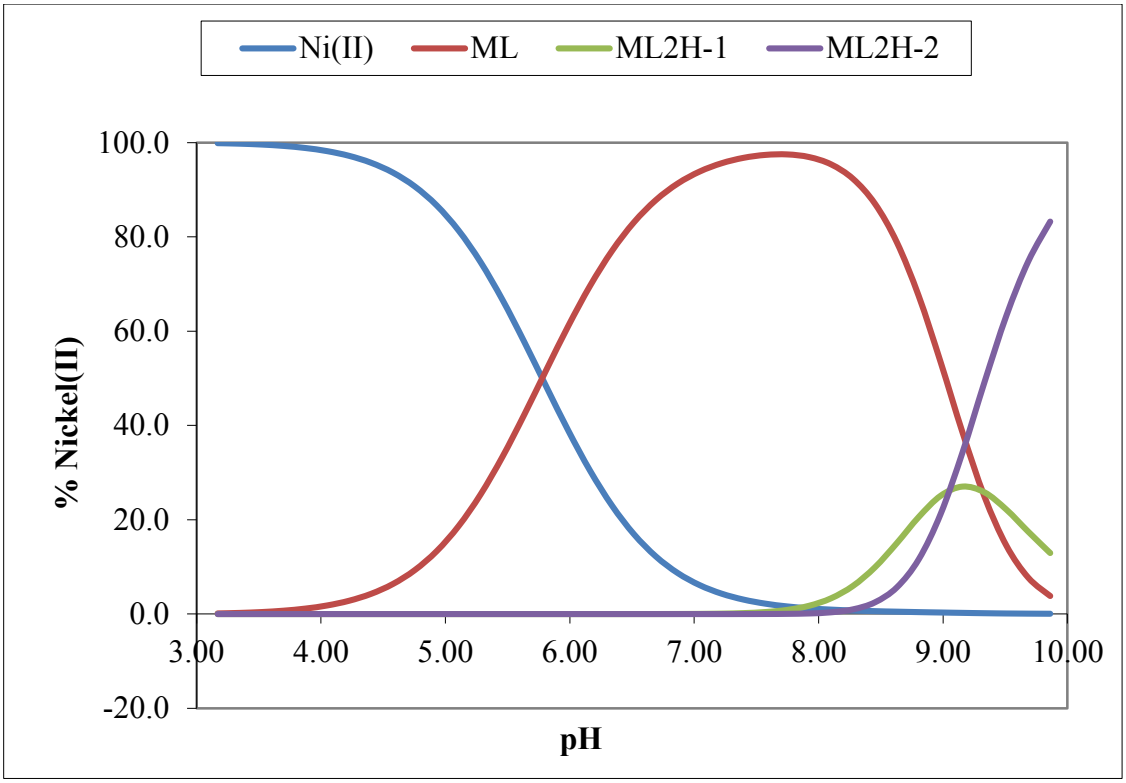

Figure 3.18: Model 2 of the protonation species distribution curve for nickel(II) and Gly-Leu-Phe (1:4 ratio) at 25 ºC in 0.15 mol.dm^{-3} of NaCl.

3.3.3(b) Ni-Sar-Leu-Phe

The complex formation function, Z_M-bar, for Model 1 and Model 2 of nickel(II) and Sar-Leu-Phe can be seen in Figure 3.19 and Figure 3.20 respectively. Both models have a good agreement between the theoretical and experimental functions. In both models, the Z_M-bar begins to level off at a value of 1, but before levelling off, the curve then curls backwards. This indicates that the formation of the ML species almost reaches 100% dominance, before the hydroxo species start forming and overlapping the ML formation. It also indicates that these hydroxo species form at high pH values while the ML species forms at middling pH values. The estimated log K_{ML} value for both Model 1 and Model 2 is 4.8, which corresponds to the calculated value.

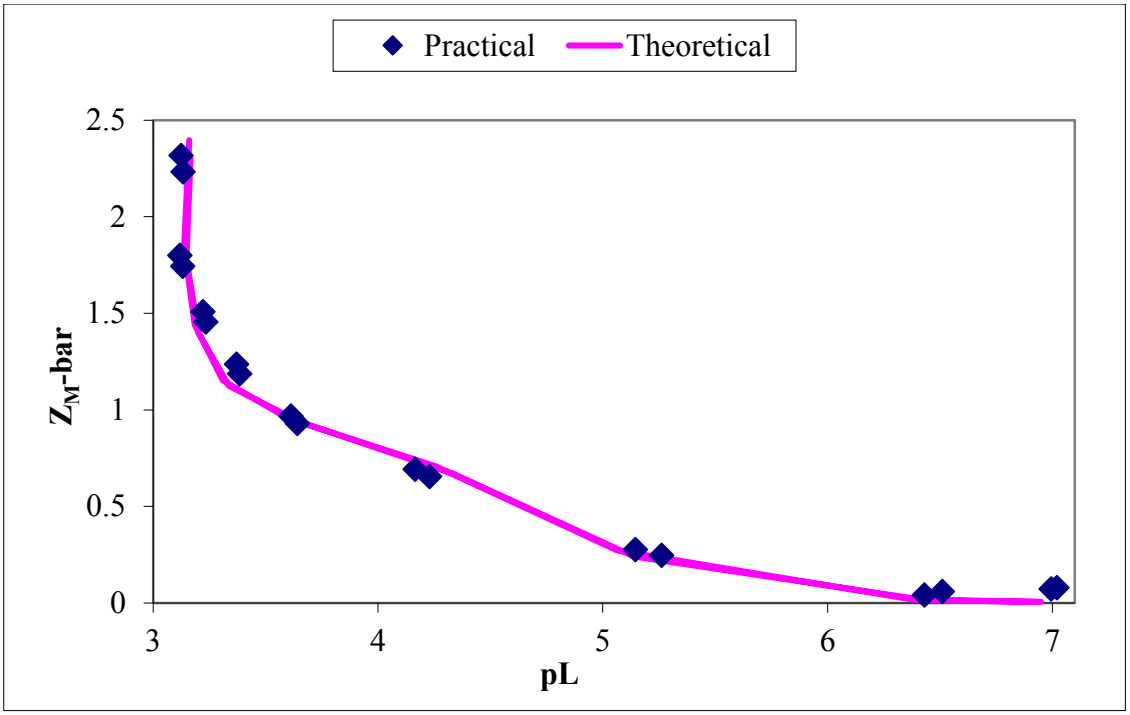

Figure 3.19: Model 1 of Z_M-bar as a function of pH for the 1:3 and 1:4 complexation of nickel(II) and Sar-Leu-Phe at 25 ^oC in 0.15 mol.dm^{-3} NaCl.

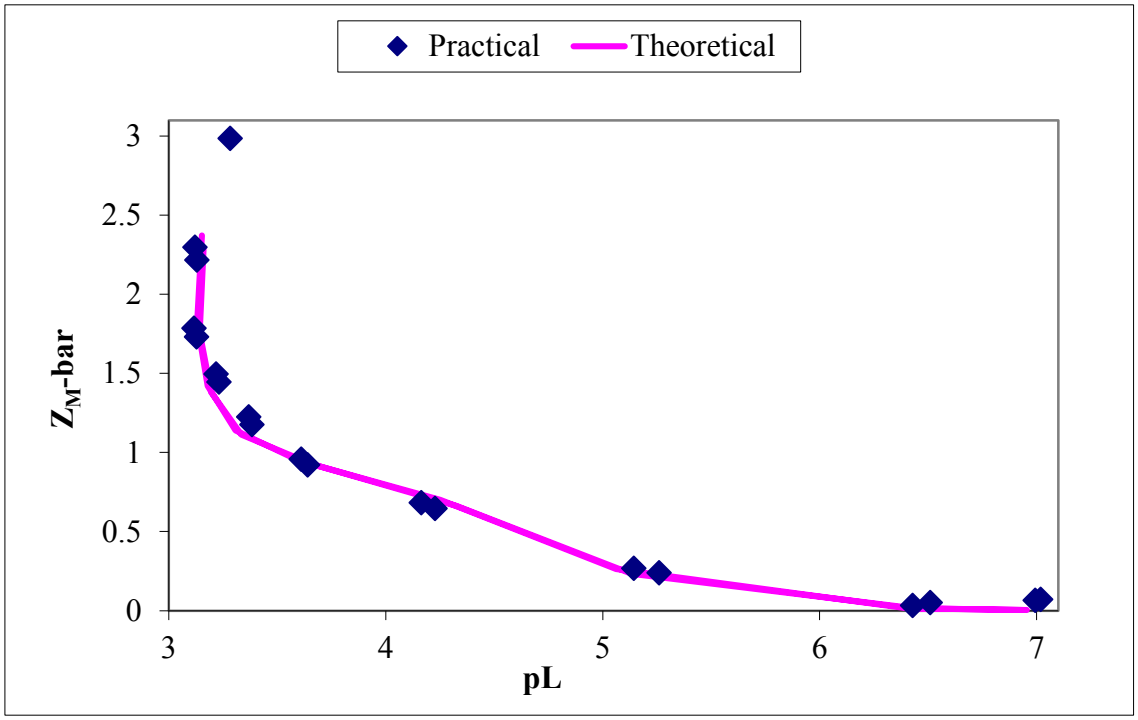

Figure 3.20: Model 2 of Z_M-bar as a function of pH for the 1:3 and 1:4 complexation of nickel(II) and Sar-Leu-Phe at 25 ^oC in 0.15 mol.dm^{-3} NaCl.

The low standard deviations of the log β values and low Hamilton R factors verify the validity of the model. The stability constants and the logarithms of the nickel(II) Sar-Leu-Phe complexation can be seen in Table 3.6 below.

Table 3.6: Model 1 and Model 2 of the stability constants (log β_{pqr}) and logarithms for the 1:4 complexation between nickel(II) and Sar-Leu-Phe at 25 ^{o}C and 0.15 mol.dm^{-3} NaCl.
Std is the standard deviation; R_f^H is the Hamilton R-factor and R_{lim}^H its limit; n_T is the number of titrations and (n_P) is the number of titration points; p, q, r are the stoichiometric coefficients of a complex with a general formula of $M_pL_qH_r$; L stands for the ligand and H stands for a hydrogen atom.

Model	Complex form	p	q	r	log β_{pqr}	log K	std	Rf	R_{lim}	$n_T(n_p)$
1	ML ML_2H_{-1} ML_2H_{-2}	1 1 1	1 2 2	0 -1 -2	4.64 -0.86 -9.99	4.64 - -9.13	0.05 0.06 0.08	0.01	0.01	2(71)
2	ML ML_2H_{-1} MLH_{-2}	1 1 1	1 2 1	0 -1 -2	4.62 -0.97 -12.74	4.62 - -	0.05 0.08 0.06	0.01	0.01	2(71)

The pK_a values from the experimental data could not be calculated and therefore could not be compared to the pK_a value from Ni(H_2O) to NiOH.

The deprotonation function, Q_M-bar, for Model 1 and Model 2 of nickel(II) and Sar-Leu-Phe can be seen in Figure 3.21 and Figure 3.22 respectively. Model 1 and Model 2 have a relatively good agreement between the theoretical and experimental functions. Similarly, in both models the n-bar plot line levels off at a value of 1, which indicates the formation of the LH species. At a pH of 4.4 in both models, the n-bar plot line starts to increase, indicating the formation of the LH_2 species. The low pH values indicate that this extra proton is due to the protonation of the carboxyl group. However, since there is no indication that a complex has formed at those low pH values, the LH_2 species is never present during complexation. At a pH of 7.4, the Q_M-bar plot line reaches a value of 1 and begins to level off, which indicates

the presence of the ML species. However, before levelling has been completed, the curve continues to increase to a value of 2. This indicates that the hydroxo species start to form just before the ML species can finish forming.

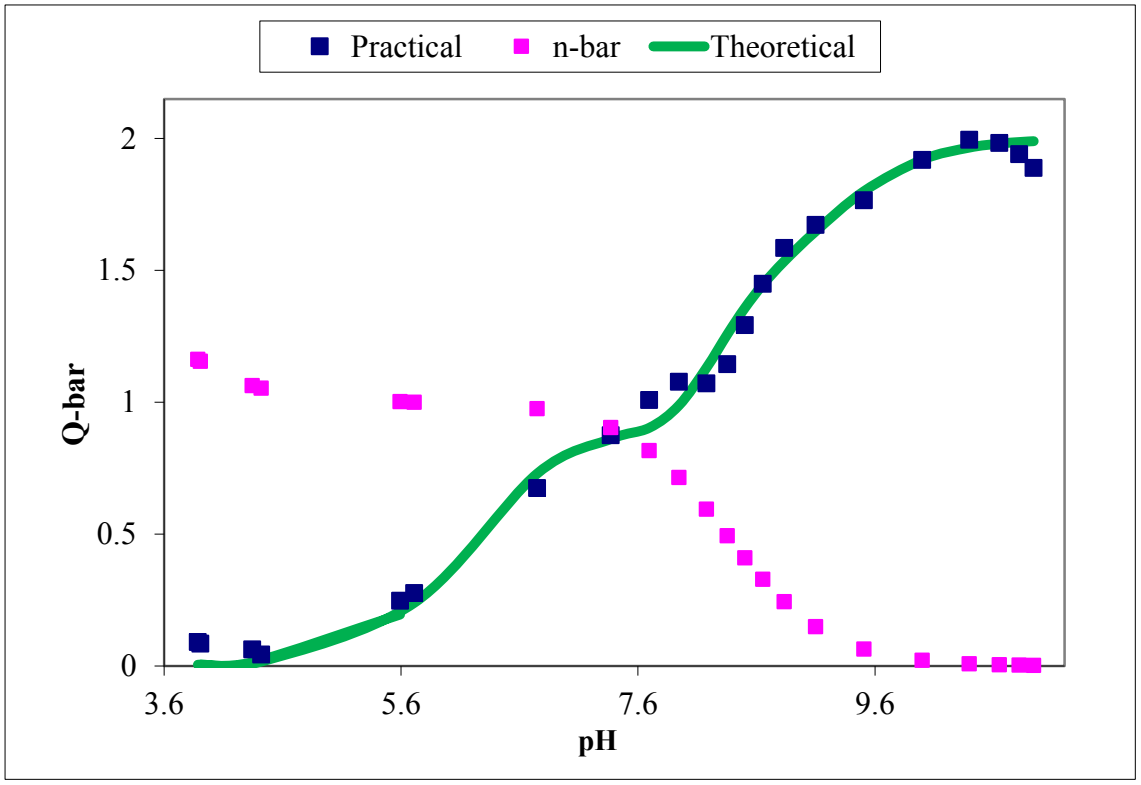

Figure 3.21: Model 1 of Q_M-bar as a function of pH for the 1:3 and 1:4 complexation of nickel(II) and Sar-Leu-Phe at 25 ^{o}C in 0.15 mol.dm^{-3} NaCl.

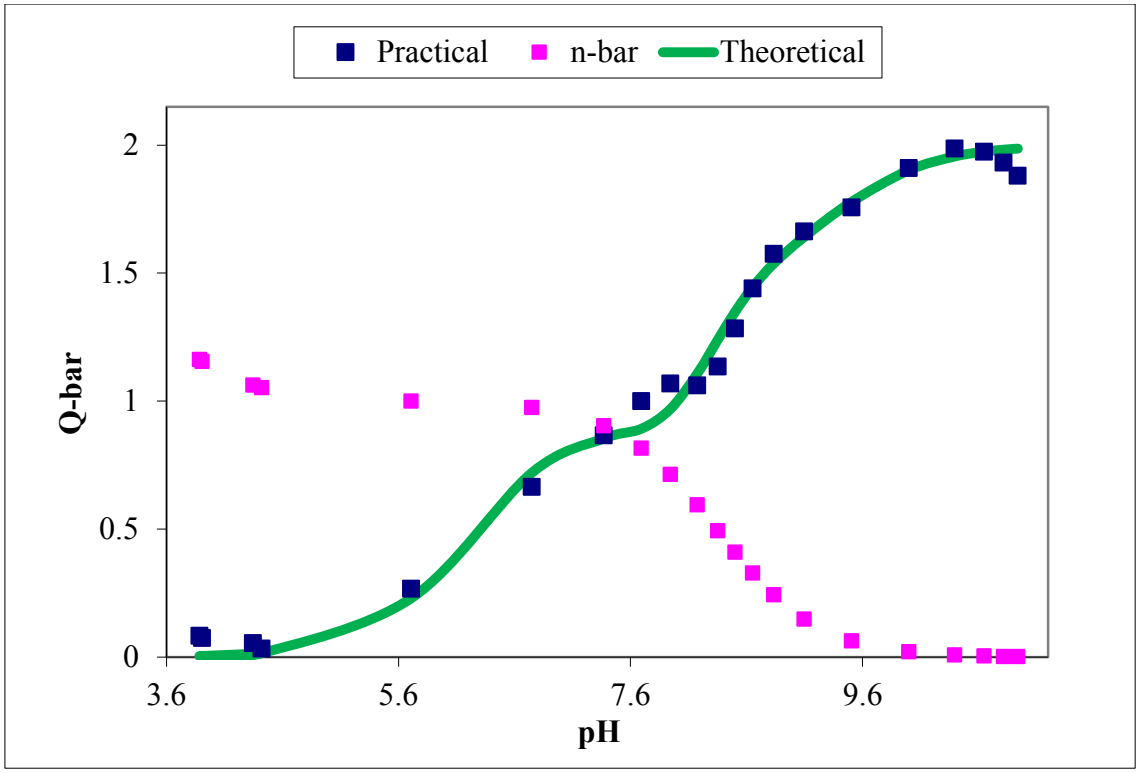

Figure 3.22: Model 2 of Q_M-bar as a function of pH for the 1:3 and 1:4 complexation of nickel(II) and Sar-Leu-Phe at 25 ºC in 0.15 mol.dm^{-3} NaCl.

The species distribution for Model 1 and Model 2 of the nickel(II) Sar-Leu-Phe system can be seen in Figure 3.23 and Figure 3.24 respectively. In both models the distribution shows that the complexation of the ML species is present in the pH range from about 3.5 to 9.3. The formation of the hydroxo species, ML_2H_{-1} and ML_2H_{-2}, in Model 1 and the hydroxo species, ML_2H_{-1} and MLH_{-2}, in Model 2 all start at a pH value of about 8 and all end beyond the analysed pH scale. The species distribution graph also shows that the ML species in both models almost reaches 100% dominance, but before this is achieved, the ML_2H_{-1} species already begins to form. This therefore corresponds to the Z_M-bar and Q_M-bar functions of both models.

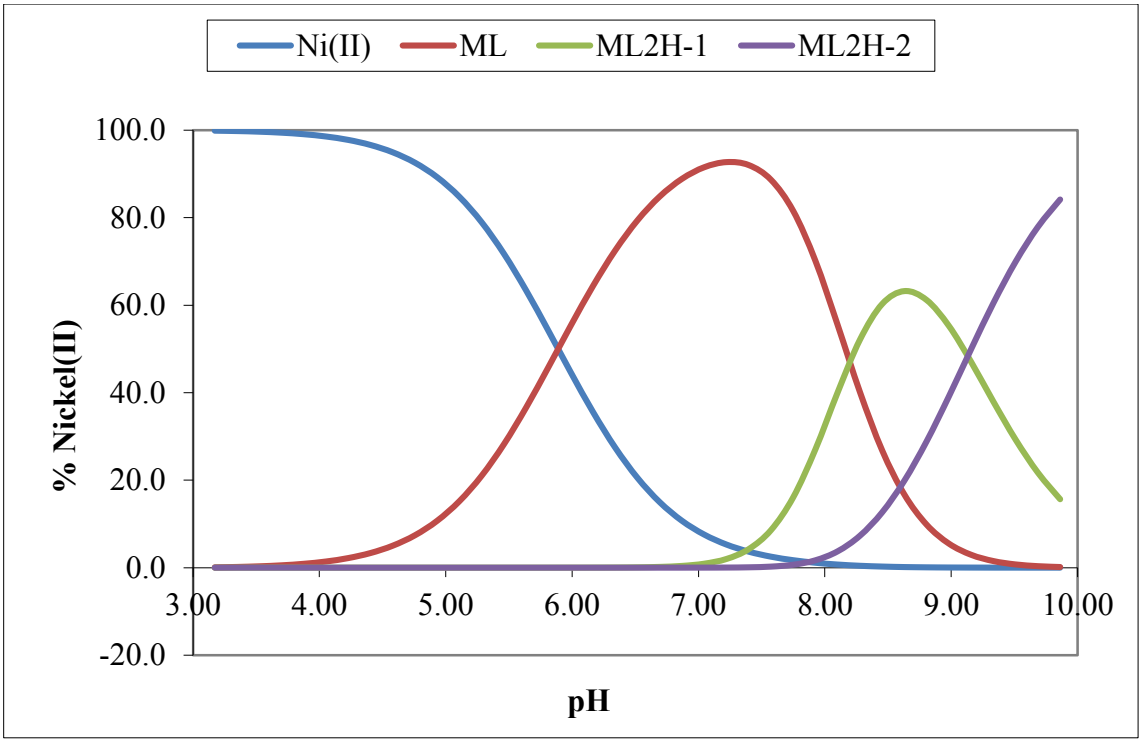

Figure 3.23: Model 1 of the protonation species distribution curve for nickel(II) and Sar-Leu-Phe (1:4 ratio) at 25 °C in 0.15 mol.dm^{-3} of NaCl.

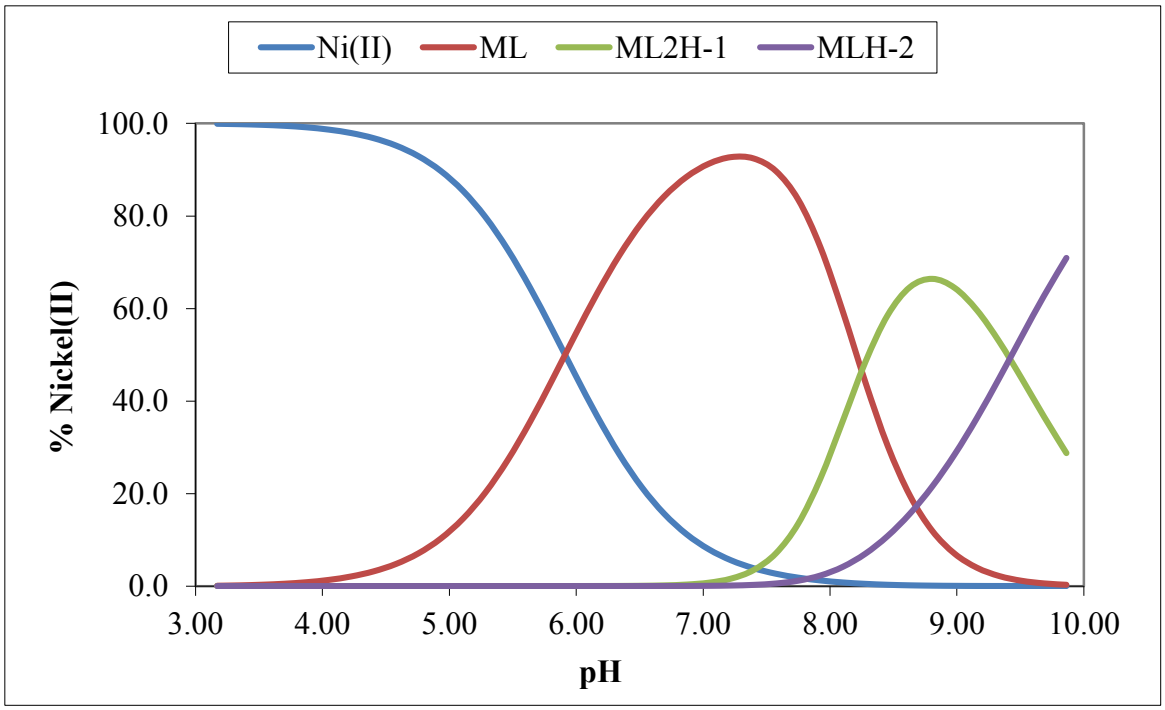

Figure 3.24: Model 2 of the protonation species distribution curve for nickel(II) and Sar-Leu-Phe (1:4 ratio) at 25 °C in 0.15 mol.dm^{-3} of NaCl.

3.3.4 Zinc(II) complexation of Gly-Leu-Phe and Sar-Leu-Phe

The stability constants (log β_{pqr}) for the zinc(II) Gly-Leu-Phe and zinc(II) Sar-Leu-Phe complexation of both a 1:3 and a 1:4 zinc(II) ligand ratio, were found using ESTA suite of programs and used to determine Z_M-bar, Q_M-bar and the species distribution functions. Similarly, these ligand ratios were chosen in order to be consistent with the copper(II) ligand ratios.

3.3.4(a) Zn-Gly-Leu-Phe

The complex formation function, Z_M-bar, for the zinc(II) Gly-Leu-Phe complexation can be seen in Figure 3.25. There is a good agreement between the theoretical and experimental functions. The Z_M-bar function curls backwards at low pL values without first levelling off. This indicates that the hydroxo species start to form at high pH values and overlap the formation of the ML species, which also forms at middling pH values.

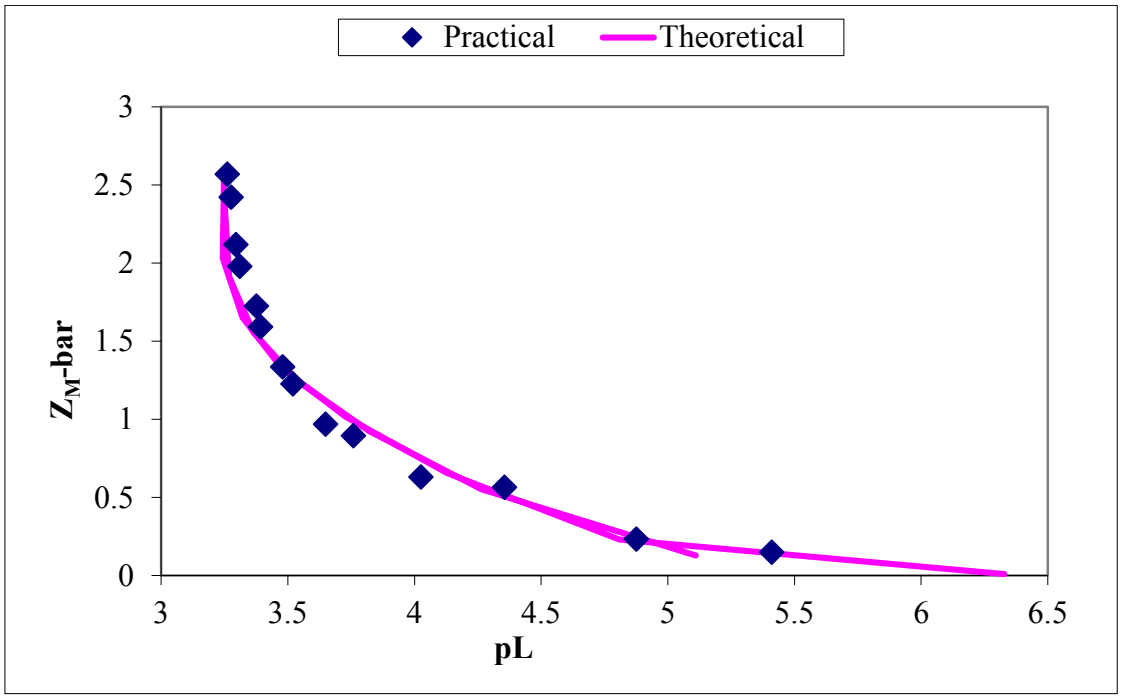

Figure 3.25: Z_M-bar as a function of pH for the 1:3 and 1:4 complexation of zinc(II) and Gly-Leu-Phe at 25 ^oC in 0.15 mol.dm^{-3} NaCl.

The low standard deviations of the log β values and low Hamilton R factors verify the validity of the model. The stability constants and the logarithms of the zinc(II) Gly-Leu-Phe complexation can be seen in Table 3.7 below.

Table 3.7: Stability constants (log β_{pqr}) and logarithms for the 1:4 complexation between zinc(II) and Gly-Leu-Phe at 25 ^{o}C and 0.15 mol.dm^{-3} NaCl.
Std is the standard deviation; R_f^H is the Hamilton R-factor and R_{lim}^H is its limit; n_T is the number of titrations and (n_P) is the number of titration points; p, q, r are the stoichiometric coefficients of a complex with a general formula of $M_pL_qH_r$; L stands for the ligand and H stands for a hydrogen atom.

Ligand	p	q	r	log β_{pqr}	log K	std	Rf	R_{lim}	$n_T(n_p)$
ML	1	1	0	4.28	4.28	0.05			
MLH_{-1}	1	1	-1	-3.51	-7.79	0.05	0.01	0.01	2(69)
MLH_{-2}	1	1	-2	-12.38	-8.87	0.05			

The pK_a of Zn(H_2O) to ZnOH is -8.96.[25] Therefore the pK_a from ML to MLH_{-1}, which has a value of -7.79, could be due to either the loss of a proton from the amide or from water. The pK_a from MLH_{-1} to MLH_{-2} has a value of -8.87 and therefore the second proton is lost from water.

The deprotonation function, Q_M-bar, can be seen in Figure 3.26. There is a relatively good agreement between the theoretical and experimental functions. The n-bar plot line levels off at a value of 1, which indicates the formation of the LH species. The n-bar plot and the Q_M-bar curve intersect at a pH of 7.1 and therefore at this pH the ML complex is present. The Q_M-bar plot line then rises to a value of 2, which indicates that the hydroxo species start forming before the ML species can finish forming. There is a dip in the Q_M-bar plot line at a pH of 8.3, but according to the species distribution, which can be seen in Figure 3.27, the ML species is barely present at that pH and therefore the dip cannot indicate that the ML species has just finished forming. This dip is rather due to the dominance of the hydroxo species.

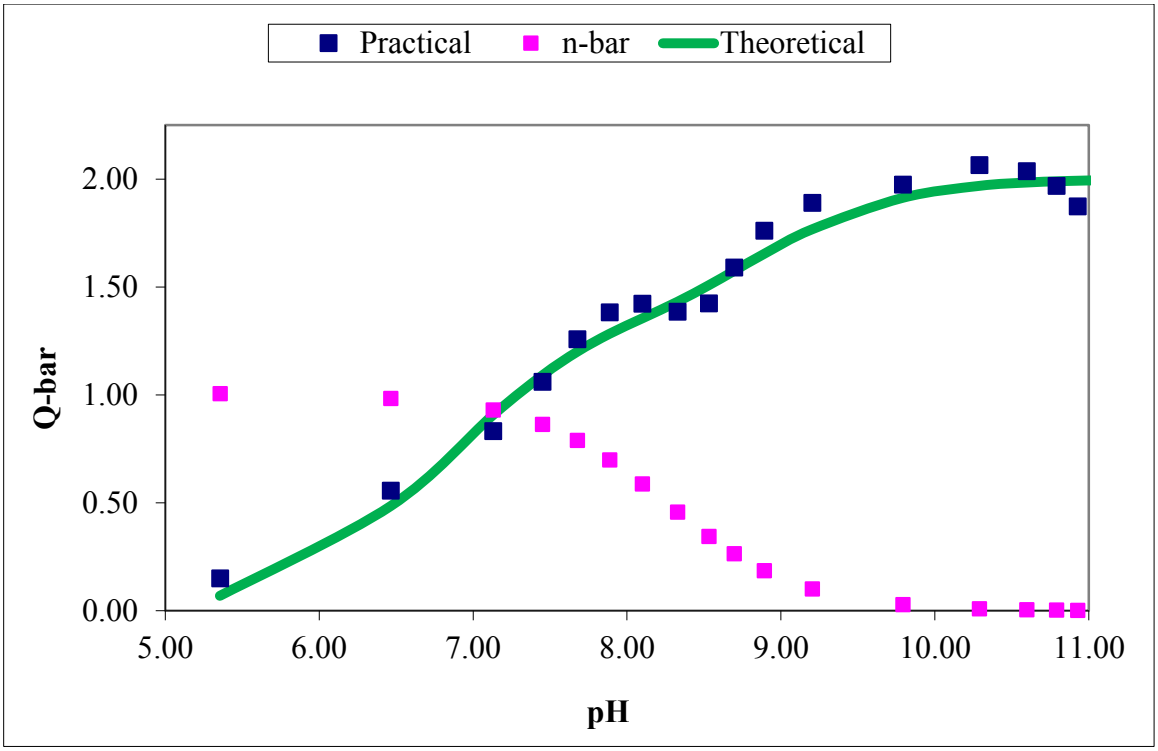

Figure 3.26: Q_M-bar as a function of pH for the 1:3 and 1:4 complexation of zinc(II) and Gly-Leu-Phe at 25 ^oC in 0.15 mol.dm^{-3} NaCl.

The species distribution in Figure 3.27 shows that the complexation of the ML species starts at a pH of about 4.0 and ends at a pH of about 8.8 with a maximum occurrence at a pH of 6.9. The MLH_{-1} hydroxo species starts forming at a pH of 6.2, which is before the ML species can reach its maximum formation and ends beyond the analysed pH scale. The maximum occurrence of MLH_{-1} is at a pH of 8.1. The MLH_{-2} species starts forming at a pH of about 7.8 and is still reaching its maximum occurrence when the analysed pH scale ends. This shows and verifies that the dip in the Q_M-bar graph is not due to the end of the ML formation, but due to the end of the MLH_{-1} species formation and the start of the MLH_{-2} species. The presence of each species at different pH values, as well as the percentage distributions, corresponds to both the Z_M-bar and Q_M-bar graphs.

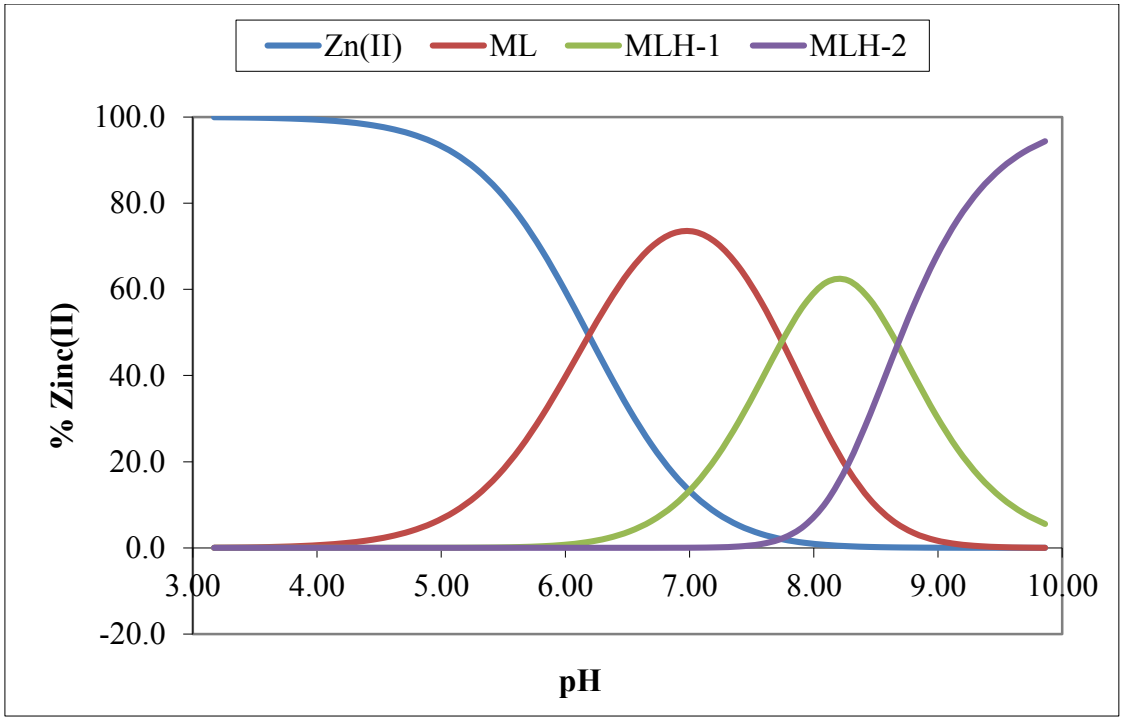

Figure 3.27: Protonation species distribution curve for zinc(II) and Gly-Leu-Phe (1:4 ratio) at 25 ^{o}C in 0.15 mol.dm^{-3} of NaCl.

3.3.4(b) Zn-Sar-Leu-Phe

The complex formation function, Z_M-bar, for the zinc(II) Sar-Leu-Phe complexation can be seen in Figure 3.28. There is a good agreement between the theoretical and experimental functions. The Z_M-bar function curls backwards at low pL values without first levelling off. This indicates that the hydroxo species start to form at high pH values before the ML complex can become dominant.

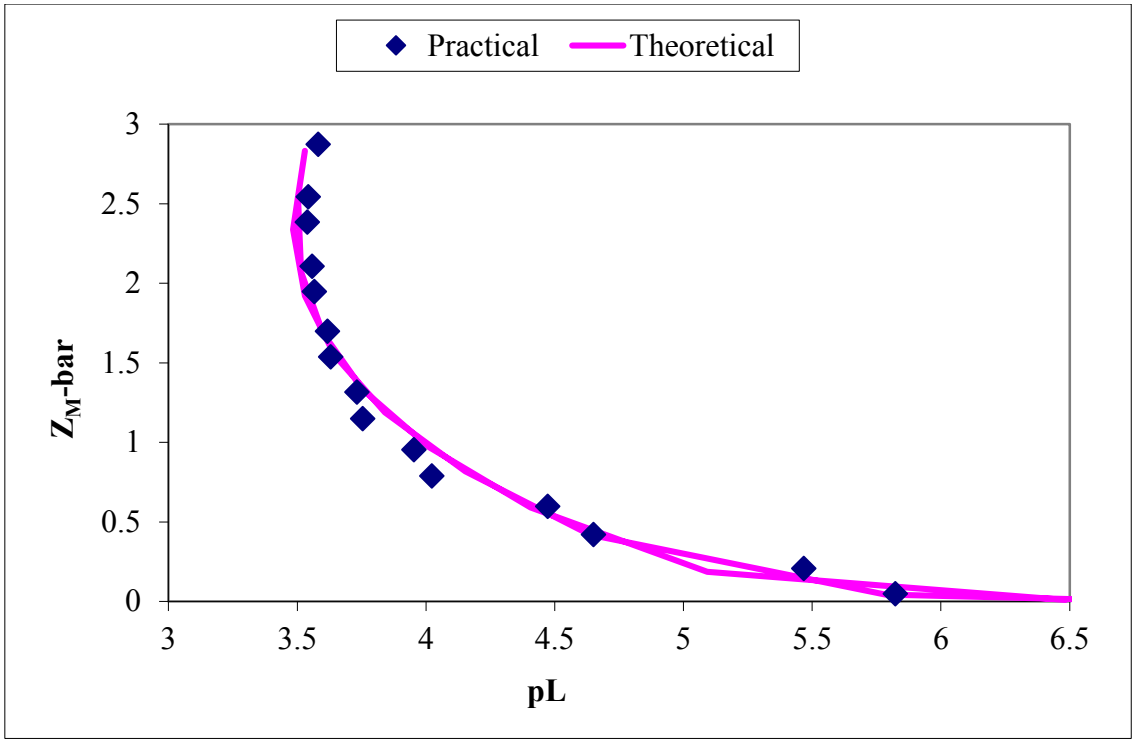

Figure 3.28: Z_M-bar as a function of pH for the 1:3 and 1:4 complexation of zinc(II) and Sar-Leu-Phe at 25 °C in 0.15 mol.dm^{-3} NaCl.

The low standard deviations of the log β values and low Hamilton R factors verify the validity of the model. The stability constants and the logarithms of the zinc(II) Sar-Leu-Phe complexation can be seen in Table 3.8 below.

Table 3.8: Stability constants (log β_{pqr}) and logarithms for the 1:4 complexation between zinc(II) and Sar-Leu-Phe at 25 °C and 0.15 mol.dm^{-3} NaCl.

Std is the standard deviation; R_f^H is the Hamilton R-factor and R_{lim}^H is its limit; n_T is the number of titrations and (n_P) is the number of titration points; p, q, r are the stoichiometric coefficients of a complex with a general formula of $M_pL_qH_r$; L stands for the ligand and H stands for a hydrogen atom.

Ligand	p	q	r	log β_{pqr}	log K	std	Rf	R_{lim}	$n_T(n_p)$
ML	1	1	0	4.41	4.41	0.07			
MLH_{-1}	1	1	-1	-3.11	-7.52	0.06	0.02	0.02	2(35)
MLH_{-2}	1	1	-2	-11.31	-8.20	0.09			

The pK_a from $Zn(H_2O)$ to ZnOH is -8.96.[25] Therefore, since the pK_a from ML to MLH_{-1} is -7.52, the loss of the proton is due to the amide and not from water. The pK_a from MLH_{-1} to MLH_{-2} has a value of -8.20 and therefore the second proton can be lost from either the amide or from water.

The deprotonation function, Q_M-bar can be seen in Figure 3.29. There is a relatively good agreement between the theoretical and experimental functions, with a slight deviation between the pH values of 8.3 and 10.1. The n-bar plot line levels off at a value of 1, which indicates the formation of the LH species. The n-bar plot curve and the Q_M-bar curve intersect at a pH of 7.0 and therefore at this pH the ML complex is present. The Q_M-bar then rises above the n-bar plot line and reaches a value of 1.9. This indicates that a maximum of two protons have been dissociated due to complexation, which then forms the MLH_{-1} species. Between the pH values of 8.3 and 9.1 the n-bar and Q_M-bar curves are parallel, which indicates that the protons are no longer being displaced from the ligand. However, at the pH of 9.1 the Q_M-bar plot line starts to increase, which indicates the presence and formation of hydroxo groups.

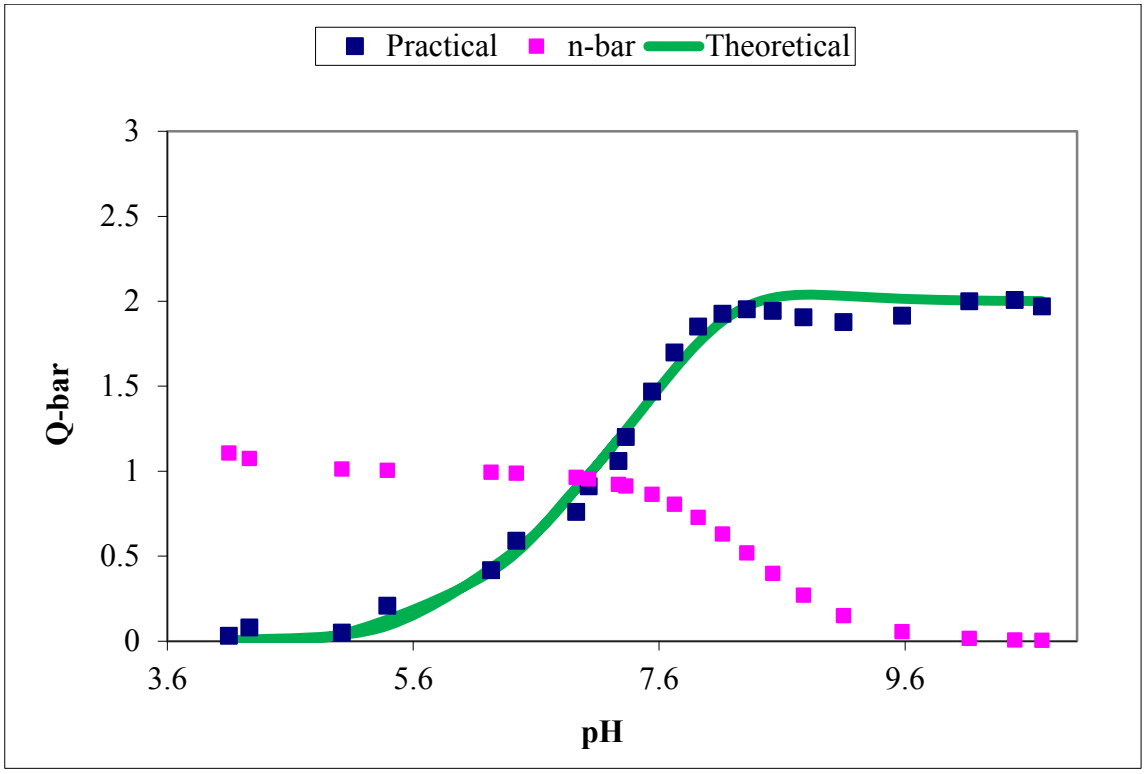

Figure 3.29: Q_M-bar as a function of pH for the 1:3 and 1:4 complexation of zinc(II) and Sar-Leu-Phe at 25 ^oC in 0.15 $mol.dm^{-3}$ NaCl.

The species distribution for zinc(II) Sar-Leu-Phe can be seen in Figure 3.30 below. The distribution shows that the complexation of the ML species starts at a pH of about 4.4 and ends at a pH of about 8.3. The formation of MLH_{-1} starts and ends at a pH value of about 6.1 to 9.9 and MLH_{-2} starts at a pH of about 7.4 and continues to exist at values which are out of the analysed pH scale. The existence of the complex species in these particular pH ranges corresponds to the Q_M-bar function. The MLH_{-1} species starts to form before the ML species has reached a dominant distribution and therefore corresponds to the Z_M-bar function. Therefore the increase in the Q_M-bar curve, from the pH of 9.1, is mainly due to the MLH_{-2} hydroxo species formation.

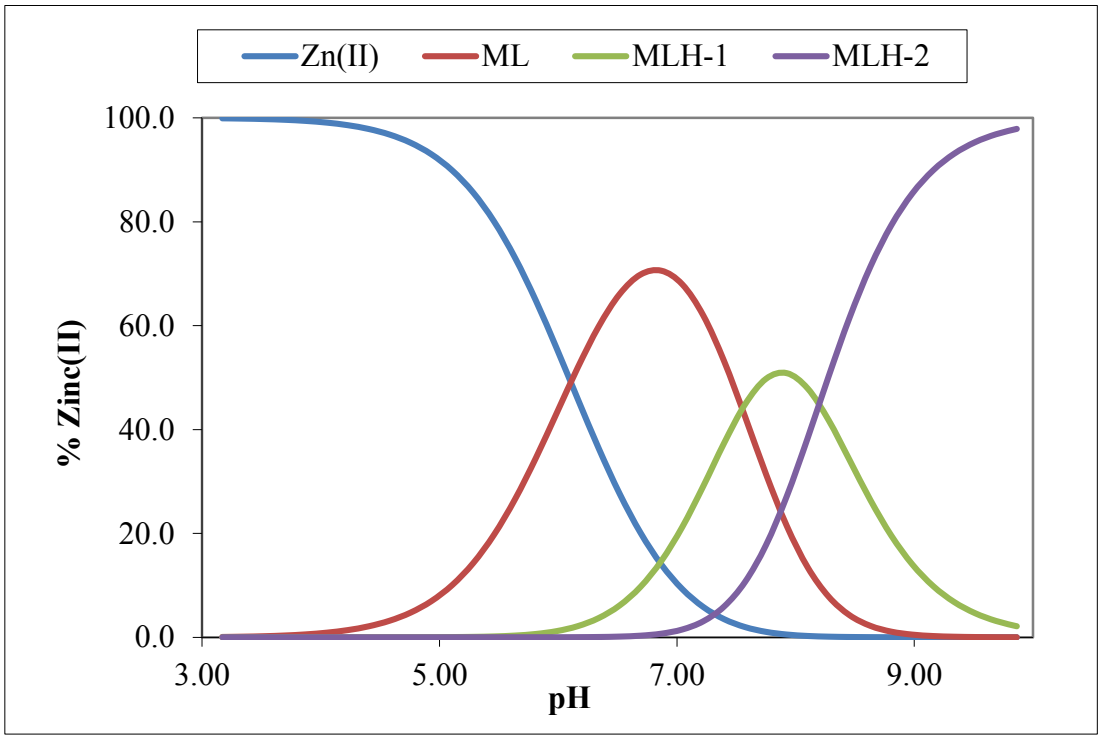

Figure 3.30: Protonation species distribution curve for zinc(II) and Sar-Leu-Phe (1:4 ratio) at 25 ^{o}C in 0.15 mol.dm^{-3} of NaCl.

3.4 Discussion

Copper(II) binds to protein molecules in blood plasma, and therefore it is essential that the copper(II) ligand complexes in this study are sufficiently stable, so that the ligand can transport copper(II). However, the stability cannot be so strong that the complex does not release copper(II). The protonation and stability constants for the ligands Gly-Leu-Phe and Sar-Leu-Phe can be seen in Table 3.9 and Table 3.10 respectively. These values were compared to literature values, which can also be seen in Table 3.9 and Table 3.10.

The literature values used were either from tripeptides or dipeptides. These had the same amine and carboxyl groups as Gly-Leu-Phe and Sar-Leu-Phe. Therefore the structures were similar and would have similar stability constants. This was verified for most protonation and complexation stability constants, except for the ML_2H_{-1} species of Ni-Sar-Leu-Phe and all the zinc(II) complexes, which deviated slightly from literature values.

The ligands Gly-Leu-Phe and Sar-Leu-Phe only differ by the methyl on the amine group of sarcosine. This methyl group has an inductive effect and was therefore expected to increase the stability of the complexes. When comparing the amine protonation constants, the amine protonation from the Sar-Leu-Phe ligand is 0.09 log units bigger than the amine protonation of Gly-Leu-Phe. This increase is not significant and therefore the methyl group did not seem to have an effect on the stability of the tripeptides.

Table 3.9: Protonation constants for the ligands, Gly-Leu-Phe and Sar-Leu-Phe, as well as literature values for diglycine (Gly-Gly) and triglycine (Gly-Gly-Gly).[27]

Ligand (exp)	***p q r***	**log β_{pqr} (exp)**	**Gly-Gly log β_{pqr} (lit)**	**Gly-Gly-Gly log β_{pqr} (lit)**
Gly-Leu-Phe	0 1 1 0 1 2	8.25 11.46	8.13 11.30	7.93 11.25
Sar-Leu-Phe	0 1 1 0 1 2	8.34 11.52	8.13 11.30	7.93 11.25

The stability constants for the metal ligand complexes were also compared with the two ligands to determine the effect of the methyl group on the stability of the complex. The stability constants of the copper(II) ligand species, showed that the Gly-Leu-Phe ligand is significantly more stable than the Sar-Leu-Phe copper(II) species, with increased values ranging from 0.38 to 1.67 log units. The only species from the nickel(II) complexes that could be compared were the ML, ML_2H_{-1} and ML_2H_{-2} species, since these are the only similar species for both ligands. There was no significant change in stability for the ML species, but there was a significant increase in stability of 1.3-1.4 log units for both the ML_2H_{-1} and ML_2H_{-2} species of the Sar-Leu-Phe compound. The stability constants of the zinc(II) ligand species, showed that the Sar-Leu-Phe ligand is more stable than the Gly-Leu-Phe ligand, since all of the species have an increased stability ranging from 0.13 to 1.07 log units.

Table 3.10: Stability constants for the complexes formed between the two ligands, Gly-Leu-Phe and Sar-Leu-Phe and the metals, Cu(II), Ni(II) and Zn(II), as well as the literature values for diglycine (Gly-Gly),[27] triglycine (Gly-Gly-Gly),[27] glycyl-L-phenylalanine (Gly-Phe)[14] and sarcosyl-L-phenylalanine (Sar-Phe).[14]

Metal	**Ligand**	**p q r**	**log β_{pqr} (exp)**	**Gly-Gly log β_{pqr} (lit)**	**Gly-Gly-Gly log β_{pqr} (lit)**	**Gly-Gly log β_{pqr} (lit)**	**Gly-Phe log β_{pqr} (lit)**	**Gly-Gly log β_{pqr} (lit)**	**Sar-Phe log β_{pqr} (lit)**
Cu(II)	**Gly-Leu-Phe**	1 1 0 1 1 -1 1 1 -2 1 2 -1	5.63 -0.14 -7.02 4.02	5.56 1.33 -8.04 4.46	5.25 0.16 -7.02 3.23				
Cu(II)	**Sar-Leu-Phe**	1 1 0 1 1 -1 1 1 -2 1 2 -1	4.72 -0.52 -8.69 3.45	5.56 1.33 -8.04 4.46	5.25 0.16 -7.02 3.23				
Ni(II) Model 1	**Gly-Leu-Phe**	1 1 0 1 1 -1 1 2 -2	4.65 -4.95 -11.34	3.96 -4.91 -11.99	3.75 -5.45 -				

Ni(II) Model 2	**Gly-Leu-Phe**	1 1 0 1 2 -1 1 2 -2	4.66 -2.27 -11.32	3.96 -2.51 -11.99	3.75 - -				
Ni(II) Model 1	**Sar-Leu-Phe**	1 1 0 1 2 -1 1 2 -2	4.64 -0.86 -9.99	3.96 -2.51 -11.99	3.75 - -				
Ni(II) Model 2	**Sar-Leu-Phe**	1 1 0 1 2 -1 1 1 -2	4.62 -0.97 -12.74	3.96 -2.51 -	3.75 - -				
Zn(II)	**Gly-Leu-Phe**	1 1 0 1 1 -1 1 1 -2	4.28 -3.51 -12.38			3.25 - -	2.70 -4.39 -14.0		
Zn(II)	**Sar-Leu-Phe**	1 1 0 1 1 -1 1 1 -2	4.41 -3.11 -11.31					3.25 - -	2.96 -3.96 -13.5

Since there was not an overall increase in the protonation and stability constants for the species with the N-methylated group, this suggests that the methyl group also has steric effects as well as inductive effects. This causes the inductive effects to be less prominent. Another explanation as to why the inductive effects were not prominent is due to the preference of the ammonium ions or charged amine to form a hydrogen bond with water. This effect was seen for alkylamines in a solvent, where the base strength was found to be in the order of $NH_3<RNH_2$, $R_2NH >R_3N$. The true base strengths should have been $NH_3<RNH_2< R_2NH <R_3N$, because the electron density to the nitrogen atom is increasing, since the number of methyl groups is increasing. However, the deviation was explained by the preference of the charged amine to solvate through hydrogen bonding.[28]

A comparison of the stability of the same species with the three different metals corresponds to the Irving Williams series, since the overall stability of the copper(II) complexes are more stable than the nickel(II) complexes and the nickel(II) complexes are more stable than the zinc(II) complexes.[29,30]

Mohajane found that the Cu-Gly dipeptides were slightly more stable than the Cu-Sar dipeptides.[14] The explanation given was the possibility that the methyl group caused a steric effect as well as an inductive effect. However, since the two results were comparable, the conclusion was that the N-methylated dipeptides would not affect the stability of the complex, but would still improve the lipophilicity of the complex, since N-methylated groups are more lipophilic than non-N-methylated groups. It was therefore suggested that the tripeptides, Sar-Leu-Phe and Gly-Leu-Phe should be analysed to study the stability and subsequent properties of the metal complexes.[14] However, the stability of the Cu-Sar-Leu-Phe complexes was found to be less than the Cu-Gly-Leu-Phe complexes. Therefore, this shows that the added methyl group on this tripeptide does affect the stability of the complex, which could indicate that Cu-Sar-Leu-Phe is more suitable for releasing copper(II) *in vivo* than Cu-Gly-Leu-Phe.

The overall stability of the copper(II) tripeptide complexes in this study was lower than the dipeptide complexes found in literature, except for the MLH_{-1} species of Sar-Leu-Phe.[14] This was unexpected, since tripeptides should have increased the stability of the complexes, due to their increased coordination. The comparison can be seen in Table 3.11 below.

Table 3.11: Comparison between dipeptides from literature and the tripeptides, Gly-Leu-Phe and Sar-Leu-Phe.[14]

Ligand	*p q r* with corresponding stability constants (log β_{pqr})			
	1 1 0	1 1-1	1 1 -2	1 2 -1
Sar-Phe	6.54	1.03	-8.89	-
Sar-Leu	6.32	-1.25	-11.6	-
Sar-Leu-Phe	4.72	-0.52	-8.69	3.45
Gly-Phe	6.37	-	-	-
Gly-Leu	5.79	1.08	-	4.19
Gly-Leu-Phe	5.63	-0.14	-7.02	4.02

Potentiometric titrations indirectly contributed to the determination of the structure of the metal ligand complex, since the complex species were given. The pK_a values of the

complexes could be compared to the pK_a value of CuOH, NiOH and ZnOH, which could indicate if the loss of a proton was from the amide or from water.

The complexation between nickel(II) and Gly-Leu-Phe resulted in two speciation models. Both models have the same standard deviations and R-factors and therefore the one model cannot be favoured over the other with regard to statistical grounds. Consequently, chemical and thermal grounds have to be used to determine which model is the more favourable model. Model 1 has ML, MLH_{-1} and ML_2H_{-2} and Model 2 has ML, ML_2H_{-1} and ML_2H_{-2}. The only difference in species between the two models is that Model 1 has the MLH_{-1} species and Model 2 has the ML_2H_{-1} species. It is therefore more likely that Model 1 will be favoured, since to form the species, ML_2H_{-1}, only one ligand must lose a proton. For example, if one ligand loses a proton, the other should also be able to lose a proton. Therefore, since the MLH_{-1} complex has only one ligand and one proton to lose, it is more likely to form.

The complexation between nickel(II) and Sar-Leu-Phe also resulted in two speciation models. Both models also have the same standard deviations and R-factors and therefore chemical and thermal groups also have to be used to determine which model is more favourable. Model 1 has ML, ML_2H_{-1} and ML_2H_{-2} and Model 2 has ML, ML_2H_{-1} and MLH_{-2}. Therefore the only difference is between the ML_2H_{-2} and MLH_{-2} species. Thus it is more likely that Model 1 will be favoured, since it is more favourable for the complex to lose one proton and then a second proton, instead of losing one proton, as well as losing the ligand along with another proton.

3.5 Conclusion

The objective to measure the thermodynamic stability of two specific tripeptides and compare them to the stability of previously studied dipeptides was achieved.[14] The expected increase in stability of a tripeptides compared to these dipeptides was not seen. Unlike the comparable stability between the N-methylated and non-N-methylated copper(II) complexes seen in literature,[14] Cu-Sar-Leu-Phe was found to be less stable than Cu-Gly-Leu-Phe. However, the decreased stability could indicate that copper(II) will be released more easily *in vivo* by Sar-Leu-Phe than by Gly-Leu-Phe.

References

1. J. Liyanage, *J. Sci. Univ. Kelaniya,* 2003, **1**, 1-13.
2. E. Lindner and B. D. Pendley, *Anal. Chim. Acta*, 2013, **762**, 1-13.
3. I. Pašti, T. Lazarević-Pašti and S. V. Mentus, *J. Electroanalytical Chem*., 2012, **665**, 83-89.
4. M. Cuartero, J. A. Ortuño, . Garcia and F. Martinez-Ortiz, *Electrochim. Acta*, 2012, **69**, 152-159.
5. P. May, K. Murray and D. R. Williams, *Talanta*, 1988, **35**, 927.
6. M. Michelon, A. Sabatini and A. Vacca, *Inorg. Chim. Acta*, 1977, **25**, 41-48.
7. O. Yamauchi and A. Odani, *Pure Appl. Chem*., 1996, **68**, 469-496.
8. H. M. Irving and H. S. Rossotti, *J. Chem. Soc.*, 1954, 2904-2910.
9. H. M. Irving and H. S. Rossotti, *Acta Chem. Scandinavica*, 1956, **10**, 72-93.
10. W. J. O'Sullivan and D. D. Perrin, *Biochem.*, 1964, **3**, 18-26.
11. A. Albert and E. P. Serjeant, *Determination of Ionization Constants, A Laboratory Manual*, Springer, Holland, 3rd edn., 1984, ch. 10, pp. 176-191.
12. S. C. Wallis, L. R. Gahan, B. G. Charles, T. W. Hambley and P. A. Duckworth, *J. Inorg. Biochem.*, 1996, **62**, 1-16.
13. A. E. Martell and R. D. Hancock, *Metal Complexes in Aqueous Solutions*, Springer, New York, 1996, ch. 7, pp. 217-240.
14. M. Mohajane, PhD Thesis, University of Cape Town, 2013.
15. J. N. Zvimba, PhD Thesis, University of Cape Town, 2005.
16. K. Murray and P. M. May, *Equilibrium Simulation For Titration Analysis,* Version 1.1, University of Wales Institute of Science and Technology, 1984.
17. J. A. Liyanage*, J. Sci. Univ. Kelaniya*, 2003, **1**, 1-13.
18. P. M. May, K. Murray and D. R. Williams, *Talanta*, 1985, **32**, 483-489.
19. P. M. May, K. Murray and D. R. Williams, *Talanta*, 1988, **35**, 825-830.
20. A. I. Vogel, *Vogel's Qualitative Inorganic Analysis,* Longman, London, 3rd edn, 1961.
21. F. J. C. Rossotti and H. Rossotti, *Journal of Chemical Education,* 1965, **42,** 375-378.
22. ChemPages Netorials, http://www.chem.wisc.edu/deptfiles/genchem/netorial/modules/biomolecules/modules/protein1/prot11.htm, (accessed September 2013).

23. Chemistry at Illinois, http://butane.chem.uiuc.edu/cyerkes/Chem104ACSpring2009/Lecture_Notes_104/lect27c.html, (accessed September 2013).
24. Stability Constants (log K_1) of Various Metal Chelates, http://www.george-eby-research.com/html/stability_constants.html, (accessed September 2013).
25. K. J. Powell, Academic software and database: Structure and displays V. Solov'ev, 1992-2000.
26. J. N. Zvimba and G. E. Jackson, *J. Inorg. Biochem*., 2007, **101**, 148-158.
27. C. G. Agoston, Z. Miskolczy, Z. Nagy and I. Sovago, *Polyhedron*, 2003, **22**, 2607-2615.
28. H. K. Hall, *J. Phys. Chem*., 1956, **60**, 63-70.
29. H. Irving and R. J. P. Williams, *J. Chem. Soc.,* 1953, 3192-3210.
30. Y. Altun, F. Köseoğlu, H. Demirelli, İ. Yilmaz, A. Çukurovah and N. Kavak, *J. Braz. Chem. Soc.*, 2009, **20**, 299-308.

4 Structural Studies

4.1 Ultraviolet-Visible (UV-Vis) Spectrophotometry

4.1.1 Introduction

Electronic spectroscopy is the study of electronic transitions between orbitals of different energies in transition metals, which have chelated with ligands to form a complex. These transitions are called *d-d* transitions, because the transitions involve molecular orbitals, which have the characteristic of *d* metals. The energy levels have spaces which correspond to the wavelengths of visible light. Therefore the UV-Vis spectra are formed when electromagnetic radiation in the UV-Vis wavelength region interacts with the transition metal complexes and absorption of the wavelength takes place. During the transition, an electron is excited from the highest occupied energy orbital to the lowest unoccupied energy orbital and this excitation results in absorption bands, which are labelled as *d-d* bands and have an energy that corresponds to the difference between the two energy levels.[1-3] These absorption bands appear in the ultraviolet and visible regions of the electromagnetic spectrum.[4] The spaces of the energy levels depend on aspects such as the geometry of the complex, the type of ligand that forms a complex with the metal ion and the oxidation of the metal ion.[2] Therefore UV-Vis spectroscopy can give information about the structure of the complex.

Selection rules govern the intensities of absorption bands. These rules include the Laporte rule, which specifies that transitions are only allowed if there is a change of parity in molecules. Therefore only transitions from a *gerade* to an *ungerade*($g \rightarrow u$) or an *ungerade* to a *gerade* ($u \rightarrow g$) is allowed. Molecules with a centre of symmetry have transitions from $g \rightarrow g$ or $u \rightarrow u$ and therefore they are said to be Laporte forbidden. Another rule states that the transition has to maintain the same multiplicity. Therefore if the spin of an electron changes during the transition, this transition is said to be multiplicity forbidden.[5]

For an octahedral complex the five d orbitals are split into a triply degenerate, t_{2g} set and a double degenerate, e_g set. The e_g orbitals (d_{z^2}, $d_{x^2-y^2}$) are higher in energy, since these orbitals have ligands directly on the x, y and z axes and therefore experience a stronger

electron repulsion than the t_{2g} orbitals (d_{xy}, d_{xz}, d_{yz}), which have ligands between the x, y and z axes and therefore experience weaker election repulsion. The energy difference between these two energy levels is called the Crystal Field Splitting Enegy (Δ_{oct}). Octahedral complexes have a centre of symmetry and therefore are Laporte forbidden. These complexes should be colourless. However in d^9 complexes, the selection rules are relaxed by vibrations due to Jahn Teller distortion. This causes the symmetry of the complex to become less symmetrical, which results in axial or equatorial elongation and an allowed electron transition. Axial elongation for d^9 complexes have one electron in the $d_{x^2-y^2}$ orbital and two electrons in the d_{z^2} orbital. This causes the orbitals with a z component to become stabilized and the d_{xy} and $d_{x^2-y^2}$orbitals to become destabilised. For equatorial elongation the d_{xy} and $d_{x^2-y^2}$ orbitals are stabilised and the z component orbitals are destabilized. These complexes are therefore paramagnetic and coloured, with a low intensity in the spectra.[3,5,6]

For a square planar complex there is no ligand along the z axis, which results in less electron repulsion in the d_{xz}, d_{yz} and d_{z^2} orbitals. This therefore causes these orbitals to be considerably lower in energy than the $d_{x^2-y^2}$ and d_{xy} orbitals. However, the d_{z^2} energy is slightly higher than the d_{xz} and d_{yz} orbitals due to electron density in the x and y axes. The $d_{x^2-y^2}$ orbital has the highest energy due to the direct axial alignment of the ligands and the d_{xy} orbital is second highest in energy.[3] This results in the energy levels to increase in the following order: e_g, b_{2g}, a_{1g} and b_{1g}.[7] This splitting pattern causes complexes with d^8metal ions to be low spin and diamagnetic.[3,5]

UV-Vis spectroscopy measures the absorbance corresponding to the maximum wavelength (λ_{max}) of each species that is present in the solution. From this wavelength the energy of the absorbed radiation can be calculated from the expression:

$$E = h\nu = \frac{hc}{\lambda} \tag{14}$$

where c is the speed of light and h is Planck's constant. This energy is also the ligand field stabilization energy.[3]

UV-Vis spectroscopy sends a beam of light into an analyte solution. The amount of radiation absorbed by a species can be represented in the Beer-Lambert law, which can be expressed as:

$$\log_{10}\frac{I_0}{I} = \varepsilon c b \tag{15}$$

where I_o is the intensity of the incident radiation and I is the intensity of the transmitted radiation. ε is the extinction coefficient or molar absorption coefficient, which represents the fraction of radiation absorbed by a species at a specific wavelength. c is the molar concentration of the species which absorbs the radiation and b is the thickness of the absorbing layer. The $\log_{10}\frac{I_0}{I}$ term can be represented as the symbol A, which is then regarded as the absorbance. Therefore the law can be rewritten as:

$$A = \varepsilon c b \tag{16}$$

If there is more than one species that is absorbing radiation at a specific wavelength, then the Beer-Lambert Law can be written as:

$$\begin{aligned} A^{\lambda} &= b(\varepsilon_1^{\lambda} c_1 + \varepsilon_2^{\lambda} c_2 + \varepsilon_3^{\lambda} c_3 + \ldots\ldots \varepsilon_i^{\lambda} c_i) \\ &= b\sum \varepsilon_i^{\lambda} ci \end{aligned} \tag{17}$$

where the superscript λ, represents a particular wavelength and the subscripts $1,2,3\ldots i$ represent the species that are absorbing radiation.[8]

Each species in solution will absorb light at different wavelengths and therefore there is a correlation between the structure of a species and λ_{max} for each absorption. Therefore the structures of complexes can be predicted using the λ_{max} of a particular species. Billo proposed an empirical method which can be used to calculate the λ_{max} (nm) for groups coordinated to the equatorial plane of a tetragonally distorted octahedral copper(II) complex.[9,10] Billo's equation can be expressed as:

$$\bar{\nu}_{\text{exp}} = \sum_i n_i \bar{\nu}_i$$

or

$$\lambda_{\text{max}} = \frac{10^3}{\sum_{i=1}^{4} n_i \bar{\nu}_i} \qquad (18)$$

where $\bar{\nu}_{\text{exp}}$ is the experimental absorption wavenumber (μm^{-1}), $\bar{\nu}_i$ is the contribution from each donor group to the ligand field of the complex and n_i is the number of equatorial donor groups. Even though this equation can predict structures of complexes with a reasonable accuracy, it cannot predict the structures which have axial coordinating ligands.

The ligands used in this study have four groups which donate electrons. These groups are the amine-N, the carboxyl-O, the amide-N and the carbonyl-O. Water can also donate electrons through the oxygen.[10] The groups which donate electrons to the metal and their corresponding contribution to the ligand field can be seen in Table 4.1 below.

Table 4.1: Relevant electron donor groups and their corresponding contribution to the ligand field.[10]

Electron donor group	Contribution to ligand field ($\bar{\nu}_i$) (μm^{-1})
N_{amino}	0.453
$N_{peptide}$	0.485
$O_{carboxylate}$	0.342
$O_{carbonyl/water}$	0.301

4.1.2 Experimental

The same ligand solutions that were prepared for potentiometic titrations were used for UV-Vis analysis, where each solution contained HCl and background electrolyte. 1:4 metal to ligand ratios were then prepared for copper(II) and nickel(II) ligand solutions. The pH of these solutions was then adjusted with NaOH to obtain a pH range from 2-11 in increments of pH 1. Exact metal ligand volumes and exact NaOH volumes which had been added were noted. The pH of the solution was measured with an accuracy of 0.1 using a Crison micropH 2000 pH meter, which was equipped with a Ω Metrohm glass electrode and the pH of each solution was recorded. The solutions were kept at a constant temperature of 25 ^{o}C. Spectrophotometric absorbance measurements were carried out on a Cray 50 recording spectrophotometer using a range from 200-800 nm. A blank was used to set the absorbance to zero. The calculation for the molar extinction coefficients for individual species cannot be achieved directly from the spectra. This is because there are mixed species present at each pH and the absorbance values will therefore include mixed species. ESTA suite of programs was therefore used to deconvolute the UV-Vis spectra and they were analysed in an in-house spectral fitting program (UV-SPEC) in order to obtain spectra of the individual copper(II) species present in the solution. From these spectra, proposed structures could then be obtained.

4.1.3 Results

During the potentiometric titrations, colour changes occurred in the copper(II) and nickel(II) ligand solutions. The copper(II) ligand solutions turned to a violet colour and the nickel(II) ligand solutions turned to a yellow colour as the pH was increased, while the zinc(II) ligand solutions remained colourless. The changing colour indicated that different complex species had formed at different pH values and each had different absorption spectra.[11]

4.1.3(a) Copper(II) complexes

The absorption spectra for the complexes formed from copper(II) and the two ligands, Gly-Leu-Phe and Sar-Leu-Phe can be seen in Figure 4.1 and Figure 4.2 respectively as a function of pH. As the pH increases from a very low value in both figures, the absorbance bands shift to a shorter wavelength in a blue shift manner and the intensity increases. The increase in intensity indicates that the colour of the solution is becoming more prominent. According to the Beer Lambert Law, this could either indicate that the extinction coefficients are increasing or the concentration of a particular complex species is increasing.[8] The shift to shorter wavelengths of between 538-561 nm indicates that the Crystal Field Splitting Energy between the e_g and t_{2g} orbitals is increasing.[11] This could indicate that a different coordination between the ligands and the metals is taking place between the pH values.[6] Alternatively, since each of these absorption bands are a combination of different complex species, some absorption bands could appear at an average wavelength for all the respective species. According to the speciation distribution diagrams for Cu-Gly-Leu-Phe and Cu-Sar-Leu-Phe, which can be seen in Figures 3.9 and 3.12 respectively, copper(II) complexes start forming from a pH of approximately 5. The absorption bands that show a maximum absorbance at a wavelength of approximately 770 nm for both ligands only occur at low pH values. This indicates that they are due to $Cu(H_2O)_6$, since $Cu(H_2O)_6$ has been recorded to have a wavelength band from 600-1000 nm, with a maximum at approximately 800 nm.[12] In Figures 4.1 and 4.2, the absorbance bands with a maximum of between 538-561 nm also correspond to the species distribution diagrams, because the species distribution diagrams show that the concentration and speciation of species change as the pH is increased. Since the

absorbance bands change in intensity as the pH increases, it therefore shows that the concentration and speciation of the species have changed with increasing pH values.

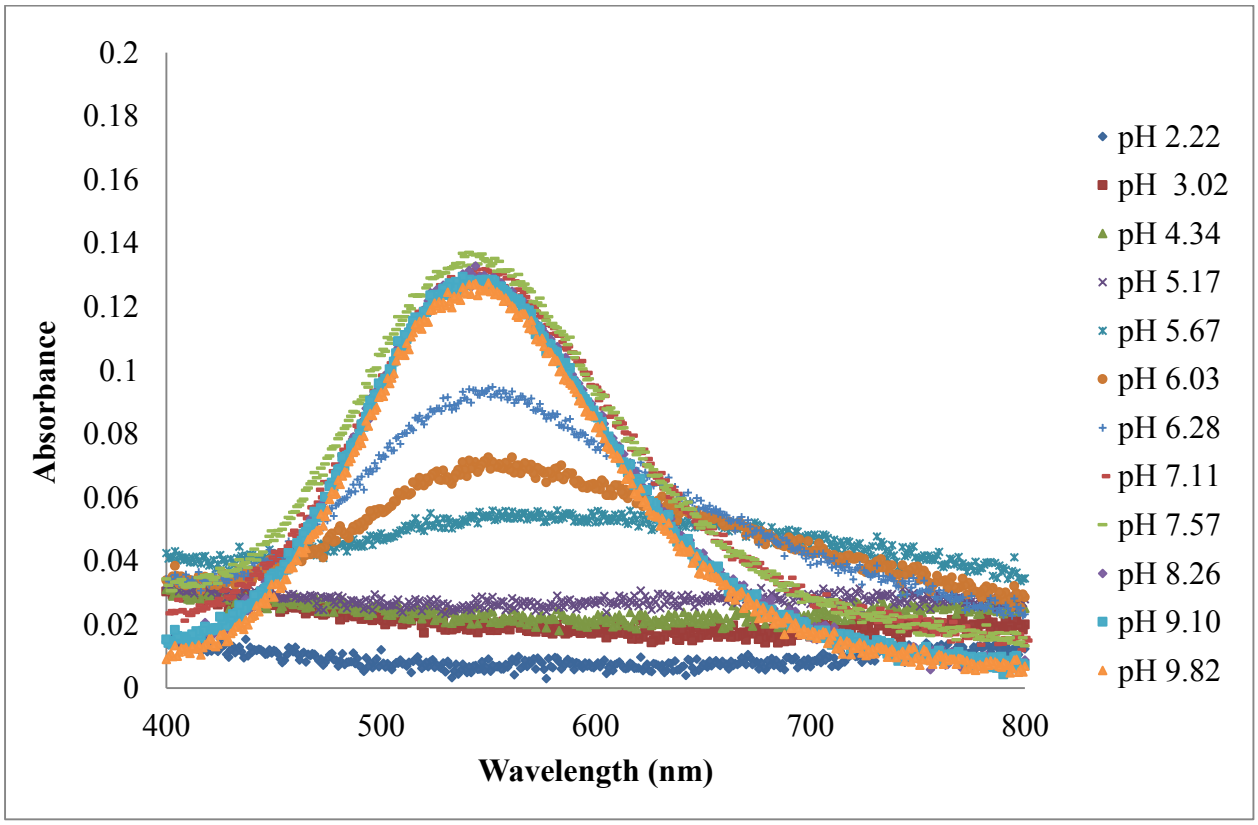

Figure 4.1: Electronic spectra for solutions containing 7.63 x10^{-4} mol.dm^{-3} of copper(II) and 0.0025 mol.dm^{-3} of Gly-Leu-Phe.

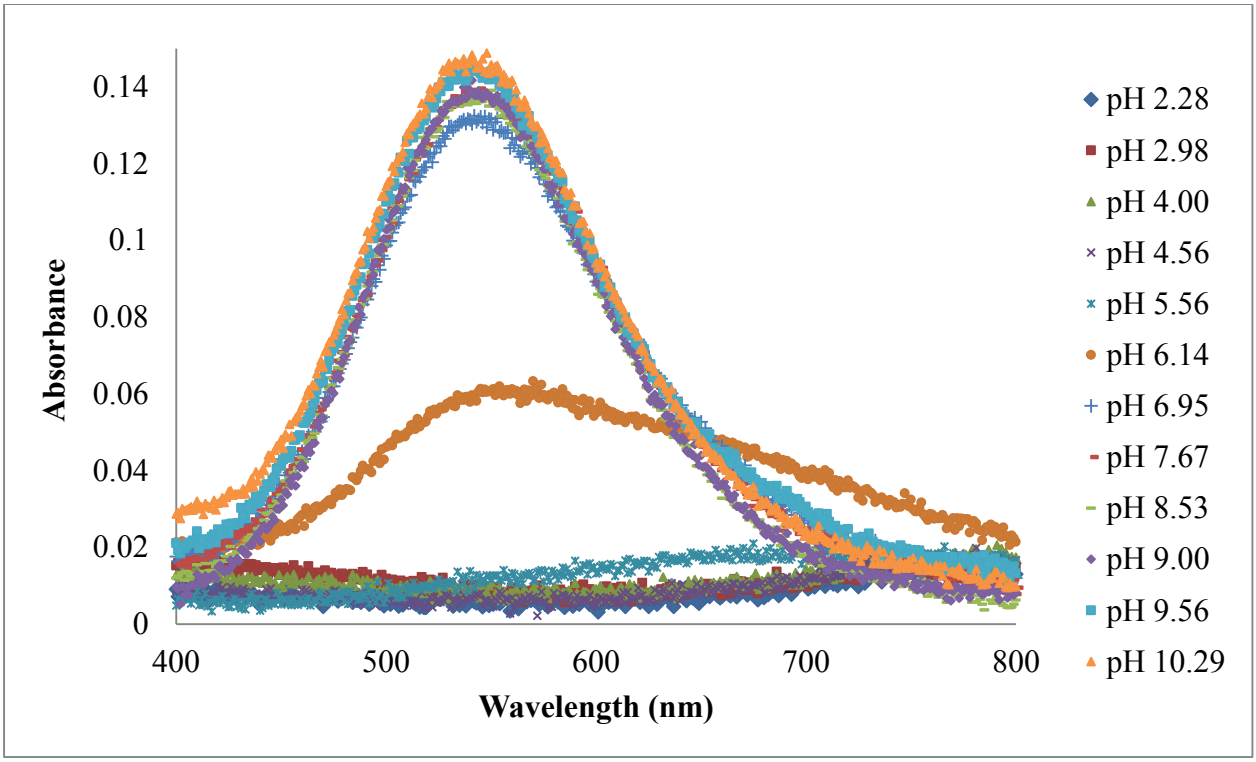

Figure 4.2: Electronic spectra for solutions containing 7.04 x 10^{-4} mol.dm^{-3} of copper(II) and 0.0025 mol.dm^{-3} of Sar-Leu-Phe.

After deconvoluting the spectra, using ESTA suite of programs, the spectra for individual species of copper(II) complexes for both ligands were plotted. The graphs which gave the molar absorption coefficients for each species of both the complexes, Cu-Gly-Leu-Phe and Cu- Sar-Leu-Phe as a function of wavelength, can be seen in Figures 4.3 and 4.4 respectively. Both graphs show smooth spectra, which verifies that the models are reasonable and correspond to the proposed potentiometric models. The change in molar absorption coefficients for copper(II) indicates that there is a change in the symmetry and coordination sphere of copper(II).[6] Figures 4.3 and 4.4 verify that copper(II) forms $Cu(H_2O)_6$, which was speculated from the presence of an absorption band occurring at low pH values seen in Figures 4.1 and 4.2.

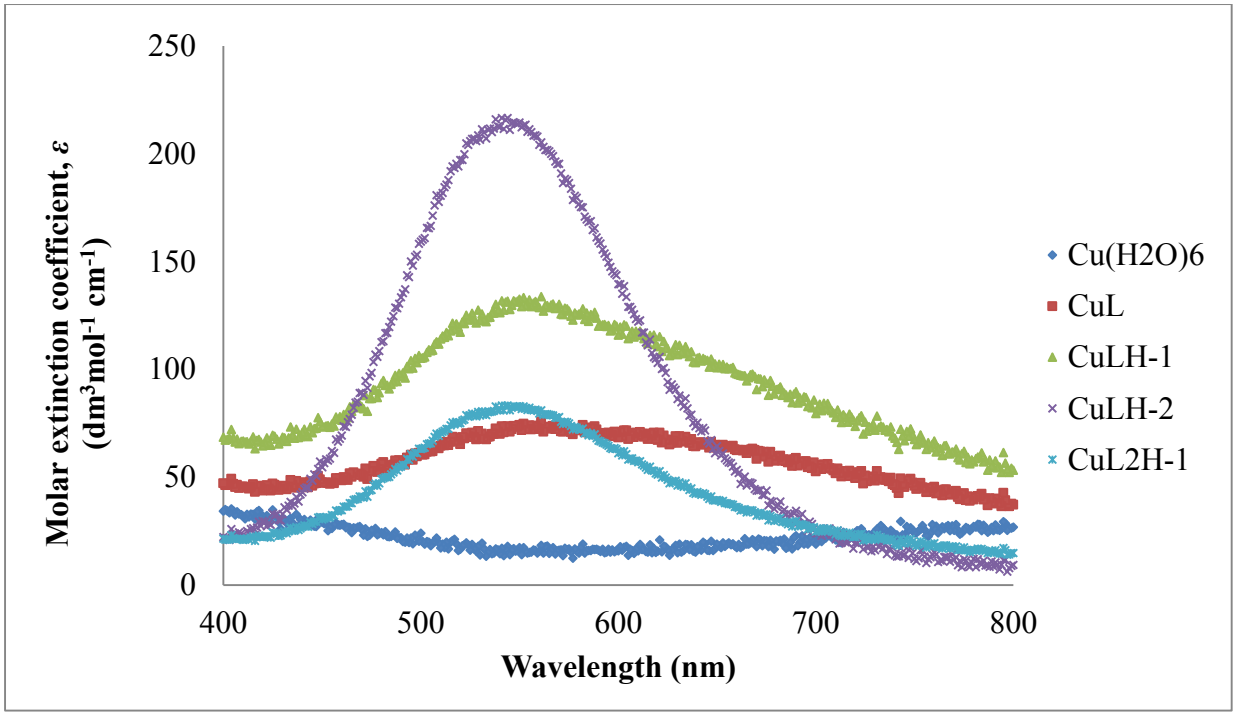

Figure 4.3: Calculated species absorption spectra for the copper(II) and Gly-Leu-Phe complexes as a function of wavelength.

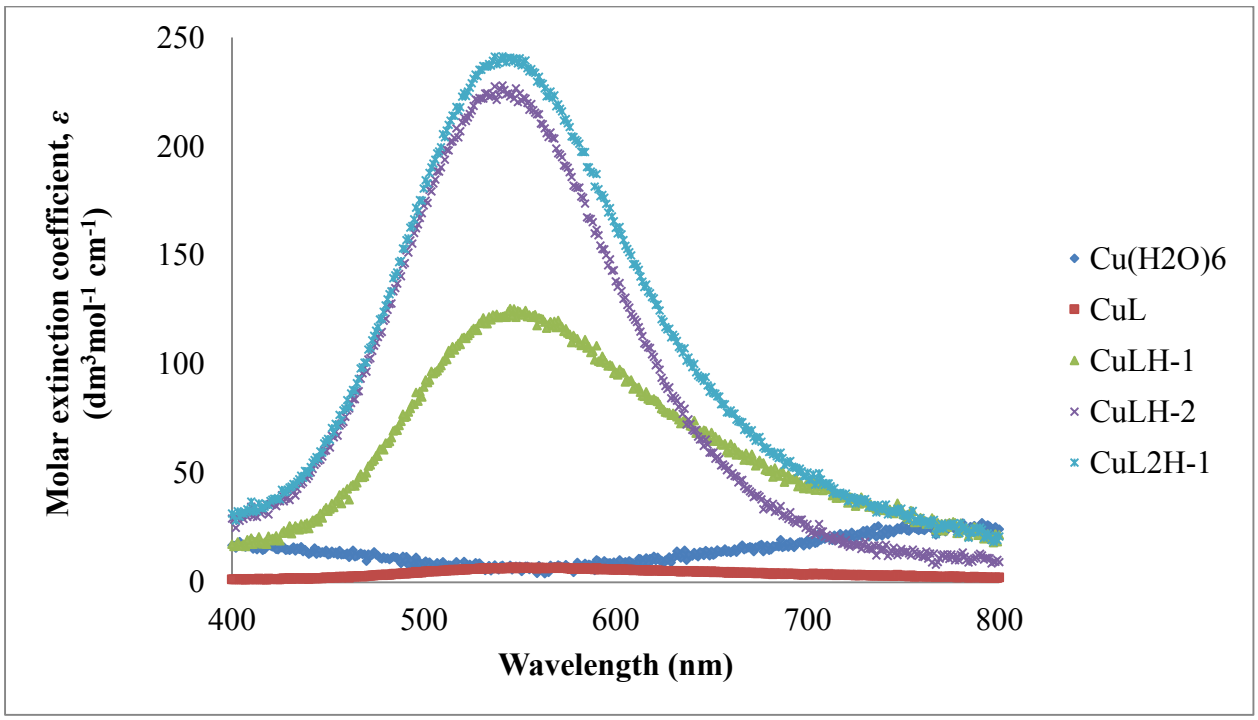

Figure 4.4: Calculated species absorption spectra for the copper(II) and Sar-Leu-Phe complexes as a function of wavelength.

The extinction coefficients and their corresponding wavelengths for the copper(II) complexes of Gly-Leu-Phe and Sar-Leu-Phe can be seen in Tables 4.2 and 4.3 respectively. Copper(II) ions have a d^9 configuration and are expected to form tetragonally distorted octahedral complexes. However, both ligands formed complexes which were a violet colour instead of the expected blue-violet colour and their single absorption band is around a wavelength of 538-561 nm instead of approximately 600 nm.[13] This could suggest that the complexes are highly tetragonally distorted octahedral complexes, which could also tend towards a square planar coordination. This is because a square planar coordination has a wavelength of 526 nm, which is close to the observed wavelengths of 538-561 nm.[14] The more distorted the octahedral coordination is, the more it will undergo axial or equatorial elongation. If it undergoes axial elongation it will tend towards a square planar complex coordination.[5,15]

The molar absorption coefficients range from 76 to 216 $dm^3mol^{-1}cm^{-1}$ for the Cu-Gly-Leu-Phe species and 124 to 240 $dm^3mol^{-1}cm^{-1}$ for the Cu-Sar-Leu-Phe species. The ML species from the Sar-Leu-Phe ligand was recorded to have a molar absorption coefficient of 8 $dm^3mol^{-1}cm^{-1}$, which is lower than the recorded molar absorption coefficient of $Cu(H_2O)_6$. This indicates that the molar absorption coefficient for the ML species of Cu-Sar-Leu-Phe is not realistic. A possible reason can be seen in the species distribution diagram in Figure 3.17. The maximum concentration of the ML species has a prevalence of approximately 20% and forms at the same pH as the formation of the MLH_{-1} species and therefore it is not possible to calculate the spectrum of each species. Thus the UV-SPEC programs could not deconvolute the spectra for the ML species, which resulted in the low and unrealistic molar absorption coefficient.

A typical octahedral environment extinction coefficient is about 10 $dm^3mol^{-1}cm^{-1}$.[5] Therefore the observed molar absorption coefficients verify that the coordination of the complex is unsymmetrical, since the larger the coefficient is, the less symmetrical the coordination is.[15] The lack of symmetry is due to Jahn Teller distortion, which allows the Laporte forbidden, spin allowed *d-d* transition of an octahedral complex to undergo electron *d-d* transitions and form an absorption band.[5] The absorption band for each species is a single broad band. However, for a tetragonally distorted octahedral system there are three spin allowed transitions. These transitions are $^2A_{1g} \leftarrow {}^2B_{1g}$, $^2B_{2g} \leftarrow {}^2B_{1g}$ and $^2E_g \leftarrow {}^2B_{1g}$. Since the absorption band for each species is broad, the separation between the three transitions cannot be distinguished and instead they appear as a single absorption.[16] The copper(II) species, which have low molar absorption coefficients could indicate that the complexes tend to be more

octahedral in coordination and the electron transition is more Laporte forbidden, which will result in a weak colour and hence low absorbance intensities.

Table 4.2: Maximum wavelengths corresponding to the molar absorption coefficients of individual complex species of copper(II) and Gly-Leu-Phe.

Species	λ_{max} (nm)	ε ($dm^3mol^{-1}cm^{-1}$)
$M(H_2O)_6$	775	25
ML	561	76
MLH_{-1}	546	132
MLH_{-2}	538	216
ML_2H_{-1}	543	83

Table 4.3: Maximum wavelengths corresponding to the molar absorption coefficients of individual complex species of copper(II) and Sar-Leu-Phe.

Species	λ_{max} (nm)	ε ($dm^3mol^{-1}cm^{-1}$)
$M(H_2O)_6$	768	22
ML	560	8
MLH_{-1}	542	124
MLH_{-2}	535	224
ML_2H_{-1}	541	240

4.1.3(b) Nickel(II) complexes

The absorption spectra for the complexes formed between nickel(II) and the two ligands, Gly-Leu-Phe and Sar-Leu-Phe can be seen in Figure 4.5 and Figure 4.6 respectively as functions of pH. Similarly to the copper(II) ligand absorbance bands, the intensities increase as the pH increases. Unlike the copper(II) ligand absorbance bands which start forming at low pH values, both Figures 4.5 and 4.6 show that the first absorbance bands only start forming at high pH values. This could indicate that the species formed at those low pH values either had very low concentrations or their extinction coefficients were too low to be detectable. This included the expected $Ni(H_2O)_6$ absorbance band, which should show an absorbance peak at 410 nm.[17] In both figures, baseline drifting can be seen. This could be due to the baseline drifting from the corrected value in the spectrophotometer. It could also be due to a large peak, which does not reach the baseline in the observed wavelength, but inevitably does at lower or higher wavelengths.

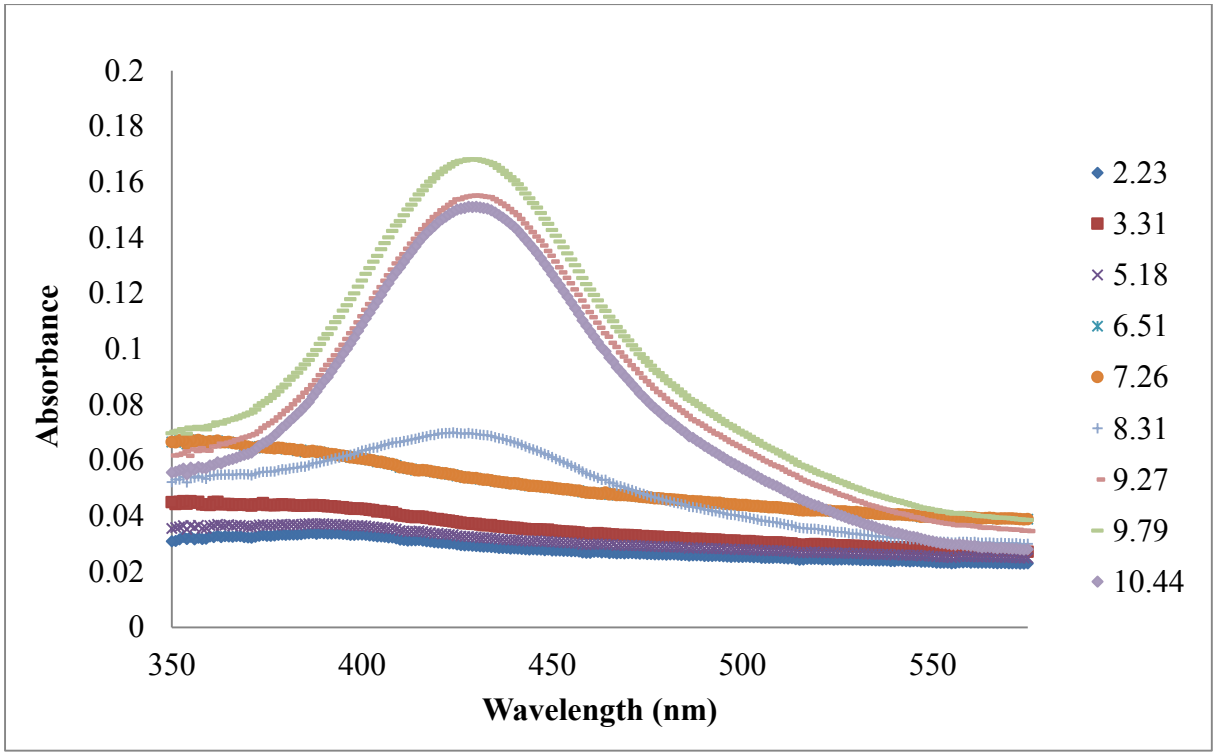

Figure 4.5: Electronic spectra for solutions containing 0.0009 $mol.dm^{-3}$ of nickel(II) and 0.0036 $mol.dm^{-3}$ of Gly-Leu-Phe.

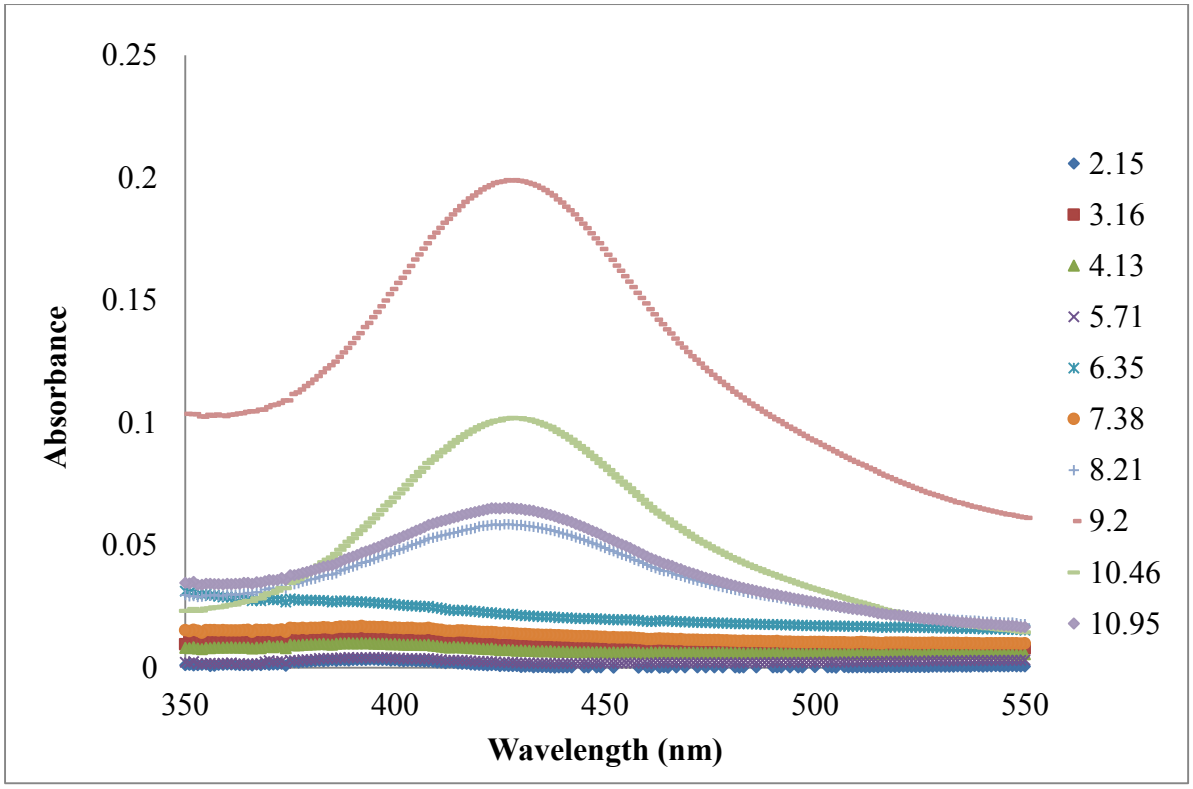

Figure 4.6: Electronic spectra for solutions containing 0.0009 mol.dm^{-3} of nickel(II) and 0.0037 mol.dm^{-3} of Sar-Leu-Phe.

Similarly to the copper(II) complexes, after deconvoluting the spectra, the spectra for individual species of nickel(II) for both ligands were plotted. The graphs, which gave the molar absorption coefficients for each nickel(II) species as a function of wavelength, can be seen in Figures 4.7-4.10. Figure 4.7 and 4.8 represent Model 1 and Model 2 of Ni-Gly-Leu-Phe respectively and Figure 4.9 and 4.10 represent Model 1 and Model 2 of Ni-Sar-Leu-Phe respectively. As was seen with the copper(II) complexes, all the graphs show smooth spectra and the change in molar absorption coefficients also indicates the change in symmetry and coordination sphere of nickel(II).[18] Figures 4.7-4.10, show absorption bands for the ML species as well as nickel(II) ions, which coordinate to water at low pH values. However, no visible absorption band was found in the pH range that would have contained these species. Therefore the spectrophotometer is most probably reading the baseline drift as an absorbance and giving it a molar absorption coefficient. Therefore all the molar absorption coefficient peaks which correspond to an ML species or to the nickel(II) ions are not credible.

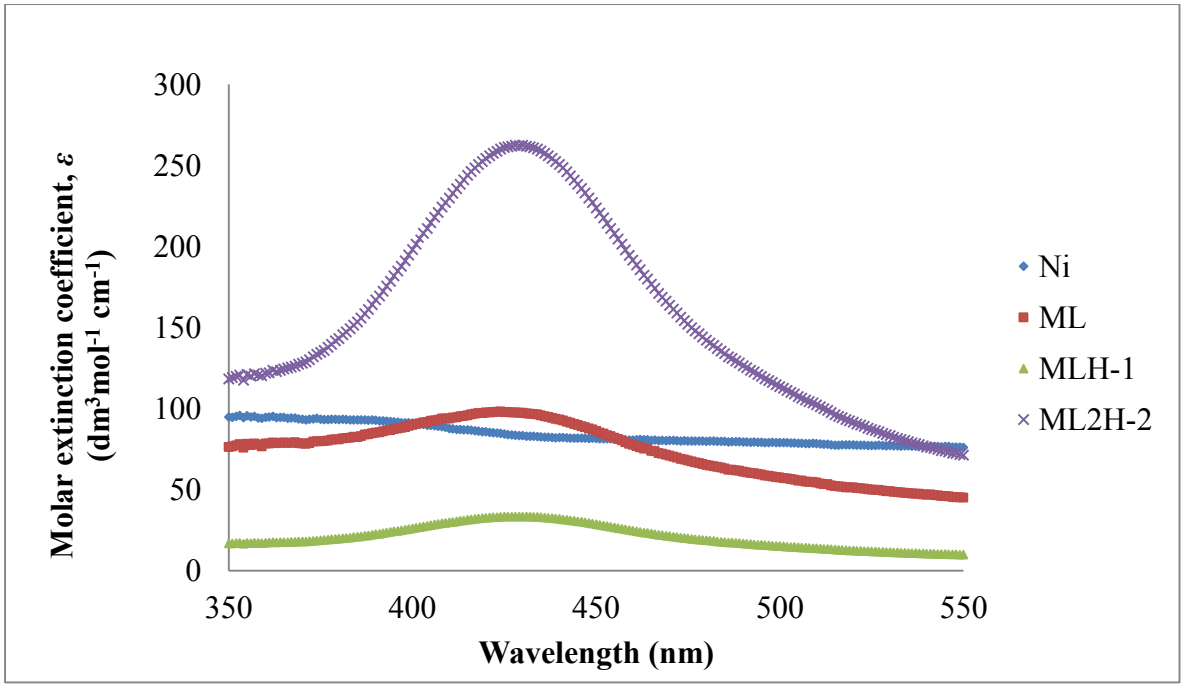

Figure 4.7: Calculated species absorption spectra of Model 1 for the nickel(II) and Gly-Leu-Phe complexes as a function of wavelength.

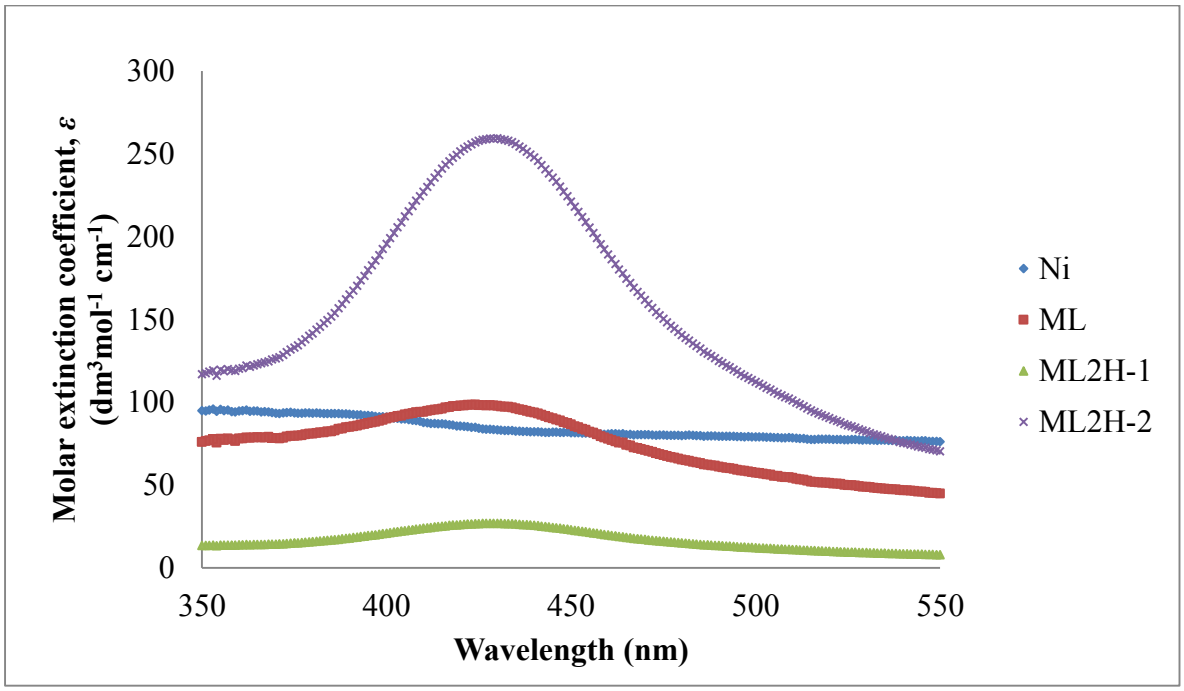

Figure 4.8: Calculated species absorption spectra of Model 2 for the nickel(II) and Gly-Leu-Phe complexes as a function of wavelength.

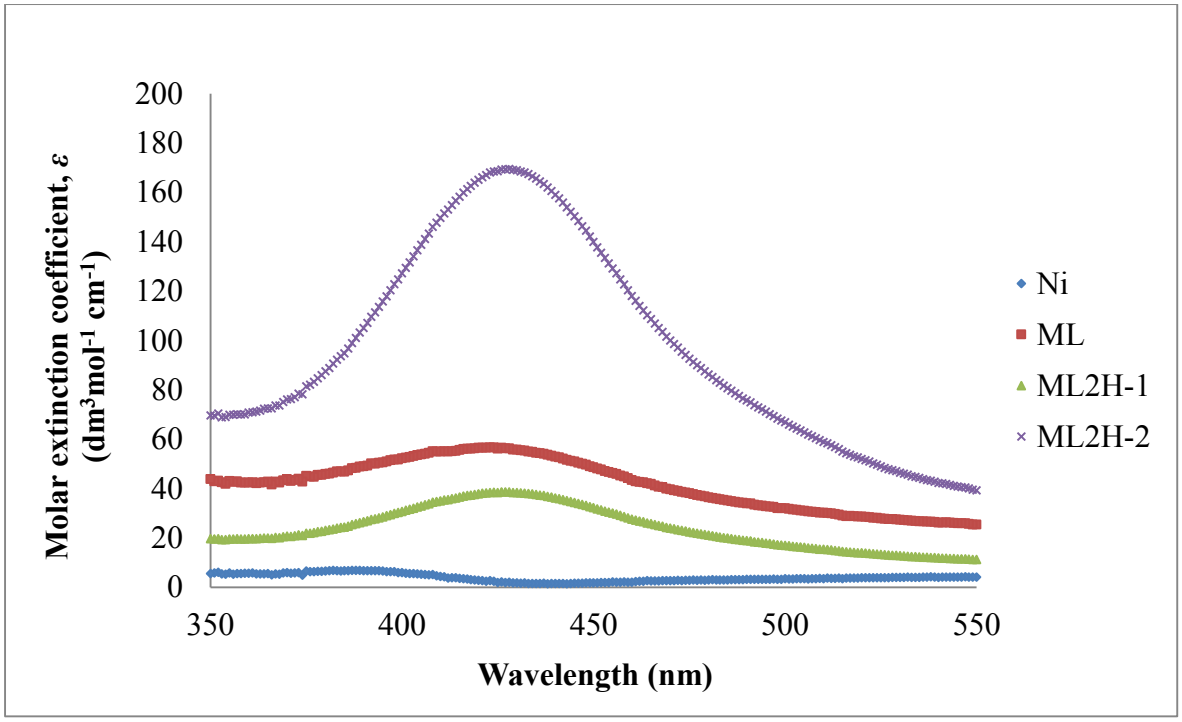

Figure 4.9: Calculated species absorption spectra of Model 1 for the nickel(II) and Sar-Leu-Phe complexes as a function of wavelength.

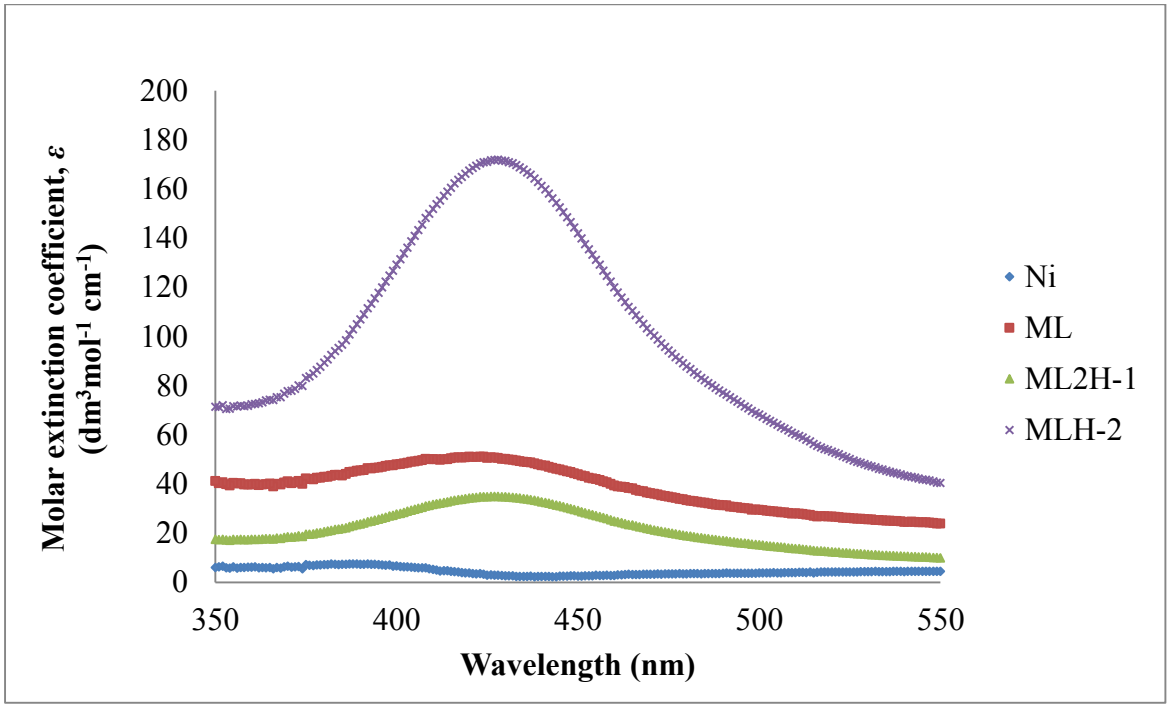

Figure 4.10: Calculated species absorption spectra of Model 2 for the nickel(II) and Sar-Leu-Phe complexes as a function of wavelength.

Nickel(II) is a d^8 configuration and since these complexes formed a yellow colour and all the wavelengths for the nickel(II) species were between 422-430 nm, it suggests that the structure of the nickel(II) complexes are square planar. The molar absorption coefficients all range between 33-260 $dm^3mol^{-1}cm^{-1}$, which also suggests that the coordination of nickel(II) is square planar.[19,20] These molar absorption coefficients and their corresponding wavelengths for the nickel(II) species can be seen in Tables 4.4 and 4.5 The square planar coordination of nickel(II) usually shows two absorption bands, which are close in wavelength. However, all these species absorption bands show a single broad absorption. The second absorption peak appears between 330-430 nm. If it appears in the higher wavelength region, both the first and second wavelength could form a single broad band. If the second absorption peak appears towards the lower wavelength region, then the spectrophotometer cannot measure it at those low wavelength values. The two absorption bands are due to the $^1A_{2g}\leftarrow{}^1A_{1g}$ and $^1B_{1g}\leftarrow{}^1A_{1g}$ *d-d* transitions.[19]

Table 4.4: Maximum wavelengths corresponding to the molar absorption coefficients of individual complex species for Model 1 and Model 2 of nickel(II) and Gly-Leu-Phe.

Species	λ_{max} (nm)	ε ($dm^3mol^{-1}cm^{-1}$)
	Model 1	
MLH_{-1}	430	33
ML_2H_{-2}	430	262
	Model 2	
ML_2H_{-1}	427	26
ML_2H_{-2}	429	259

Table 4.5: Maximum wavelengths corresponding to the molar absorption coefficients of individual complex species for Model 1 and Model 2 of nickel(II) and Sar-Leu-Phe.

Species	λ_{max} (nm)	ε ($dm^3mol^{-1}cm^{-1}$)
	Model 1	
ML_2H_{-1}	428	38
ML_2H_{-2}	428	169
	Model 2	
ML_2H_{-1}	427	34
MLH_{-2}	428	171

4.1.4 Discussion

The potentiometric titrations data provided a basis for determining the structures of the metal ligand complexes, since the formation of the specific species was determined, as well as whether the dissociated protons were from the amide or from water.

4.1.4(a) Copper(II) complexes

The ML, MLH_{-1}, MLH_{-2} and ML_2H_{-1} species all have a wavelength between 538-561 nm. The dipeptides, Gly-Phe and Sar-Phe have complex species corresponding to wavelengths of approximately 635 nm.[21] Since these dipeptides should have very similar ML, MLH_{-1}, ML_2H_{-1} and MLH_{-2} coordinations to the tripeptides in this study, a valid comparison can be made. The higher wavelengths for the dipeptides compared to these tripeptides show that the Crystal Field Splitting Energy is larger than expected. Amides are high on the spectrochemical series and therefore cause substantial crystal field splitting, which then corresponds to a shorter wavelength. Therefore the amides could be responsible for splitting the crystal field more than expected. Since the ML species has no amide coordination it should have the longest wavelength. The ML species of Cu-Gly-Leu-Phe has a slightly longer wavelength than the other species and thus corresponds to the assumption. Even though the molar absorption coefficient of the ML species of Cu-Sar-Leu-Phe was found to be unrealistic, the wavelength is realistic and since this ML species also has a slightly longer wavelength than the other species, it also correspond to the assumption.

Odisitse *et al*. found that the wavelengths corresponding to tetragonal distortion in a copper(II) complex were approximately 600 nm.[11,13] However, a third study by Odisitse *et al*. found absorption peaks for tetragonally distorted copper(II) complexes to be between 560-570 nm, which is closer to the wavelengths found for Cu-Gly-Leu-Phe and Cu-Sar-Leu-Phe.[18] However, comparing the wavelengths of Cu-Gly-Leu-Phe and Cu-Sar-Leu-Phe to the wavelengths in literature, it verifies that these wavelengths are smaller than expected and therefore the coordination could be square planar rather than the expected tetragonally distorted octahedral coordination.[11,13,18,21]

When Billo's equation was used, the calculated λ_{max} values did not correspond to any of the observed wavelength values for any of the species of both copper(II) complexes. Billo's equation does not incorporate axial donor groups besides axial water and therefore does not account for the subsequent possible structures.[9,10] This therefore suggests that the species of both copper(II) complexes could have donor groups coordinated in the axial positions, or that the complexes could tend towards a square planar geometry rather than a tegragonally distorted octahedral geometry.

As mentioned previously amides are high on the spectrochemical series and therefore cause substantial crystal field splitting. Based on the observed λ_{max} value of each species, a correlation can be made between the number of amide-N groups which copper(II) coordinates to and the λ_{max} values. As has already been discussed, the ML species for both copper(II) complexes have the longest observed λ_{max} values and thus copper(II) has not coordinated to the amide-N groups. The MLH_{-1} and ML_2H_{-1} species of both copper(II) complexes have approximately the same wavelength, while the MLH_{-2} species of both copper(II) complexes have a slightly shorter wavelength. This could indicate that copper(II) coordinates to one amide-N group in the MLH_{-1} and ML_2H_{-1} species and to possibly two in the MLH_{-2} species. Since the wavelengths are all very similar to one another, the differences between them could be within experimental error and therefore negligible. The potentiometic results indicated that the MLH_{-1} species in both copper(II) complexes lost the hydrogen from an amide-N. It also indicated that the MLH_{-2} species in the Cu-Gly-Leu-Phe complex lost the second hydrogen from an amide-N, but in the Cu-Sar-Leu-Phe complex the second hydrogen was either lost from an amide-N group or from water. Therefore the UV-Vis results agree with the potentiometric results.

4.1.4(b) Nickel(II) complexes

For the nickel(II) species, even though the ML species was not found in this UV-Vis study, it has been suggested by Agoston *et al*., that the ML species of square planar Ni(II) tripeptides involves nickel(II) coordinating to the amine-N and the carbonyl-O at the N-terminal as well as to two water molecules.[22] It has also been suggested, that the MLH_{-1}, ML_2H_{-1} and ML_2H_{-2} species are all formed from the deprotonation of one amide group with the overall coordination to the amine-N, amide-N, carboxyl-O and to one water molecule.[22] Lastly, it

was suggested that the MLH_{-2} species are formed from the deprotonation of two amide groups with the overall coordination to the amine-N, two amide-Ns and a carboxyl-O.[22] It was also noted by Agoston *et al*. that all the ML species of the nickel(II) tripeptides are paramagnetic and octahedral and that the MLH_{-2} species are always accompanied by a yellow colour, representing a square planar nickel(II) species.[22] This corresponded to the results that were obtained for the nickel(II) complex species in this study, since the ML species did not appear. Therefore it can be suggested that this is due to the Laporte forbidden octahedral coordination of the ML species. It also corresponded to the MLH_{-2} species, because of the large molar absorption coefficient associated with this species, which signifies that the coordination is non-symmetrical and thus will have an absorption band. The potentiometric species distribution graph verified this, since it showed that the MLH_{-2} species appears in the same pH range where the characteristic yellow colour of the square planar coordination was observed. The proposed coordinations of the nickel(II) species and their corresponding wavelengths can be seen in Table 4.6, including the unobserved ML species.

Table 4.6: Proposed coordinations of the nickel(II) species for the two ligands Gly-Leu-Phe and Sar-Leu-Phe, as well as the observed wavelengths of each species.

Nickel(II) Species for Gly-Leu-Phe		Observed wavelength (nm)	Electron donor groups				
			N-amino	N-peptide	O-carboxylate	O-carbonyl	O-water
Model 1	ML	-	1	0	0	1	2
	MLH_{-1}	430	1	1	1	0	1
	ML_2H_{-2}	430	1	1	1	0	1
Model 2	ML	-	1	0	0	1	2
	ML_2H_{-1}	427	1	1	1	0	1
	MLH_{-2}	429	1	2	1	0	0
Nickel(II) Species for Sar-Leu-Phe							
Model 1	ML	-	1	0	0	1	2
	ML_2H_{-1}	428	1	1	1	0	1
	ML_2H_{-2}	428	1	1	1	0	1
Model 2	ML	-	1	0	0	1	2
	ML_2H_{-1}	427	1	1	1	0	1
	MLH_{-2}	428	1	2	1	0	0

The UV-analysis also determined whether there were any differences in the two models for each nickel(II) ligand complex. Since both models for each ligand had approximately the same wavelengths and corresponding molar absorption coefficients, there were no UV differences and therefore this verifies that chemical grounds had to be used to determine the favourable model.

4.1.5 Conclusion

The UV-Vis analysis showed that all the wavelengths formed a λ_{max} between 538-561 nm and were smaller than expected compared to literature values.[11,13,18,21] Billo's method for determining the coordination of tetragonally distorted octahedral copper(II) species could not calculate any coordination modes for either of the copper(II) complexes. This suggested that in all species, the ligand donor groups either formed an axial coordination or that the geometry of all the species could be square planar. When correlating the number of possible amide-N coordinations to the observed λ_{max} values for each species, it was found that the ML species of both complexes are not coordinated to an amide-N. The MLH_{-1} and ML_2H_{-1} species of both complexes are coordinated to one amide-N, while the MLH_{-2} species of Cu-Gly-Leu-Phe is coordinated to two amide-N groups and the MLH_{-2} species of Cu-Sar-Leu-Phe is coordinated to either one or two amide-N groups.

The UV-Vis analysis also showed that the nickel(II) complexes were square planar and subsequent coordinations of the species were suggested. However, the ML species did not have an absorption band. A comparison with literature, showed that the ML species are paramagnetic and octahedral in coordination and therefore are Laporte forbidden and cannot be detected by UV-absorption.

References

1. P. W. Atkins, *Physical Chemistry*, Oxford University Press, Oxford, U. K., 2nd edn., 1982, pp. 583.
2. J. E. Huheey, *Inorganic Chemistry: Principles of Structure and Reactivity*, Harper and Row, New York, 3rd edn., 1983, pp. 368-412.
3. M. S. Silberberg, *Chemistry: The Molecular Nature of Matter and Change*, McGraw-Hill, New York, 5th edn., 2009, pp. 1049-1054.
4. E. F. H. Brittain, W. O. George and C. H. J. Wells, *Introduction to Molecular Spectroscopy: Theory and Experiment*, Academic Press, London, 1970, pp. 37.
5. C. E. Housecroft and A. G. Sharpe, *Inorganic Chemistry*, Pearson, London, 3rd edn., 2008, pp. 638-663.
6. R. J. Deeth and L. J. A. Hearnshaw, *J. Chem. Soc. Dalton Trans*., 2006, 1092-1100.
7. H. H. Jaffe and M. Orchin, *Theory and Applications of Ultraviolet Spectroscopy*, John Wiley & Sons, Inc., New York, 5th edn., 1970, pp. 526.
8. F. R. Hartley, C. Burgess and R. M. Alcock, *Solution Equilibria*, Ellis Horwood, Chichester, U.K., 1980, pp. 33-144.
9. E. Prenesti, P. G. Daniele, M. Prencipe and G. Ostacoli, *Polyhedron*, 1999, **18**, 3233-3241.
10. E. Farkas, E. Csapo, P. Buglyo, C. A. Damante and G. Di Natale, *Inorg. Chim. Acta*, 2009, **362**, 753-762.
11. S. Odisitse and G. E. Jackson, *Polyhedron*, 2008, **27**, 453-464.
12. G. L. Miessler and D. A. Tarr, *Inorganic Chemistry*, Pearson Education, Inc., Philippines, 3rd edn., 2004, ch. 11, pp. 380.
13. S. Odisitse, G. E. Jackson, T. Govender, H. G. Kruger and A. Singh, J. *Chem. Soc. Dalton Trans*., 2007, 1140-1149.
14. S. Nigam and H. Mohabey, *Asian J. Chem*., 2001**, 13,** 107-110.
15. R. C. Rosenberg, C. A. Root, P. K. Bernstein and H. B. Gray, *J. Am. Chem.* Soc., 1975, **97**, 2092-2096.
16. J. N. Zvimba and G. E. Jackson, *J. Inorg. Biochem*., 2007, **101**, 148-158.
17. A. Mittal, *Chemistry*, APH Publishing, New Delhi, 2007, ch. 1 pp. 267.
18. S. Odisitse and G. E. Jackson, *Inorg. Chim. Acta*, 2009, **362**, 125-135.

19. A. B. P. Lever, *Inorganic Electronic Spectroscopy*, Elsevier Publishing Company, Amsterdam, 1968, 124-146.
20. E. T. Nomkoko, G. E. Jackson, B. S. Nakani and S. A. Bourne, *J. Chem. Soc. Dalton Trans*., 2004, 1789-1796.
21. M. Mohajane, PhD Thesis, University of Cape Town, 2013.
22. C. G. Agoston, Z. Miskolczy, Z. Nagy and I. Sovago, *Polyhedron*, 2003, **22**, 2607-2615.

4.2 Infrared (IR) Spectroscopy

4.2.1 Introduction

Infrared spectroscopy studies the covalent bonding of molecular structures. Molecular structures are constantly rotating and vibrating. Each of these vibrational motions have their own natural frequency which originates from the mass of the atoms, the type of motion the molecule under goes and the strength of the bonds between the atoms. Therefore each bond in a molecular structure acts as though it were a flexible spring. The resulting frequencies from these vibrational motions are within 2.5 to 25 μm. This region is the IR region of the electromagnetic spectrum. Therefore the energies of these molecular vibrations are quantized and fall within the same range as the energies of the IR photons. Each bond absorbs in a characteristic IR wavelength range and therefore IR spectroscopy can be used to identify molecular structures.[1-5] The structure of Gly-Leu-Phe and Sar-Leu-Phe are known. However, when these ligands coordinate to a metal, the mode of metal coordination is not known. The possible sites for coordination are through the amine-N, the amide-N, the carbonyl-O and the carboxyl-O. Therefore by comparing the IR analysis of each ligand to the IR analysis of the metal ligand complexes, any change in peaks will indicate that a specific coordination has taken place. Thus the identification of changed peaks in the IR spectrum will contribute to the determination of the metal ligand structures. At different pH values, the coordination of the metal to ligand is expected to change and therefore the IR analysis for the metal ligand complex has to be analysed at different pH values in the range from 2-11.

4.2.2 Experimental

The ligand solutions were prepared by dissolving a 0.1 M concentration of Gly-Leu-Phe and Sar-Leu-Phe in D_2O and the pH of these ligands was measured to be pH 2. Before the metal was added, these ligand solutions were analysed at 25 °C using a Bruker Tensor FTIR with an ATR attachment. Copper(II) chloride was then added to the ligand solutions so that a 1:4 metal ligand ratio was prepared. The pH of these metal ligand solutions was adjusted so that the metal ligand solution of Gly-Leu-Phe was analysed at a pH of 5, 6, 7.6 and 9.6. The pH of the metal ligand solution of Sar-Leu-Phe was adjusted to a pH of 4.5, 6, 8 and 11. These respective pH values were chosen since different species dominate at these values, which corresponded to the potentiometric species distribution graphs. The pH values were not corrected for the D_2O isotope effect.

4.2.3 Results

Sections of IR spectral data for Gly-Leu-Phe and Cu-Gly-Leu-Phe as well as for Sar-Leu-Phe and Cu-Sar-Leu-Phe at various pH values can be seen in Figures 4.11 and 4.12 respectively. D_2O was used instead of water so that any change in stretching vibration frequency for the nitrogen donor and the amide oxygen could be seen during the complexation process.[6] This is because the O-H bond in water has large vibration frequencies in the 3200-3400 cm^{-1} and 1600 cm^{-1} region which will overlap the ligand and complex signals.[7,8]

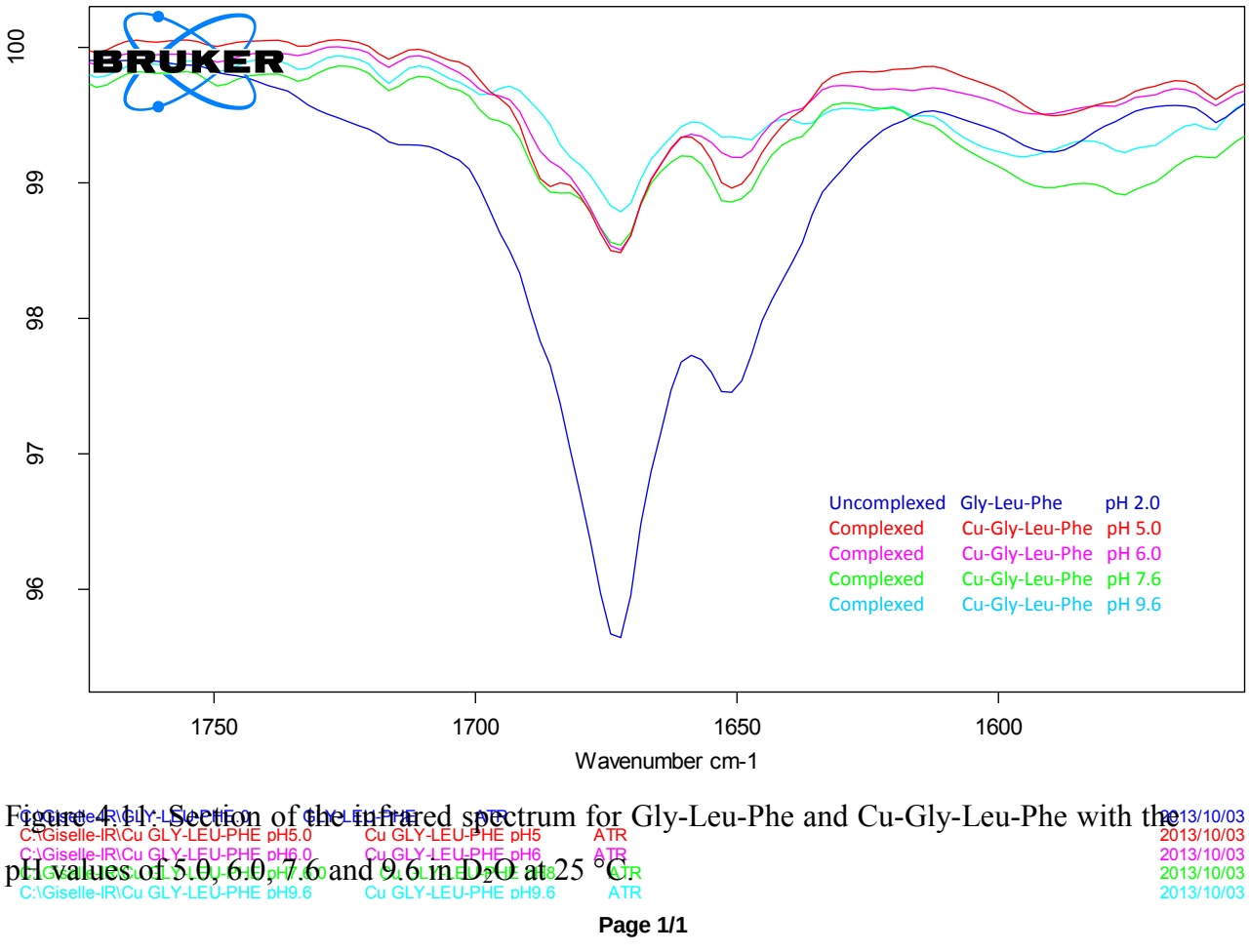

Figure 4.11: Section of the infrared spectrum for Gly-Leu-Phe and Cu-Gly-Leu-Phe with the pH values of 5.0, 6.0, 7.6 and 9.6 in D_2O at 25 °C

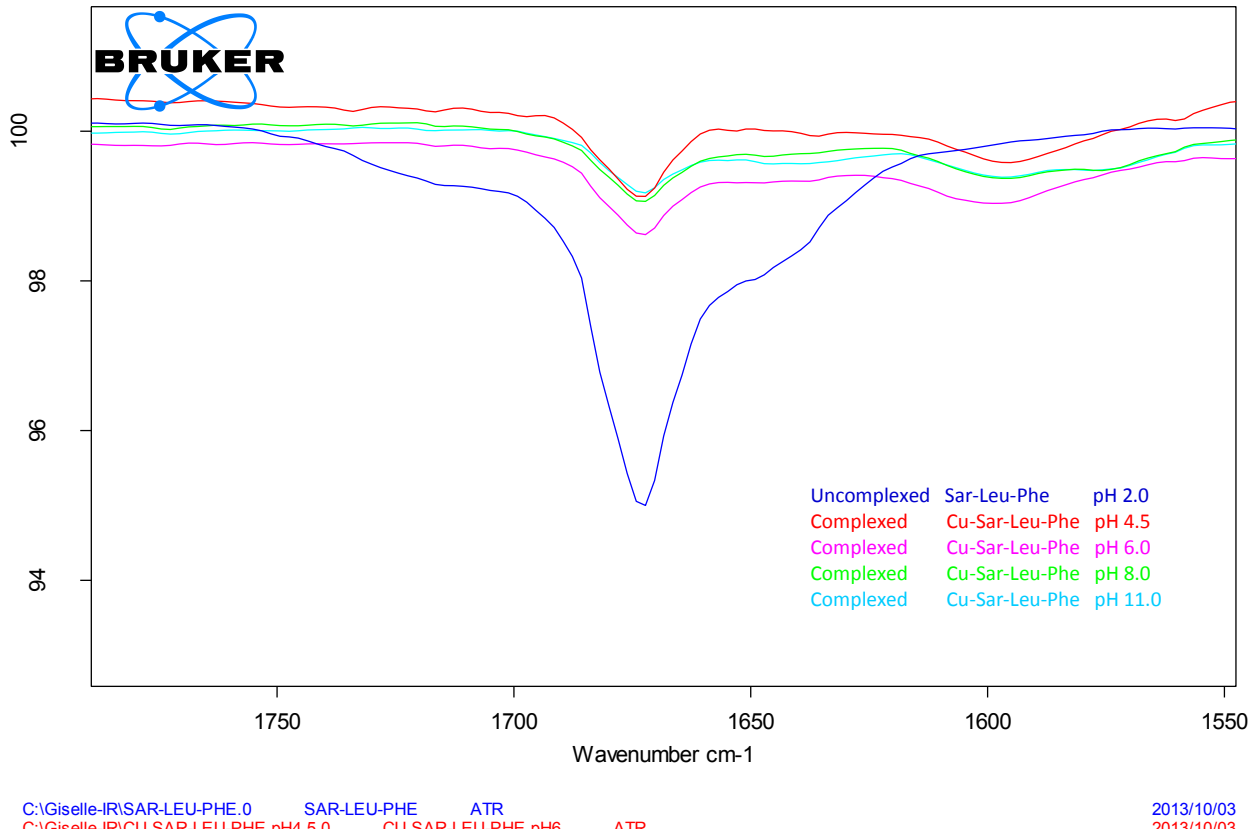

Figure 4.12: Section of the infrared spectrum for Sar-Leu-Phe and Cu-Sar-Leu-Phe with the pH values of 4.5, 6.0, 8.0 and 11.0 in D_2O at 25 °C.

4.2.4 Discussion

4.2.4(a) Gly-Leu-Phe

In Figure 4.11, the IR spectral data show that for the Gly-Leu-Phe ligand, a stretching vibration frequency for the uncoordinated amide carbonyl occurs at a frequency of 1675 cm^{-1}. A peak at 1590 cm^{-1} can also be observed in the region that was previously assigned by Odisitse *et al*.[9,10] and Steenland *et al*.[11] as the region which indicated the coordination to the amide carbonyl group through the oxygen. This region was also assigned by Kim *et al*.[7] as the region which indicates the coordination to the carboxyl group. However, the assignment for these coordinations could not be made, since the peak was already present before coordination had taken place and thus a change in the spectrums could not be seen.

A difference between the uncoordinated ligand and copper(II) coordinated ligand occurs at 1565 cm^{-1} where a new weak broad peak forms at the pH values of 6, 7.6 and 9.6. This peak corresponds to the assignment Odisitse *et al.* had made for the coordination to an amide carbonyl through the nitrogen.[9,10] Since the peak in Figure 4.11 is broad, it could also have incorporated the peak that indicates the coordination to the second nitrogen.[9,10] These peaks corresponded to the potentiometric species distribution graph, which showed that between the pH range of 6-9.6 the species lose either one or two hydrogen atoms.

The uncomplexed Gly-Leu-Phe ligand indicates a broad peak at 1720 cm^{-1}, which can be assigned as the protonated carboxyl group. Comparing this uncomplexed ligand to the metal coordinated ligand, it can be seen that the broad peak is no longer visible for all the pH values. This indicates that the protonated carboxyl peak is no longer present during complexation, which was expected since the pH had increased and therefore the carboxyl would have become deprotonated.

The coordination to either one or two amide-N groups, over the pH range from 6-9.6, also suggests that the MLH_{-1} and ML_2H_{-1} species are coordinated to one amide-N group and the MLH_{-2} species is coordinated to one or possibly two amide-N groups.

4.2.4(b) Sar-Leu-Phe

In Figure 4.12, the infrared spectrum of the uncomplexed Sar-Leu-Phe ligand, shows the presence of an uncoordinated carbonyl amide group at a stretching vibration frequency of 1675 cm^{-1}. This corresponds to the Steenland *et al*. assignment of 1665 cm^{-1}.[6,12] Comparing this uncomplexed ligand with the metal coordinated ligand at the recorded pH values of 4.5, 6, 8 and 11, the uncoordinated carbonyl amide peak decreases and a new peak forms at the frequency of 1595 cm^{-1}. This peak represents the coordination to a carbonyl amide group through the oxygen, which corresponds to the Odisitse *et al*. assignment of 1591 cm^{-1}.[9] However, the 1595 cm^{-1} peak can also be assigned to the coordinated carboxyl band, since Kim *et al*. found that the carboxyl band for triglycine occurred at 1595 cm^{-1}.[7]

There is still the presence of the uncoordinated carbonyl amide at the frequency of 1675 cm^{-1} in the complexation spectrum for all pH values. However, the area of the peak has been drastically reduced, which indicates that coordination to the carbonyl amide has taken place. Therefore the peak at 1595 cm^{-1} should represent the oxygen coordinated amide or the peak could also be a combination of the oxygen coordinated amide and the coordinated carboxyl. The presence of the uncoordinated carbonyl amide during complexation could be due to the 1:4 metal ligand ratio that was used to prepare the solution. Therefore the difference between the area of the peak in the uncoordinated ligand compared to the area of the peak in the copper(II) coordinated ligand at 1675 cm^{-1}, should represent a 3:4 ratio, since one quarter of the ligand was used for coordination to the metal. However, this was not observed. Instead only approximately one quarter of the original area remained and therefore the resulting outcome of the ligand cannot be determined.

Since, the 1595 cm^{-1} peak is present during all the pH values, the distinction between whether the peak represents the coordinated carbonyl amide through the oxygen or whether it represents the coordinated carboxyl group or both cannot be determined.

Similarly to Gly-Leu-Phe, the uncomplexed Sar-Leu-Phe ligand also shows a peak at 1720 cm^{-1}, which can be assigned as the protonated carboxyl group. This corresponds to literature, since Kim *et al*. found a protonated carboxyl group at 1720 cm^{-1}.[7] In comparison with the metal coordinated ligand, it can be seen that this peak is no longer visible for all the pH values. This also indicates that the protonated carboxyl peak is no longer present during complexation.

Another difference between the uncoordinated ligand and the metal coordinated ligand can be seen at the pH values of 8 and 11, where a new weak peak forms at a frequency of 1572 cm^{-1}. This peak could represent either the amide carbonyl that has a strong coordination through the nitrogen or, since the peak is broad, it could incorporate a second peak corresponding to the coordination to the second amide nitrogen as well. Odisitse *et al*. found that the peak at 1568 cm^{-1} corresponded to the coordination of the amide carbonyl through the nitrogen and the peak at 1578 cm^{-1} corresponded to the coordination to the second nitrogen.[9,10]

This also corresponded to the potentiometric distribution diagram, which showed that at a pH range of 8-11, the species present had lost either one or two hydrogens during coordination. However at a pH of 6, the MLH_{-1} species is dominant and the pK_a of this species suggests that the loss of hydrogen is from the amide. Therefore, the IR spectrum should also have shown a peak at 1572 cm^{-1} for the metal ligand complex at a pH of 6. A possible reason is that the peak at 1595 cm^{-1} is close to 1572 cm^{-1} and therefore the two peaks would overlap each other. The formation of a peak at 1572 cm^{-1} could therefore have been concealed.

The coordination to either the carboxyl-O or to the carbonyl-O or to both, over the pH range from 4.5-11 suggests that the ML, MLH_{-1}, MLH_{-2} and ML_2H_{-1} species are all coordinated to either one or to both groups. The coordination to either one or to two amide-Ns, over the pH range from 8-11 suggests that the ML_2H_{-1} species is coordinated to one amide-N group and the MLH_{-2} species is coordinated to one or possibly two amide-Ns.

4.2.5 Conclusion

There was substantial change in the IR spectra when comparing the spectrum of the uncoordinated ligands to the spectrum of the copper(II) coordinated ligands for different pH values. The change indicated that coordination had occurred. Many of the stretching frequencies for different coordinating groups overlapped one another and therefore it was difficult to separate them and determine the exact coordination mode of the complexes. The coordination of copper(II) to Gly-Leu-Phe could not be determined for the carboxyl-O or carbonyl-O groups, but the MLH_{-1} and ML_2H_{-1} species are coordinated to one amide-N and the MLH_{-2} species is coordinated to one or possibly two amide-Ns. In the coordination of copper(II) to Sar-Leu-Phe, the ML, MLH_{-1}, MLH_{-2} and ML_2H_{-1} species are coordinated to either carboxyl-O or to carbonyl-O or to both. The ML_2H_{-1} is also coordinated to one amide-N group and the MLH_{-2} is either coordinated to one or two amide-Ns.

References

1. M. S. Silberberg, *Chemistry: The Molecular Nature of Matter and Change*, McGraw-Hill, New York, 5th edn., 2009, ch. 23, pp. 1049-1054.
2. C. E. Housecroft and A. G. Sharpe, *Inorganic Chemistry*, Pearson, London, 3rd edn., 2008, ch. 21, pp. 638-663.
3. B. Stuart, *Biological Applications of Infrared Spectroscopy*, ed. D. J. Ando, John Wiley & Sons, Inc., New York, 1997, ch. 1, pp. 1-15.
4. M. R. Derrick, D. Stulik and J. M. landry, *Infrared Spectroscopy in Conservation Science*, *Scientific Tools for Conservation*, Getty Publications, USA, 2000, ch. 2, pp. 4-15.
5. P. Larkin, *Infrared and Raman Spectroscopy, Principles and Spectral Interpretation*, Elsevier, USA, 2011, ch. 1, pp. 1-7.
6. M. W. A. Steenland, P. Westbroek, I. Dierck, G. G. Herman, W. Lippens, E. Temmerman and A. M. Goeminne, *Polyhedron*, 1999, **18**, 3417-3424.
7. M. K. Kim and A. E. Martell, *J. Am. Chem.* Soc., 1966, **88**, 914-918.
8. N. D. Mitrofanova, L. I. Martynenko and V. I. *Inorg. Anal. Chem*., 1971, **20**, 2010-2014.
9. S. Odisitse and G. E. Jackson, *Polyhedron*, 2008, **27**, 453-464.
10. S. Odisitse and G. E. Jackson, *Inorg. Chim. Acta*, 2009, **362**, 125-135.
11. M. W. A. Steenland, P. Westbroek, I. Dierck, G. G. Herman, W. Lippens, E. Temmerman and A. M. Goeminne, *Polyhedron,* 1999, **18**, 3417-3424.
12. M. W. A. Steenland, I. Dierck, G. G. Herman, B. Devreese, W. Lippens, J. Van Beeumen and A. M. Goeminne, *J. Chem. Soc. Dalton Trans*., 1997, 3637-3642.

4.3 ^{1}H NMR Spectroscopy

4.3.1 Introduction

The properties of ^{1}H NMR techniques can be used to determine the binding sites of metal ions to ligands. Copper(II) is a paramagnetic metal ion and will thus have strong interactions between the unpaired electrons of copper(II) and the nuclei of the ligand, which can affect both the chemical shifts and relaxation rates of the ligand nuclei. The chemical shift of a nucleus in a paramagnetic complex is affected by two contributing factors; a diamagnetic factor and a paramagnetic factor. In the diamagnetic factor, the chemical shift is affected by the structural changes that occur when the metal binds to the ligand and it is also affected by the magnetic field that has been induced by the charge of the metal ion. In the paramagnetic factor the chemical shift is affected by a contact shift, which is a through-bond effect that is caused by scalar coupling between the nuclei and the unpaired electrons, as well as by a pseudocontact shift, which is a through-space effect that is caused by the interaction between the magnetic dipoles of the nuclei and the unpaired electrons.[1,2]

The relaxation rates of the nuclei are increased as a paramagnetic metal ion binds to the ligand due to a through-space effect, which again is caused by the interaction between the magnetic dipoles of the nuclei and the unpaired electrons. This increase can give information about the binding sites of the metal ion, since it depends on the distance between the nuclei of the ligand and the paramagnetic metal ion. Increased relaxation rates cause the ^{1}H MNR signals that are close to the binding sites of the metal ion to broaden and therefore indicate the location of the binding sites.[3-8] The transverse relaxation time (T_2) is what determines the line width of the peaks and the equation for line broadening can be seen below:

$$T_2 = \frac{1}{\pi W_{1/2}} \tag{19}$$

where $W_{1/2}$ is the line width at half height.[9]

When a ligand is in the presence of a copper(II) salt, the nuclear spin of the ligand exchanges between the paramagnetic bound and diamagnetic free sites.[10] Depending on the speed of the exchange with respect to the NMR time scale, the nmr spectrum will either be resolved for individual environments or taken as an average of the two environments. If the exchange rate is slower than the NMR time scale then both individual environments will be resolved, whereas an average will be seen if the exchange is faster. The NMR time scale is dependent on the field strength and on each particular experimental setup and therefore it is unique.[11]

A method that has been used to observe the broadening of ^{1}H NMR signals is to titrate the ligand with copper(II) at a predetermined pH. This will allow the broadening of the ^{1}H NMR signals to occur gradually and therefore make the structural analysis visually convenient to process.[12]

As discussed before, the structure of the ligands are known, but the coordination modes of the copper(II) complexes are not known. Therefore by titrating the ligand with copper(II) at a specific pH, where a species of the complex is expected to have the maximum concentration, the coordination modes of each species may be determined. The possible binding sites for copper(II) are the amine-N, the amide-N, the carbonyl-O and the carboxyl-O, which can be seen in Figure 4.13.

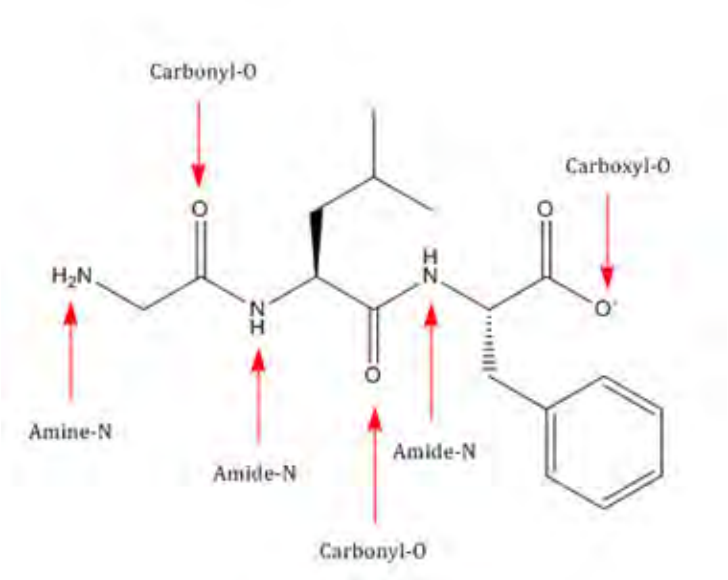

Figure 4.13: Illustration of the possible binding sites for copper(II) onto the Gly-Leu-Phe ligand. Sar-Leu-Phe has the same binding sites.

4.3.2 Experimental

A 0.0139 M solution of Sar-Leu-Phe and a 3.82 x10^{-3} M solution of Gly-Leu-Phe were prepared using D_2O. Tertiary butyl alcohol was added as an internal reference and the pD was adjusted using NaOD/DCl. A Crison micropH 2000 pH meter, which is equipped with a Ω metrohm glass electrode was used to record the pH of each solution with an accuracy of 0.1. Since a pH meter was used to measure the pD of the solution, corrections were made for the isotope effect on the pH reading according to the following equation described by Popov *et al*.[13] as well as Glasoe and Long.[14]

$$pD = \text{pH meter reading} + 0.44 \quad (20)$$

pH values were chosen to correspond to the maximum concentration of a single species according to the species distribution diagrams. A copper(II) solution of 0.01 M and 0.001 M was prepared using D_2O. The 0.01 M copper(II) solution was titrated in increments of 10-15 µl into each of the different pH solutions for Sar-Leu-Phe and the 0.001 M copper(II) solution was titrated in increments of 10-15 µl into each of the different pH solutions for Gly-Leu-Phe. During each titration the pH of each solution was checked and kept constant. ^{1}H NMR spectra were recorded on a Bruker 300 MHz spectrometer and processed using MestReNova software, version 9.1.

4.3.3 Results

The numbering for the proton assignments in the ^{1}H NMR spectra for Gly-Leu-Phe and Sar-Leu-Phe can be seen in Figures 4.14 and 4.15 respectively. This proton numbering system will be used to analyze the ^{1}H NMR spectra for the protonation of each ligand over a pH range from 2-11, as well as the ^{1}H NMR spectra as each ligand is titrated with copper(II) at a predetermined pH value.

4.4.3(a) Protonation of Gly-Leu-Phe and Sar-Leu-Phe

The two available sites for protonation in the ligands Gly-Leu-Phe and Sar-Leu-Phe are the amine and carboxyl groups. During the potentiometric analysis the pK_a values for the protonation of the carboxyl group were found to be 3.21 for Gly-Leu-Phe and 3.18 for Sar-Leu-Phe. The pK_a values for the protonation of the amine were found to be 8.25 for Gly-Leu-Phe and 8.34 for Sar-Leu-Phe. ^{1}H NMR can be used to identify the protonation sites in ligands. In this case the protonation sites of the two ligands are already known, but the chemical shifts that occur in the spectra as the pH of the solution changes, is not known. These chemical shifts are needed in order to analyze the effect copper(II) has in the ^{1}H NMR spectrum, when each ligand is titrated with copper(II). For all the ^{1}H NMR spectra, D_2O was used as a solvent and therefore the protons on the amine, amide and carboxyl groups will exchange with deuterium and cause the proton signals for these groups to disappear.[15]

Figure 4.14 and Figure 4.15 show the ^{1}H NMR spectra of Gly-Leu-Phe and Sar-Leu-Phe respectively over an increasing pH range. As the pH increased, peak **g** in Figure 4.14 shifted towards a lower ppm, which indicates that there is increased shielding. The increased shielding verifies that the amine group has been protonated. In Figure 4.15, peaks **g** and **h** also shifted towards a lower ppm as the pH increased. Similarly to Figure 4.14, the shift indicates increased shielding and also verifies the protonation of the amine group. The deprotonation of the carboxyl group in both ligands cannot be seen by the ^{1}H NMR spectra, since the pH is above the pK_a of the carboxyl group. Figure 4.16 and Figure 4.17 show the change in chemical shifts for selected protons in Gly-Leu-Phe and Sar-Leu-Phe respectively as a function of pH. Protonation constants can be estimated from the inflection point of each curve. In Figure 4.16 only ‘g’ exhibited an inflection point, which was found to be at a pH of

approximately 8.2 and therefore this is also the estimated protonation constant, which corresponds to the pK_a value of 8.25. In Figure 4.17 both ‘g’ and ‘h’ exhibited an inflection point at the same pH value, which was found to be at approximately 8.2 and therefore corresponds to the pK_a value of 8.34.

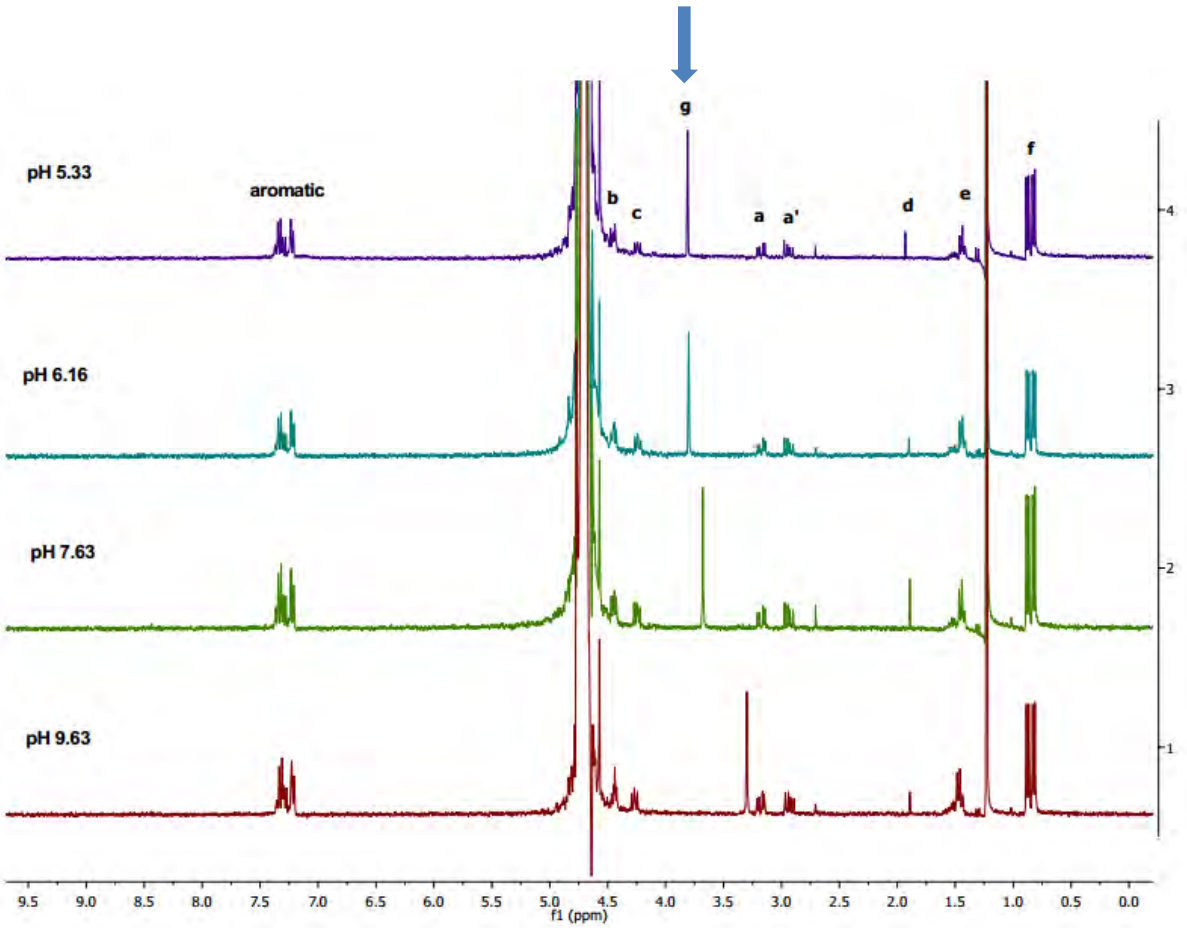

A

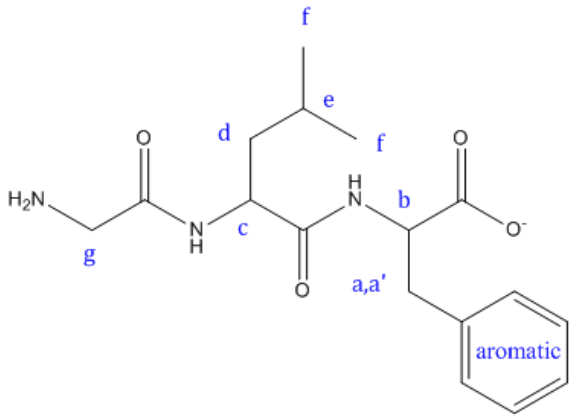

B

Figure 4.14: A: ^{1}H NMR spectra of Gly-Leu-Phe at increasing pH values from 2-11. An arrow has been added to indicate the shifting of peak **g** over increasing pH values. B: The proton assignments.

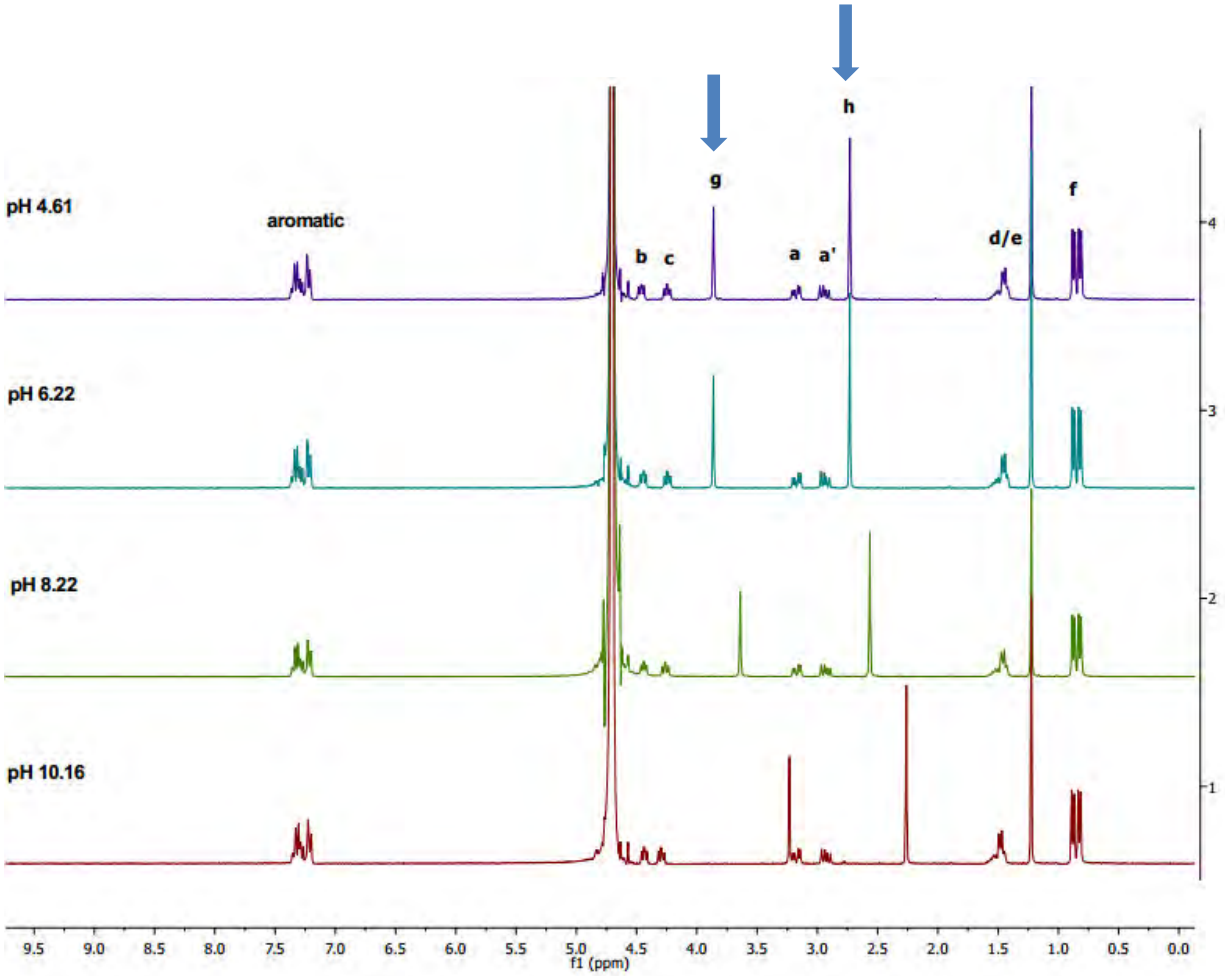

A

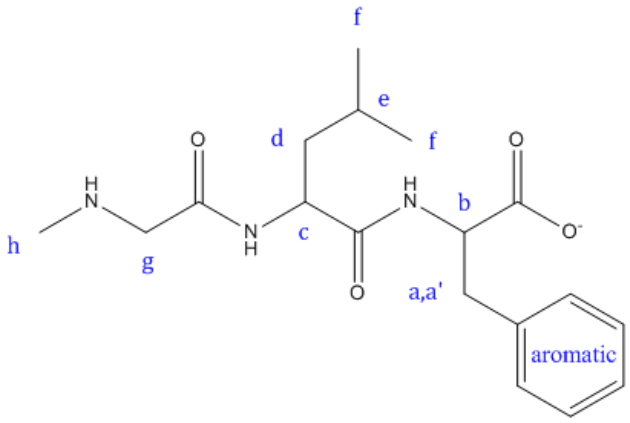

B

Figure 4.15: A: ^{1}H NMR spectra of Sar-Leu-Phe at increasing pH values from 2-11. Arrows have been added to indicate the shifting of peak **g** and **h** over increasing pH values. B: The proton assignments.

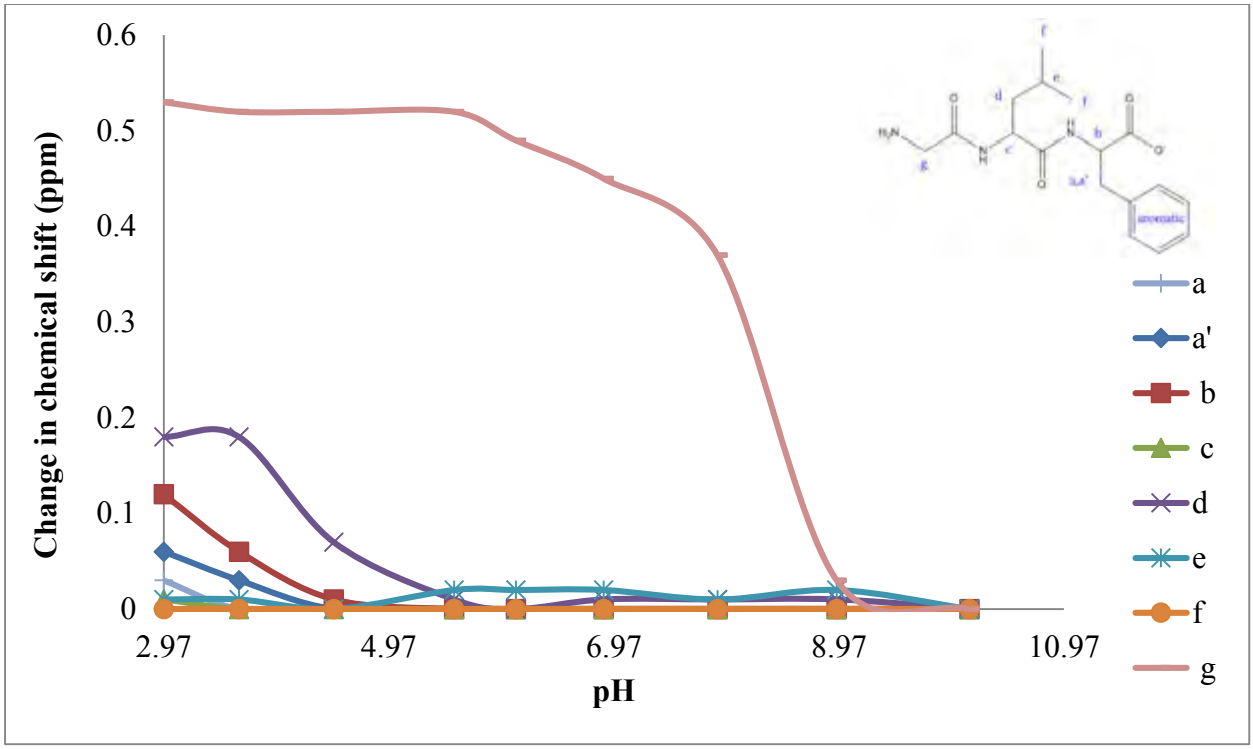

Figure 4.16: The change in Gly-Leu-Phe ^{1}H chemical shift as a function of pH.

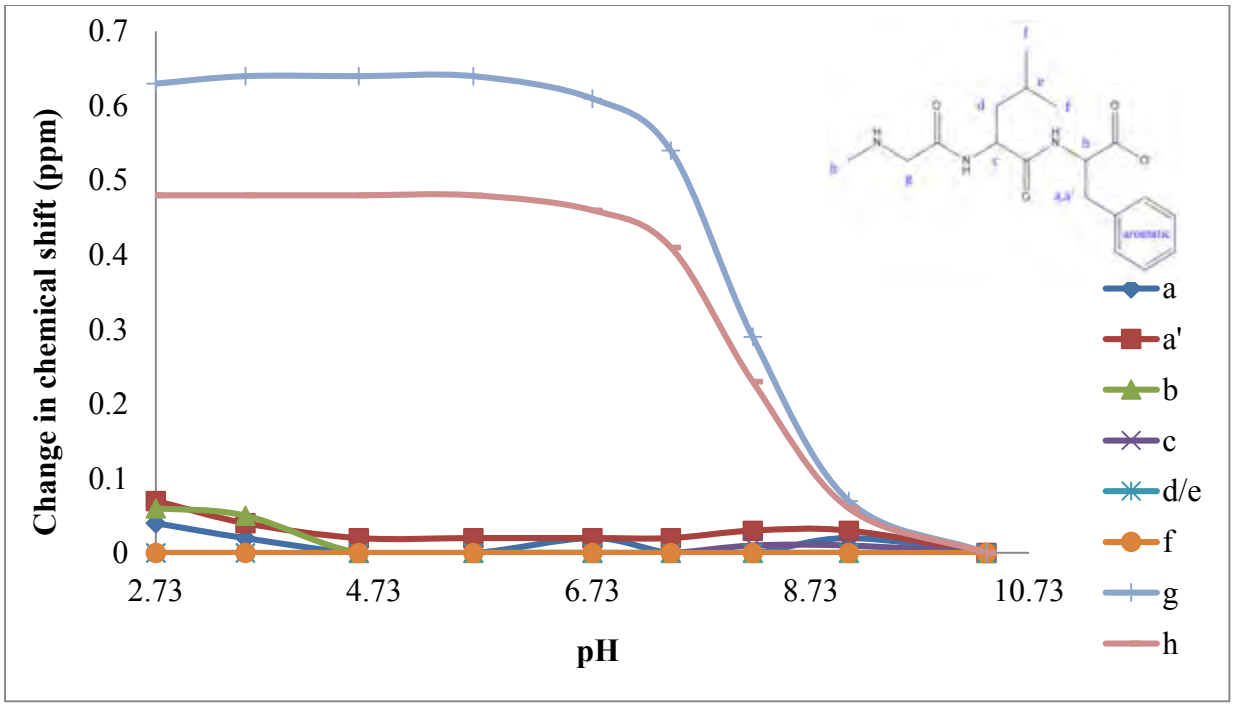

Figure 4.17: The change in Sar-Leu-Phe ^{1}H chemical shift as a function of pH.

4.3.3(b) Titration of Gly-Leu-Phe and Sar-Leu-Phe with copper(II)

For both ligand complexes, the pH values were chosen so that the maximum concentration of a single species type would be present during the copper(II) titration. However, the distribution of these species over a pH range from 2-11 is specific for a 1:4 copper(II) ligand ratio and could differ for other ratios. Therefore, when titrating each ligand with copper(II), the distribution of species for both ligands may change over the pH range from 2 to 11 and thus must be considered during the analysis. Another aspect is that the species type may also change to another form other than the four found species (ML, MLH_{-1}, ML_2H_{-1}, and MLH_{-2}) for a 1:4 metal ligand ratio.

4.3.3(b.i) Cu-Gly-Leu-Phe

The titration of Gly-Leu-Phe with copper(II) was analyzed at a pH of 5.33, 6.16, 7.62 and 9.63 and can be seen in Figures 4.18-4.21 respectively. In all pH values, peak **g** broadens greatly which indicates that copper(II) has coordinated to the amine-N in all the species.

For the pH value of 5.33, which can be seen in Figure 4.18, peak **c** broadens more than the other peaks. This indicates that copper(II) is coordinated to Leu-N, Leu-O or Gly-O. Coordination to Phe-N can be discounted because peak **b** does not broaden. The ML species is assumed to predominate at this pH, and so coordination to Leu-N, which could only occur by deprotonation of the amide, is discounted from the stoichiometry of the complex. The UV-Vis analysis also found that copper(II) in the ML species does not coordinate to the amide-N groups. Without a quantitative analysis it is not possible to distinguish between the two carbonyl groups.

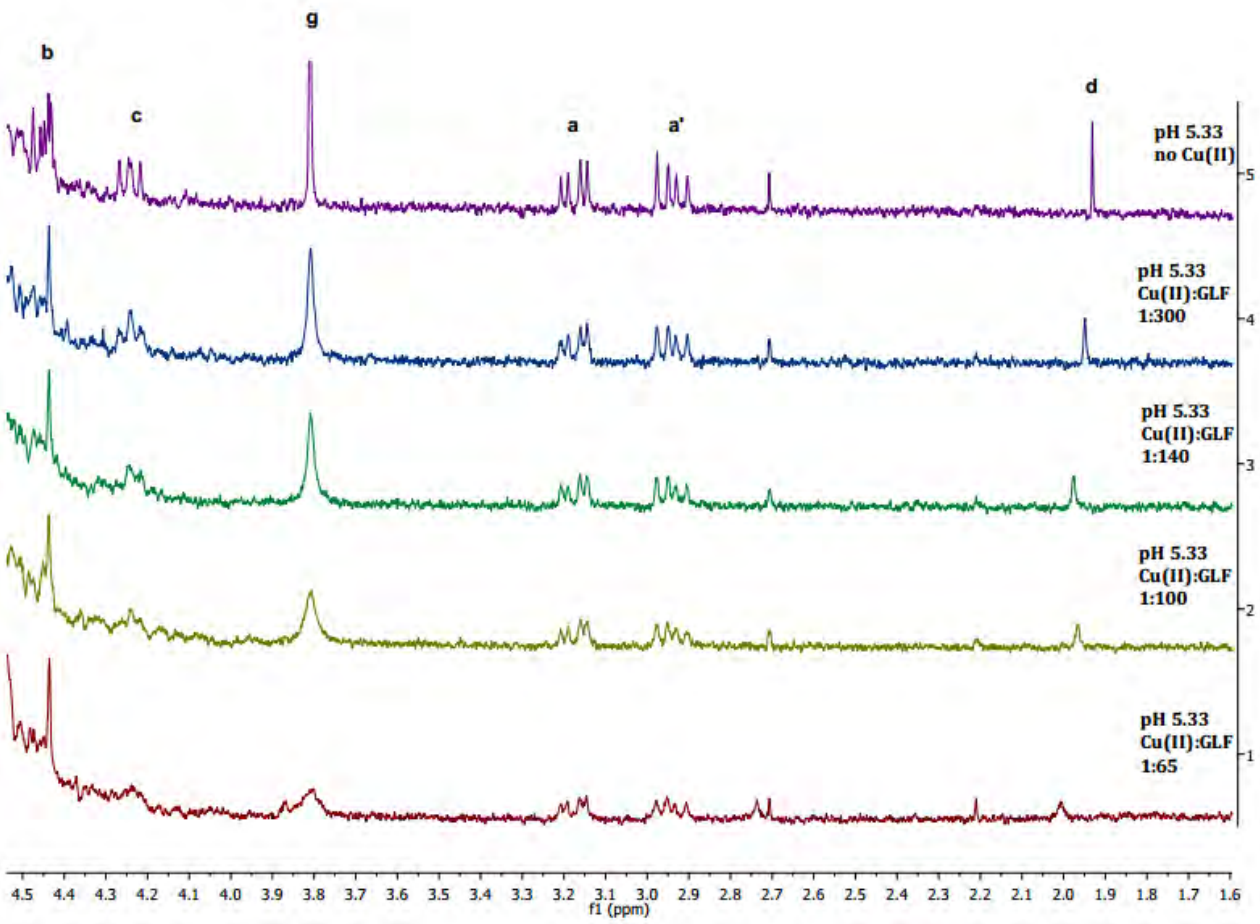

A

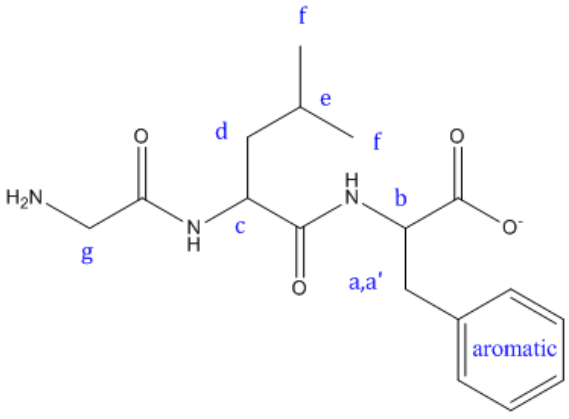

B

Figure 4.18: A: ^{1}H NMR spectra of the titration of Gly-Leu-Phe with copper(II) at a pH of 5.33 in D_2O. B: The proton assignments for Gly-Leu-Phe.

For the pH value of 6.16, which can be seen in Figure 4.19, peak **c** broadens more than the other peaks. Again this indicates that the copper(II) is coordinated to Leu-N, Leu-O or Gly-O. In this case an argument can be made that the increased broadening is due to the coordination to Leu-N as well as to Leu-O, as these sites are closer to proton **c**. The predominant species at this pH is assumed to be $MLH_{-1,}$ which is consistent with the loss of an amide proton. The potentiometric analysis also suggested that MLH_{-1} species is formed by the loss of a proton from the ligand and not water and the IR and UV-Vis analyses suggested that copper(II) is coordinated to one amide-N.

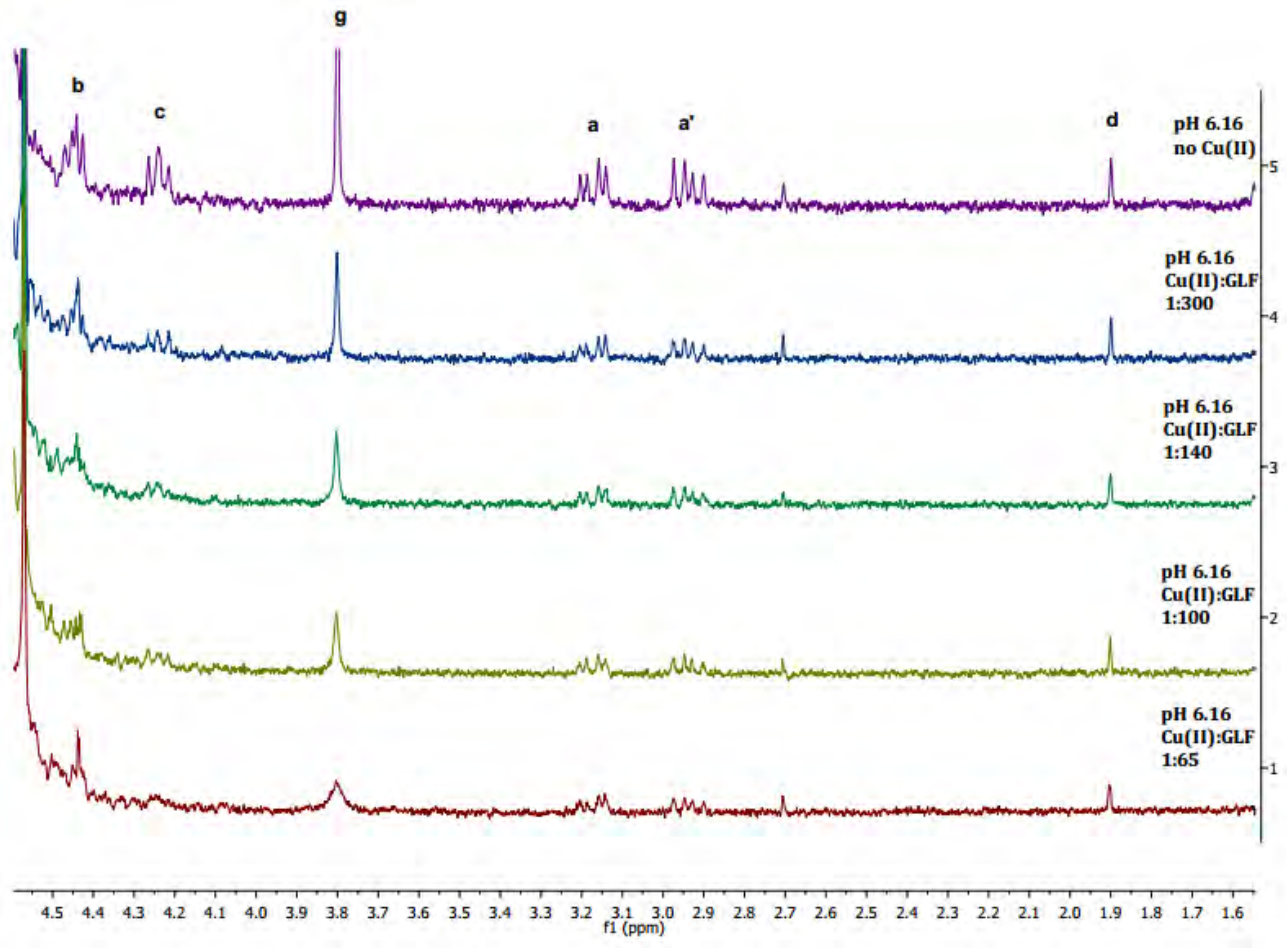

A

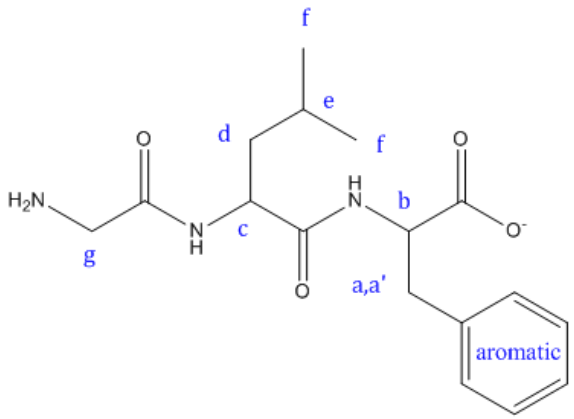

B

Figure 4.19: A: ^{1}H NMR spectra of the titration of Gly-Leu-Phe with copper(II) at a pH of 6.16 in D_2O. B: The proton assignments for Gly-Leu-Phe.

For the pH value of 7.62, which can be seen in Figure 4.20, peaks **b** and **c** broaden more than the other peaks. This indicates that the copper(II) can be coordinated to Leu-N, Leu-O, Gly-O, Phe-N or to the carboxyl-O. At this pH the ML_2H_{-1} species is assumed to be present and since this complex consists of two ligands, a large number of coordination arrangements can occur. Therefore the exact coordination mode cannot be determined without a quantitative analysis. The potentiometric, IR and UV-Vis analyses also suggested that for this species, copper(II) coordinated to the amide-N groups.

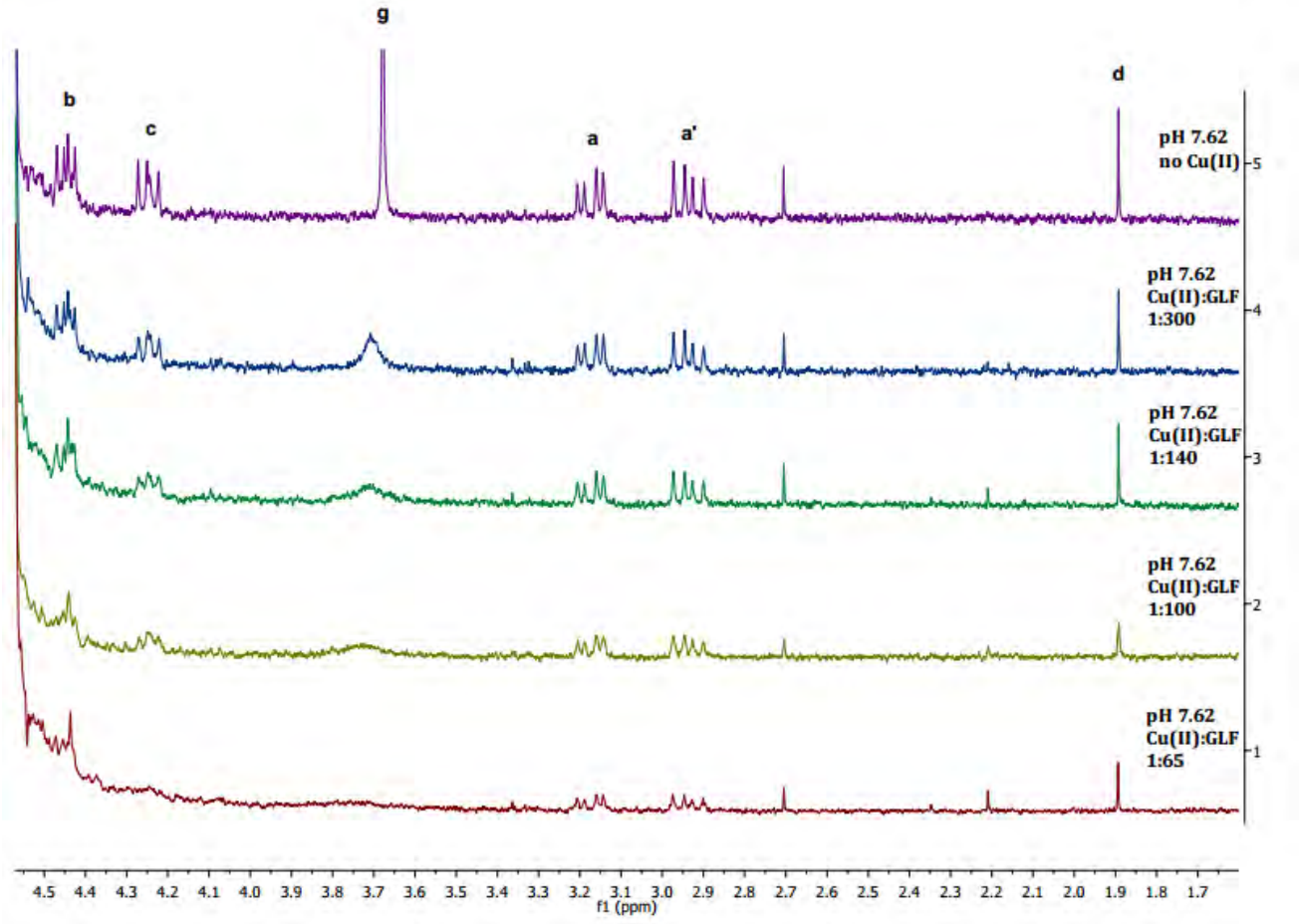

A

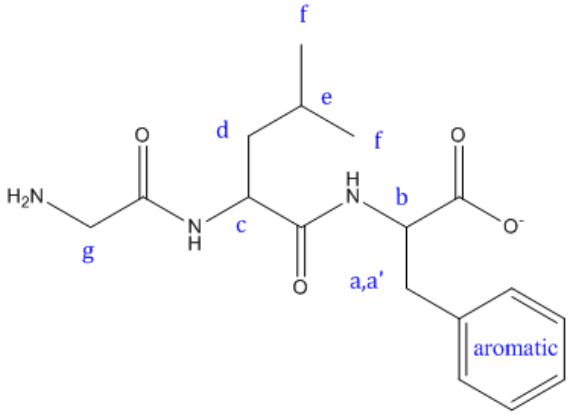

B

Figure 4.20: A: ^{1}H NMR spectra of the titration of Gly-Leu-Phe with copper(II) at a pH of 7.62 in D_2O. B: The proton assignments for Gly-Leu-Phe.

For the pH value of 9.63, which can be seen in Figure 4.21, with the exception of peak **g** which broadens greatly, all the other peaks do not appear to broaden more than the relative amount of broadening that is expected when copper(II) is present. However, at the high pH of 9.63, these peaks appear to have sharpened. This sharpening at high pH values can be explained by a decrease in the exchange rate. This causes copper(II) to become ineffective at reacting with the excess ligand, which results in the observation of all resonances and therefore the inability to determine the coordination mode of this species.[16-18] A similar observation was made by Elmagbari[19] and was seen in the ^{1}H NMR analysis for a copper(II)glycylglycylhistamine complex.[20]

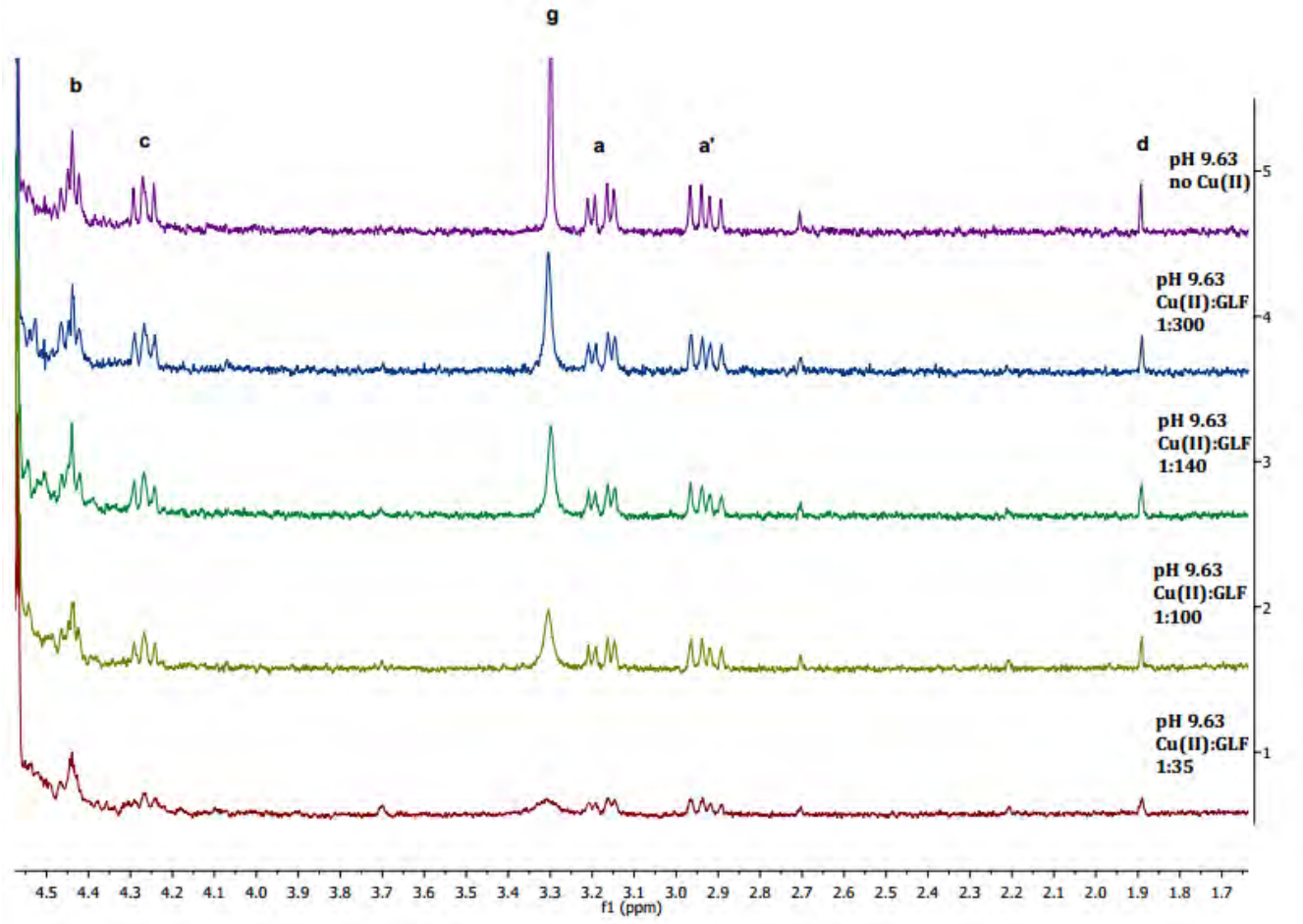

A

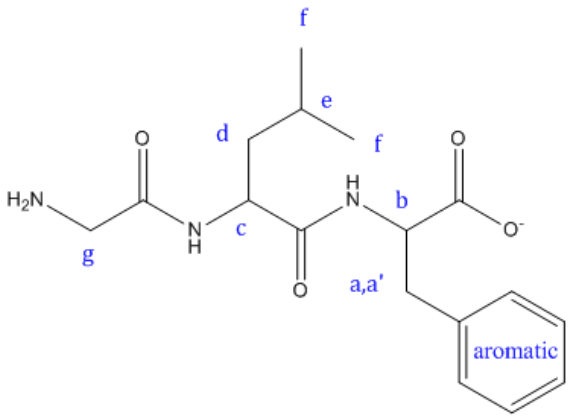

B

Figure 4.21: A: ^{1}H NMR spectra of the titration of Gly-Leu-Phe with copper(II) at a pH of 9.63 in D_2O. B: The proton assignments for Gly-Leu-Phe.

4.3.3(b.ii) Cu-Sar-Leu-Phe

The titration of Sar-Leu-Phe with copper(II) was analyzed at a pH of 4.61, 6.22, 8.22 and 10.16 and can be seen in Figures 4.22-4.25 respectively. In all pH values peaks **g** and **h** broaden greatly, which indicates that copper(II) has coordinated to the amine-N in all the species.

For the pH value 4.61, which can be seen in Figure 4.22, peaks **b** and **c** broaden slightly more than the other peaks during the titration. This indicates that copper(II) is coordinated to Gly-O, Leu-N, Leu-O, Phe-N and the carboxyl-O. However, the ML species is assumed to predominate at this pH and therefore Leu-N and Phe-N can be discounted, since coordination to these groups can only occur through deprotonation of the amide. Without a quantitative analysis, the carbonyl and carboxyl groups cannot be distinguished. The IR analysis suggested that for the ML species, copper(II) coordinated to either the carboxyl-O or to the carbonyl-O or to both. The UV-Vis analysis suggested that the ML species does not coordinate to an amide-N group.

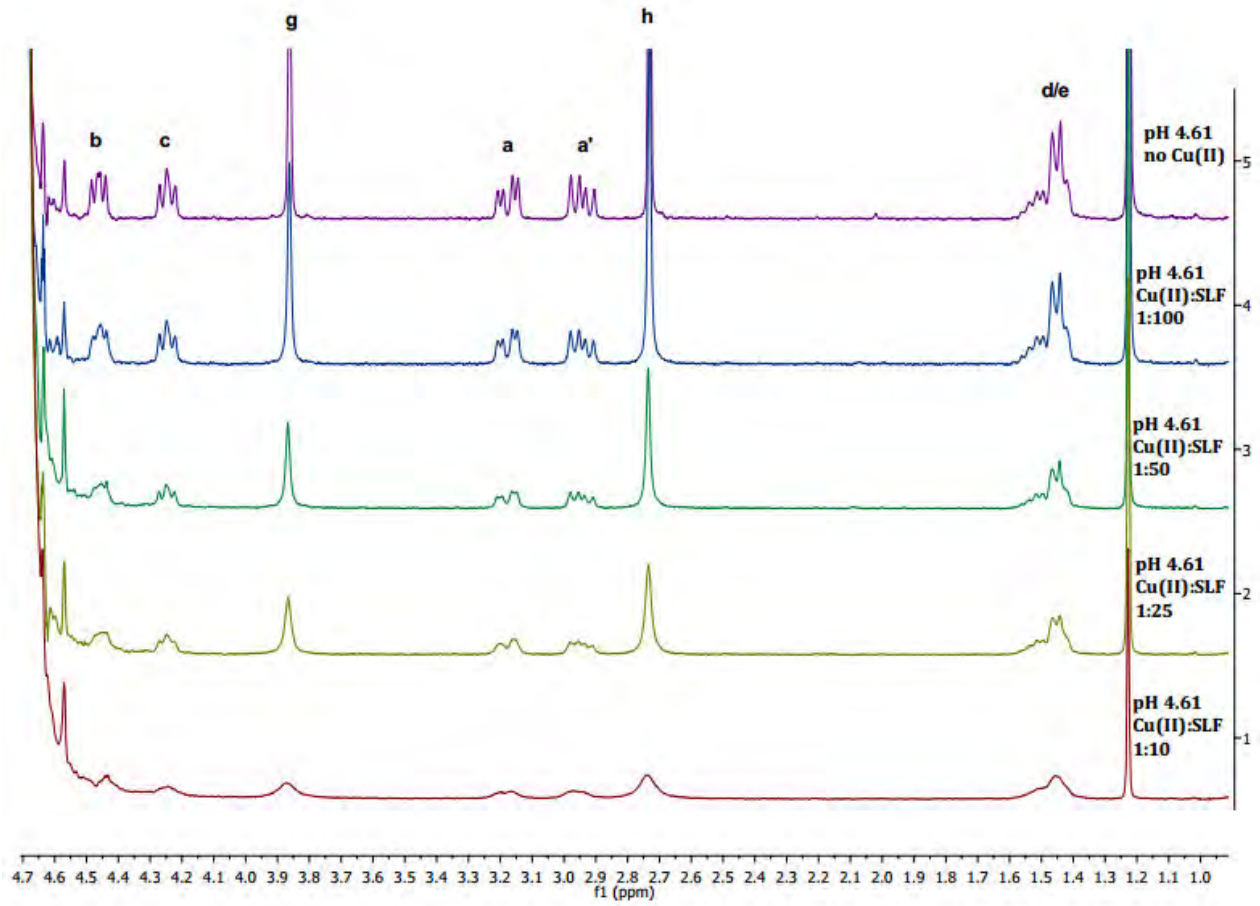

A

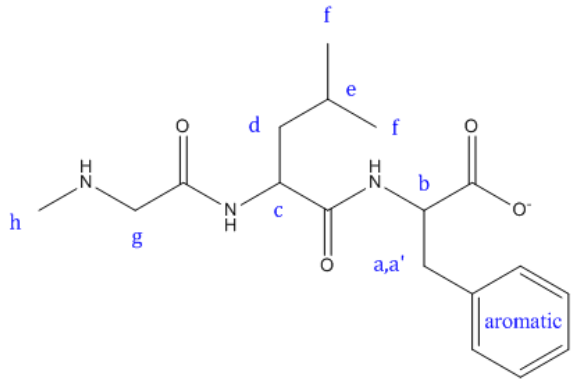

B

Figure 4.22: A: ^{1}H NMR spectra of the titration of Sar-Leu-Phe with copper(II) at a pH of 4.61 in D_2O. B: The proton assignments for Sar-Leu-Phe.

For the pH value of 6.22, which can be seen in Figure 4.23, peak **b**, peak **c** and peak **d/e** all broaden more relative to peak **a** and **a'**. This indicates that copper(II) has coordinated to Leu-N, Leu-O, Gly-O, Phe-N and the carboxyl-O. The presumed species for a pH of 6.22 is the MLH_{-1} species and therefore is consistent with copper(II) coordinating to one of the amide-N groups. However, quantitative analysis is needed to further distinguish between all of these groups. The potentiometric analysis suggested that the loss of the proton is from the ligand and not from water and the IR analysis suggested that the copper(II) coordinates to either the carbonyl-O or to the carboxyl-O or to both. The UV-Vis analysis suggested that copper(II) coordinated to one amide-N group. Therefore the ^{1}H NMR analysis and these structure determining techniques are in agreement.

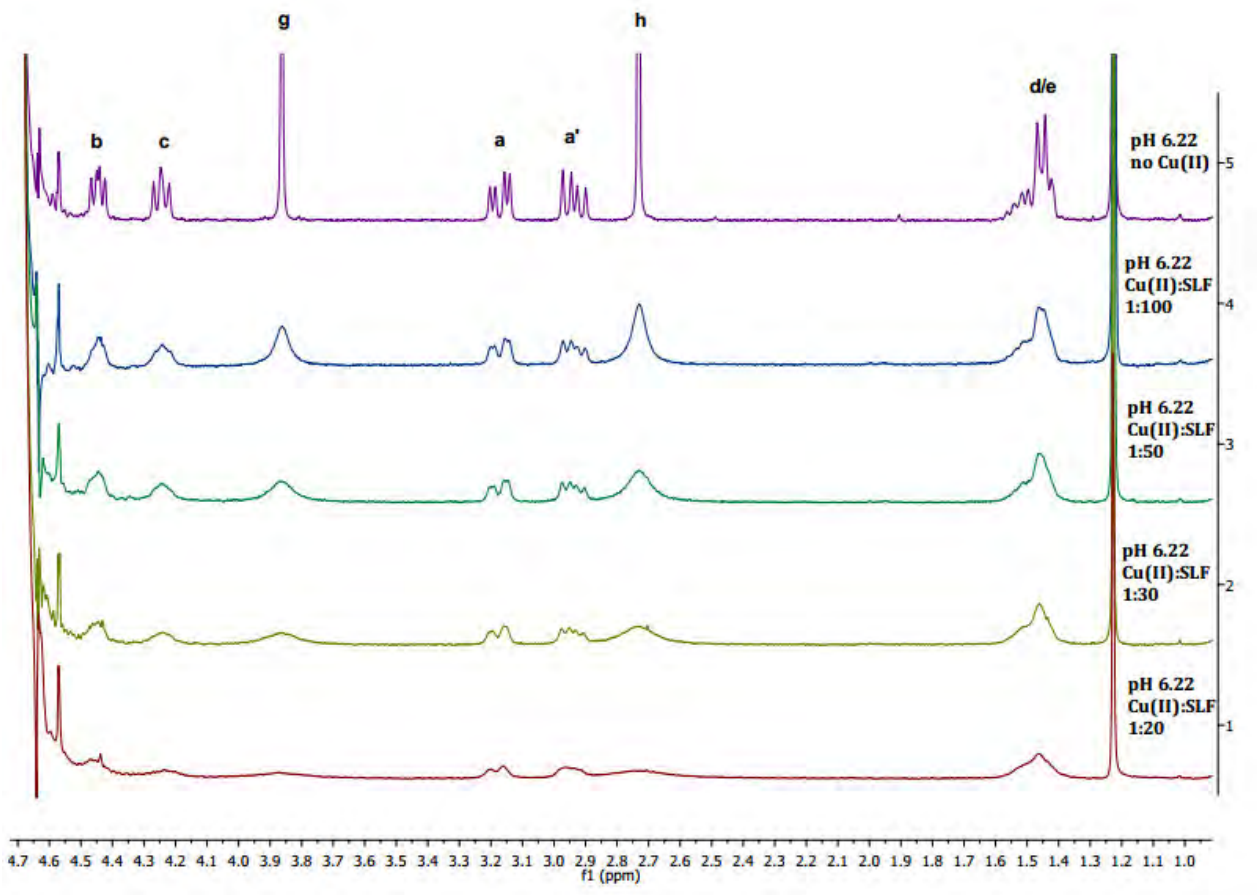

A

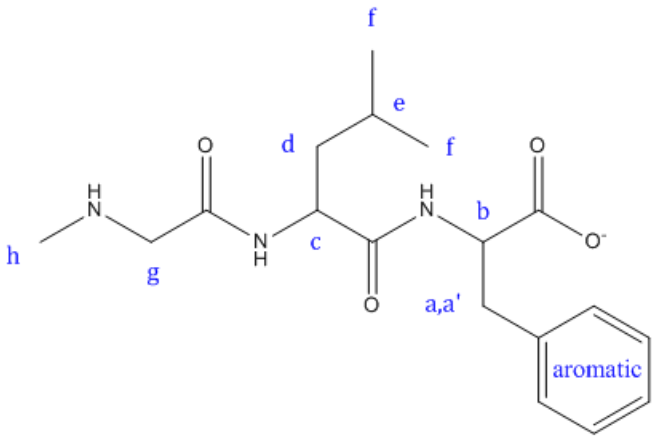

B

Figure 4.23: A: ^{1}H NMR spectra of the titration of Sar-Leu-Phe with copper(II) at a pH of 6.22 in D_2O. B: The proton assignments for Sar-Leu-Phe.

For the pH values 8.22 and 10.16, which can be seen in Figures 4.24 and 4.25 respectively, with the exception of peaks **g** and **h** which broaden greatly, all the other peaks do not appear to broaden more than the expected relative broadening that occurs when copper(II) is present. However, similarly to the peaks of the species at high pH values for Cu-Gly-Leu-Phe, these peaks which are presumed to belong to the ML_2H_{-1} and MLH_{-2} species respectively also appear to have sharpened. This can also be explained by the decrease in the exchange rate at high pH values and therefore the ability to determine the coordination modes of these species cannot be achieved.[16-18]

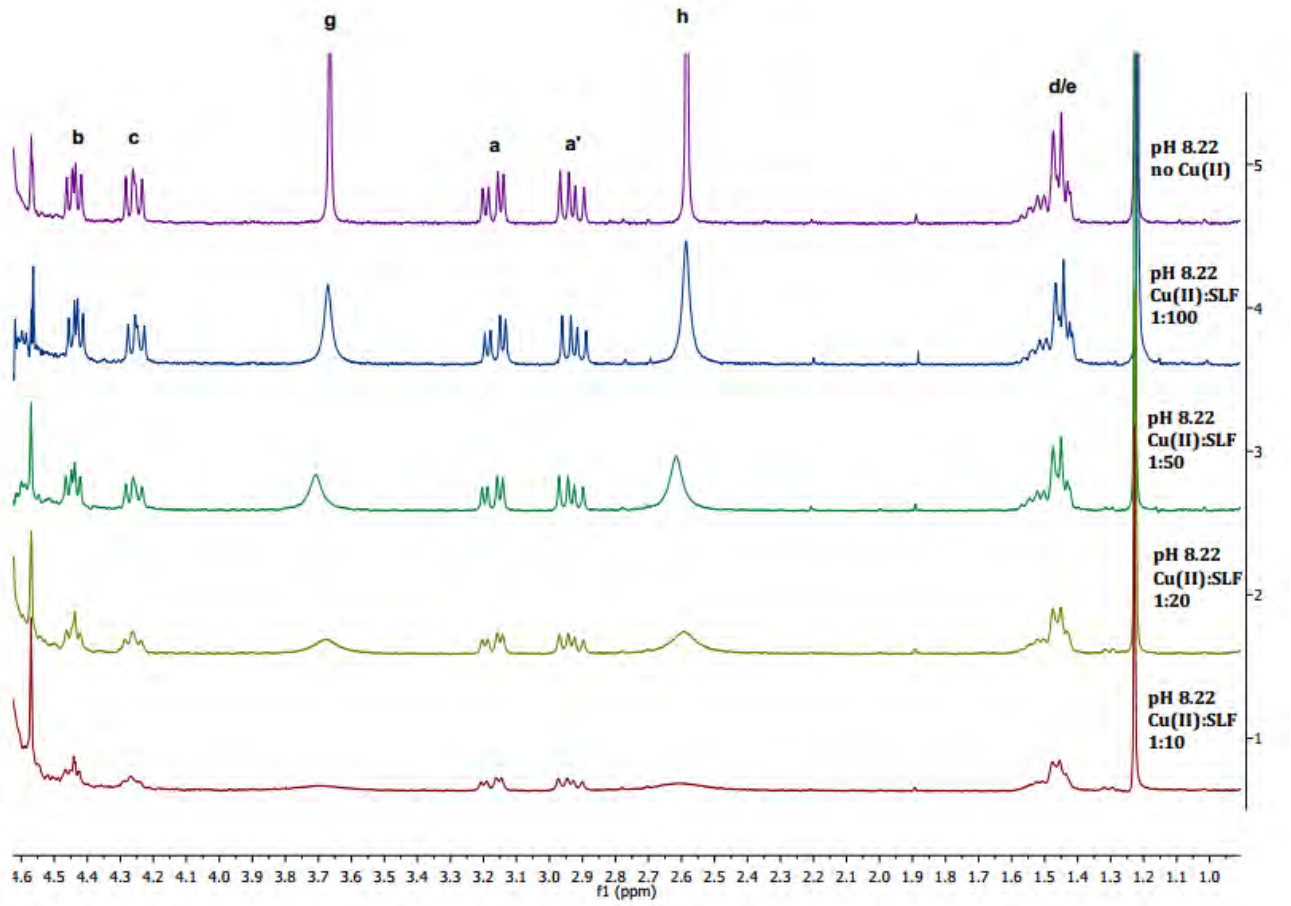

A

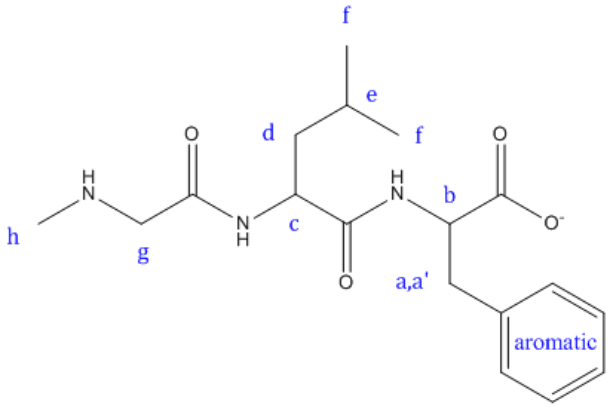

B

Figure 4.24: A: ^{1}H NMR spectra of the titration of Sar-Leu-Phe with copper(II) at a pH of 8.22 in D_2O. B: The proton assignments for Sar-Leu-Phe.

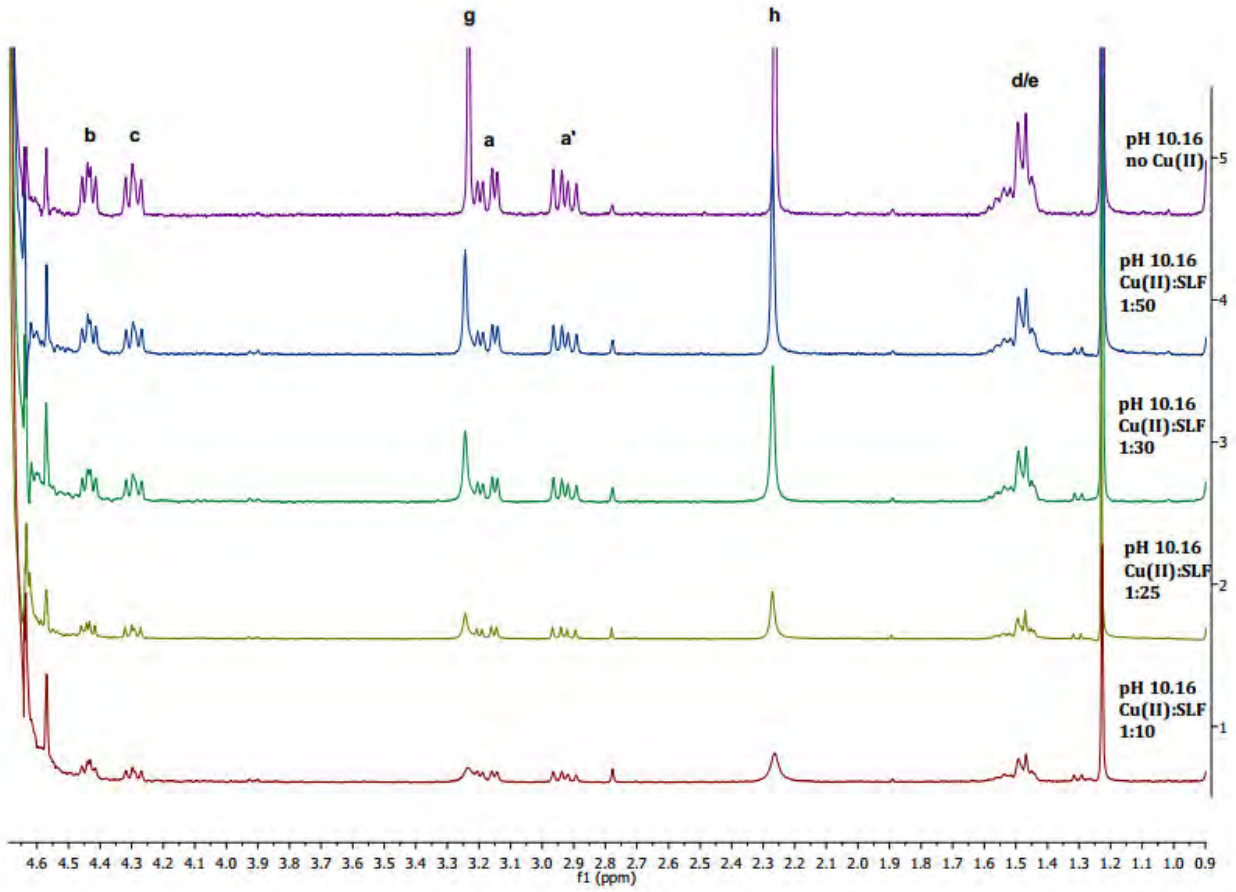

A

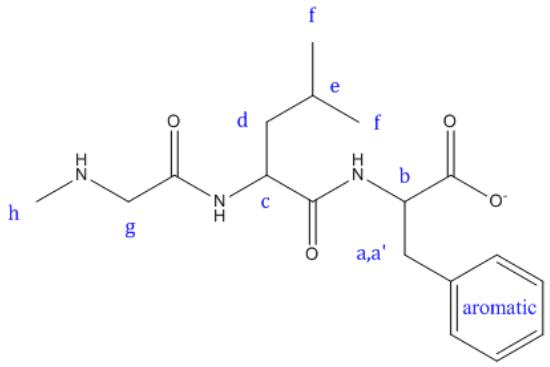

B

Figure 4.25: A: ^{1}H NMR spectra of the titration of Sar-Leu-Phe with copper(II) at a pH of 10.16 in D_2O. B: The proton assignments for Sar-Leu-Phe.

4.3.4 Discussion

Since an exchange between deuterium and the protons from the amine, amide and carboxyl groups occurred and resulted in the disappearance of these proton signals, the analysis of the titration of each ligand with copper(II) was achieved by observing the broadening of visible proton signals. Proton signals which originate from protons that are near possible coordination sites will broaden when copper(II) complexes to the ligands. The protons which produced peaks **a**, **a'**, **b**, **c**, **g** and **h** are situated on either the α or β carbons of the coordination sites. Protons which are further away are not affected to the same extent and produce peaks that have not undergone much noticeable broadening. Therefore the analysis focused on the protons which produce the above mentioned peaks.

In all the ^{1}H NMR spectra studied, which can be seen in Figures 4.18-4.25, all the peak signals showed broadening as the ligands were titrated with copper(II). This is due to a general increase in the magnetic susceptibility of the solution. However, when the metal ion coordinates to the ligand, there is a differential broadening of protons close to the site of coordination. Since this through-space effect is dependent on the distance between the nuclei of the ligand and copper(II), the ^{1}H MNR signals that are close to the binding sites of copper(II) broadened more.[3-8]

The coordination modes that were proposed by analyzing the ^{1}H NMR spectra for both copper(II) complexes are illustrated in Figures 4.26-4.30. The charges on the donor groups of the ligands have been omitted for simplicity.

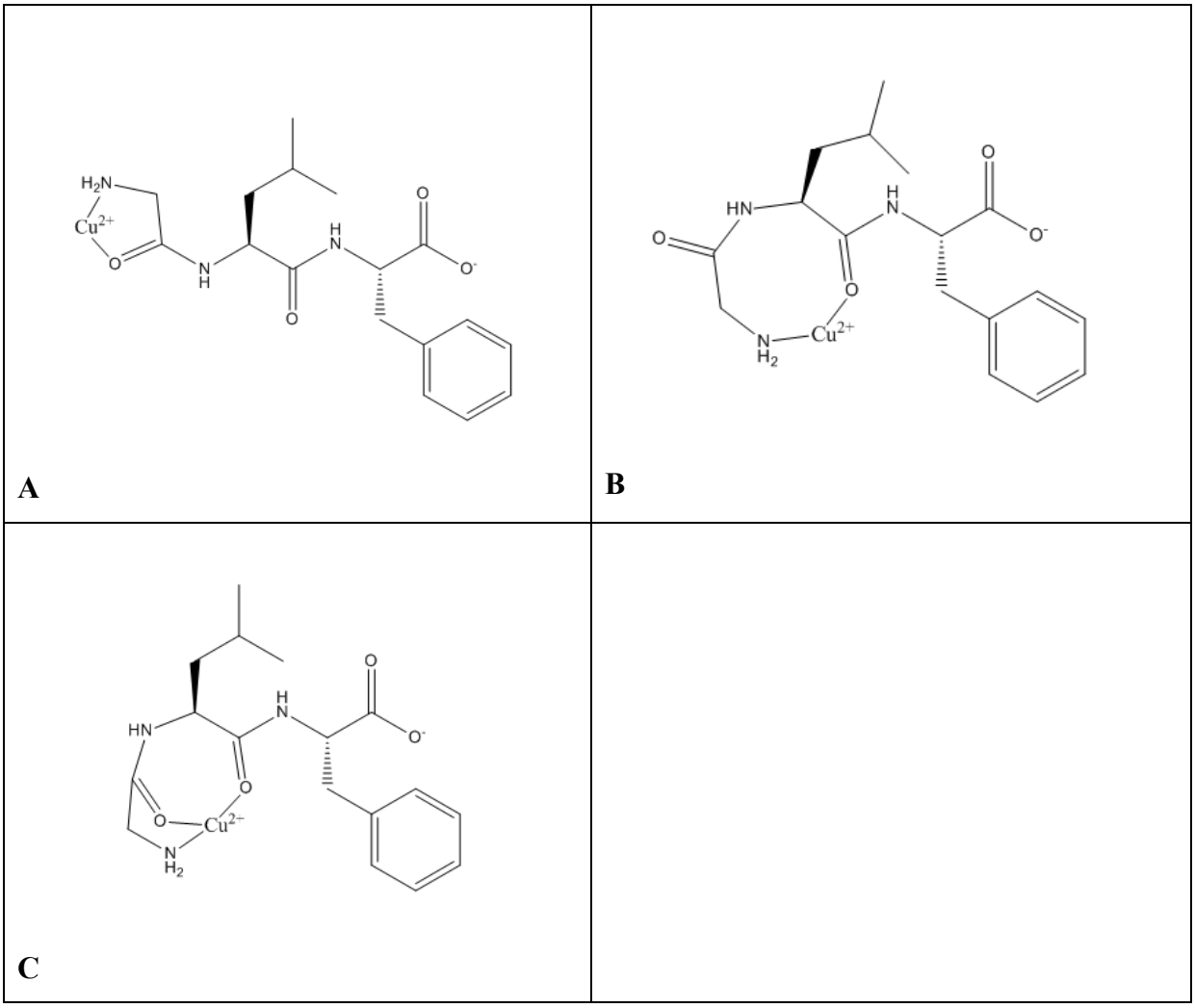

Figure 4.26: Possible metal ligand coordination modes for the ML species of Cu-Gly-Leu-Phe at a pH of 5.33.

Coordination mode **C** in Figure 4.26 could be the most probable coordination mode for the ML species of Cu-Gly-Leu-Phe, since it has two chelate ring formations and one of the chelate rings is a five-membered ring. The other possible coordination modes only have one seven or eight-membered chelate ring. The greater the number of chelate ring formations a complex has, the more stable the complex is.[21,22] In addition a five-membered chelate ring has less strain between the bonds and therefore during formation will be more stable than a seven or eight-membered ring.[23]

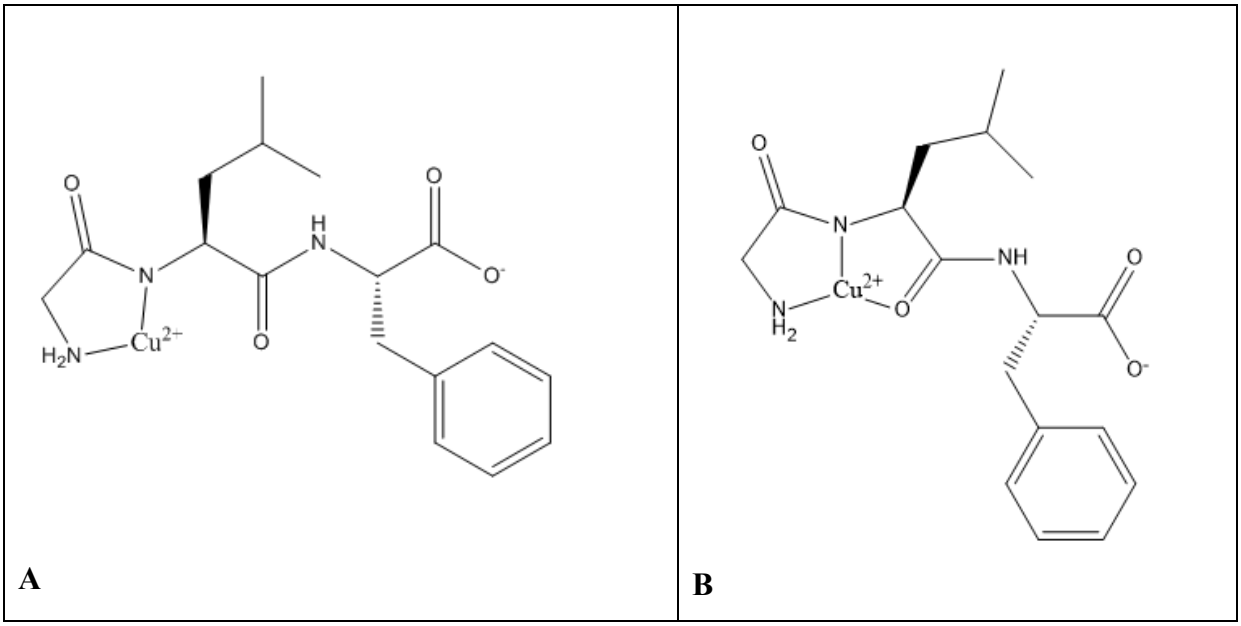

Figure 4.27: Possible metal ligand coordination modes for the MLH_{-1} species of Cu-Gly-Leu-Phe at a pH of 6.16.

From Figure 4.27 it can be seen that both coordination modes for the MLH_{-1} species of Cu-Gly-Leu-Phe have five-membered chelate rings. However, **B** has a greater chelate effect, since it is a tridentate chelate, while **A** is a bidentate chelate, and therefore coordination mode **B** is the most probable coordination mode for the MLH_{-1} species of Cu-Gly-Leu-Phe .[24]

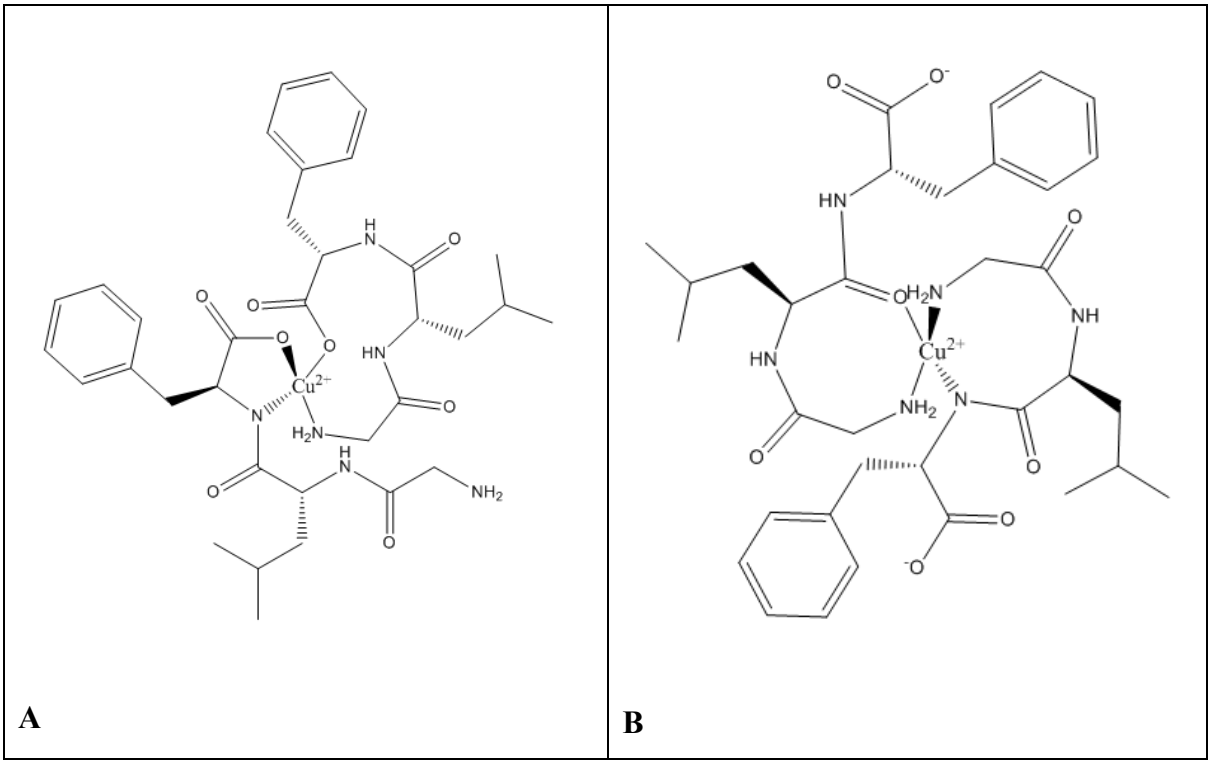

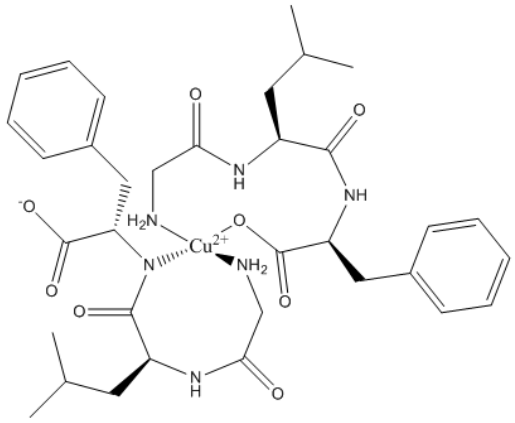

C

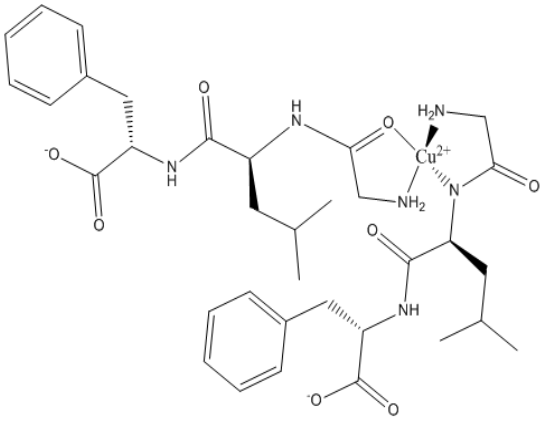

D

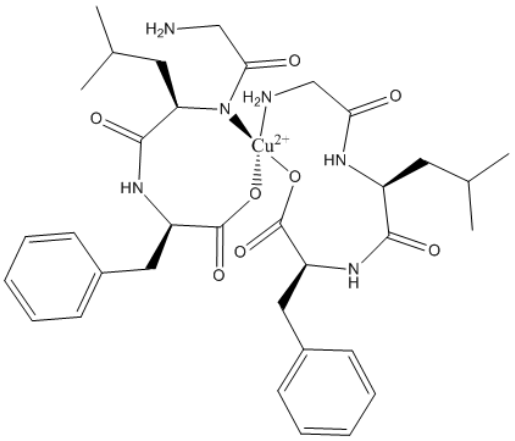

E

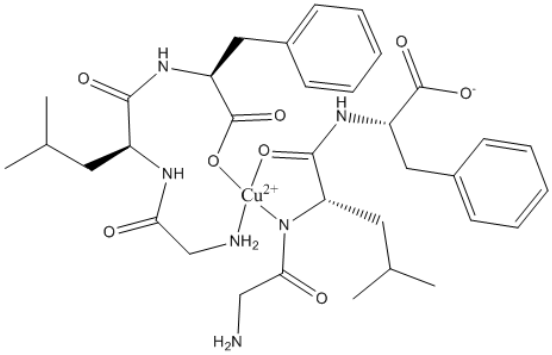

F

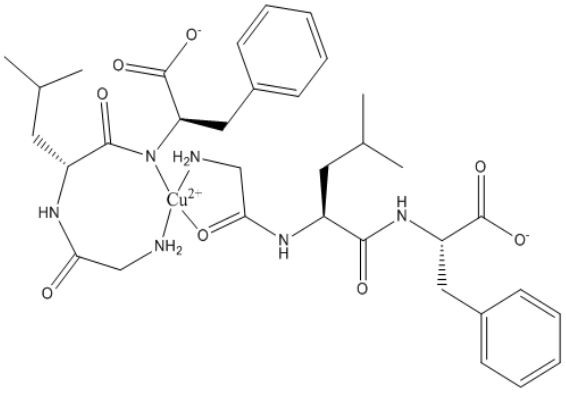

G

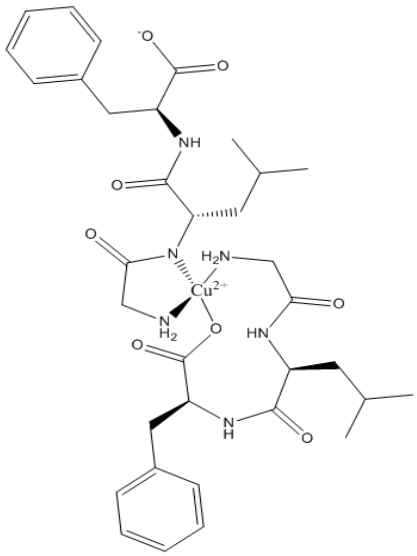

H

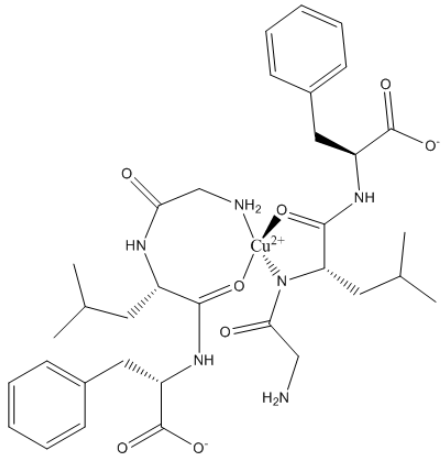

I

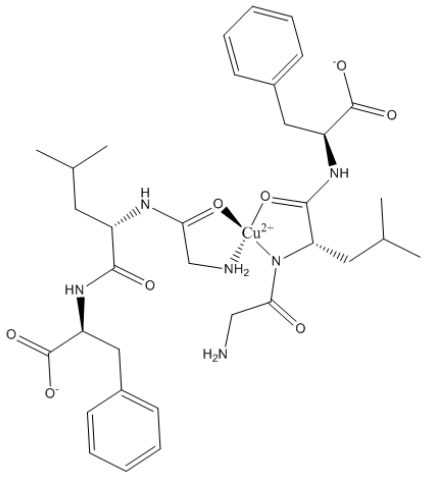

J

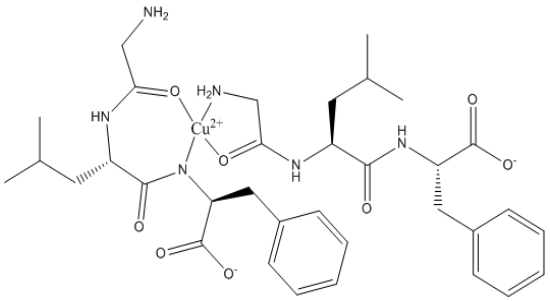

K

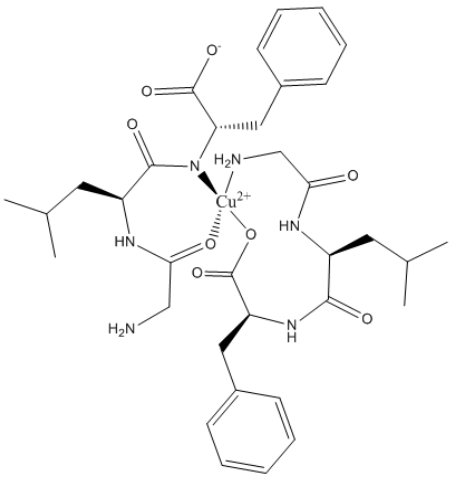

L

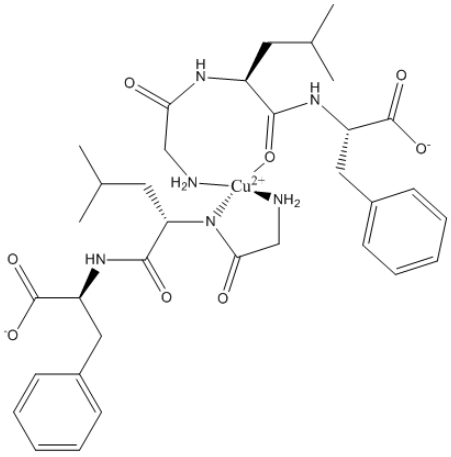

M

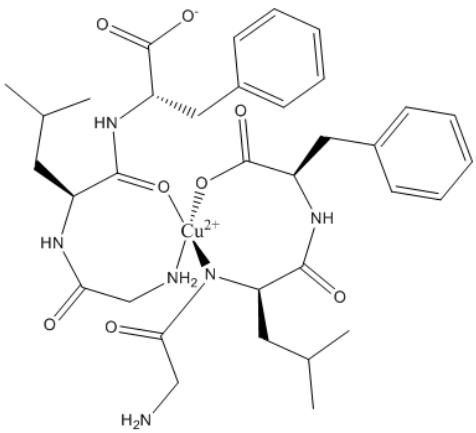

N

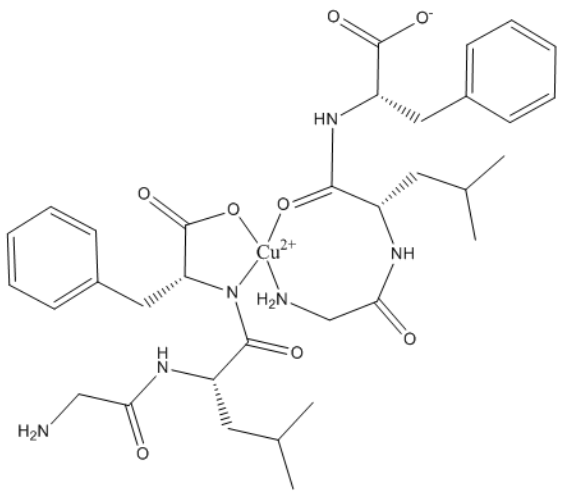

O

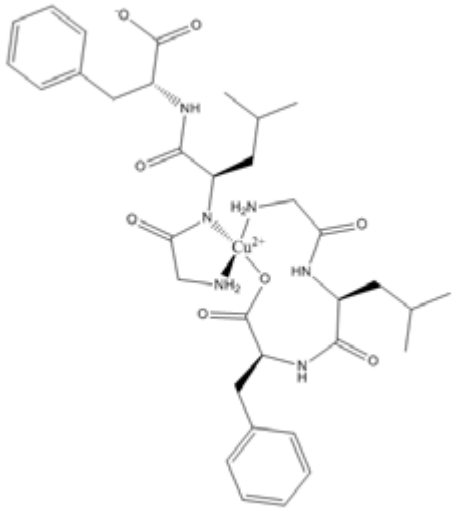

P

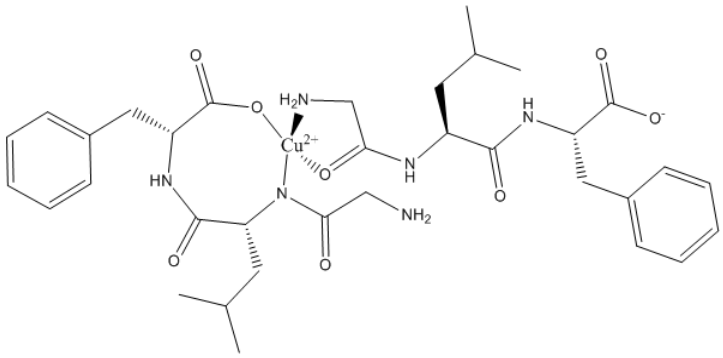

Q

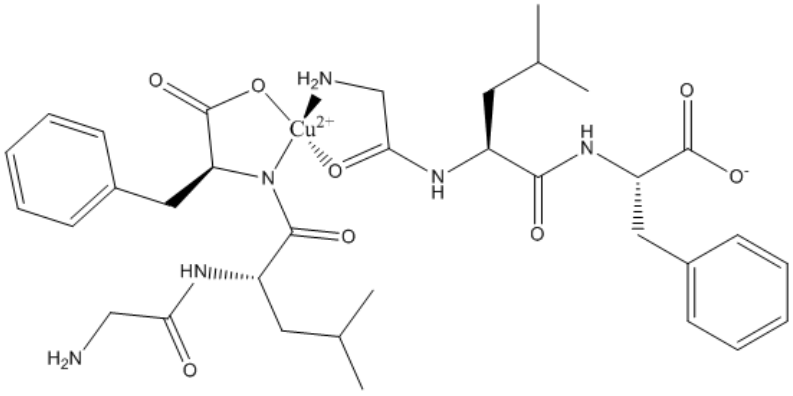

R

Figure 4.28: Possible metal ligand coordination modes for the ML_2H_{-1} species of Cu-Gly-Leu-Phe at a pH of 7.62.

In Figure 4.28 it can be seen that all the proposed coordination modes for the ML_2H_{-1} species of Cu-Gly-Leu-Phe have two chelate ring formations. However, only coordination modes **D**, **J** and **R** have two five-membered chelate ring formations and therefore these coordination modes could form more readily than the other coordination modes.

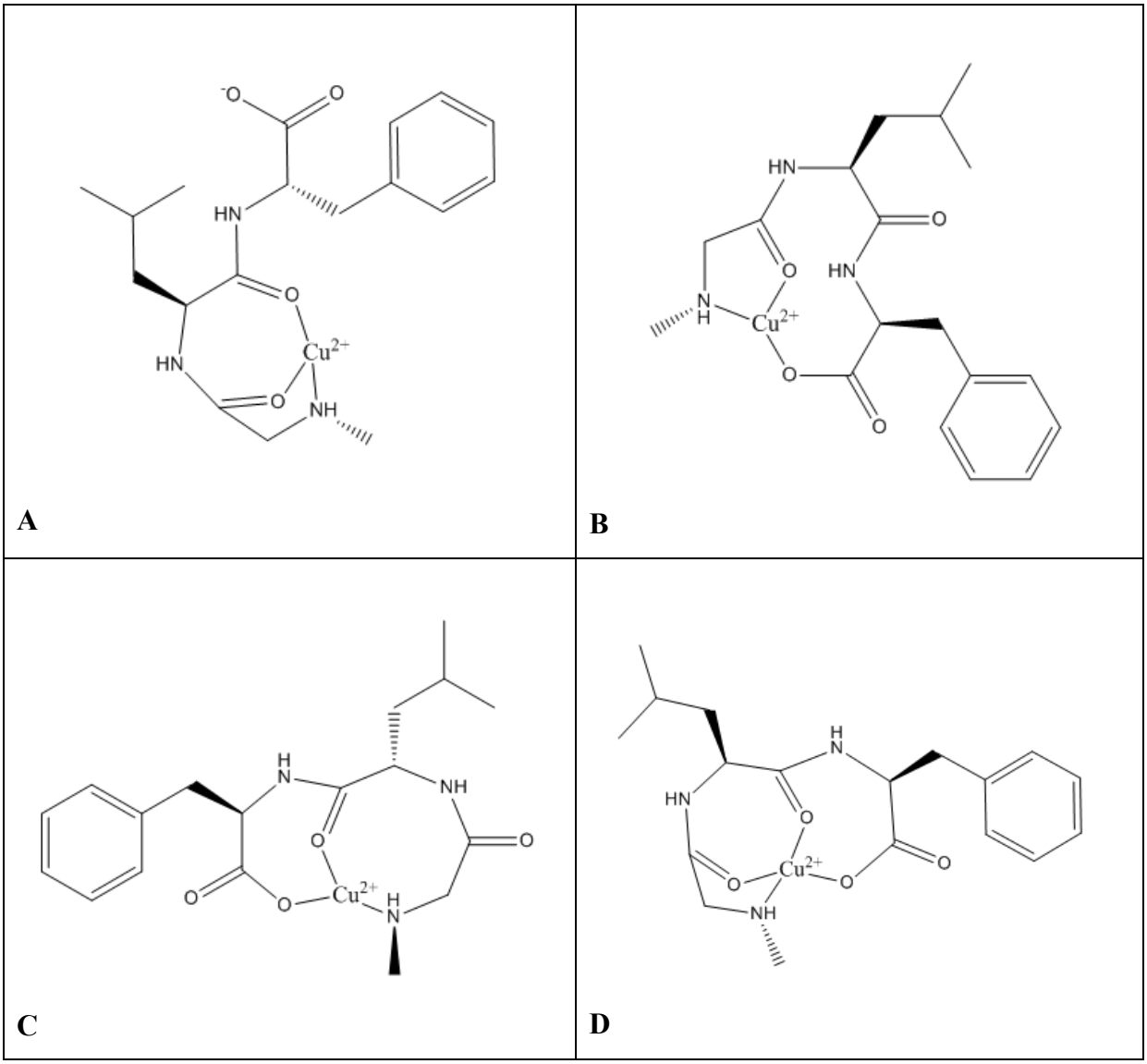

Figure 4.29: Possible metal ligand coordination modes for the ML species of Cu-Sar-Leu-Phe at a pH of 4.61.

Coordination modes **A**, **B** and **C**, which can be seen in Figure 4.29 for the ML species of Cu-Sar-Leu-Phe all form two chelate rings, while **D** forms three. Therefore coordination mode **D** has a higher probability of forming than the other coordination modes.

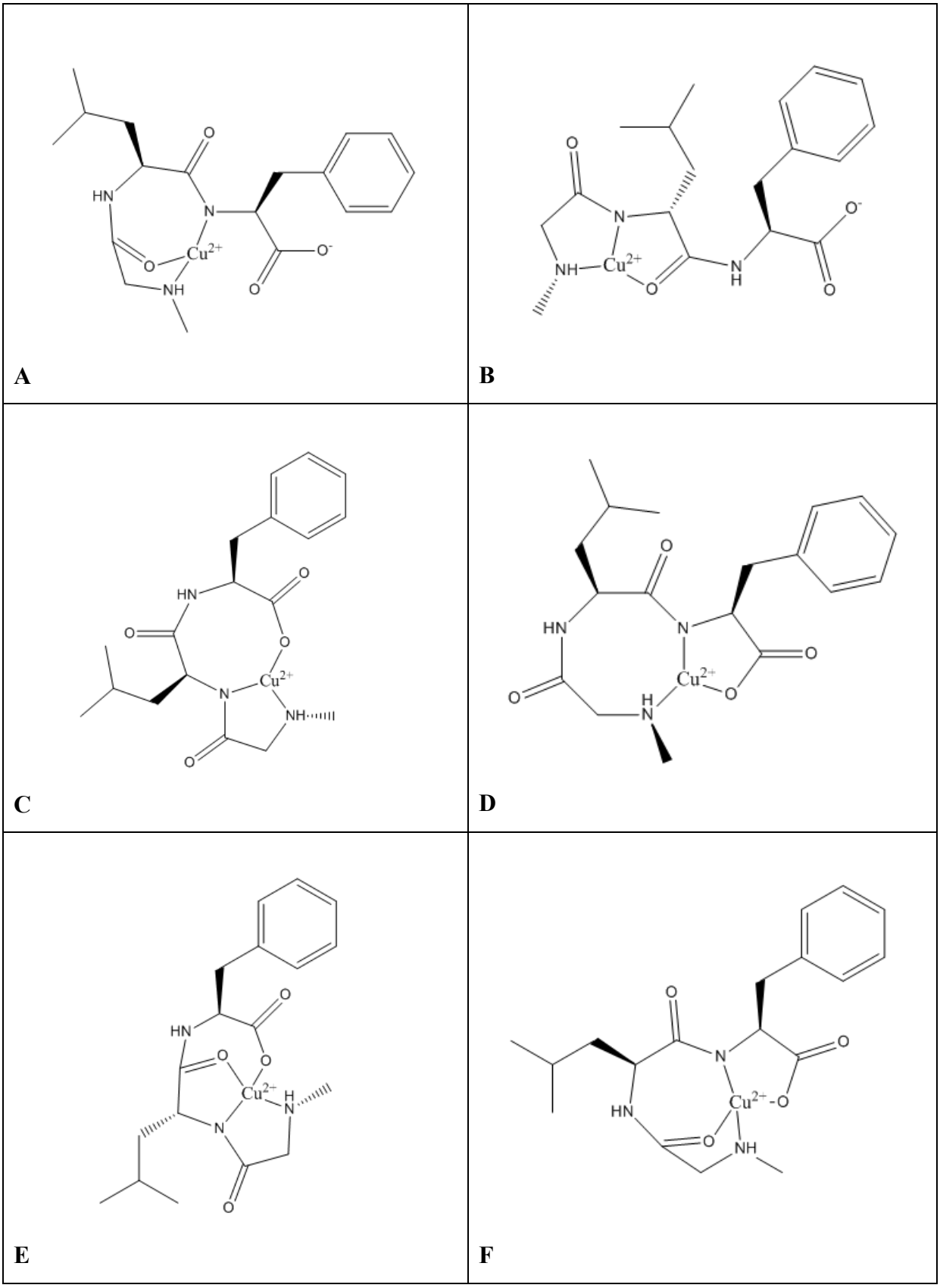

Figure 4.30: Possible metal ligand coordination modes for the MLH_{-1} species of Cu-Sar-Leu-Phe at a pH of 6.22.

Coordination mode **B**, which can be seen in Figure 4.30 for the MLH_{-1} species of Cu-Sar-Leu-Phe, has two five-membered chelate rings, while all the other coordination modes have seven or more membered chelate rings. Thus the probable coordination mode of the MLH_{-1} species is **B**, since it will form with the most stability.

4.3.5 Conclusion

The method to determine the coordination of copper(II) to Gly-Leu-Phe and Sar-Leu-Phe via a titration technique is based on the assumption that at high metal to ligand ratios the species distribution and species type is the same as that of a 1:4 metal ligand ratio. As copper(II) coordinated to the ligands, the ^{1}H NMR spectra for the protons surrounding the coordination site were expected to broaden significantly, which would indicate a definite binding site. However, substantial peak broadening only occurred in the protons that surround the amine group in both ligands for all pH values. This showed that in all species, copper(II) had coordinated to the amine-N. For the ML and MLH_{-1} species of both ligands, as well as the ML_2H_{-1} species of Cu-Gly-Leu-Phe, peak broadening occurred in the protons that surround the other coordination sites. However, because these sites are all close to one another, a quantitative analysis is needed to find the exact coordination mode of each species. Therefore possible coordination modes were suggested. The coordination modes of the MLH_{-2} species of Cu-Gly-Leu-Phe, as well as the ML_2H_{-1} and MLH_{-2} species of Cu-Sar-Leu-Phe, could not be determined, because peak sharpening had occurred.

References

1. R. T. Morrison and R. N. Boyd, *Organic Chemistry*, Allyn and Bocon, Inc., Boston, 5th edn., 1987, pp. 578-580.
2. I. R. Kleckner and M. P. Foster, *Biochim. Biophys. Acta*, 2010, DOI: 10.1016/jbbapap.2010.10.012.
3. R. T. Morrison and R. N. Boyd, *Organic Chemistry*, Allyn and Bocon, Inc., Boston, 5th edn., 1987, pp. 578-580.
4. X. Z. Zhao, T. Jiang, L. Wang, H. Yang, S. Zhang and P. Zhou, *J. Mol. Structure*, 2010, DOI: 10.1016/jmolstruc.2010.09.049.
5. L. Hou and M. G. Zagorski, *J. Am. Chem. Soc.,* 2006, **128**, 9260-9261.
6. B. Liang, J. H. Bushweller and L. K. Tamm, *J. Am. Chem. Soc*., 2006, **128**, 4389-4397.
7. Nuclear Magnetic Resonance: An Introduction, http://instructor.physics.lsa.umich.edu/adv-labs/NMR/Ch12_NMRTEC.pdf, (accessed July 2015).
8. *Chemical Speciation in the Environment*, ed. A. Ure and C. Davidson, Blackwell Science Ltd., United Kingdom, 2nd edn., 2002, ch. 3, pp. 46.
9. R. A. Marusak, K. Doan and S. D. Cummings, *Integrated Approach to Coordination Chemistry: An Inorganic Laboratory Guide*, John Wiley & Sons, Inc., New Jersey, 2007, pp. 232.
10. E. Gaggelli, N. D' Amelio, D. Valensin and G. Valensin, *Magn. Reson. Chem*., 2003, **41**, 877-883.
11. R. G. Bryant, *J. Chem. Edu.*, 1983, **60**, 933-935.
12. M. A. Wells, C. Jelinska, L. L. P. Hosszu, J. Craven, A. R. Clarke, J. Collinge, J. P. Waltho and G. S. Jackson, *Biochem. J.*, 2006, **400**, 501-510.
13. K. Popov, H Rönkkömäki and L. H. J. Lajunen, *Pure Appl. Chem*., 2006, **78**, 663-675.
14. P. K. Glasoe and F. A. Long, *J. Phys. Chem*., 1960, **64**, 188-190.
15. Nuclear Magnetic Resonance Spectroscopy, http://www2.chemistry.msu.edu/faculty/reusch/VirtTxtJml/Spectrpy/nmr/nmr1.htm, (accessed March 2015).
16. S. Lau, J. Laussac and B. Sarkar*, Biochem. J.*, 1989, **257**, 745-750.
17. J. Laussac, R. Haran and B. Sarkar, *Biochem. J.*, 1983, **209**, 533-539.

18. Z. Szabó, *Coord. Chem. Rev.*, 2008, **252**, 2362-2380.
19. F. M. A. Elmagbari, PhD Thesis, University of Cape Town, 2015.
20. T. Gajda, B. Henry, A. Aubry and J. Delpuech*, Inorg. Chem*., 1996, **35**, 586-593.
21. *Analytical Chemistry: Twenty-sixth International Congress of Pure and Applied Chemistry*, T. Takeuchi, Pergamon press, Oxford, 1977, vol. 3, pp. 815.
22. S. Prakash, G. D. Tuli, S. K. Basu and R. D. Madan, *Advanced Inorgandic Chemistry*, S. Chand Publishing, India, 17th edn., 2000, vol. 2, pp. 32.
23. J. Clayden, N. Greeves, S. Warren and P. Wothers, *Organic Chemistry*, Oxford University Press, Inc., New York, 1st edn., 2001, ch. 18, pp. 454-455.
24. C. E. Housecroft and A. G. Sharpe, Inorganic Chemistry, Pearson Education Limited, England, 3rd edn., 2008, ch. 7, pp. 203-205.

4.4 Molecular Modelling

4.4.1 Introduction

Molecular modelling is a computational set of techniques that is used to determine the molecular geometry, energies, transition states, chemical reactivity, IR, UV and NMR spectra of molecules. The methods that are used to solve these chemical properties can be grouped into five broad classes:

1. Molecular mechanics uses a balls-and-springs model to describe the structures and relative energies of molecular configurations.
2. Ab initio calculations solve the Schrödinger equation of a molecule to give the energy and wave function. Approximations are used, since the Schrödinger equation cannot be solved exactly for a molecule with more than one electron.
3. Semi-empirical calculations are similar to ab initio calculations, since they are also based on the Schrödinger equation and give the energy and wave function. However, semi-empirical calculations have more approximations and are parameterized with experimental values.
4. Density Functional Theory (DFT) calculations are also based on the Schrödinger equation, but derive an electron distribution directly instead of calculating a wave function.
5. Molecular dynamics calculations simulate the motions of molecules by applying the laws of motion to the molecules.[1]

Other PhD theses, as well as journals that have investigated the coordination mode of copper(II) complexes, have used a molecular mechanical approach.[2-7] However, quantum mechanical modelling is more computationally intensive and provides more accurate models, since it includes electronic contributions, transition states and excited states, all of which are not included in molecular mechanics.[8-11]

Therefore DFT was used instead of the molecular mechanical approach to calculate the binding energies of molecules.[12,13] The structure with the lowest binding energy from a series of possible coordination combinations for the species of Cu-Gly-Leu-Phe and Cu-Sar-Leu-Phe can then be proposed as a possible structure for each species.

In quantum mechanics, the wave function is used to describe a system. The wave function is calculated from the Schrödinger equation and for a system that has more than one electron or termed as a many-electron system, the equation is represented in Equation 21 as:

$$\left[\sum_{i}^{N}\left(-\frac{\hbar^2\nabla_i^2}{2m}+v(\boldsymbol{r}_i)\right)+\sum_{i<j}U(\boldsymbol{r}_i,\boldsymbol{r}_j)\right]\psi(\mathbf{r_1},\mathbf{r_2}\ldots,\mathbf{r_N})=\mathrm{E}\psi(\mathbf{r_1},\mathbf{r_2}\ldots,\mathbf{r_N}) \tag{21}$$

where N is the number of elections, ħ is the Planck constant, ∇^2 is the Laplacian, m is the reduced mass, $v(\boldsymbol{r}_i)$ is the potential energy, ψ is the wave function and U($\boldsymbol{r}_i$, $\boldsymbol{r}_j$) is the electron-electron interaction.[12]

Solving the Schrödinger equation for large molecules is problematic, because it places high demands on computational resources and the methods used to solve the Schrödinger equation then become inefficient.[1,12] DFT provides an alternative for calculating the chemical properties of molecules, since it describes a many-electron system completely in terms of the electron probability density function, which is a probability per unit volume and is designated as $\rho(x, y, z)$.[1,14,15] The fundamental nature of DFT can be stated in two theorems that were found and published by Hohenberg and Kohn in 1964.[16] The first theorem says every observable quantity of a stationary quantum mechanical system can be described as a functional in terms of its ground state density alone.[16-18] The second theorem says that by using a variational principle, the energy of any trial electron density function will be greater or equal to the true ground state energy.[1,14,16,18] A functional is a mathematical term for mapping a set of functions to a set of numbers and the variational principle assures that the calculation of an approximate energy will be greater than or equal to the exact energy.[1,19]

The first theorem indicates that the ground-state properties, which include the energy of molecules, can be calculated from the electron density in a three-dimensional space and represented in Equation 22 as:

$$\rho_0(x, y, z) \longrightarrow E_0 \tag{22}$$

where $\rho_0(x, y, z)$ is the electron density function and E_0 is the energy.[1]

The second theorem can be represented in Equation 23 as:

$$E_v[\rho_t] \geq E_0[\rho_0] \tag{23}$$

where $E_v[\rho_t]$ is the electronic energy functional of the ground state electron density, ρ_t is the trial density and $E_0[\rho_0]$ is the exact ground state energy.[1]

The exact functional, ($E_v[\rho_t]$), that will transform the ground state electron density function into the ground state energy is unknown, and the nature, as well as how to find the functional, is also unknown. Therefore Kohn-Sham found a solution, which current molecular DFT calculations are based on.[20] The energy functional, E_0 consists of three terms which can be seen in Equation 24 below:

$$E_0 = \langle T[\rho_0] \rangle + \langle V_{Ne}[\rho_0] \rangle + \langle V_{ee}[\rho_0] \rangle \tag{24}$$

where $\langle T[\rho_0] \rangle$ is the expectation value of the kinetic energy, $\langle V_{Ne}[\rho_0] \rangle$ is the expectation value of the nuclear-electron attraction potential energy and $\langle V_{ee}[\rho_0] \rangle$ is the expectation value of the electron-electron potential energy.[1] The kinetic and electron-electron functionals are the unknown functionals for which Kohn-Sham found a solution.[21] This was achieved by expressing the molecular energy as a sum of terms, where the unknown functional is only one relatively small term and can be seen in Equation 25. This ensures that large errors in the functional term will not lead to large errors in the total energy.[1,21]

$$\mathrm{E}_0 = -\sum_{\text{Nuclei A}} \mathrm{Z}_A \int \frac{\rho_0(\mathbf{r}_1)}{\mathbf{r}_{1\mathrm{A}}} d\mathbf{r}_1 - \frac{1}{2}\sum_{i=1}^{2n} \left\langle \psi_i^{KS}(1) \middle| \nabla_1^2 \middle| \psi_i^{KS}(1) \right\rangle + \frac{1}{2}\iint \frac{\rho_0(\mathbf{r}_1)\rho_0(\mathbf{r}_2)}{r_{12}}\, d\mathbf{r_1} d\mathbf{r_2} + E_{\mathrm{xc}}[\rho_0]$$

(25)

In this equation, Z_A is the nuclear charge on nuclei A, $\psi_i^{KS}(1)$ are the Kohn-Sham spatial orbitals that are arbitrarily assigned as electron number 1 and ∇^2 is the Laplacian. The $E_{\mathrm{xc}}[\rho_0]$ term is the relatively small term that contains the unknown functional and is subjected to the most error. This term is called the exchange-correlation energy functional. The electron density ρ should be initially guessed and then used to calculate an estimation of the Kohn-Sham orbitals, which can be seen in Equation 26.[1]

$$\rho_0 = \rho_r = \sum_{i=1}^{2n} \left| \psi_i^{KS}(1) \right|^2$$

(26)

This estimation is then used to refine the orbitals until the final orbitals are used to calculate the electron density. This electron density will then be used to calculate the energy. By substituting Equation 26 into Equation 25 and varying E_0 with respect to ψ_i^{KS}, provided E_0 and ψ_i^{KS} remain orthonormal, the Kohn-Sham equations can be derived and seen in Equation 27.

$$\left[-\frac{1}{2}\nabla_{\mathrm{i}}^2 - \sum_{\text{nuclei A}} \frac{\mathrm{Z_A}}{\mathbf{r}_{1\mathrm{A}}} + \int \frac{\rho(\mathbf{r}_2)}{\mathbf{r}_{12}} d\mathbf{r_2} + v_{\mathrm{XC}}(1) \right] \psi_i^{KS}(1) = \epsilon_i^{KS} \psi_i^{KS}(1)$$

(27)

where ϵ_i^{KS} are the Kohn-Sham energy levels and $v_{\mathrm{XC}}(1)$ is the exchange correlation potential. Therefore since Equation 25 is precise, the exact energy could be found if the density function $\rho_0(\mathbf{r})$ and the exchange-correlation energy functional $E_{\mathrm{xc}}[\rho_0]$ are known.[1]

Gaussian 09 is the newest version of the Gaussian® series which are electronic structure programs that can predict the properties of molecules and complexes, as well as other reactive systems.[13,22] Gaussian 09 finds the minimum energy of a molecule by geometry optimization. This involves calculating the energy and the wave function at an initial geometry and then searching to find a new geometry with a lower energy. This is then repeated until the geometry with the lowest energy is found. In order to achieve this, the force on each atom is calculated by finding the gradient of the energy with respect to the position of the atoms. Algorithms then select a new geometry at each step, which focuses on converging the geometry with the lowest energy and as soon as convergence occurs, the calculation stops.[23,24] Gaussian 09 uses the Berny algorithm that works with GEDIIS in redundant internal coordinates.[13,25] When convergence occurs and if the system is stable, then a global minimum or a local minima would have been reached on the potential energy surface. However, if a saddle point was reached instead, then the system will be unstable.[23,24] The stability can be checked by evaluating the frequencies of each structure. If there is a negative frequency, it indicates that the structure is unstable and has reached a saddle point on the potential energy surface, whereas positive frequencies indicate stability and that the structure has reached a global minimum or a local minima.[24]

4.4.2 Experimental

All coordination modes for the ML, MLH_{-1}, ML_2H_{-1} and MLH_{-2} species of Cu-Gly-Leu-Phe and Cu-Sar-Leu-Phe were generated using GaussView 5.0.9.[26] In all the generated coordination modes, copper(II) was bound to the amine-N and then to combinations of other possible binding sites for each species. Minimization in GaussView 5.0.9 was carried out and the multiplicity and charge of each resulting structure was checked and calculated by Gaussian 09 Revision C. 01.[13,26] The multiplicity for each complex is a doublet, since copper(II) has one unpaired electron and the charge for the ML, MLH_{-1}, ML_2H_{-1} and MLH_{-2} species is +1, 0, -1 and -2 respectively. These structures were obtained at the M06-2x/def2-svp level of theory.[27-29] Once the ground state energy of each structure was obtained, the frequencies were checked to determine if the structures were stable.

4.4.3 Results

All the possible coordination modes for each species of Cu-Gly-Leu-Phe and Cu-Sar-Leu-Phe were calculated by Gaussian 09 and can be seen in Figures 4.31-4.50 below. In all of these figures, except for Figure 4.49, the side views labelled "i" show the geometry of each complex and the top down views labelled "ii" show the coordination. Any axial water molecules in the top down views were removed for clarity. Figure 4.49 shows both the geometry and the coordination in a side view labled "i". In all the figures the grey, white, blue, red and orange spheres are the carbon, hydrogen, nitrogen, oxygen and copper(II) atoms respectively. All the coordination modes that did not converge can be seen in the Appendix in Figures 1-8.

4.4.3(a) Cu-Gly-Leu-Phe

Two different coordination modes, labelled **a** and **b** were found for the ML species of Cu-Gly-Leu-Phe and can be seen in Figures 4.31 and 4.32 respectively. Both coordination modes have tetragonally distorted octahedral geometries. In coordination mode **a**, water molecules are in the axial positions, while in coordination mode **b,** the carbonyl-O is in the one axial position. When comparing the ground state energies, coordination mode **b** is approximately 200,000 kJ/mol less than coordination mode **a** and therefore coordination mode **b** is more likely to form. This corresponds to the UV-Vis analysis, since copper(II) does not coordinate to an amide-N. This coordination mode also agrees with the coordination mode that was suggested by the ^{1}H NMR analysis. However, in the ^{1}H NMR analysis the coordination to the carboxyl-O could not be seen, because the nearest proton was too distant to be affected by copper(II).

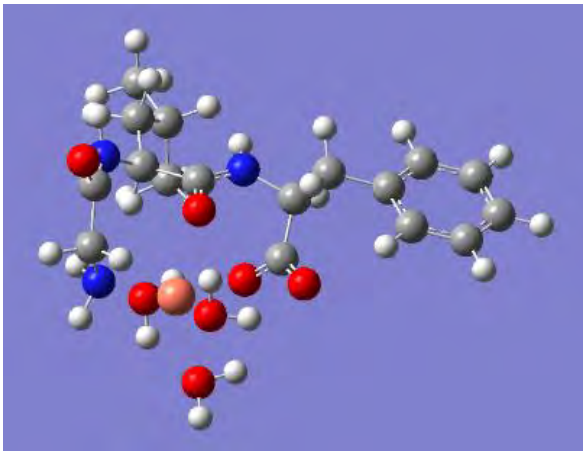

i

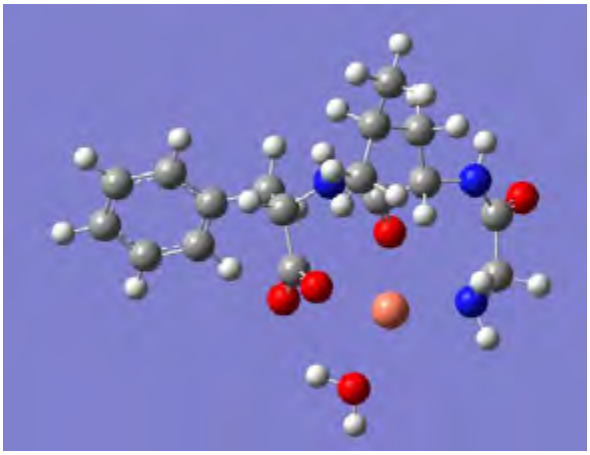

ii

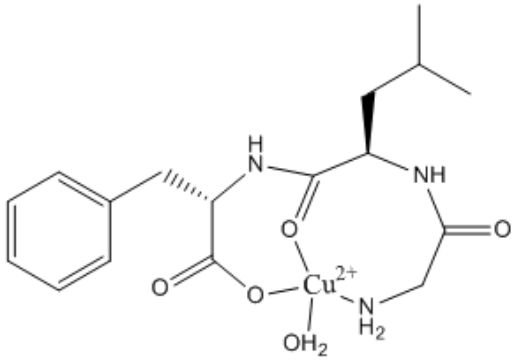

iii

Figure 4.31: i: Gaussian 09 side view, ii: Gaussian 09 top down view and iii: a line drawing of coordination mode **a** from the ML species in Cu-Gly-Leu-Phe, which has a ground state energy of -7,864,187.52 kJ/mol. Axial water molecules have been omitted in the top down view and in the line drawing for clarity.

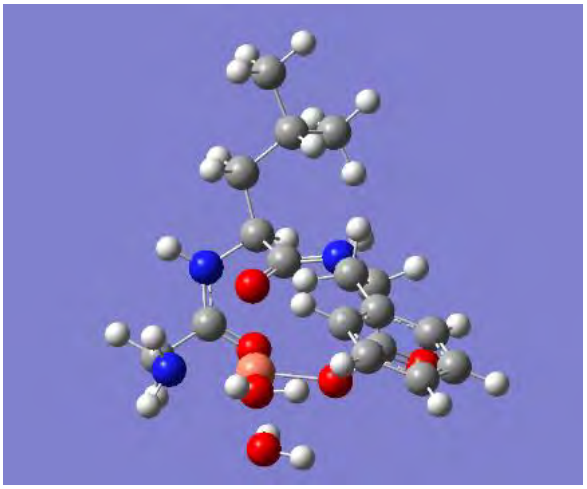

i

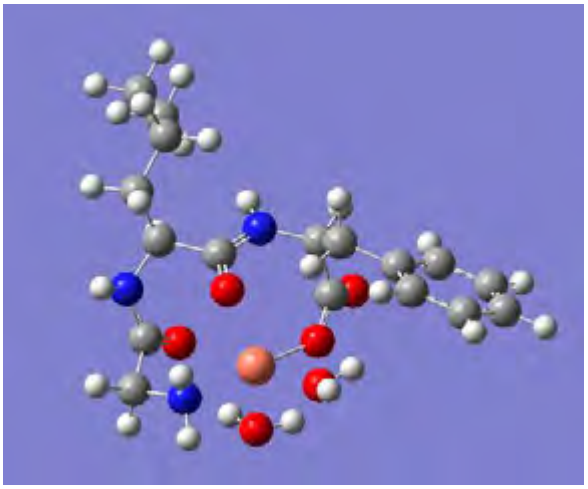

ii

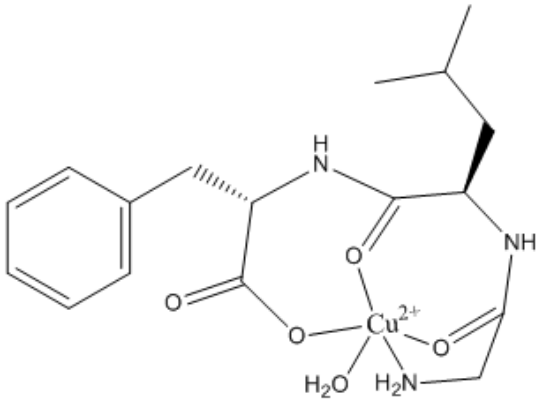

iii

Figure 4.32: i: Gaussian 09 side view, ii: Gaussian 09 top down view and iii: a line drawing of coordination mode **b** from the ML species in Cu-Gly-Leu-Phe, which has a ground state energy of -7,663,766.02 kJ/mol.

Four different coordination modes, labelled from **a-d** were found for the MLH_{-1} species of Cu-Gly-Leu-Phe, which can be seen in Figures 4.33-4.36 respectively. Coordination mode **a**, **b** and **c** were all found to have tetragonally distorted octahedral geometries and both the axial positions were occupied by water molecules. Coordination mode **d** was found to have a square pyramidal geometry and copper(II) was coordinated to the carboxyl-O in the one axial position. For all the coordination modes, the loss of the proton came from an amide-N. When comparing the ground state energies, coordination modes **a-c** have energies that are within approximately 150 kJ/mol of one another, while coordination mode **d** has an energy that is approximately 200,500 kJ/mol less than the other coordination modes. Therefore, since

coordination mode **d** has a much lower energy, it is more likely to form. This corresponds to the potentiometric analysis, which found that the loss of the proton came from the ligand and not from the water. It also corresponds to the IR and UV-Vis analyses which showed that copper(II) coordinated to an amide-N. This coordination mode also agrees with the coordination mode that was suggested by the ^{1}H NMR analysis. However, similarly to the ML species, in the ^{1}H NMR analysis the coordination to the carboxyl-O could not be seen, because the nearest proton was too distant to be affected by copper(II).

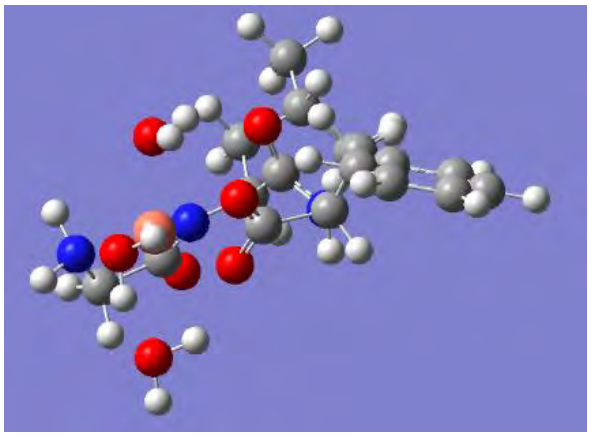

i

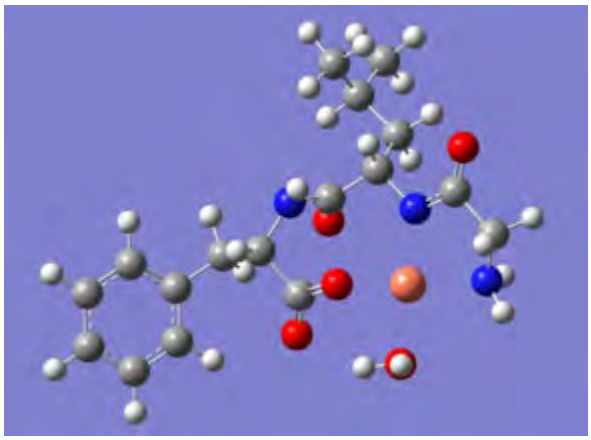

ii

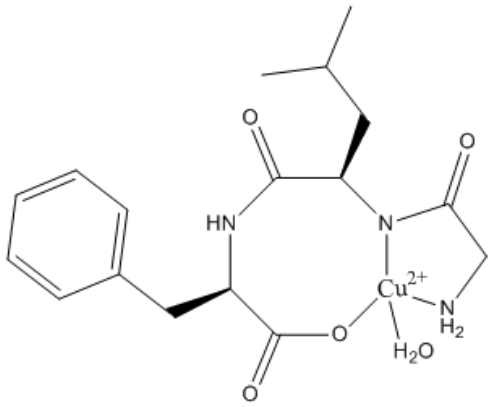

iii

Figure 4.33: i: Gaussian 09 side view, ii: Gaussian 09 top down view and iii: a line drawing of coordination mode **a** from the MLH_{-1} species in Cu-Gly-Leu-Phe, which has a ground state energy of -7,863,208.27 kJ/mol. Axial water molecules have been omitted in the top down view and in the line drawing for clarity.

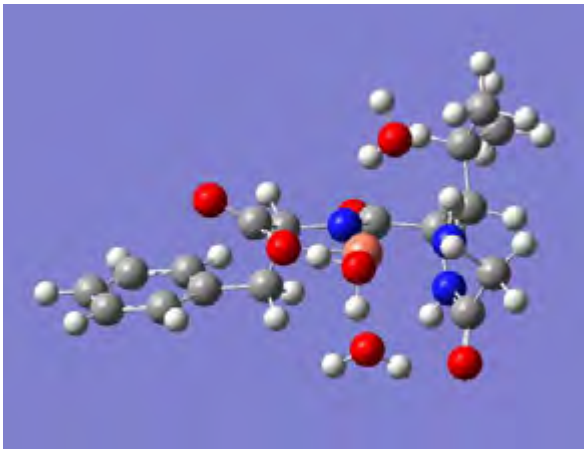

i

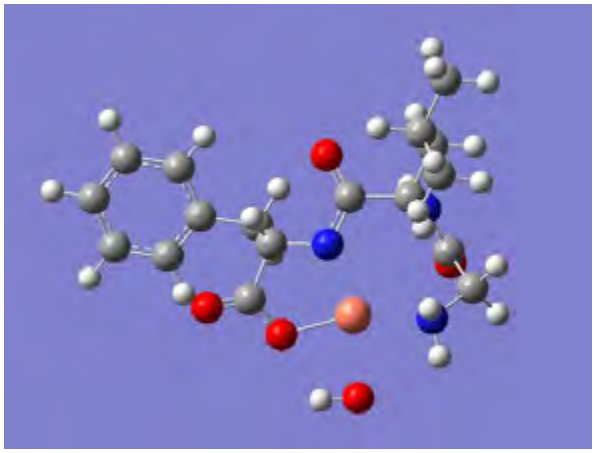

ii

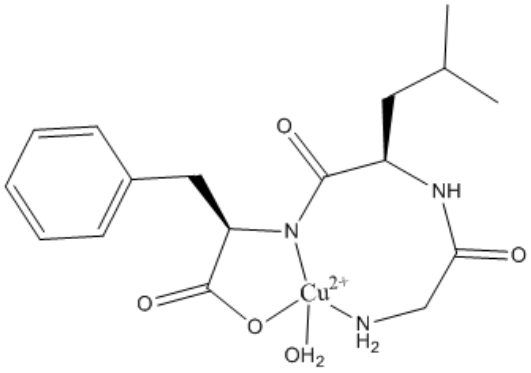

iii

Figure 4.34: i: Gaussian 09 side view, ii: Gaussian 09 top down view and iii: a line drawing of coordination mode **b** from the MLH_{-1} species in Cu-Gly-Leu-Phe, which has a ground state energy of -7,863,142.37 kJ/mol. Axial water molecules have been omitted in the top down view and in the line drawing for clarity.

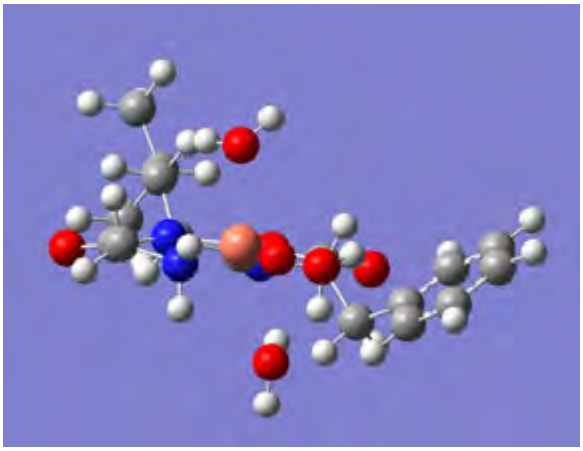

i

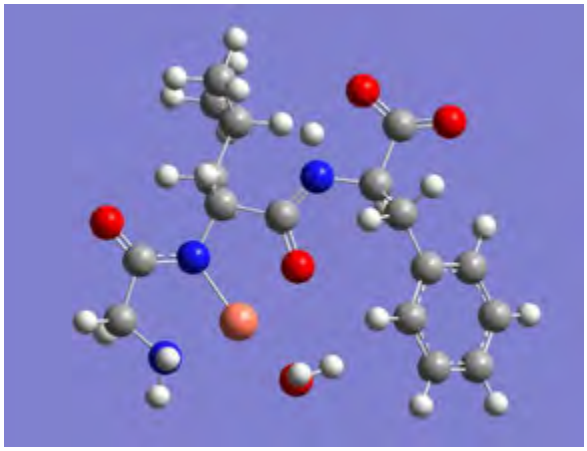

ii

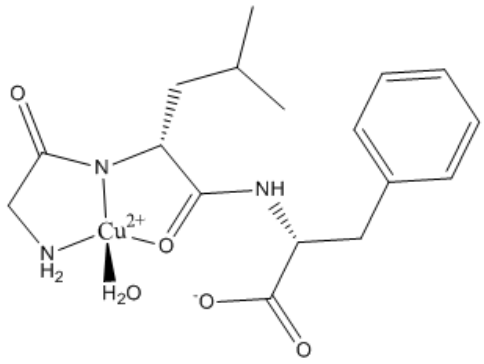

iii

Figure 4.35: i: Gaussian 09 side view, ii: Gaussian 09 top down view and iii: a line drawing of coordination mode **c** from the MLH_{-1} species in Cu-Gly-Leu-Phe, which has a ground state energy of -7,863,055.34 kJ/mol. Axial water molecules have been omitted in the top down view and in the line drawing for clarity.

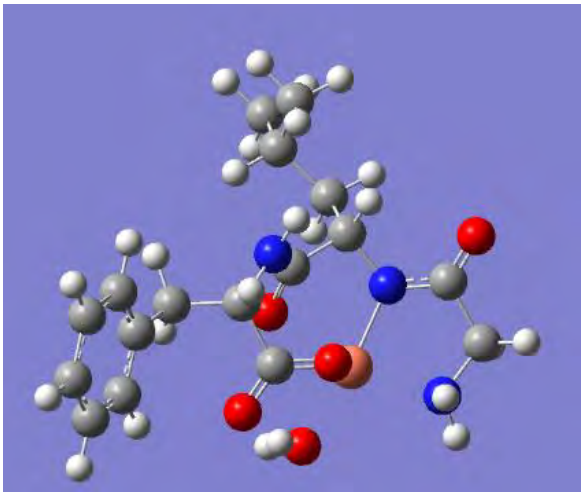

i

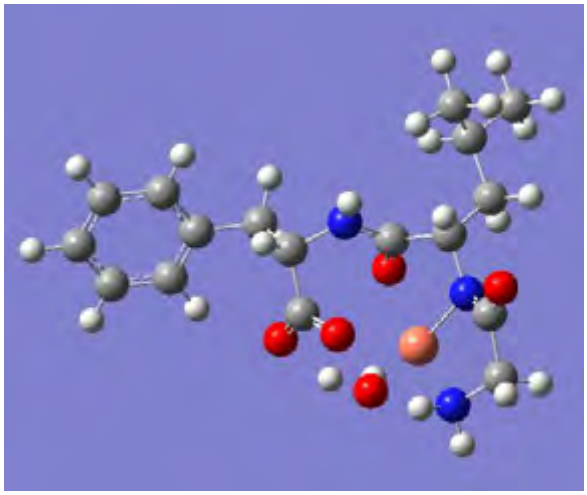

ii

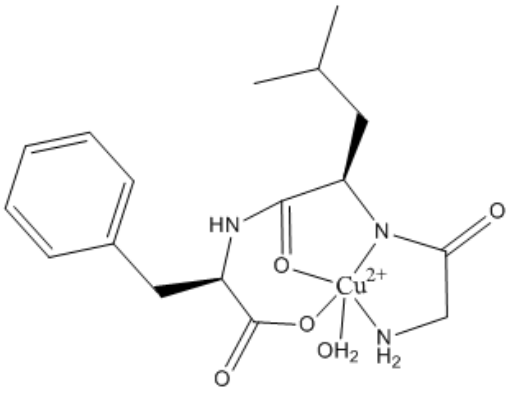

iii

Figure 4.36: i: Gaussian 09 side view, ii: Gaussian 09 top down view and iii: a line drawing of coordination mode **d** from the MLH_{-1} species in Cu-Gly-Leu-Phe, which has a ground state energy of -7,662,718.67 kJ/mol.

Eighteen different coordination modes were evaluated for the ML_2H_{-1} species of Cu-Gly-Leu-Phe and of these only two refined successfully. The other sixteen are shown in the appendix. The two different coordination modes, **a** and **b**, that were found, can be seen in Figures 4.37 and 4.38 respectively. Both coordination modes formed a tetragonally distorted octahedral geometry and lost the proton from an amide group. When comparing the ground state energies, coordination mode **a** is approximately 5500 kJ/mol lower in energy than coordination mode **b** and therefore more likely to form. The potentiometric, IR and UV-Vis analyses agree with this coordination mode, since copper(II) coordinated to the amide-N. This coordination mode was also suggested as a coordination mode in the ^{1}H NMR analysis.

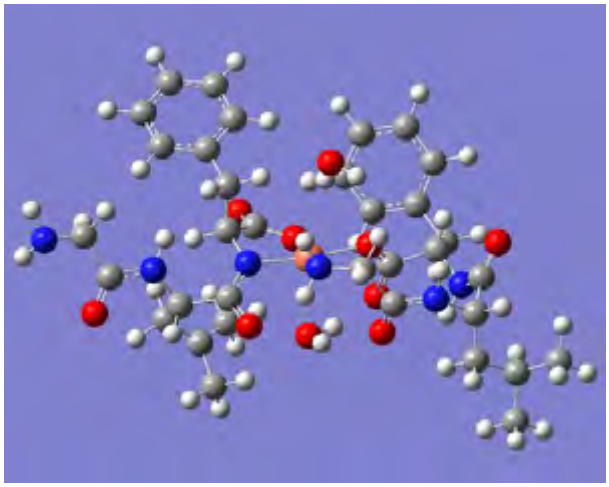

i

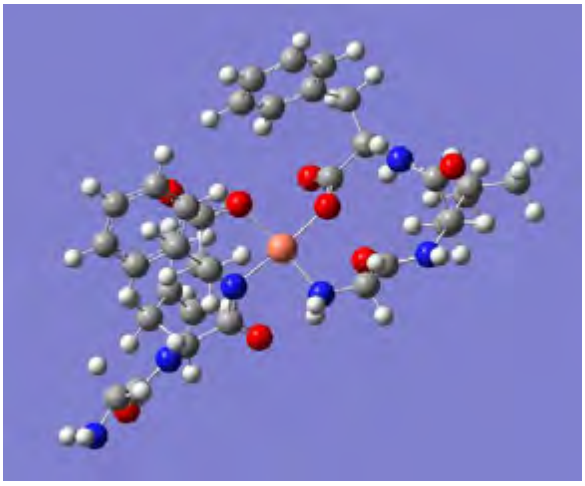

ii

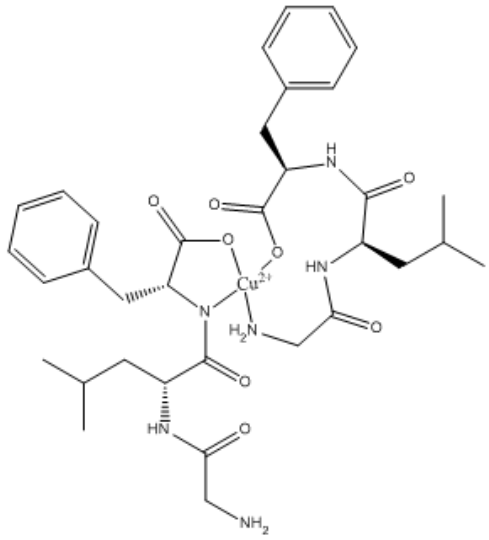

iii

Figure 4.37: i: Gaussian 09 side view, ii: Gaussian 09 top down view and iii: a line drawing of coordination mode **a** from the ML_2H_{-1} species in Cu-Gly-Leu-Phe, which has a ground state energy of -10,614,276.27 kJ/mol. Axial water molecules have been omitted in the top down view and in the line drawing for clarity.

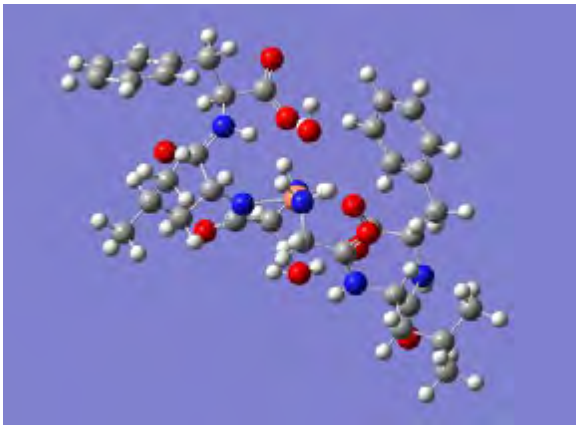

i

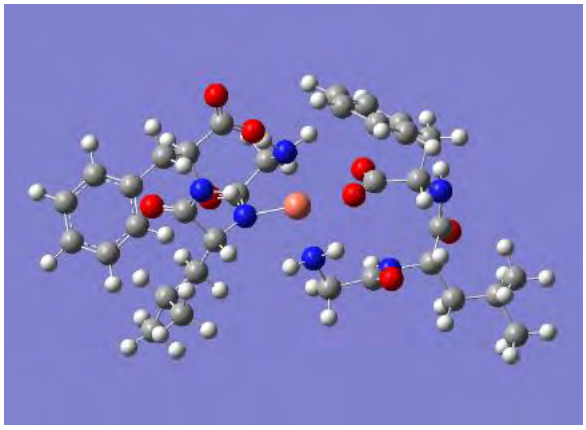

ii

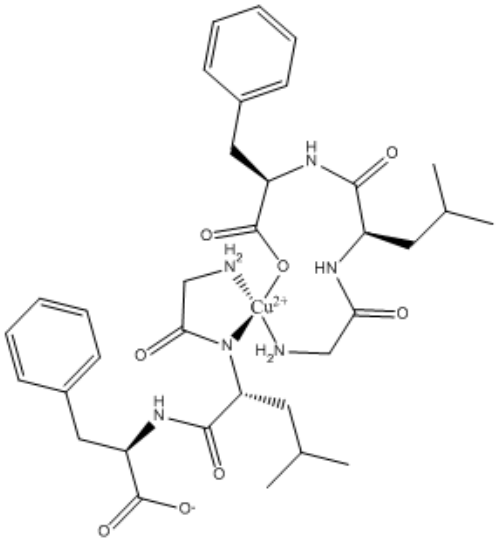

iii

Figure 4.38: i: Gaussian 09 side view, ii: Gaussian 09 top down view and iii: a line drawing of coordination mode **b** from the ML_2H_{-1} species in Cu-Gly-Leu-Phe, which has a ground state energy of -10,619,800.63 kJ/mol. Axial water molecules have been omitted in the top down view and in the line drawing for clarity.

Two different coordination modes **a** and **b** were found for the MLH_{-2} species of Cu-Gly-Leu-Phe and can be seen in Figures 4.39 and 4.40 respectively. Coordination mode **a** has a tetragonally distorted octahedral geometry with axial water molecules, while coordination mode **b** has a square planar geometry. In coordination **a**, one proton was lost from an amide and another proton was lost from water, while in coordination mode **b**, both protons were lost from the amide groups. The ground state energy of coordination mode **b** is approximately 200,000 kJ/mol lower than coordination mode **a** and therefore is the preferred structure. This agrees with the potentiometric analysis, since both protons are lost from the ligand and not from water. It also agrees with the UV-Vis analysis, since copper(II) has coordinated with amide groups.

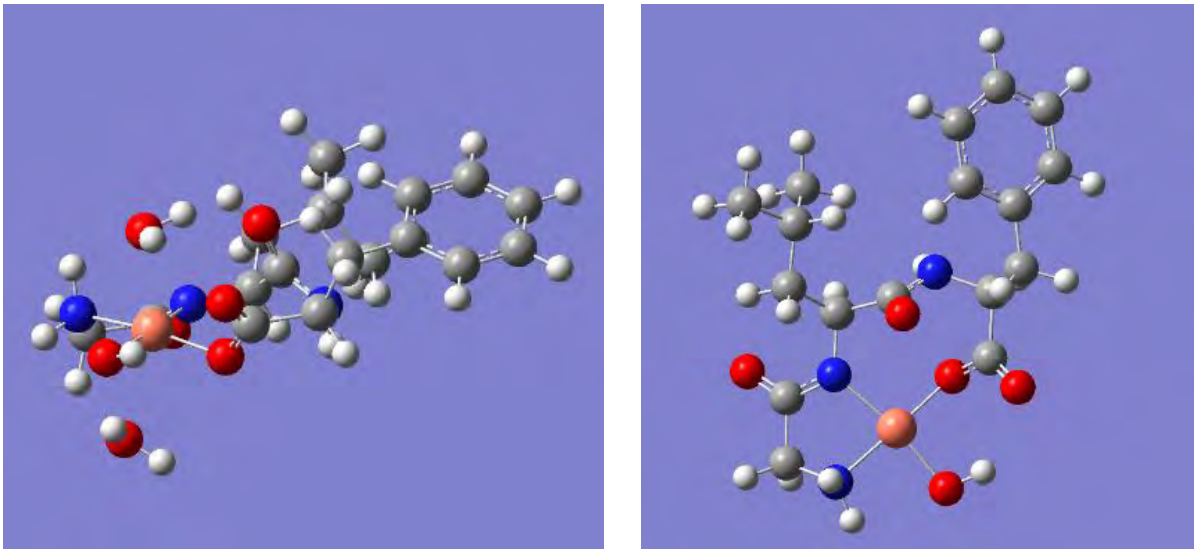

i ii

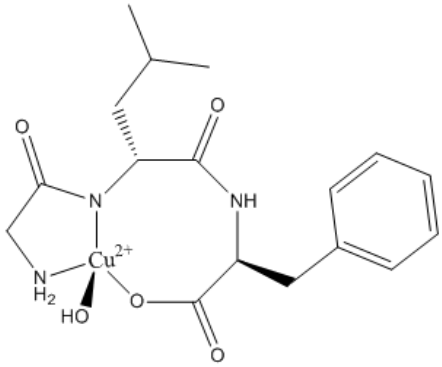

iii

Figure 4.39: i: Gaussian 09 side view, ii: Gaussian 09 top down view and iii: a line drawing of coordination mode **a** from the MLH_{-2} species in Cu-Gly-Leu-Phe, which has a ground state energy of -7,861,342.53 kJ/mol. Axial water molecules have been omitted in the top down view and in the line drawing for clarity.

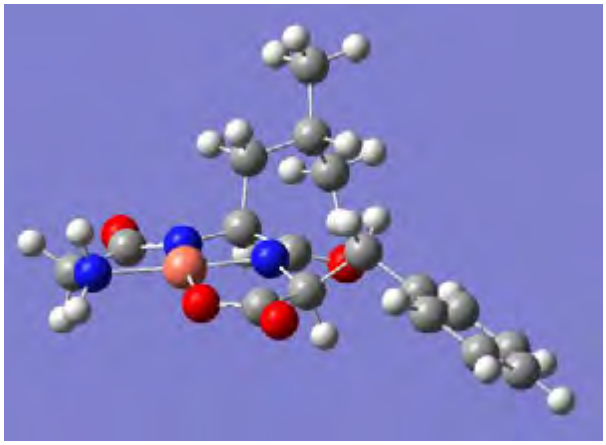

i

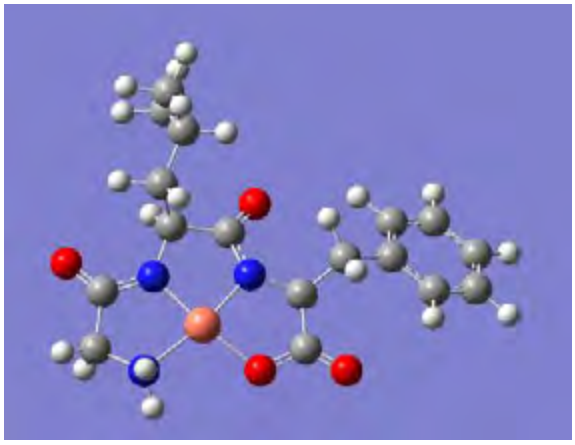

ii

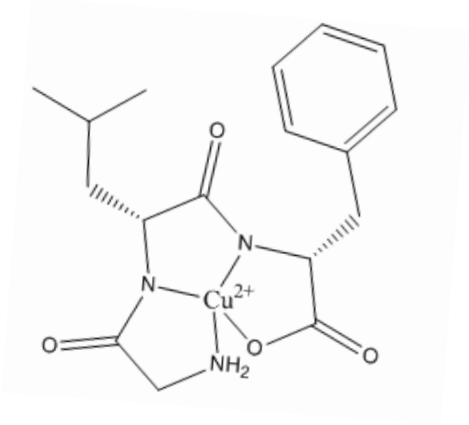

iii

Figure 4.40: i: Gaussian 09 side view, ii: Gaussian 09 top down view and iii: a line drawing of coordination mode **b** from the MLH_{-2} species in Cu-Gly-Leu-Phe, which has a ground state energy of -7,660,922.49 kJ/mol.

4.4.3(b) Cu-Sar-Leu-Phe

Four coordination modes were found for the ML species of Cu-Sar-Leu-Phe, namely coordination mode **a**, **b**, **c** and **d** and can be seen in Figures 4.41-4.44 respectively. The molecular geometries of coordination modes **a** and **b** could not be determined clearly, since water molecules appear to cluster randomly around copper(II) in both coordination modes. Coordination modes **c** and **d** were found to have a tetragonally distorted octahedral geometry. Coordination mode **c** has two water molecules in the axial positions, while coordination mode **d** has one water molecule and one donor group (a carbonyl group) in the axial positions. When comparing the ground state energies, coordination modes **a** and **b** are similar in energy with a difference of approximately 600 kJ/mol, while coordination mode **c** is approximately

200,000 kJ/mol lower in energy and coordination mode **d** is approximately another 200,000 kJ/mol lower in energy than coordination mode **c**. Therefore since coordination mode **d** has the lowest ground state energy, it is more likely to form compared to the other coordination modes. This corresponds to the UV and IR analyses, since the UV-analysis suggested that the ML species does not coordinate to an amide-N group and the IR-analysis suggested that copper(II) coordinated to either the carboxyl-O or to the carbonyl-O or to both. The ^{1}H NMR analysis also suggested this coordination mode.

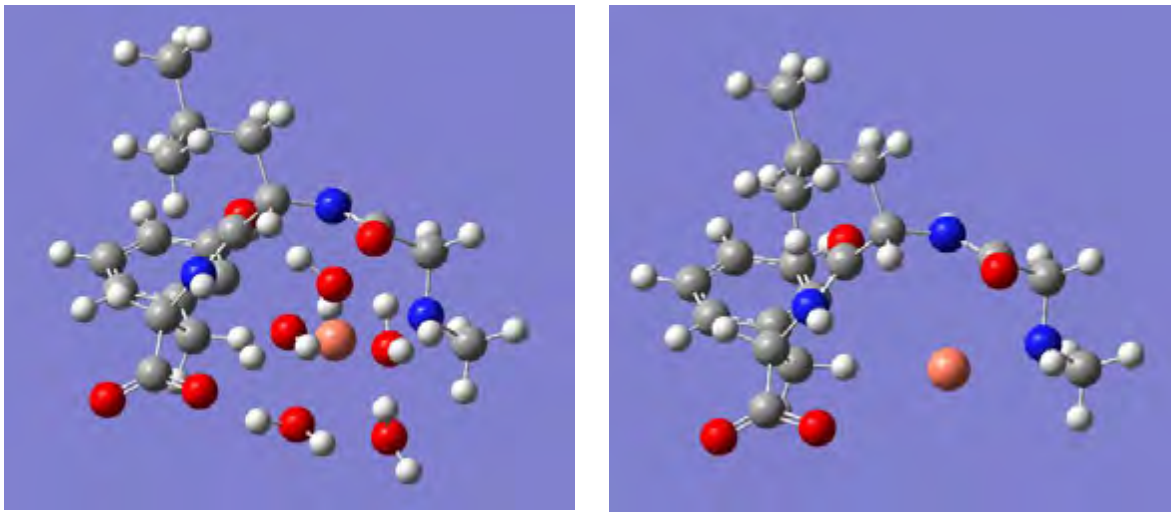

i ii

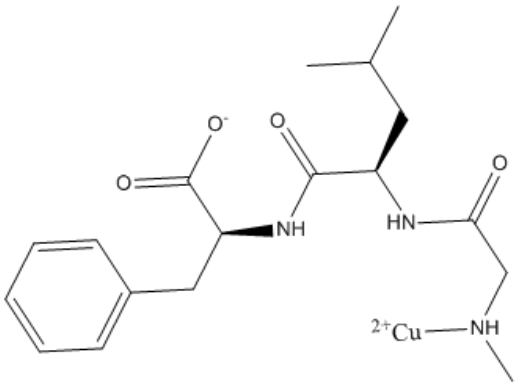

iii

Figure 4.41: i: Gaussian 09 side view, ii: Gaussian 09 top down view and iii: a line drawing of coordination mode **a** from the ML species in Cu-Sar-Leu-Phe, which has a ground state energy of -8,166,964.67 kJ/mol. Water molecules have been omitted in the top down view and line drawing for clarity.

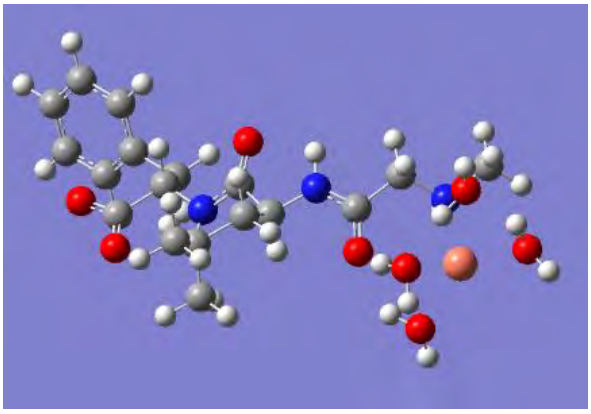

i

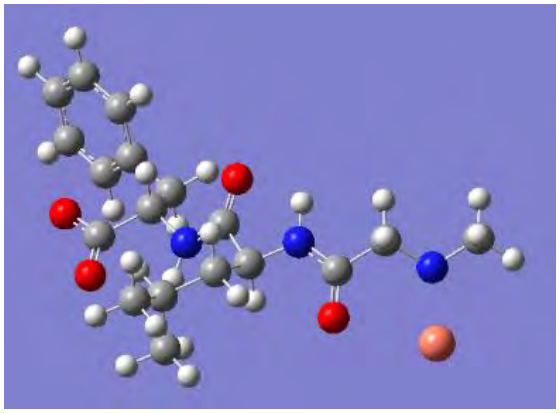

ii

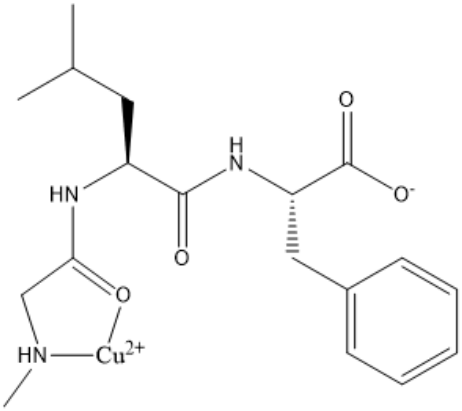

iii

Figure 4.42: i: Gaussian 09 side view, ii: Gaussian 09 top down view and iii: a line drawing of coordination mode **b** from the ML species in Cu-Sar-Leu-Phe, which has a ground state energy of -8,167,557.10 kJ/mol. Water molecules have been omitted in the top down view and in the line drawing for clarity.

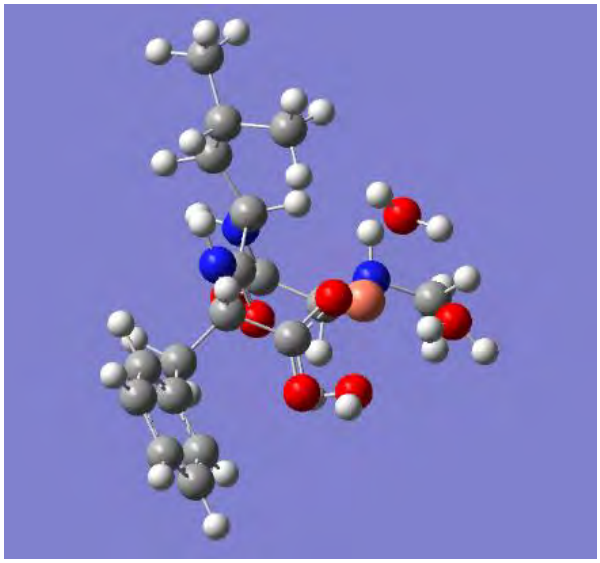

i

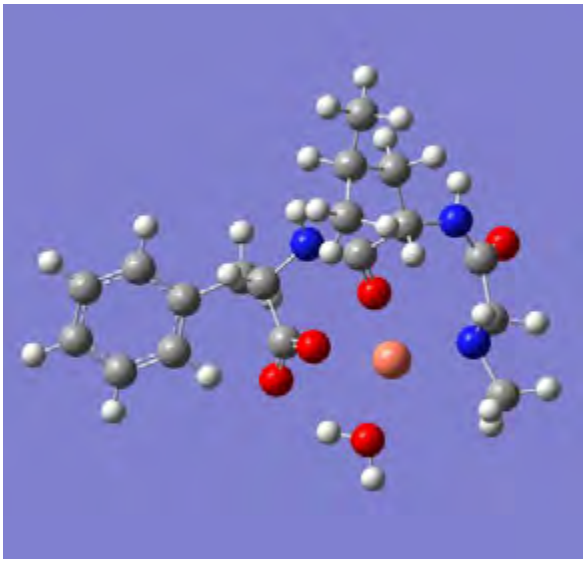

ii

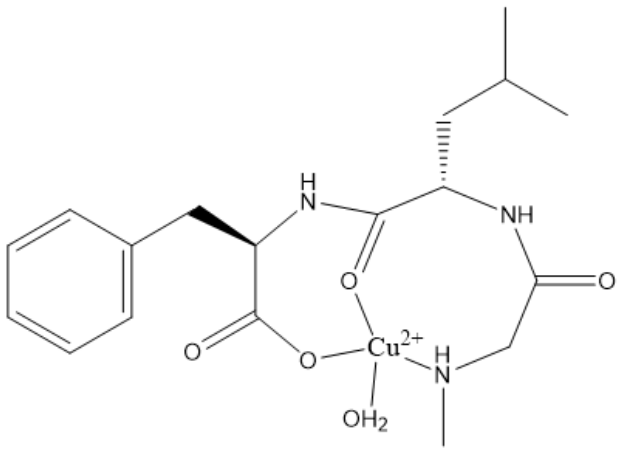

iii

Figure 4.43: i: Gaussian 09 side view, ii: Gaussian 09 top down view and iii: a line drawing of coordination mode **c** from the ML species in Cu-Sar-Leu-Phe, which has a ground state energy of -7,967,259.42 kJ/mol. Water molecules have been omitted in the top down view and in the line drawing for clarity.

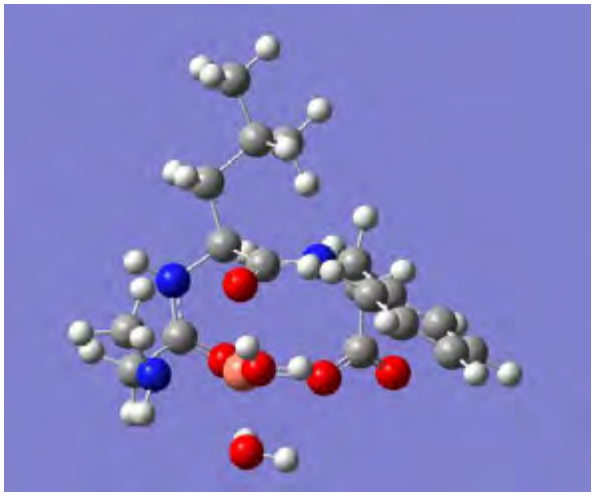

i

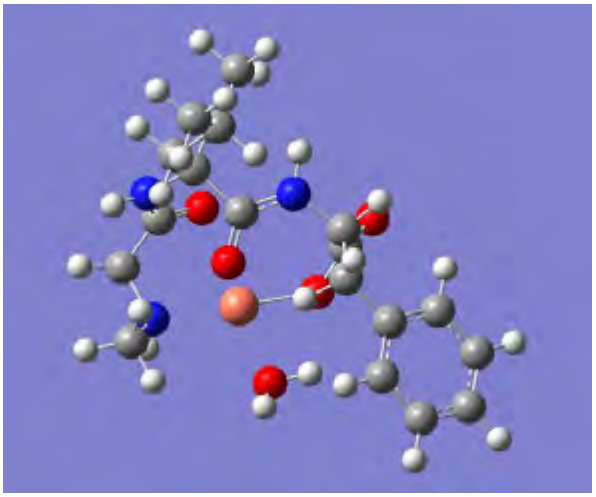

ii

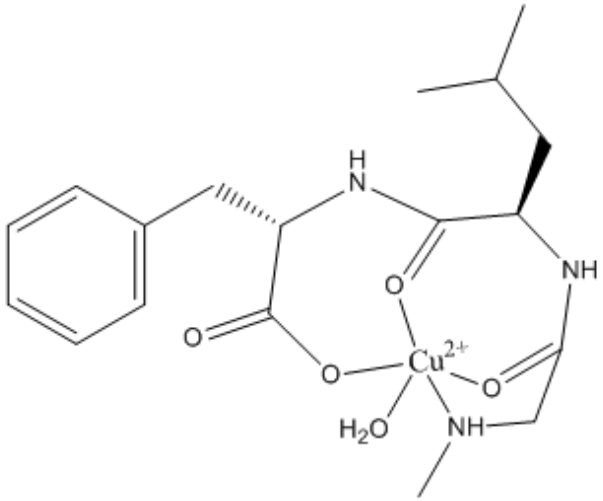

iii

Figure 4.44: i: Gaussian 09 side view, ii: Gaussian 09 top down view and iii: a line drawing of coordination mode **d** from the ML species in Cu-Sar-Leu-Phe, which has a ground state energy of -7,766,840.08 kJ/mol. Water molecules have been omitted in the top down view and in the line drawing for clarity.

Two different coordination modes, labelled **a** and **b** were found for the MLH_{-1} species of Cu-Sar-Leu-Phe, which can be seen in Figures 4.45 and 4.46 respectively. The geometry of coordination mode **a** has a tetragonally distorted octahedral geometry and coordination mode **b** has a square pyramidal geometry. In both coordination modes the proton was lost from the amide-N. Coordination mode **a** was found to be approximately 150 kJ/mol lower than coordination mode **b**. This difference in energy could indicate that coordination mode **a** could form slightly more readily than coordination mode **b.** This corresponds to the potentiometric analysis, since the loss of the proton was from the amide-N group in both coordination modes

and not from water. It also agrees with the UV-Vis analysis and IR analysis, as copper(II) coordinated to an amide-N and to the carboxyl-O respectively. The results from the ^{1}H NMR analysis also suggest that both coordination modes could form.

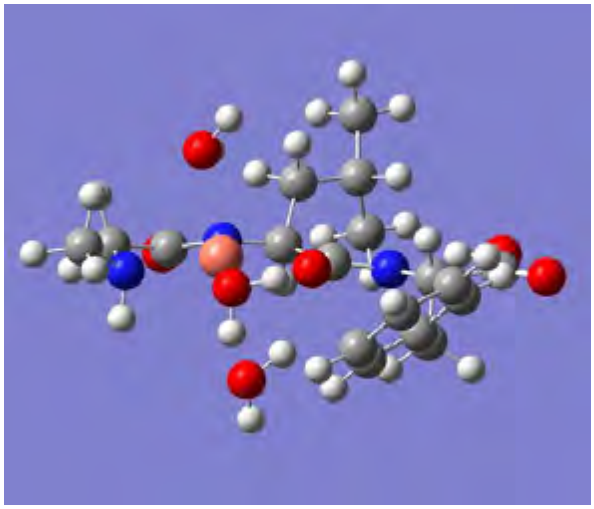

i

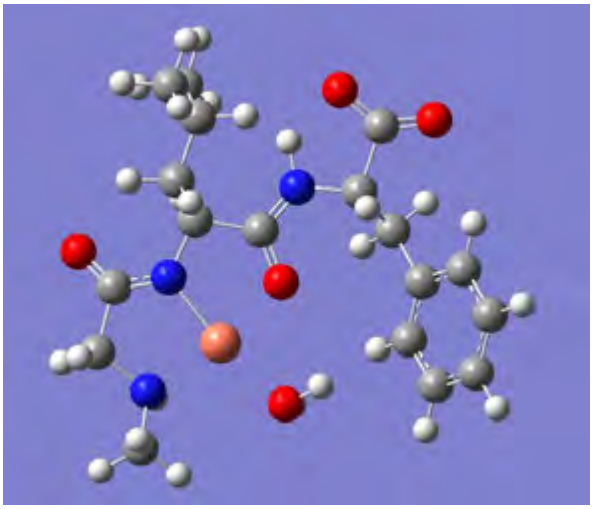

ii

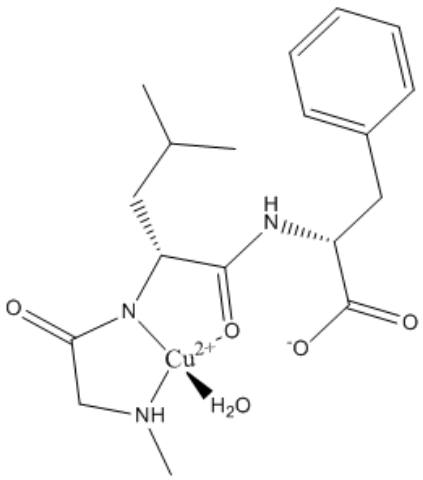

iii

Figure 4.45: i: Gaussian 09 side view, ii: Gaussian 09 top down view and iii: a line drawing of coordination mode **a** from the MLH_{-1} species in Cu-Sar-Leu-Phe, which has a ground state energy of -7,966,126.71 kJ/mol. Axial water molecules have been omitted in the top down view and in the line drawing for clarity.

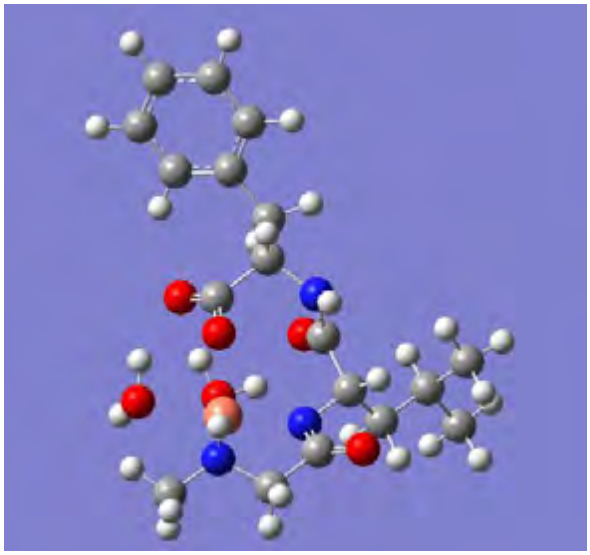

i

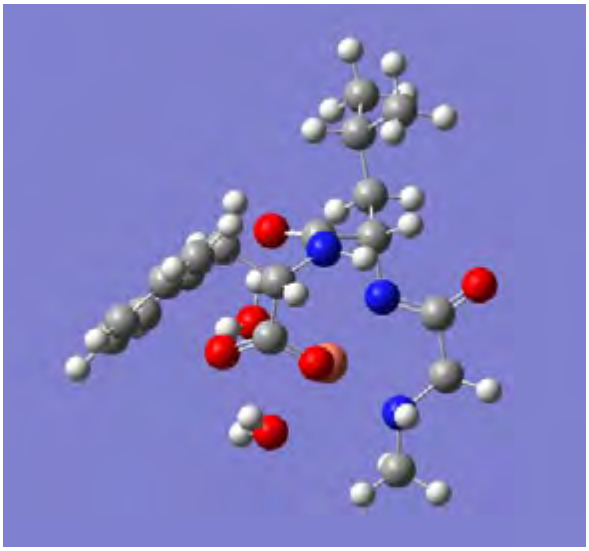

ii

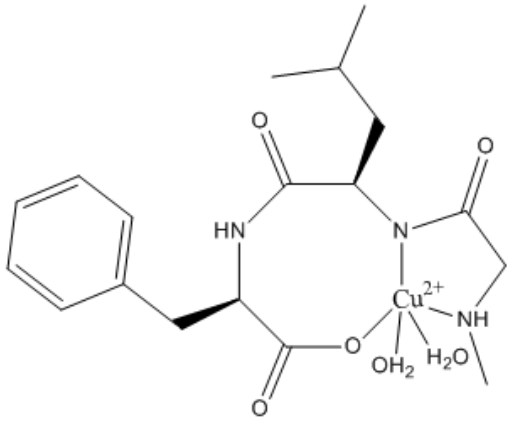

iii

Figure 4.46: i: Gaussian 09 side view, ii: Gaussian 09 top down view and iii: a line drawing of coordination mode **b** from the MLH_{-1} species in Cu-Sar-Leu-Phe, which has a ground state energy of -7,966,277.78 kJ/mol.

Only one coordination mode, named coordination mode **a**, was found for the ML_2H_{-1} species, which can be seen in Figure 4.47. This coordination mode was found to have a square planar geometry and even though its ground state energy cannot be compared to the ground state energies of the ML_2H_{-1} species from Cu-Gly-Leu-Phe, their magnitudes have a difference of approximately 200,000 kJ/mol. This indicates that the ground state energy for the ML_2H_{-1} species of Cu-Sar-Leu-Phe is reasonable. The computational results agree with the potentiometric and UV-Vis analyses, since copper(II) coordinated to the amide-N group. It also agrees with the IR analysis, since copper(II) coordinated to an amide-N and to a carboxyl-O.

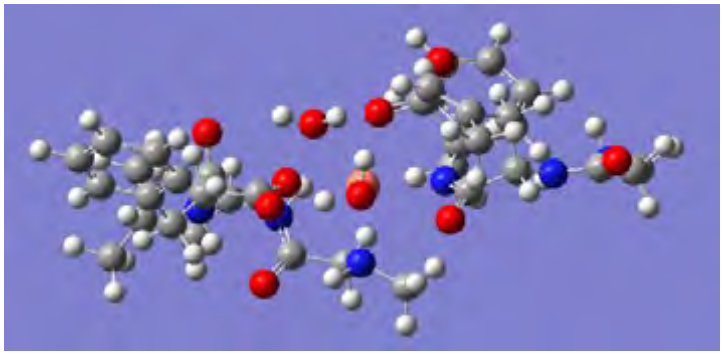

i

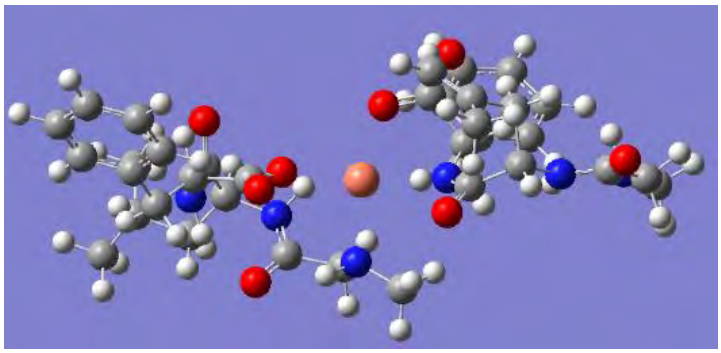

ii

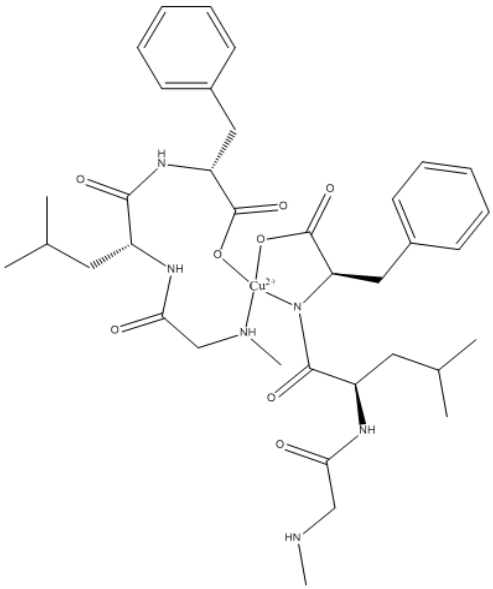

iii

Figure 4.47: Gaussian 09 side view, ii: Gaussian 09 top down view and iii: a line drawing of coordination mode **a** from the ML_2H_{-1} species in Cu-Sar-Leu-Phe, which has a ground state energy of -10,824,337.87 kJ/mol. Axial water molecules have been omitted in the top down view and in the line drawing for clarity.

Three coordination modes were found for the MLH_{-2} species, namely coordination mode **a**, **b** and **c**, which can be seen in Figure 4.48-4.50 respectively. Coordination mode **a** and **c** were found to have a tetragonally distorted octahedral geometry, while coordination mode **b** was found to have a square planar geometry. In coordination modes **a** and **b** the first proton was lost from the amide-N and the second proton was lost from a water molecule, while in coordination mode **c**, both protons were lost from the amide-N groups. Coordination modes **a** and **b** have similar ground state energies that are within 40 kJ/mol of each other, while coordination mode **c** was found to be approximately 200,000 kJ/mol lower in energy and therefore more likely to form. The potentiometric analysis suggested that the first hydrogen is lost from the amide-N and the second could either be lost from another amide-N or from a water molecule. The UV-Vis and IR analyses suggested that copper(II) coordinated to the amide-N groups. The IR analysis also suggested that copper(II) coordinated to a carbonyl-O group.

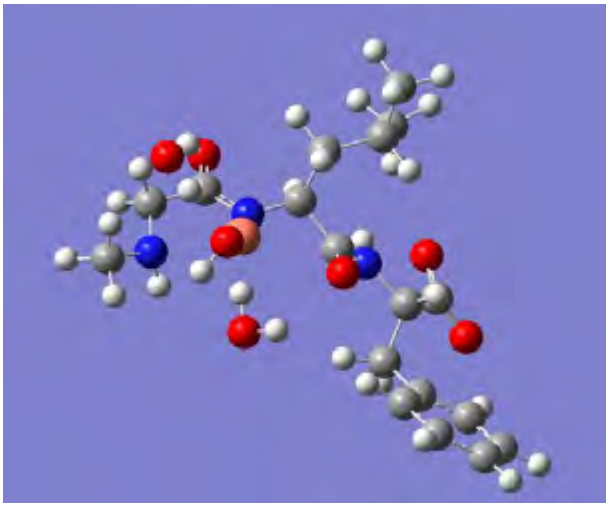

i

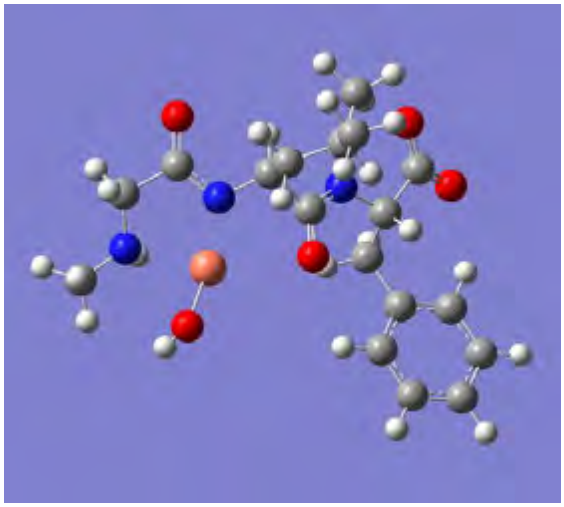

ii

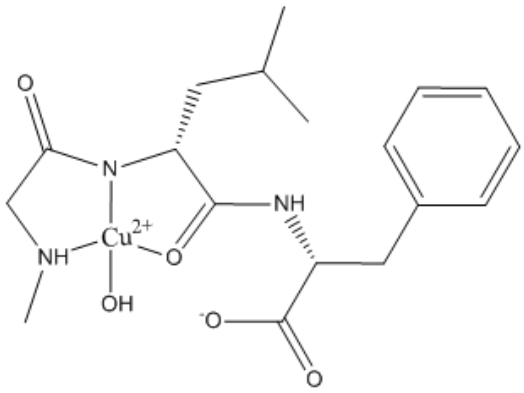

iii

Figure 4.48: i: Gaussian 09 side view, ii: Gaussian 09 top down view and iii: a line drawing of coordination mode **a** from the MLH_{-2} species in Cu-Sar-Leu-Phe, which has a ground state energy of -7,964,717.81 kJ/mol. Axial water molecules have been omitted in the top down view and in the line drawing for clarity.

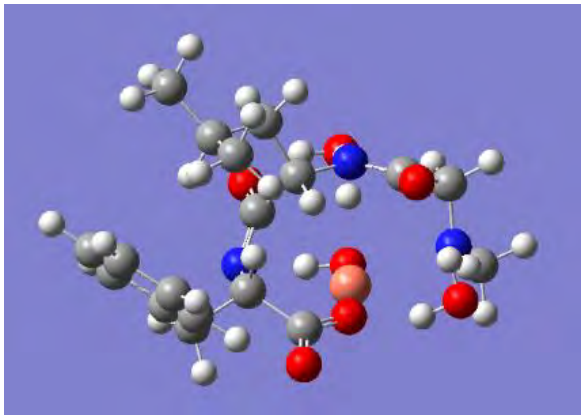

i

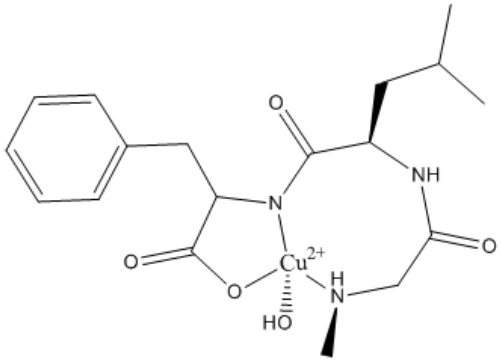

ii

Figure 4.49: i: Gaussian 09 side view and ii: a line drawing of coordination mode **b** from the MLH_{-2} species in Cu-Sar-Leu-Phe, which has a ground state energy of -7,964,678.07 kJ/mol.

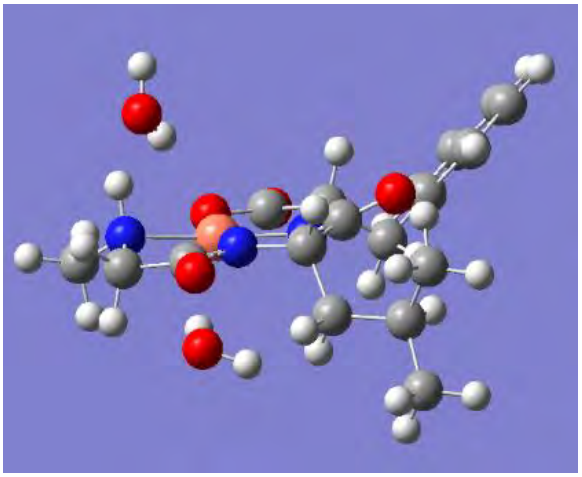

i

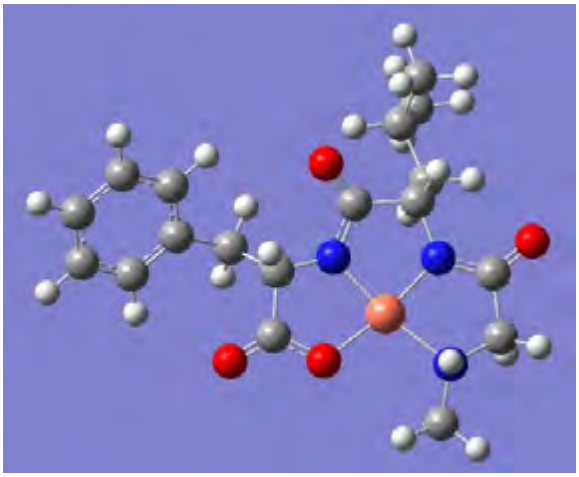

ii

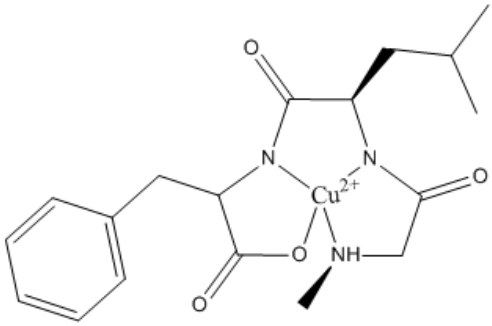

iii

Figure 4.50: i: Gaussian 09 side view, ii: Gaussian 09 top down view and iii: a line drawing of coordination mode **c** from the MLH_{-2} species in Cu-Sar-Leu-Phe, which has a ground state energy of -7,763,994.47 kJ/mol. Axial water molecules have been omitted in the top down view and in the line drawing for clarity.

4.4.4 Discussion

In the UV-analysis Billo's method was used to determine the coordination modes of each species for each copper(II) complex. As discussed in the UV-analysis, Billo proposed an empirical method which can be used to calculate the λ_{max} (nm) from groups coordinated to the equatorial plane of a tetragonally distorted octahedral copper(II) complex.[30,31] However, the method could not determine any of the coordination modes and these computational results have suggested reasons for this. In the ML species of both copper(II) complexes the ligand donor groups are in the axial positions, which should be occupied by water molecules for Billo's method to work. The ML_2H_{-1} species of Cu-Gly-Leu-Phe and the MLH_{-2} species of Cu-Sar-Leu-Phe both formed a tetragonally distorted octahedral geometry with water molecules in the axial positions. Billo's method should have been able to calculate these coordination modes, but was unable to do so. However, a possible reason could be due to the bond lengths of the axial water molecules. As discussed below, in sections 4.4.4(a.iii) and 4.4.4(b.iv), the bond lengths were found to be of a magnitude that causes the complexes to tend towards a square planar geometry and therefore Billo's method cannot calculate these species. The MLH_{-1}, MLH_{-2} species of Cu-Gly-Leu-Phe and the ML_2H_{-1} species of Cu-Sar-Leu-Phe formed square pyramidal, square planar and again square planar geometries respectively. Billo's method can only calculate tetragonally distorted octahedral geometries and therefore could not calculate the coordination modes of these species. For the MLH_{-1} species of Cu-Sar-Leu-Phe, both coordination modes had similar ground state energies and therefore both could form. However, since Billo's method could not calculate the coordination mode, this suggests that coordination mode **b** could form more readily than coordination mode **a**, because it has a square pyramidal geometry.[30,31]

The proposed coordination modes for the species of Cu-Gly-Leu-Phe and Cu-Sar-Leu-Phe can be seen in Table 4.7 and Table 4.8 respectively with their corresponding bond lengths, geometries, bite angles and relative energies with respect to a particular coordination mode.

Table 4.7: Proposed coordination modes for the species of Cu-Gly-Leu-Phe with their relative energies with respect to a particular coordination mode, geometries, ring sizes, bond lengths and bite angles.

Species	Relative energies with respect to a particular coordination mode kJ/mol	Geometry	Ring size	Bond length Å	Bite angle
ML					
Coordination mode **a**	200,421.50	Tetragonally distorted octahedral	7,8	Cu-N (amine) = 2.048 Cu-O (carboxyl) = 1.957 Cu-O (carbonyl) = 2.439	O-Cu-O = 79.87° O-Cu-N = 85.47°
Coordination mode **b**	0	Tetragonally distorted octahedral	5,7,7	Cu-N (amine) = 2.097 Cu-O (carboxyl) = 1.907 Cu-O (carbonyl) = 2.050 Cu-O_{axial} (carbonyl) = 2.573	N-Cu-O = 76.68° O -Cu-O = 75.86° - 98.06°
MLH_{-1}					
Coordination mode **a**	200,489.60	Tetragonally distorted octahedral	5,8	Cu-N (amine)= 2.067 Cu-N (amide) = 1.984 Cu-O (carboxyl) = 2.045	N-Cu-N = 81.78° O-Cu-N = 94.84°
Coordination mode **b**	200,423.70	Tetragonally distorted	5,8	Cu-N (amine)= 2.084	N-Cu-N = 107.28°

		octahedral		Cu-N (amide) = 2.010 Cu-O (carboxyl) = 1.918	O-Cu-N = 85.34°
Coordination mode **c**	200,336.67	Tetragonally distorted octahedral	5,5	Cu-N (amine) = 2.089 Cu-N (amide) = 1.930 Cu-O (carbonyl) = 1.980	N-Cu-N = 83.05° O-Cu-N = 82.36°
Coordination mode **d**	0	Square pyramidal	5,5,7	Cu-N (amine) = 1.949 Cu-N (amide) = 2.066 Cu-O (carbonyl) = 2.127 $Cu\text{-}O_{axial}$ (carboxyl) = 2.257	N-Cu-N = 83.78° N-Cu-O = 80.52° O-Cu-O =79.77°
ML_2H_{-1}					
Coordination mode **a**	0	Tetragonally distorted octahedral	5,11	Cu-N (amine) = 1.875 Cu-N (amide) = 1.909 Cu-O (carboxyl) = 1.904-1.917 $Cu\text{-}H_2O_{axial}$ = 2.500-3.042	O-Cu-N = 83.92°-92.06°
Coordination mode **b**	5,524.36	Tetragonally distorted octahedral	5,11	Cu-N (amine) = 2.043-2.098 Cu-N (amide) = 1.993 Cu-O (carboxyl) =	N-Cu-N = 81.62° O-Cu-N = 84.67°

				1.990 Cu-H_2O_{axial} = 2.491-2.607	
MLH_{-2}					
Coordination mode **a**	200,420.04	Tetragonally distorted octahedral	5,8	Cu-N (amine) = 1.930 Cu-N (amide) = 1.933 Cu-O (carboxyl) = 1.864	N-Cu-N = 81.89° O-Cu-N = 96.48°
Coordination mode **b**	0	Square planar	5,5,5	Cu-N (amine) = 1.974 Cu-N (amide) =1.831-1.832 Cu-O (carboxyl) = 1.881	N-Cu-N = 85.21°-85.60° O-Cu-N = 86.45°

Table 4.8: Proposed coordination modes for the species of Cu-Sar-Leu-Phe with their relative energies with respect to a particular coordination mode, geometries, ring sizes, bond lengths and bite angles.

Species	Relative energies with respect to a particular coordination mode kJ/mol	Geometry	Ring size	Bond length Å	Bite angle
ML					
Coordination mode **a**	400,124.59	undetermined	-	Cu-N (anime) = 2.183	-
Coordination mode **b**	400,717.02	undetermined	5	Cu-N (amine) = 2.146 Cu-O (carbonyl) = 2.849	N-Cu-O = 68.47°
Coordination mode **c**	200,419.39	Tetragonally distorted octahedral	7,8	Cu-N (amine) = 2.0365 Cu-O (carbonyl) = 2.431 Cu-O (carboxyl) = 1.951	N-Cu-O = 87.81° O-Cu-O = 80.20°
Coordination mode **d**	0	Tetragonally distorted octahedral	5,7,7	Cu-N (amine) = 2.095 Cu-O (carbonyl) = 2.074 $Cu\text{-}O_{axial}$ (carbonyl) = 2.599 Cu-O (carboxyl) = 1.910	N-Cu-O = 77.45°-89.51° O -Cu-O = 74.49°
MLH_{-1}					
Coordination mode **a**	0	Tetragonally distorted	5,5	Cu-N (amine) = 2.079	N-Cu-N = 84.11°

		octahedral		Cu-N (amide) = 1.931 Cu-O (carbonyl) = 1.974	N-Cu-O = 92.59°
Coordination mode **b**	151.07	Square pyramidal	5,8	Cu-N (amine) = 2.045 Cu-N (amide) = 1.991 Cu-O (carboxyl) = 2.192	N-Cu-N = 84.73° N-Cu-O = 94.43°
ML_2H_{-1}					
Coordination mode **a**	0	Square planar	5,11	Cu-N (amine) = 2.240 Cu-N (amide) = 2.303 Cu-O (carboxyl) = 2.120-2.154	N-Cu-O = 77.28° – 91.19°
MLH_{-2}					
Coordination mode **a**	200,723.34	Tetragonally distorted octahedral	5,5	Cu-N (amine) = 2.470 Cu-N (amide) = 2.018 Cu-O (carbonyl) = 2.951	N-Cu-N = 74.135° N-Cu-O = 66.65°
Coordination mode **b**	200,683.60	Square planar	5,8	Cu-N (amine) = 2.519 Cu-N (amide) = 2.779 Cu-O (carboxyl) = 1.991	N-Cu-O = 71.67° – 107.88° O-Cu-O = 90.93°
Coordination mode **c**	0	Tetragonally distorted octahedral	5,5,5	Cu-N (amine) = 1.837 Cu-N (amide)	N-Cu-N = 85.01° – 85.65°

				=1.837-1.979 Cu-O (carboxyl) = 1.883 Cu-H_2O_{axial} = 2.411-2.969	O-Cu-N = 86.62°

Copper(II) formed a range of geometries for the different coordination modes. The geometries of the proposed coordination modes were found to be either square-pyramidal, tetragonally distorted octahedral or square planar and each of these geometries have an optimum bond angle of 90°. However, the formation of the chelate rings will cause strain on these bite angles and result in a deviation from the ideal 90° angle.[32] Bond lengths that were found in literature were in the ranges of 2.002 Å [33] -2.050 Å[34] for the copper(II) amine bonds, 1.977 Å [33] - 2.050 Å[34] for the copper(II) amide bonds, 1.934 Å[35] - 2.010 Å[34] for the copper(II) carboxyl bonds, 1.902 Å -1.974 Å[36] for the copper(II) carbonyl bonds and 2.225 Å[37]- 2.470 Å [34] for the copper(II) water bonds. Axial copper(II) carboxyl bond lengths were found to be 2.616 Å[35] and axial copper(II) carbonyl bond lengths were found to be 2.880 Å.[38] The more the proposed structures deviate from their optimum bond angles and the bond lengths, the more the steric energy of the complex will increase. The energy of the complex will also be affected by the formation of chelate rings between the copper(II) ion and the ligand.[39] The greater the number of chelate ring formations there are in a single complex, the greater the stability of the complex. The overall stability of the chelate ring sizes are 5>6>3>7>4>8-10.[40-42] All of these factors were considered when analysing why one coordination mode for a particular species had a lower or higher energy than another coordination mode from that same species. The analysis for each coordination mode can be seen below.

4.4.4(a) Cu-Gly-Leu-Phe

4.4.4(a.i) ML coordination modes

Coordination mode **a** from the ML species was found to have the lowest energy. Comparing the structural properties of the two ML coordination modes, coordination mode **a** and coordination mode **b** have bond lengths that are within the range that was found in literature, as well as bond lengths that are close to the range. These longer than expected Cu-O bond lengths could increase the energy of each coordination mode to approximately the same degree, since they are relatively the same in length. The deviation in bite angles from the optimum 90° for both coordination modes are approximately the same and therefore could also increase the energy of each coordination mode to approximately the same degree. The biggest difference in both coordination modes are the chelate ring formations, since coordination mode **b** has smaller ring sizes as well as more ring formations. Therefore coordination mode **b** is a more stable structure than coordination mode **a**, which led to a lower energy.

4.4.4(a.ii) MLH_{-1} coordination modes

Coordination mode **d** from the MLH_{-1} species was found to have the lowest energy. The bond lengths of all four MLH_{-1} coordination modes were found to be within, as well as close to the literature ranges. The bond angles for all of the coordination modes deviated from 90° to approximately the same degree. Therefore neither the bond lengths nor the bite angles are responsible for causing the difference in energy between the MLH_{-1} coordination modes. Coordination modes **a**, **b** and **c** all have similar energies, while coordination mode **d** has a significantly lower energy. Coordination mode **d** has three chelate ring formations, which all have stable ring sizes, while the other coordination modes have two chelate ring formations with only one stable five-membered ring. This difference in the number of chelate ring formations and ring sizes therefore caused coordination mode **d** to have a lower energy than coordination modes **a**, **b** and **c**.

4.4.4(a.iii) ML_2H_{-1} coordination modes

Of the two coordination modes that were found for the ML_2H_{-1} species, coordination mode **a** had a lower energy than coordination mode **b**. When comparing the physical properties of these coordination modes, the bond lengths are all close to the literature values and the bond angles deviated slightly from the optimum 90°. The bond lengths of the axial water molecules in both coordination modes are large and therefore cause the geometry of the complex to tend towards a square planar geometry, which could verify why Billo's method could not calculate this coordination mode. The chelate ring formations in both coordination modes consist of one five-membered and one eleven-membered ring formation. Even though the chelate ring formations, as well as the bond length and bond angle deviations, are all similar between the two coordination modes, coordination mode **a** is lower in energy than coordination mode **b**. A possible cause is the result of fewer accumulative bond length and bond angle deviations throughout the whole complex of coordination mode **a** compared to coordination mode **b**.

4.4.4(a.iv) MLH_{-2} coordination modes

Of the two coordination modes that were found for the MLH_{-2} species, coordination mode **b** had the lowest energy. The bond lengths found in both coordination modes were all close to the literature ranges. The bond angles in both coordination modes slightly deviated from the optimum angle of 90°. However, the cause of the vast difference in energy is due to the chelate ring formations. Coordination mode **b** has three five-membered chelate rings, while coordination mode **a** has two chelate rings and only one is a five-membered ring. This difference caused coordination mode **b** to become more stable, which therefore resulted in a lower energy.

4.4.4(b) Cu-Sar-Leu-Phe

4.4.4(b.i) ML coordination modes

Coordination modes **a** and **b** from the ML species were found to be the least stable, which is due to each of these coordination modes either forming one or no chelate rings. It is also due to the formation of bond lengths that are longer than the values found in literature, as well as forming bite angles that are small and therefore strained. Coordination mode **d** was found to have the lowest energy and when comparing coordination mode **d** to **c**, both coordination modes have bond lengths that fall within, as well as close to the literature values. They also have bite angles that deviate to approximately the same degree from the optimum 90° angle. The biggest factor that is affecting the difference in energies between coordination modes **c** and **d** are the chelate ring formations. Coordination mode **c** has two chelate rings, while coordination mode **d** has three. The chelate ring formations from coordination mode **d** are also smaller in size than coordination mode **c** and therefore both of these factors cause coordination mode **d** to be more stable and thus have a lower energy.

4.4.4(b.ii) MLH_{-1} coordination modes

The two coordination modes that were found for the MLH_{-1} species had similar energies, where coordination mode **a** had a slightly lower energy than coordination mode **b**. It can be seen that all of the bond lengths are either within or close to the range found in literature and the bite angles deviate within a similar range from the expected 90° angle. Both coordination modes also formed two chelate rings, although coordination mode **b** formed one five-membered and one eight-membered ring, while coordination mode **a** formed two five-membered rings. This slight difference could be the reason for the slightly higher energy in coordination mode **b** than in **a**.

4.4.4(b.iii) ML_2H_{-1} coordination modes

The one coordination mode that was found for the ML_2H_{-1} species has two chelate ring formations with one five-membered ring and one eleven-membered ring. The bond lengths that are slightly larger than literature values and the bite angles that deviate from the optimum 90° all contribute to decreasing the stability of the complex. This therefore increases the energy of the complex.

4.4.4(b.iv) MLH_{-2} coordination modes

In the MLH_{-2} species, out of the three coordination modes that were found, coordination mode **c** was found to have the lowest energy. When looking at the physical properties it can be seen that coordination mode **a** and coordination mode **b** both have bond lengths and bite angles that fall far outside of the literature range. This, as well as having only two chelate ring formations, makes these two coordination modes less stable than coordination mode **c**, which has three chelate ring formations that all consist of five-membered rings. Coordination mode **c** also has bite angles that are close to the optimum angle of 90°. The axial bond lengths of coordination mode **c** are large and therefore cause the geometry to tend towards a square planar geometry, which could verify why Billo's method could not calculate this coordination mode.

4.4.5 Conclusion

Gaussian 09 was able to propose the most probable coordination modes for the species of Cu-Gly-Leu-Phe and Cu-Sar-Leu-Phe by finding the minimum energy of each possible coordination mode for each species. Once the minimum energies were found, all the proposed coordination modes for a particular species were compared and the coordination mode with the lowest minimum energy was then proposed to be the most probable. The geometry, as well as the bite angles and bond lengths, were also found and used to determine the most probable coordination modes. The geometry for each most probable coordination mode of each species of Cu-Gly-Leu-Phe was found to be tetragonally distorted octahedral for the ML and ML_2H_{-1} species, square pyramidal for the MLH_{-1} species and square planar for the MLH_{-2} species. The geometry for each most probable coordination mode of each species of Cu-Sar-Leu-Phe was found to be tetragonally distorted octahedral for the ML, MLH_{-1} and MLH_{-2} species and square planar for the ML_2H_{-1} species.

References

1. E. G. Lewars, *Computational Chemistry: Introduction to the Theory and Applications of Molecular and Quantum mechanics*, Kluwer Academic Publishers, Massachusetts, 2003, ch. 7, pp. 385-394.
2. F. M. A. Elmagbari, PhD Thesis, University of Cape Town, 2015.
3. M. Mohajane, PhD Thesis, University of Cape Town, 2013.
4. A.Hammouda, PhD Thesis, University of Cape Town, 2015.
5. J. N. Zvimba, PhD Thesis, University of Cape Town, 2005.
6. J. N. Zvimba and G. E. Jackson, *J. Inorg. Biochem.*, 2007, **101**, 1120-1128.
7. S. Odisitse and G. E. Jackson, *Polyhedron*, 2008, **27**, 453-464.
8. J. C. A. Boeyens and P. Comba, *Coord. Chem. Rev.,* 2001, **212**, 3-10.
9. A. K. Rappe, C. J. Casewit, K. S. Colwell, W. A. Goddard and W. M. Skiff, *J. Am. Chem.* Soc., 1992, **114,** 10024-10035.
10. T. A. Halgren, *J. Comp. Chem.,* 1996, **17**, 490-519.
11. F. K. Winkler and J. D. Dunitz, *J. Mol. Biol.*, 1971, **59**, 169-182.
12. K. Capelle, *Brazzilian J. Phys*., 2006, **36,** 1318-1342.
13. M. J. Frisch, G. W. Trucks, H. B. Schlegel, G. E. Scuseria, M. A. Robb, J. R. Cheeseman, G. Scalmani, V. Barone, B. Mennucci, G. A. Petersson, H. Nakatsuji, M. Caricato, X. Li, H. P. Hratchian, A. F. Izmaylov, J. Bloino, G. Zheng, J. L Sonnenberg, M. Hada, M. Ehara, K. Toyota, R. Fukuda, J. Hasegawa, M. Ishida, T. Nakajima, Y. Honda, O. Kitao, H. Nakai, T. Vreven, J. A. Montgomery, Jr., J. E. Peralta, F. Ogliaro, M. Bearpark, J. J. Heyd, E. Brothers, K. N. Kudin, V. N. Staroverov, T. Keith, R. Kobayashi, J. Normand, K. Raghavachari, A. Rendell, J. C. Burant, S. S. Iyengar, J. Tomasi, M. Cossi, N. Rega, J. M. Millam, M. Klene, J. E. Knox, J. B. Cross, V. Bakken, C. Adamo, J. Jaramillo, R. Gomperts, R. E. Stratmann, O. Yazyev, A. J. Austin, R. Cammi, C. Pomelli, J. W. Ochterski, R. L. Martin, K. Morokuma, V. G. Zakrzewski, G. A. Voth, P. Salvador, J. J. Dannenberg, S. Dapprich, A. D. Daniels, O. Farkas, J. B. Foresman, J. V. Ortiz, J. Cioslowski, and D. J. Fox, Gaussian 09 (Revision D.01), Gaussian Inc., Wallingford CT, 2010.
14. E. K. U. Gross and S. Kurth, *Relativistic and Electron Correlation Effects in Molecules and Solids*, ed. G. L. Malli, Plenum Press, New York, 1994, pp. 367.

15. U. von Barth, *Phys. Scr.*, 2004, **T109**, 9-39.
16. P. Hohenberg and W. Kohn, *Phys. Rev.*, 1964, **136**, B864-B875.
17. A. Hinchliffe, *Modelling Molecular Structures*, John Wiley & Sons, Inc., New York, 1996, ch. 4, pp. 55.
18. W. F. Huebner and W. D. Barfield, *Opacity*, Springer Science and Business media, New York, 2014, ch. 3, pp. 75.
19. A. Hinchliffe, *Molecular Modelling for Beginners*, John Wiley & Sons, Inc., 2003, ch. 20, pp. 347-358.
20. W. Kohn and L. J. Sham, *Phys. Rev.*, 1965, **140**, A1133-A1138.
21. N. M. Harrison, *Computational Materials Science*, ed. R. Catlow and E. Kotomin, IOS Press, Amsterdam, 2003, pp. 45-70.
22. The official Gaussian website, http://www.gaussian.com/g_prod/g09b.htm, (accessed August 2015).
23. *Ion/Molecule Attachment Reactions: Mass Spectrometry*, ed. T. Fujii, Springer, New York, 2015, ch. 3, pp. 52.
24. Gaussian 09W Tutorial: An Introduction to Computational Chemistry using G09W and Avogadro Software, http://www.molcalx.com.cn/wp-content/uploads/2015/01/Gaussian09W_tutorial.pdf, (accessed September 2015).
25. Gaussian 09 User's Reference, http://www.gaussian.com/g_tech/g_ur/k_opt.htm, (accessed September 2015).
26. R. Dennington, T. Keith, and J. Millam, GaussView (Version 5), Semichem, Inc., Shawnee Mission, KS, 2009.
27. Y. Zhao and D. G. Truhlar, *Acc. Chem. Res.,* 2008, **41**, 157-167.
28. Y. Zhao and D. G. Truhlar, *Theor. Chem. Acc.,* 2008, **120**, 215-241.
29. F. Weigend and R. Ahlrichs, *Phys. Chem. Chem. Phys.*, 2005, **7**, 3297-3305.
30. E. Prenesti, P. G. Daniele, M. Prencipe and G. Ostacoli, *Polyhedron*, 1999, **18**, 3233-3241.
31. E. Farkas, E. Csapo, P. Buglyo, C. A. Damante and G. Di Natale, *Inorg. Chim. Acta*, 2009, **362**, 753-762.
32. A. Majumder, G. Pilet, M. Teresa, G. Rodriquez and S. Mitra, *Polyhedron*, 2006, **25**, 2550-2558.
33. Q. Wang, C. F. Bi, D. Q. Wang and Y. H. Fan, Acta Cryst., 2009, DOI: 10.1107/S1600536809010149.

34. J. F. Blount, K. A. Fraser, H. C. Freeman, J. T. Szymanski, C. H. Wang and F. R. N. Gurd, *Chem. Comm*., 1966, **756,** 23-24.
35. B. O. Patrick, C. L. Stevens, A. Storr and R. C. Thompson, *Polyhedron*, 2003, **22**, 3025-3035.
36. P. F. Lee, C. Yang, D. T. Yang, D. Fan. J. J. Vittal and J. D. Randford, *Polyhedron*, 2003, **22**, 2781-2786.
37. A. W. Addison, T. N. Rao, J. Reedijk, J. van Rijn and G. C. Verschoor, *J. Chem. Soc*. *Dalton Trans.*, 1984, 1349-1356.
38. N. Camerman, A. Camerman and B. Sarkar, *Can. J. Chem*, 1976, **54**, 1309-1316.
39. H. Irving, R. J. P. Williams, D. J. Ferrett and A. E. Williams, *J. Chem. Soc.,*1954, 3494-3504.
40. J. Clayden, N. Greeves, S. Warren and P. Wothers, *Organic Chemistry,* Oxford University Press, Oxford, 2009.
41. *Analytical Chemistry: Twenty-sixth International Congress of Pure and Applied Chemistry, T. Takeuchi*, Pergamon press, Oxford, 1977, vol. 3, pp. 815.
42. S. Prakash, G. D. Tuli, S. K. Basu and R. D. Madan, *Advanced Inorgandic Chemistry*, S. Chand Publishing, India, 17th edn., 2000, vol. 2, pp. 32.

5 Dermal Absorption

5.1 Introduction

Copper(II) complexes can be administered into the body through oral, or parenteral or transdermal methods. With oral administration, copper(II) would have to be absorbed through a variety of body compartments and are subject to the low stomach pH. Absorption through these body compartments is difficult for copper(II) complexes, because the complexes must be uncharged and lipophilic to penetrate stomach and intestinal membranes.[1] The resulting non-absorbed copper(II) salts are irritants, which cause oedema to occur in the tissues as well as form ulcers. If absorption does occur, copper(II) will be subjected to protein binding in the plasma and will result in a further decrease in the bioavailability of copper(II).[2,3] Therefore this administration path is not favourable. Parenteral administration of simple copper salts, such as copper(II) chloride, has been shown to reduce inflammation by an amount that is proportional to the amount of copper(II) injected.[3] Jackson *et al.* showed that copper(II) complexes will also protect against the formation of oedema, which is directly proportional to the amount of copper(II) administered.[2] However, parenteral administration of copper(II) complexes can also cause an irritation at the site of injection.[4,5] This, as well as the inconvenience of patients having to seek professional help to administer the treatment for rheumatoid arthritis via an injection, has led to the consideration of transdermal methods, in the form of a topical application.

Administration of the copper(II) ligand complex into blood plasma via the skin is limited to the ability of the ligand to promote diffusion of the metal ion across the skin barrier. The properties of the ligand that govern the diffusion ability are the lipophilicity and protein binding properties.[6,7]

The skin is divided into three layers, namely the epidermis, the dermis and the subcutis. Out of the three layers, the epidermis is considered to be the rate-limiting barrier for chemicals. The epidermis consists of five layers, with the stratum corneum being the outermost layer of the epidermis and therefore the skin. The stratum corneum usually has a thickness of 10-30 cells of keratinized corneocytes and in between these cells are lipids, called lamellar

membranes, which are arranged in bilayers and fill the space between the cells. An illustration of the stratum corneum can be seen in Figure 5.1 below. It is this surrounding lipid layer that causes the stratum corneum to become essentially lipophilic and therefore the rate-limiting barrier for chemicals to pass through the skin.[8-11]

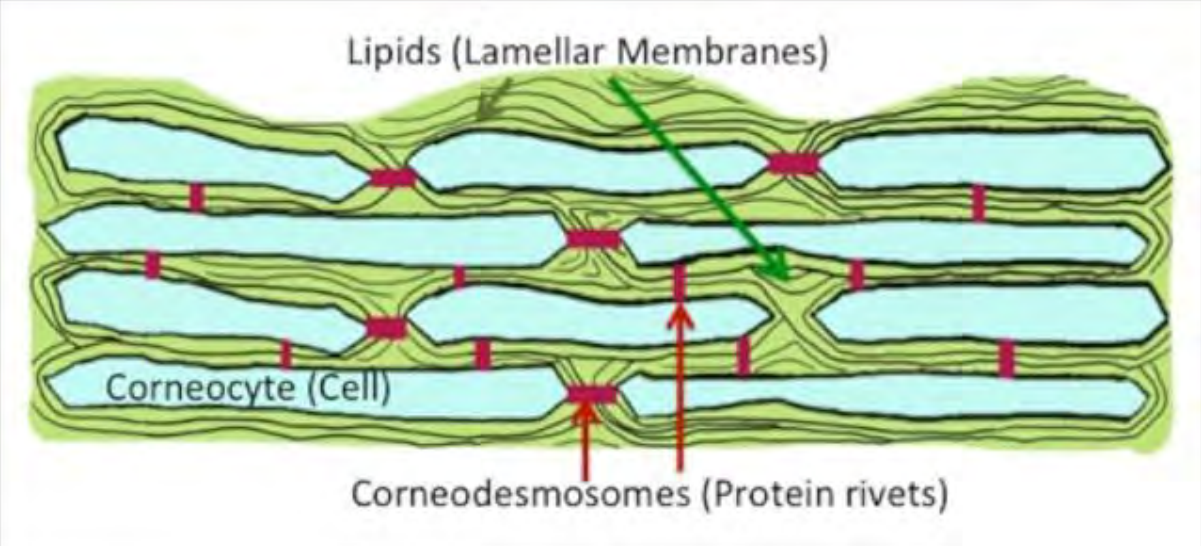

Figure 5.1: Illustration of the stratum corneum.[9]

The dermis is composed mainly of collagen, with elastin implanted in a mix of mucopolysaccharides. These cell layers in the dermis cause less of a diffusion barrier for chemicals than the stratum corneum. The rate of diffusion is dependent on interstitial-fluid, blood flow and the interaction between the chemicals and the dermal components. Chemicals will diffuse through the connective tissue of the dermis and then enter the blood capillaries, which are situated in the dermis, before reaching the subcutis.[8,12]

The chemicals that diffuse through the skin can diffuse through three possible pathways in the stratum corneum, depending on the nature of the chemicals. The major diffusion pathway is through the lipid bilayer and therefore the chemicals used for dermal absorption should have a non-polar lipophilic nature. Another possible pathway is via the corneocytes, although since the corneocytes are filled with keratin, which is a highly diffusion-resistant protein, only polar hydrophilic substances may undergo diffusion through these cells and the diffusion route can be perceived as aqueous channels in the protein. The final pathway is via lipophilic appendages, such as hair follicles, sebaceous glands and sweat glands. However, these routes only account for 0.1-1 % of the skin surface area and therefore the total flux will be low.[11,13]

Two methods to determine transdermal absorption were used. The first is the Flask Shake method, which gives the octanol/water partition coefficients and the second is the Franz cell diffusion method, which gives the permeability coefficients.

The permeability and partition coefficients can both be used to determine how effective the copper(II) ligand complexes are at undergoing dermal absorption.

5.2 Octanol/Water Partition Coefficient

5.2.1 Flask Shake method

Octanol/water partition coefficients were measured to determine the lipophilicity of the copper(II) ligand complex, which is represented as a partition coefficient. To measure the octanol/water partition coefficients, the most common method is the Flask Shake method, whereby a known concentration of analyte is added to water. A known volume of organic solvent is then used to extract the analyte and the amount of analyte remaining in the water layer and the amount of analyte present in the organic layer is measured. For metal complexes the partition coefficient can be defined in Equation 28 as:

$$\log P_{oct/aq} = \log \left(\frac{[\mathrm{Cu(II)}]_{\mathbf{oct}}}{[\mathrm{Cu(II)}]_{\mathbf{aq}}} \right) \tag{28}$$

where $[Cu(II)]_{oct}$ is the concentration of copper(II) that is extracted into the organic phase and $[Cu(II)]_{aq}$ is the concentration of copper(II) that remains in the aqueous phase.[8,14]

5.2.2Experimental

A 1:4 copper(II) ligand ratio was prepared in miliQ water for both Gly-Leu-Phe and Sar-Leu-Phe. 5 ml of the copper(II) ligand solution was added to nine glass vials for each ligand. The pH of the solution in each glass vial was adjusted using NaOH so that the pH increased in increments of 1 from a pH of 2 to a pH of 10. Subsequently 5 ml of saturated 1-octanol solution was added to each glass vial for both ligands. The vials were then shaken for 1 min and left to stand for 10 min so that the two phases could separate.

3 ml of each organic layer was withdrawn from each vial and placed into separate vials. 7 ml of 5 % HNO_3 was added to the withdrawn organic phase, so that copper(II) could be extracted back into an aqueous phase. 5 ml of the 5 % HNO_3 aqueous phase for each vial was withdrawn and placed into another vial so that the concentration of copper(II) could be determined.

A copper(II) concentration of between 1-2 ppm for the aqueous phase of the copper(II) ligand solutions was required. Therefore after the two phases had separated, in order to get a copper(II) concentration of between 1-2 ppm, 1 ml of the aqueous phase of each ligand and each pH was extracted and placed into separate vials. 5 ml of 5% HNO_3 was then added to each vial. 5 ml of this aqueous solution in each vial was withdrawn and placed into another vial so that the concentration of copper(II) could be determined.

The concentrations of copper(II) were determined by using the Agilent 4100 Microwave Plasma Atomic Emission Spectrometer (4100 MP-AES) with Agilent technologies and the data were analysed using MP Expert, Microwave Plasma Instrument software, version 1.1.1.45895. Standard solutions of 0.01, 0.2, 0.5, 1 and 2 ppm of copper(II), using miliQ water, were prepared for both phases and used in the 4100 MP-AES to obtain the copper(II) concentrations. The 4100 MP-AES was set to a wavelength of 324.795 nm, which is the optimum wavelength that will measure copper(II) concentrations of approximately 0.1 ppm.

A flow diagram outlining the method can be seen in Figure 5.2 below.
The measured concentrations of copper(II) in the aqueous and organic phases were then used to calculate the partition coefficient according to Equation 28.

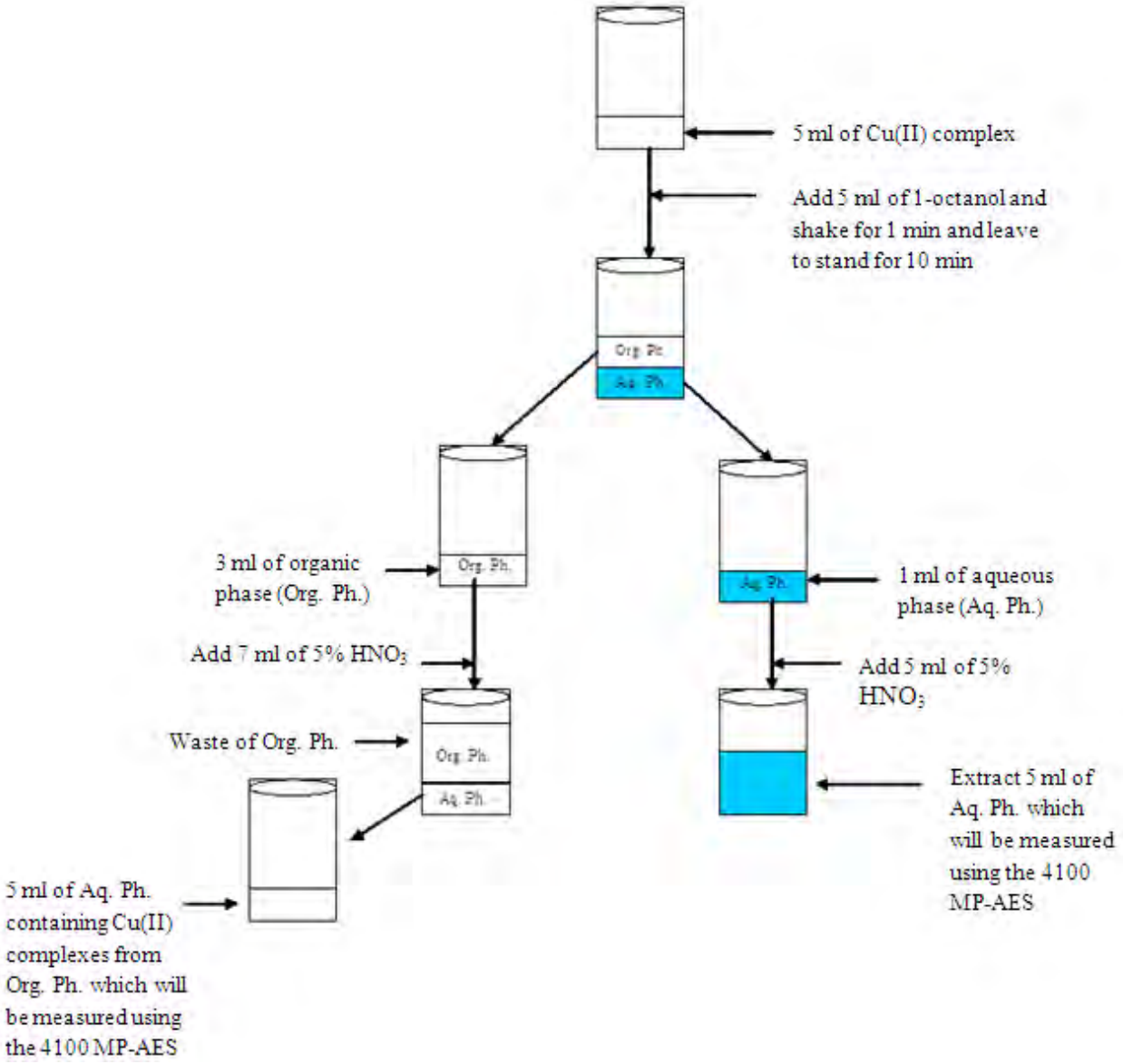

Figure 5.2: Flow diagram depicting the method outlined for determining the partition coefficients.[15]

5.2.3 Results

The partition coefficients (log $P_{oct/aq}$) for Cu-Gly-Leu-Phe and Cu-Sar-Leu-Phe were plotted against a function of pH and overlaid with the corresponding species distribution curves so that a comparison could be made, which can be seen in Figure 5.3 and Figure 5.4 respectively. The partition coefficients for both metal ligand complexes are negative over a pH range from 2-10. Before complex formation occurs in both metal ligand complexes, hydrated copper $[Cu(OH_2)_6]^{2+}$ predominates and therefore the -3 partition coefficient values that are seen at low pH values in Figure 5.3 and Figure 5.4 are due to hydrated copper(II). Other studies of copper(II) complexes also found that low partition coefficient values, before complex formation occurred, was due to hydrated copper(II).[16-18]

At low pH values, the partition coefficient for Cu-Gly-Leu-Phe in Figure 5.3 remains at -3 until a pH of 3.4 is reached, at which point the values begin to increase. A peak is reached at a pH of 6.2 with a partition coefficient of -1.6, after which the values for the partition coefficient decrease to a value of -2.2 at the end of the pH range. The overlaid speciation curve of Cu-Gly-Leu-Phe, shows that species only start forming at a pH of 3.4. This corresponds to the increase in partition coefficients at a pH of 3.4. The speciation curve also indicates that at any particular pH value between a pH of 4-8, more than one out of the four (ML, ML_2H_{-1}, MLH_{-1} and MLH_{-2}) species are present. Therefore the partition coefficient values between a pH of 3.4 and 4 are due to the ML species, while all the other partition coefficient values are due to a mixture of species. At the physiological pH of 7.4 the partition coefficient was measured to be approximately -1.8 and the species which predominates is the ML_2H_{-1} species.

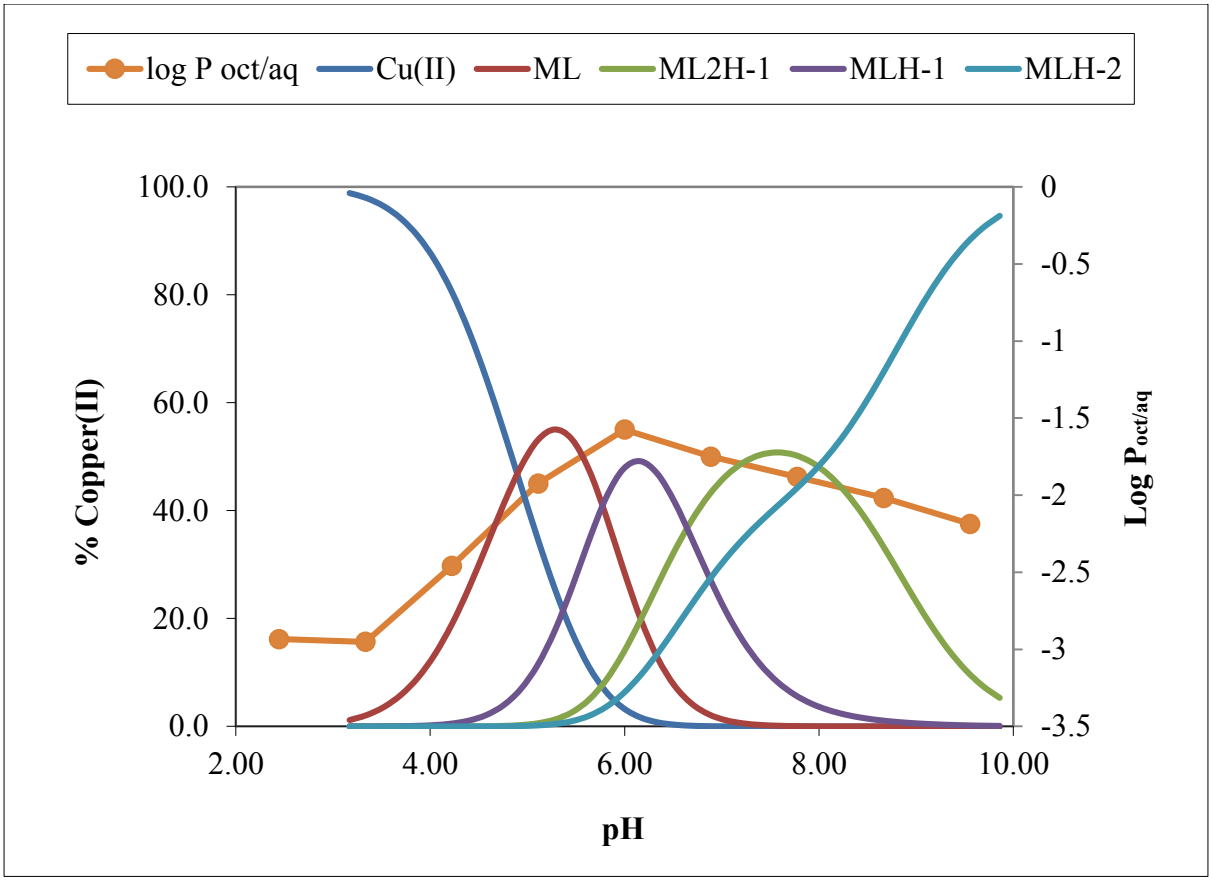

Figure 5.3: Protonation species distribution curve for Cu-Gly-Leu-Phe at 25 ºC in 0.15 mol.dm^{-3} of NaCl overlaid with the partition coefficient values of Cu-Gly-Leu-Phe (1:4) over a pH range from 2-10. (error bars are ± 0.01)

At low pH values, the partition coefficient values for Cu-Sar-Leu-Phe in Figure 5.4 also remain at -3 until a pH of 4.4. From a pH of 4.4 to 6.5 it increases to -1.6, after which the partition coefficient values decrease to -2.2 at the end of the pH range. The overlaid speciation curve for Cu-Sar-Leu-Phe in Figure 5.4 indicates that species only start forming at a pH of 4.2, which corresponds to the increase in partition coefficient values at a pH of 4.4. The speciation curve also indicates that until a pH of 4.8, the increase in partition coefficient is due to the ML species, after which all the other partition coefficient values are due to a combination of the four possible species (ML, ML_2H_{-1}, MLH_{-1} and MLH_{-2}). At the physiological pH of 7.4 the ML_2H_{-1} species predominates and has a partition coefficient of approximately -1.7.

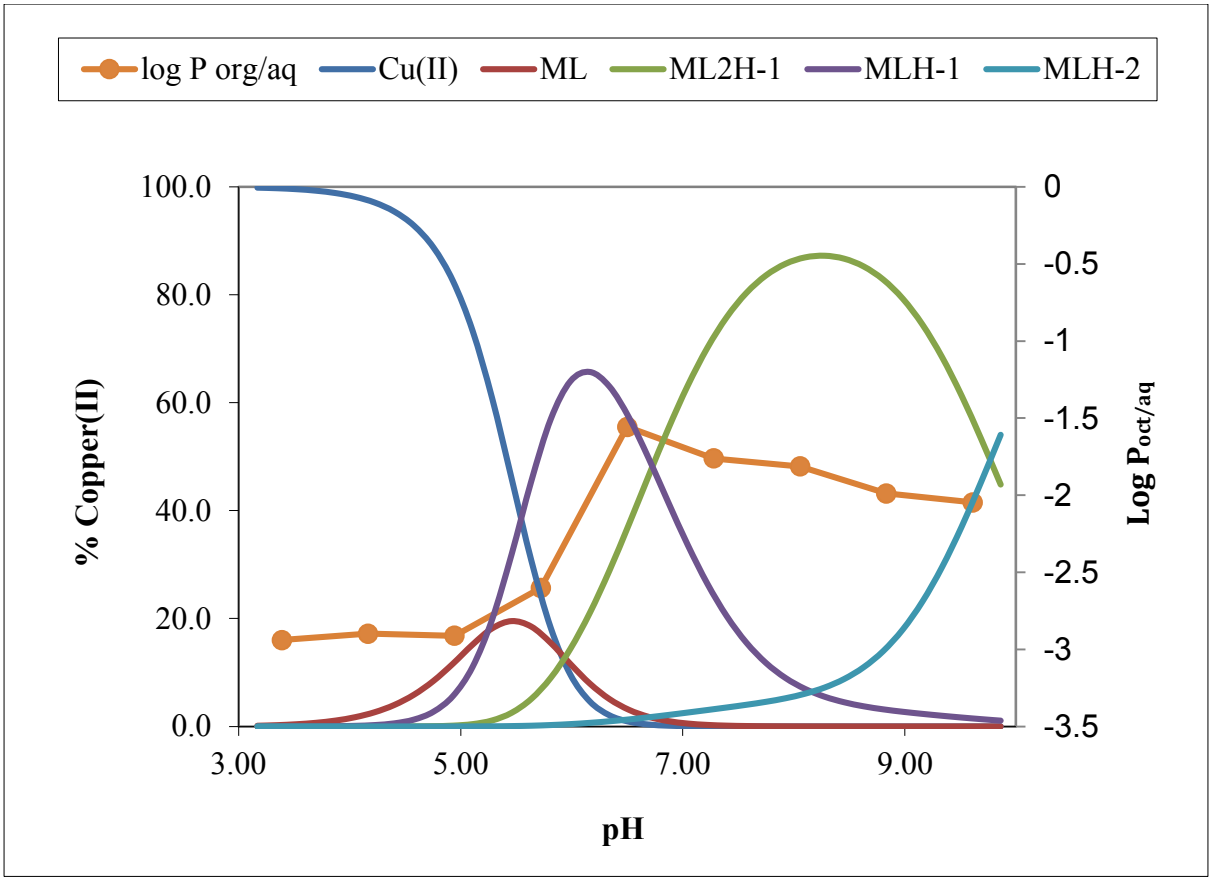

Figure 5.4: Protonation species distribution curve for Cu-Sar-Leu-Phe at 25 ^{o}C in 0.15 mol.dm^{-3} of NaCl overlaid with the partition coefficient values of Cu-Sar-Leu-Phe (1:4) over a pH range from 2-10. (error bars are $\pm$ 0.01)

In both complexes the partition coefficients increase beyond the pH where the formation of the ML species takes place and peak at the pH where the MLH_{-1} species predominates. Therefore the MLH_{-1} species could cause the partition coefficient values to increase. In both complexes the decrease in partition coefficients occurs at a pH of approximately 6.3. For both complexes the ML_2H_{-1} species starts forming at a pH of approximately 5.5 and therefore the decrease in partition coefficients could be due to the ML_2H_{-1} species. However, since the formation of the ML_2H_{-1} species rapidly decreases at high pH values while the MLH_{-2} species are forming, the decrease in partition coefficient values could also be due to the formation of the MLH_{-2} species.

The experimental error was calculated using the method outlined by Gardiner.[19]

5.2.4 Discussion

According to Gertz *et al*. a drug can be classified into one of the four distinct areas of lipophilicity.[20] A low lipophilicity is log P = 0-2.5, an intermediate lipophilicity is log P = 2.5-5, a high lipophilicity is log P = 5-7 and a very high lipophilicity is log P ≥ 7. However, Zvimba *et al*. found that log P must be at least 0.6 to be considered lipophilic, which will then allow for trans-dermal absorption.[21] Therefore, the negative log $P_{oct/aq}$ values that were found for both metal ligand complexes, indicate that these complexes are hydrophilic.[21] Even though the overall nature of the complexes are hydrophilic, there are species which are more lipophilic than others. At the pH value where speciation takes place the ligands have a charge of -1, since the carboxyl group has lost a hydrogen and copper(II) has a charge of +2. Therefore the ML species have a charge of +1, the MLH_{-1} species are neutral, the ML_2H_{-1} species have a charge of -1 and the MLH_{-2} species have a charge of -2. The less charged a species is, the more lipophilic it is and the more likely it is to move into the octanol phase. This is due to the polar nature of water in the aqueous phase, which stabilises the charges and so the species that are the most lipophilic are the MLH_{-1} species, then the ML and the ML_2H_{-1} species and then the MLH_{-2} species. This corresponds to the trends seen in the partition coefficients for both Figure 5.3 and Figure 5.4.

The initial increase in partition coefficient values for both the Cu-Gly-Leu-Phe and Cu-Sar-Leu-Phe complexes is because the ML species are less charged than the copper(II) ions and therefore a possible cause for the increase in partition coefficient values. The partition coefficient values continue to increase while the MLH_{-1} species form and then decrease as the ML_2H_{-1} and MLH_{-2} species form. Since the MLH_{-1} species is more lipophilic than the ML_2H_{-1} and MLH_{-2} species, the partition coefficient trend corresponds to the order in lipophilicity for the species. Tsang *et al.*[22] worked with positively charged compounds and found the partition coefficients to be between 0.84 and 3.00, indicating that the compounds are lipophilic. This shows that electrostatic interactions are not the only factors affecting the partition coefficients.

At the physiological pH of 7.4, the partition coefficient was found to be approximately -1.79 for the Cu-Gly-Leu-Phe complexes and approximately -1.72 for the Cu-Sar-Leu-Phe complexes. This indicates approximately a 1.6 % and a 1.9% copper(II) extraction into the

octanol phase for the Cu-Gly-Leu-Phe and Cu-Sar-Leu-Phe complexes respectively. The predominant species at this pH is the ML_2H_{-1} species.

N-methylated groups are more lipophilic than non-N-methylated groups and therefore it was predicted that the Cu-Sar-Leu-Phe complexes would be more lipophilic than the Cu-Gly-Leu-Phe complexes. The partition coefficients of -1.79 and -1.72 at a pH of 7.4 for the Cu-Gly-Leu-Phe and Cu-Sar-Leu-Phe complexes respectively, show that the Cu-Sar-Leu-Phe complexes are slightly more lipophilic than the Cu-Gly-Leu-Phe complexes. However, the difference is so slight that it falls within the range of experimental error.

Previously, Mohajane found that the partition coefficients of dipeptide copper(II) complexes ranged from -1.4 to -0.8 at a pH of 7.4.[14] When comparing this range with the partition coefficient values for the Cu-Gly-Leu-Phe and Cu-Sar-Leu-Phe complexes, Cu-Gly-Leu-Phe and Cu-Sar-Leu-Phe are less lipophilic than these dipeptides. Mahajane also found that the N-methyl substituent on the terminal amine increased the lipophilicity between the Cu-Gly-Leu and Cu-Sar-Leu complexes at a pH of 7.4, but only showed an increase in lipophilicity between the Cu-Gly-Phe and Cu-Sar-Phe complexes at higher pH values.[14] However, these increases were also slight and within the experimental margin.[14] The comparison between the partition coefficients of Cu-Gly-Leu-Phe and Cu-Sar-Leu-Phe and these dipeptide copper(II) complexes can be seen in Table 5.1.

Table 5.1: Comparison of the partition coefficient values at a pH of 7.4 between dipeptides from literaure[14] and the tripeptides, Gly-Leu-Phe and Sar-Leu-Phe.

Complex	Log $P_{oct\backslash aq}$ at pH 7.4
Cu-Gly-Leu	-0.96
Cu-Sar-Leu	-0.80
Cu-Gly-Phe	-1.0
Cu-Sar-Phe	-1.4
Cu-Gly-Leu-Phe	-1.79 ± 0.01
Cu-Sar-Leu-Phe	-1.72 ± 0.01

Tripeptides complexed to copper(II) were also studied by Hammouda.[23] The first position in the tripeptide was sarcosine, which is therefore similar to the Sar-Leu-Phe tripeptide. The

other positions in the tripeptides were alternated by histidine, glycine and lysine. At a pH of 7.4, Hammouda found that the partition coefficient values for the copper(II) tripeptides ranged between -2.05 to -3.02, while the partition coefficient values for Cu-Gly-Leu-Phe and Cu-Sar-Leu-Phe at a pH of 7.4 are significantly higher and therefore more lipophilic.[23] The main difference between the tripeptides in this study compared to the tripeptides in literature, is that in the literature study an imidazole group is present in the histidine amino acid and an amine side chain is present in the lysine amino acid.[23] Both of these groups make the tripeptides in literature more hydrophilic than the tripeptides in this study.[23,24] The comparison between these partition coefficients can be seen in Table 5.2.

Table 5.2: Comparison of the partition coefficient values at pH 7.4 between the tripeptides from literature[23] and the tripeptides, Gly-Leu-Phe and Sar-Leu-Phe.

Copper(II) Complexes	Log $P_{oct\backslash aq}$ at pH 7.4
Cu-Sar-His-Lys	-3.02 ± 0.01
Cu-Sar-Lys-His	-2.05 ± 0.01
Cu-Sar-His-His	-2.96 ± 0.01
Cu-Sar-Lys-Lys	-2.63 ± 0.01
Cu-Sar-Gly-His	-2.40 ± 0.01
Cu-Gly-Leu-Phe	-1.79 ± 0.01
Cu-Sar-Leu-Phe	-1.72 ± 0.01

Other studies containing copper(II) complexes have found that at a pH of 7.4 the partition coefficients ranged from -1.65 to 0.08.[16,17,18,21] Therefore the results obtained in this study are just below this range. The only studies of knowledge, which have found positive partition coefficient values for copper(II) complexes are in a study by Green[25] and in another study by Sri-Aran *et al.*[26] Green[25] found that a ^{64}Cu complex of pyrucaldehyde bis(N4-methylthiosemicarbazone) has a partition coefficient of 1.97 and Sri-Aran *et al.*[26] found that a ^{67}Cu complex of N-(2-pyridylmethyl)-N'-(salicylaldimino)-1,3-propanediamine has a partition coefficient of 0.75.

5.2.5 Conclusion

The Flask Shake method found that the partition coefficients indicated that the overall nature for the copper(II) complexes was hydrophilic, but with varying degrees of hydrophilicity, which depended on the charge of each species. The most lipophilic species were the MLH_{-1} species, then the ML and the ML_2H_{-1} species and then the MLH_{-2} species. By layering the species distribution curve over the partition coefficient values for a pH range from 2-10 for each metal ligand complex, it was also found that the trend in partition coefficient values over this pH range corresponded to the degree of lipophilicity for each species.

The objective to compare the lipophilicity of these copper(II) complexes with the lipophilicity of the dipeptide copper(II) complexes from literature, namely Cu-Gly-Leu, Cu-Sar-Leu, Cu-Gly-Phe and Cu-Sar-Phe, was achieved.[14] The N-methylated groups were suspected to be more lipophilic than non-N-methylated groups. However, the difference in lipophilicity found between the Cu-Sar-Leu-Phe and Cu-Gly-Leu-Phe complexes was within experimental error and therefore not significant enough to verify the statement. This was also found in the dipeptides from literature.[14]

5.3 Modified Franz cell: Permeability Coefficient

5.3.1 Franz cell diffusion method

The permeability coefficient physically measures how well the copper(II) ligand complex can undergo dermal absorption. Dermal absorption of the metal ligand complexes will be measured using a modified Franz cell. This is an apparatus that consists of two primary chambers separated by an artificial membrane. Dermal absorption is measured by monitoring the rate at which copper(II) diffuses passively through the membrane and into the other chamber. A representation of the modified Franz cell setup can be seen in Figure 5.5 below.[27-29]

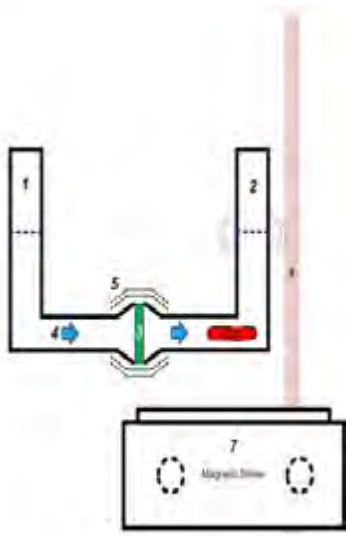

1. Donor chamber
2. Receiver chamber
3. Artificial membrane.
4. Passive diffusion direction
5. Clamp
6. Stirrer bar
7. Magnetic stirrer
8. Burette stand with clamp.

Figure 5.5: A modified Franz cell.[15]

Fick's first law relates flux (J) to the concentration gradient of a solute, which can be seen in Equation 29 below:

$$J = - D \frac{dC}{dX} \tag{29}$$

where, D is the diffusion coefficient of the solute (cm^2/h), dC is the change in concentration of the solute (mg/cm^3) and dX is the change in distance of the solute (cm). The negative sign

indicates that the concentration in the donor chamber is decreasing with increasing distance. However, during the process, flux continuously increases and therefore is a positive entity.[30-32] This equation is used to relate a steady state flux to the permeability coefficient, which can be seen below in Equation 30:

$$K_{\mathrm{p}} = \frac{J}{C_i} \tag{30}$$

where, K_{p} is the permeability coefficient (cm/h), J is the mass that passes through a unit area of the membrane in a unit time, which is known as the steady state flux (mg/cm^{2}h) and C_i is the initial concentration from the solution of the donor chamber. [27,33]
The steady state flux, J, can also be expressed in Equation 31 as:

$$J = \frac{1}{S}\frac{dM}{dt} \tag{31}$$

where, dM is the change in mass (mg), dt is the change in time (h) and S is the surface area of the membrane separating the two chambers (cm^2).[27,28,31]
The steady state flux can therefore be calculated from the gradient of the linear region in an accumulative absorption-time curve and then by dividing it by the surface area of the membrane separating the two chambers. Subsequently, the permeability coefficient can be calculated by dividing the steady state flux rate by the initial concentration of the solution in the donor chamber.[34-36]

The steady state flux can only be calculated when the diffusion rate of the solute becomes constant. The time it takes for the system to reach a steady state flux is called the lag time. The lag time is a result of the solute developing an equilibrium between the donor phase and the membrane when diffusion takes place. Therefore lag time is a function of the thickness of skin, diffusivity and the solute entering into the stratum corneum and dermis.[30]

5.3.2 Experimental

A 20 ml 1:4 copper(II) ligand ratio was prepared in miliQ water for both Gly-Leu-Phe and Sar-Leu-Phe. The pH of both solutions was adjusted to the physiological pH of 7.4. A 20 ml copper(II) chloride solution, with the same concentration as the copper(II) added to the ligand solutions, was prepared in miliQ water. The pH of the copper(II) chloride solution was adjusted to a pH of 4.2. The copper(II) chloride was adjusted to a lower pH because at high pH values $Cu(OH)_2$ would precipitate. All three solutions were prepared with no background electrolyte. A total of three Franz cell setups were used, one for each copper(II) ligand solution and one for the copper(II) chloride solution. The diameter of the opening in each chamber belonging to the Franz cell, was measured. The available area where diffusion can take place for Cu-Gly-Leu-Phe, Cu-Sar-Leu-Phe and copper(II) chloride was 0.63, 0.59 and 0.60 cm^2 respectively. The artificial membrane was made using Whatman International Ltd filter paper, which has a thickness of 0.0012 cm. The area of the filter paper was chosen to fit the diameter of each Franz cell. The filter paper was soaked in Cerasome 9005 lipid solution at 25 °C and any excess lipid solution was shaken off. The amount of lipid solution absorbed was determined by the difference in masses of the lipid absorbed filter paper and the non-lipid absorbed filter paper, which was between 0.045-0.055 g for all three experiments.

Each of the solutions was added to the donor chamber of each Franz cell and 20 ml of miliQ water was added to the receiver chambers of each Franz cell. The Franz cells were placed in a temperature controlled environment of 25 °C and covered so that minimal water vapour would escape. Magnetic stirrer bars were placed in all the chambers. For each experiment, at time zero, 0.5 ml samples were taken from both the donor and receiver phases and then after 10.5 hours, samples were taken from both the donor and receiver phases at random regular intervals, until a total of 48 hours had passed. For the copper(II) chloride solution, 0.5 ml was also taken from both the receiver and donor phases at time zero and then after 10.25 hours, samples were taken from both chambers at random regular intervals, until a total of 47 hours had passed. 4.5 ml of 5 % nitric acid solution was added to each of the collected receiver phase samples to make up a total volume of 5 ml. In addition 12 ml of 5 % nitric acid solution was added to the first donor chamber samples taken at time zero to make a total of 12.5 ml. A total of 12.5 ml was required so that the concentration in the donor phase was approximately 2 ppm. The concentrations of copper(II) were determined using an Agilent

4100 Microwave Plasma Atomic Emission Spectrometer (4100 MP-AES) and the data were analysed using MP Expert, Microwave Plasma Instrument software, version 1.1.1.45895. Standard solutions of 0.5, 0.75 0.1, 1.5 and 2 ppm of copper(II), were prepared using miliQ water. The MP-AES was set to a wavelength of 324.795 nm.

5.3.3 Results

The concentration of copper(II) that was measured in the receiver phase during the three experiments is shown in Table 5.3 and Table 5.4 below. The copper(II) complexes were adjusted to the biological pH of 7.4 and the copper(II) chloride to a pH of 4.2.

Table 5.3: Measured copper (II) concentration in the receiver phase of the Franz cell as a function of time after the copper (II) complexes at a pH of 7.4 diffused through a Cerasome 9005 lipid membrane.

Time (h) for copper(II) complexes	Cu-Gly-Leu-Phe (ppm)	Cu-Sar-Leu-Phe (ppm)
0	0	0
10.5	7.1 ± 0.1	3.4 ± 0.1
13	8.4 ± 0.1	4.3 ± 0.1
14.75	9.0 ± 0.1	4.9 ± 0.1
15.5	9.9 ± 0.1	5.4 ± 0.1
16.5	10.4 ± 0.1	6.1 ± 0.1
17.5	11.4 ± 0.2	6.4 ± 0.1
18.5	12.2 ± 0.2	7.2 ± 0.1
21.5	13.6 ± 0.2	8.3 ± 0.1
23.75	15.0 ± 0.2	9.2 ± 0.1
27	16.3 ± 0.2	10.3 ± 0.1
36.25	19.4 ± 0.2	13.7 ± 0.1
38.75	20.9 ± 0.2	14.2 ± 0.2
41.25	21.4 ± 0.2	14.6 ± 0.2
43.83	22.9 ± 0.2	15.9 ± 0.2
46	23.3 ± 0.2	16.1 ± 0.2
48	23.5 ± 0.2	16.7 ± 0.2

Table 5.4: Measured copper (II) concentration in the receiver phase of the Franz cell as a function of time after copper (II) chloride at a pH of 4.2 diffused through a Cerasome 9005 lipid membrane.

Time (h) for copper(II) chloride	$CuCl_2.2H_2O$ (ppm)
0	0
10.25	4.3 ± 0.2
11.5	5.2 ± 0.1
12.5	5.6 ± 0.1
13.5	5.5 ± 0.1
14.5	6.1 ± 0.1
15.5	6.1 ± 0.1
18.75	7.3 ± 0.1
22.5	8.3 ± 0.1
25	9.5 ± 0.1
34.85	12.7 ± 0.1
36	13.4 ± 0.1
37.85	14.1 ± 0.1
44	17.7 ± 0.1
47	15.5 ± 0.1

From Table 5.3 and Table 5.4 it can be seen that the difference in time between the first and second reading is 10.5 and 10.25 hours respectively. This was engineered so that the lag time occurred during the night. The lag time concentrations are not included into the calculation to find the steady state flux and therefore receiving those concentrations are not necessary. However, by engineering the lag time to occur at night, it meant that during the day, when it is possible to collect samples, the system would have already reached a steady state of flux. Therefore this allowed a greater number of samples in a steady state flux to be collected and used to obtain the gradient, before the system reached equilibrium.

A graphical representation of the measured copper(II) concentrations in the receiver phase plotted against time can be seen in Figure 5.6.

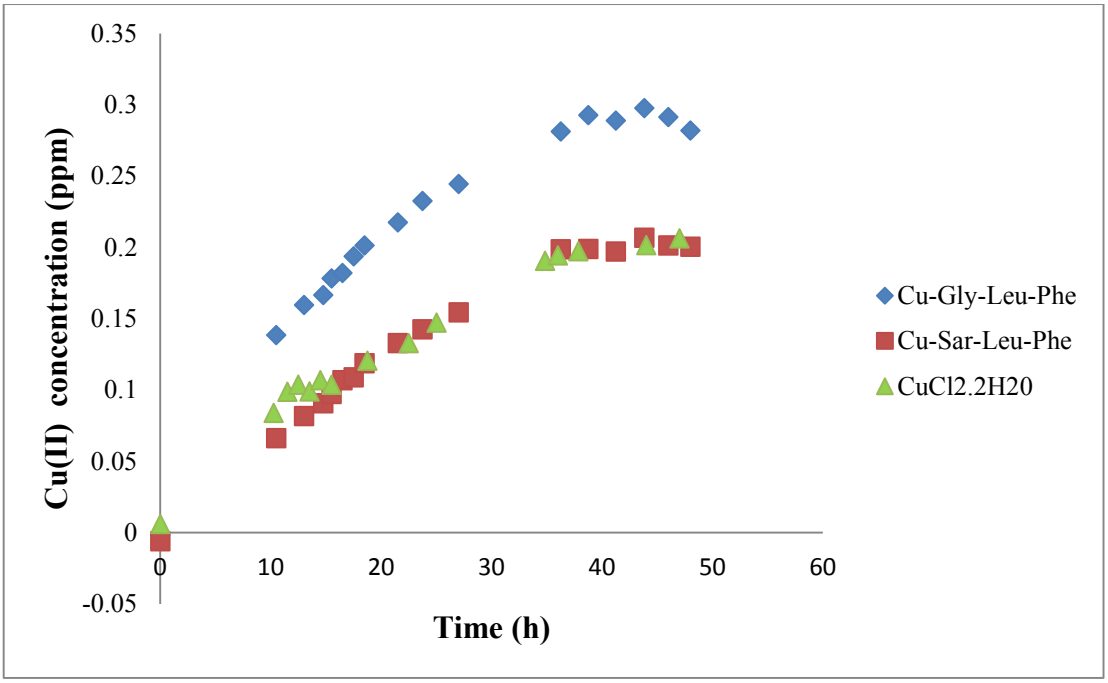

Figure 5.6: Graphical representation of the copper(II) concentration in the receiver phase of the Franz cell plotted against time after the copper(II) complexes at a pH of 7.4 and copper(II) chloride at a pH of 4.2 diffused through the Cerasome 9005 lipid membrane.

In Figure 5.6 it can be seen that a steady state of flux occurred approximately between 10-38 hours, after which an equilibrium between the solutes of the donor and receiver phases was reached. The calculated gradients from the linear region in Figure 5.6 can be seen in Figure 5.7.

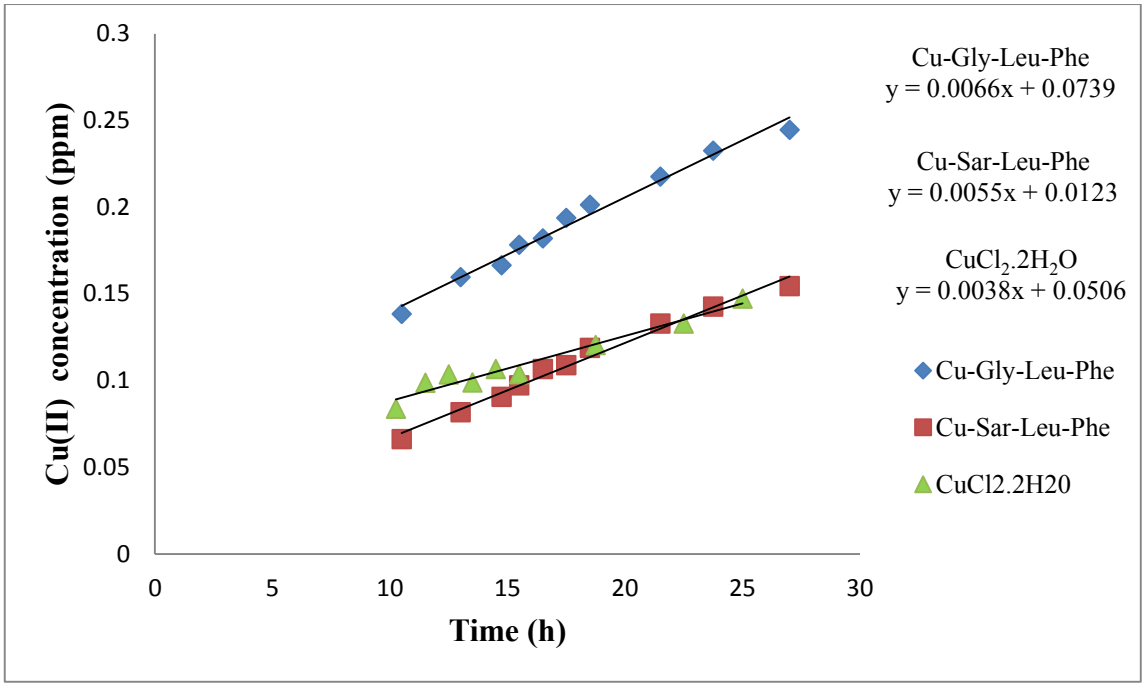

Figure 5.7: Gradient of the linear region in an accumulative absorption-time curve of copper(II) concentration in the receiver phase for Cu-Gly-Leu-Phe, Cu-Sar-Leu-Phe and $CuCl_2.2H_2O$.

From Figure 5.7 it can be seen that the gradients for the Cu-Gly-Leu-Phe, Cu-Sar-Leu-Phe and $CuCl_2.2H_2O$ were found to be 0.0066, 0.0055 and 0.0038 respectively. These gradients were then used to calculate the steady state fluxes using Equation 31 and then the permeability coefficients could be calculated using Equation 30, which are given in Table 5.5. A graphical representation of the steady state flux can be seen in Figure 5.8 and a graphical representation of the permeability coefficients can be seen in Figure 5.9.

Table 5.5: Steady state flux, J, and permeability coefficient, K_p, of Cu-Gly-Leu-Phe, Cu-Sar-Leu-Phe and $CuCl_2.2H_2O$ after diffusion through the Cerasome 9005 lipid membrane has taken place. The experimental errors were calculated using the method outlined by Gardiner.[19]

Complexes	J (mg/cm^{2}h)	K_p (cm/h)
Cu-Gly-Leu-Phe	0.010 ± 0.002	0.225 ± 0.019
Cu-Sar-Leu-Phe	0.009 ± 0.002	0.206 ± 0.019
$CuCl_2.2H_2O$	0.006 ± 0.002	0.137 ± 0.019

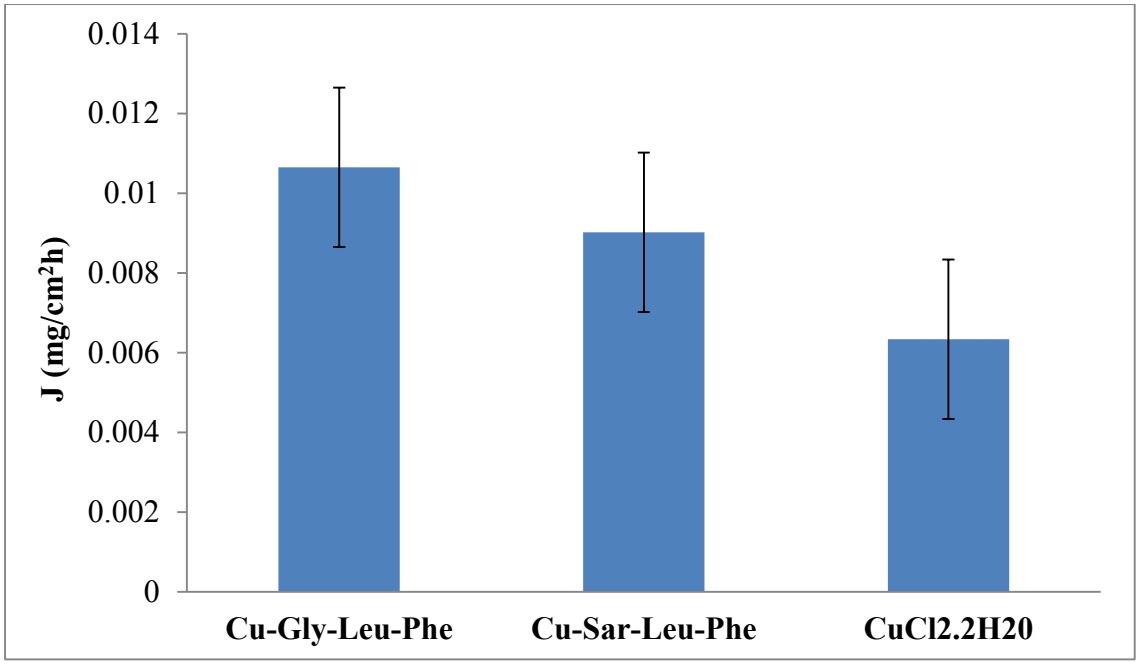

Figure 5.8: Graphical representation of the steady state flux for Cu-Gly-Leu-Phe, Cu-Sar-Leu-Phe and $CuCl_2.2H_2O$ after diffusion through the Cerasome 9005 lipid membrane has taken place.

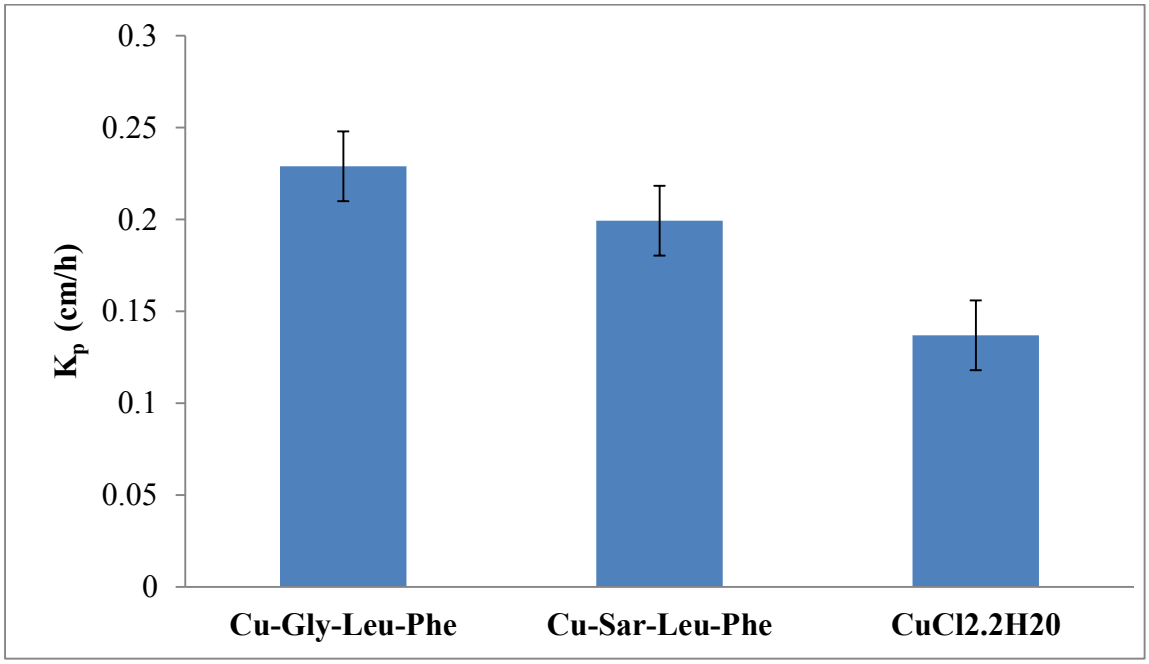

Figure 5.9: Graphical representation of the permeability coefficient for Cu-Gly-Leu-Phe, Cu-Sar-Leu-Phe and $CuCl_2.2H_2O$.

Table 5.5 as well as Figure 5.8 and Figure 5.9 show that the copper(II) complexes have a higher steady state flux and a higher permeability coefficient than that of copper(II) chloride. It also shows that Cu-Gly-Leu-Phe has a slightly higher steady state flux and permeability coefficient than Cu-Sar-Leu-Phe. However, since the values are within experimental error, the copper(II) complexes can be considered to have the same steady state flux and permeability coefficient values.

5.3.4 Discussion

The higher steady state fluxes and permeability coefficients of Cu-Gly-Leu-Phe and Cu-Sar-Leu-Phe compared to copper(II) chloride indicates that the complexation of copper(II) ions with the two tripeptides increases the permeation rate of copper ions. The similarity in the permeability coefficients for Cu-Gly-Leu-Phe and Cu-Sar-Leu-Phe shows that the N-methyl substituent on the terminal amine does not have an effect on the permeation rate of copper(II) ions.

5.3.4(a) Physiochemical properties

Membrane permeation is affected by physiochemical properties such as molecular size, compound ionization, solubility and hydrogen bonding capacities.[30]

5.3.4(a.i) Molecular size

The molecular size of a compound can be described from the molecular weight and compounds with a molecular weight lower than 50 g/mol are considered small. These small compounds have a larger than expected permeability coefficient, because they can diffuse more efficiently through the lipid bilayer of the stratum corneum.[37-41] Compounds that have a molecular weight greater than 500 g/mol are too large to diffuse in between the corneocytes of the stratum corneum and therefore cannot penetrate the skin.[42] At a pH of 7.4 the predominant species, which can be seen in the speciation curves in Figure 5.3 and Figure 5.4, for both Cu-Gly-Leu-Phe and Cu-Sar-Leu-Phe complexes are ML_2H_{-1} and this gives a similar molecular weight of 749.33g/mol and 777.39 g/mol respectively. This similarity complements the similarity found between the permeability coefficients of the two complexes. However, the molecular weights are over the upper limit of 500 g/mol, which could mean that this predominant species will not penetrate through the stratum corneum, but could penetrate through the Cerasome 9005 lipid membrane, since the artificial membrane does not have corneocytes to hinder the diffusion. It can also be seen that at a pH of 7.4 the MLH_{-2} species is significant for the Cu-Gly-Leu-Phe complex and the MLH_{-1} species is

significant for the Cu-Sar-Leu-Phe complex. These non-dominant species are all below the upper limit of 500 g/mol and therefore could penetrate through the stratum corneum.

5.3.4(a.ii) Compound ionisation

Proteins, such as corneocytes, in the stratum corneum are positively and negatively charged. This, as well as the lipophilic nature of the stratum corneum, prevents ionised compounds from undergoing dermal absorption. However, there are more negatively than positively charged proteins, which cause the stratum corneum to have a negative net ionic charge and therefore favours cationic absorption over anionic absorption. Non-ionized molecules are thus the most favourable for dermal absorption, because they will not be affected by the charged stratum corneum and will tend to be more lipophilic in their non-ionised forms.[30,43,44] At a pH of 7.4, both Cu-Gly-Leu-Phe and Cu-Sar-Leu-Phe complexes have a negatively charged ML_2H_{-1} dominant species. This could indicate that in the stratum corneum, the permeability coefficient will be lower than expected since diffusion of the complexes will be hindered by the negative charge. However, Cu-Gly-Leu-Phe also has MLH_{-2} as a non-dominant but significant species and Cu-Sar-Leu-Phe also has MLH_{-1}. The MLH_{-2} species is more negatively charged than the ML_2H_{-1} species and therefore will be more hindered by the stratum corneum, but the MLH_{-1} species is neutral and therefore will not be affected. Thus in terms of ionization, the Cu-Sar-Leu-Phe complex could yield better permeability coefficients.

5.3.4(a.iii) Hydrogen bonding

The lipid and protein composition of the stratum corneum contains groups that are capable of hydrogen bonding with the compounds that are diffusing through the stratum corneum, provided those compounds also have groups that can form hydrogen bonds. The strength of the hydrogen bond will determine by how much the diffusion of the compound will slow down.[40,43,45] The two copper (II) complexes both have one amine group, two amide groups and one carboxylic acid group that can undergo hydrogen bonding. The amine and amide groups undergo weaker hydrogen bonding than the carboxylic acid group, although collectively all the hydrogen bonding could have an effect on the permeability of the complexes in the stratum corneum. Therefore the ability of the two copper(II) complexes to

form hydrogen bonds in the stratum corneum could also cause the permeability coefficients to be lower than expected.

5.3.4(a.iv) Solubility

The solubility of a compound originates from its ability to partition into the stratum corneum. A lipophilic compound will partition into the lipid bilayer and a highly hydrophilic compound will not. However, if the compound is highly lipophilic it will partition into the stratum corneum, but it will not partition out into the underlying hydrophilic epidermal tissue. An octanol-water partition coefficient (log P) of between 1 and 3 is therefore optimal for skin absorption.[41,43] Both Cu-Gly-Leu-Phe and Cu-Sar-Leu-Phe complexes were found to have a log P of -1.79 and -1.72 respectively at a pH of 7.4 , which fell into the range of other results from literature, but does not fall into the range for optimal skin absorption. However, even though these partition coefficient values do not fall into the optimal range for skin absorption, extraction into the stratum corneum will still occur, since it was found that approximately a 1.6 % and 1.9% copper (II) extraction for Cu-Gly-Leu-Phe and Cu-Sar-Leu-Phe complexes respectively will extract into the octanol phase.

It has generally been accepted that the permeability coefficient is a more reliable expression to describe the dermal absorption of a chemical substance than the flux, since it takes the donor phase concentration into account and therefore is theoretically consistent over a range of concentrations. However, Korinth *et al*. found that the permeability coefficient is dependent on the concentration and therefore the influence the concentration has on liquid compounds in percutaneous absorption cannot be quantified.[36] Therefore K_p cannot be used when comparing the dermal absorption abilities between the complexes. Thus to compare the permeability between complexes, a ratio can be found by calculating the difference between the permeability coefficients of the copper(II) complex and copper(II) chloride from the same study and comparing it with the difference in permeability coefficients of the copper(II) complex and copper(II) chloride of another study.

Mazurowska and Mojski[28] studied the permeability of Cu(II)-glycyl-L-histidyl-L-lysine (Cu-Gly-His-Lys), while Hammouda[23] studied five complexes namely, Cu(II)-sarcosyl-L-histidyl-L-lysine (Cu-Sar-His-Lys), Cu(II)-sarcosyl-L-lysyl-L-histidine (Cu-Sar-Lys-His), Cu(II)-

sarcosyl-L-histidyl-L-histidine (Cu-Sar-His-His), Cu(II)-sarcosyl-L-lysyl-L-lysine (Cu-Sar-Lys-Lys), Cu(II)-sarcosyl-L-glycyl-L-histidine (Cu-Sar-Gly-His). A comparison of permeability can be seen in Table 5.6.

Table 5.6: A comparison between the permeability of Cu-Gly-Leu-Phe and Cu-Sar-Leu-Phe with the copper(II) tripeptide complexes investigated in the study by Mazurowska and Mojski[28] and by Hammouda,[23] by calculating the difference in permeability coefficients of the copper(II) complex and copper(II) chloride from the same studies and comparing the resultant ratios.

	K_p of $CuCl_2.2H_2O$ ($cm.h^{-1}$)	K_p of copper(II) complexes($cm.h^{-1}$)	(K_p of copper(II) complexes) – (K_p of $CuCl_2.2H_2O$) ($cm.h^{-1}$)
Cu-Gly-Leu-Phe	0.137	0.225 ± 0.02	0.088 ± 0.02
Cu-Sar-Leu-Phe	0.137	0.206 ± 0.02	0.069 ± 0.02
Cu-Gly-His-Lys	$(9.72 \pm 1.8) \times 10^{-4}$	$(22.7 \pm 2.16) \times 10^{-3}$	0.013
Cu-Sar-His-Lys	0.028 ± 0.07	0.049 ± 0.01	0.021 ± 0.01
Cu-Sar-Lys-His	0.028 ± 0.07	0.047 ± 0.01	0.019 ± 0.01
Cu-Sar-His-His	0.028 ± 0.07	0.041 ± 0.01	0.013 ± 0.01
Cu-Sar-Lys-Lys	0.028 ± 0.07	0.038 ± 0.01	0.01 ± 0.01
Cu-Sar-Gly-His	0.028 ± 0.07	0.061 ± 0.01	0.033 ± 0.01

From Table 5.6 it can be seen that the copper(II) complexes investigated in this study are between 2.1 to 8.8 times more permeable than the copper(II) complexes investigated in the study by Mazurowska and Mojski[28] and by Hammouda.[23] The difference between the tripeptides in this study and the tripeptides in these other studies is that the tripeptides in this study have the amino acids, leucine and phenylalanine, while the other studies have histidine and lysine. Leucine has a non-polar, aliphatic isobutyl side chain and phenylalanine has a non-polar benzyl side chain. Histidine has a polar imidazole function group and lysine has a polar amine side chain. Leucine and phenylalanine therefore have groups that make the overall tripeptides in this study more lipophilic than the tripeptides in previous studies. Thus these groups could be the cause for the higher permeability found in Cu-Gly-Leu-Phe and Cu-Sar-Leu-Phe compared to these studies.

The physiochemical properties of molecular size, compound ionization and hydrogen bonding all predicted that the permeability coefficients found in this study for Cu-Gly-Leu-Phe and Cu-Sar-Leu-Phe will all be lower than expected if the artificial membrane that was used is replaced with skin. Permeability is not only affected by physiochemical properties but also physical properties such as the thickness of the skin. This is because the flux is dependent on the distance that the complex travels through a membrane according to Equation 29.[30-32] The stratum corneum has a thickness of 0.0015-0.0020 cm, which is thicker than the artificial membrane.[28] This could also cause the permeability coefficient to be less than expected. The permeability of skin ranges from a permeability coefficient of 10^{-6} to 10^{-2} cm/h.[46] The permeability coefficients found in this study are above this range. However, since the physiochemical and physical properties predict that the permeability coefficients found will be less than expected, these permeability coefficients will decrease to within this range.

5.3.5 Conclusion

The complexation of copper(II) ions with the two tripeptides Cu-Gly-Leu-Phe and Cu-Sar-Leu-Phe increases the permeation rate of copper(II) ions compared to copper(II) chloride. The N-methyl substituent on the terminal amine does not have an effect on the permeation rate of copper(II) ions.

Cu-Gly-Leu-Phe and Cu-Sar-Leu-Phe are between 1.87 to 9.2 times more permeable than the copper(II) complexes investigated in literature.[23,28] This could be due to the lipophilic groups found in the amino acids, leucine and phenylalanine, which are not found in the tripeptides from literature.[23,28]

The physiochemical and physical properties predict that the permeability coefficients found will be less than expected. However, these properties should then decrease the high permeability coefficients found in this study to within the permeability range of skin.

References

1. G. Arena, G. Kavu and D. R. Williams, *J. Inorg. Nucl. Chem.*, 1978, **40**, 1221-1226.
2. G. E. Jackson, P. M. May and D. R. Williams, *J. Inorg. Nucl. Chem.*, 1978, **40**, 1189-1194.
3. G. E. Jackson, P. M. May and D. R. Williams, *J. Inorg. Nucl. Chem.*, 1978, **40**, 1227-1234.
4. K. D. Rainsford and M. W. Whitehouse, *J. Pharm. Pharmac.*, 1976, **28**, 83.
5. D. C. Atkinson and H. O. J. Collier, *Adv. Pharm. Chemotherapy*, Academic Press, London, 1980, vol. 17, pp. 238.
6. S. Odisitse and G. E. Jackson, *Polyhedron*, 2008, **27**, 453-464.
7. S. Odisitse and G. E. Jackson, *Inorg. Chim. Acta,* 2009, **362**, 125-135.
8. G. P. Moss, J. C. Dearden, H. Patel and M. T. D. Cronin, *Toxicol. Vitro*, 2002, **16**, 299-217.
9. What Is The Skin Barrier, And Why Does It Matter?, http://eliasandwilliams.com/skin-barrier/, (accessed March 2015).
10. P. H. Lee, R. Conradi and V. Shanmugasundaram, *Bioorganic Med. Chem. Lett*., 2010, **20**, 69-73.
11. M. Rauma and G. Johanson, *Toxicol. Vitro*, 2009, **23**, 919-926.
12. *Handbook of Occupational Dermatology*, ed. L. Kanerva, P. Elsner, J. E. Wahlberg and H. I. Maibach, Scientific Publishing Services, Heidelberg, 2000, ch. 9, pp. 81-82.
13. E. R. Copper, *J. Pharm. Sci*., 1984, **8**, 153-156.
14. M. Mohajane, PhD Thesis, University of Cape Town, 2013.
15. E. U. Tsumbu, MSc Thesis, University of Cape Town, 2010.
16. S. Odisitse, G. E. Jackson, T. Govender, H. G. Kruger and A. Singh, *Dalton Trans.*, 2007, 1140-1149.
17. J. N. Zvimba and G. E. Jackson, *J. Inorg. Biochem.*, 2007, **101**, 1120-1128.
18. J. N. Zvimba and G. E. Jackson, *J. Inorg. Biochem.*, 2007, **101**, 148-158.
19. W. P. Gardiner, *Statistical Analysis Methods for Chemists: A solfware-based Approach*, The Royal Society of Chemistry, United Kingdom, 1997, pp. 168-186.

20. M. Gertz, P. J. Kilford, J. B. Houston and A. Galetin, *Am. Soc. Pharm. Exp. Ther*., 2008, **36**, 535-542.
21. J. N. Zvimba and G. E. Jackson, *J. Inorg. Biochem.*, 2007, **26**, 2395-2404.
22. B. W. Tsang, C. J. Mathias, P. E. Fanwick and M. A. Green, *J. Med. Chem.*, 1994, **25**, 4400-4406.
23. A.Hammouda, PhD Thesis, University of Cape Town, 2015.
24. A. Patronov, I. Dimitrov, D. R. Flower and I. Doytchinova, *BMC Struct. Biol.*, 2012, **12**, 1-14.
25. M. A. Green, *Int. J. Radiat. Appl. Instrum.*, 1987, **14**, 56-61.
26. M. Sri-Aran, C. J. Mathias, J. K. Lim and M. A. Green., *Nucl. Med. Biol.*, 1998, **25**, 107-110.
27. L. Mazurowska, K. Nowak-Buciak and M. Mojski, *Anal. Bioanal. Chem.*, 2007, **388**, 1157-1163.
28. L. Mazurowska and M. Mojski, *Talanta*, 2007, **72**, 650-654.
29. F. Akomeaha, T. Nazir, G. P. Martin and M. B. Brown, *Europ. J. Pharm. Sci.*, 2004, **21**, 337-345.
30. L. Bartosova and J. Bajgar, *Curr. Med. Chem.*, 2012, **19**, 4671-4677.
31. *Handbook of Biopolymers and Biodegradable Plastics: Properties, Processing and applications,* ed. S. Ebnesajjad, Elsevier, UK, 2013, pp. 333.
32. I. Campbell, *Biophysical Techniques,* Oxford University Press, US, 2012, pp. 19.
33. R. O. Potts and R. H. Guy, *Pharm. Res*., 1992, **9**, 663-669.
34. S. C. Wilkinson and F. M. Williams, *Int. Arch. Occup. Environ. Health*, 2002, **75**, 519-527.
35. MSE 2090: Introduction to the Science and Engineering of Materials, http://people.virginia.edu/~lz2n/mse209/, (accessed April 2015).
36. G. Korinth, K. H. Schaller and H. Drexler, *Arch. Toxicol.*, 2005, **79**, 155-159.
37. *Free Radical Effects on Membranes,* ed. S. Matalon, Elsevier, USA, 2008, vol. 61, pp. 26.
38. M. E. Johnson, D. Blankschtein and R. Langer, *J. Pharm. Sci.*, 1997, **86**, 1162-1172.
39. R. O. Potts and R. H. Guy, *Pharm. Res.*, 1992, **9**, 663-669.
40. R. O. Potts and R. H. Guy, *Pharm. Res.*, 1992, **12**, 1628-1633.
41. A. L. Bunge and R. L. Cleek, *Pharm. Res.,* 1995, **12**, 88-95.

42. M. Kupczewska, M. Jakubowski and S. Czerczak, *Environ. Toxicol. Pharmacol.*, 2010, **2**, 95-102.
43. *Principles and Practice of Skin Toxicology*, ed. R. Chilcott and S. Price, John Wiley & Sons, Inc., England, 2008, pp. 85-92.
44. A. R. Denet, R. Vanbever and V. Préat, *Adv. Drug Delivery Rev*., 2004, **56**, 659-674.
45. S. D. Krämer, *Res. Focus*, 1999, **2**, 373-380.
46. *Theory and Practice of Contemporary Pharmaceutics,* ed. K. T. Ghosh and B. R. Jastipp, CRC Press, US, 2005, 431-433.

6 Blood Plasma Model

6.1 Introduction

One of the main aims of this study was to design a drug that can mobilize copper(II) in blood plasma. Even if the ligands can form a more stable complex with copper(II) than with zinc(II) and nickel(II), it does not ensure the formation of a copper(II) complex *in vivo*. Zinc(II) and nickel(II) have higher concentrations in blood plasma than copper(II) and therefore copper(II) has to compete with these metal ions to form a complex with the ligands. The concentration of zinc(II) and nickel(II) ions is 10^{-3} mol.dm^{-3} and 10^{-9} mol.dm^{-3} respectively, while the concentration of copper(II) ions is 10^{-16} mol.dm^{-3}.[1,2] The ligand therefore has to bind preferentially to copper(II) ions in order for copper(II) to compete with the higher concentration of other ions in the blood. Calcium(II) also has a high concentration in the blood plasma, but the two ligands used in this study do not bind to calcium(II).

Blood plasma contains both high and low molar mass molecules, which can combine with metal ions to form many combinations of complex species. The low molar mass molecules are responsible for the transfer of metal ions and therefore it is the equilibrium distribution between these low molar mass molecules and the metal ions that is required.[3] In order to analyse all the metal complex species of low molar mass molecules that are present in blood plasma, a computer model can be used, provided there is the assumption that all the components of blood plasma are in equilibrium.[4]

The program, Evaluation of Constituent Concentrations in Large Equilibrium Systems, (ECCLES) was used, which has a list of metals and ligands that can be found in blood plasma. The program also has a list of complex species that can be formed between the metals and ligands as well as their stability constants. The program calculates the speciation of all the metals and ligands found in blood plasma and includes competition of other species.[5] The program generates 5000 complexes found in the blood plasma from 7 metal ions and 40 ligands.[6,7] The program can then estimate the equilibrium concentration of individual species. The movement of a metal ion from a high molar mass complex to a low molar mass complex can be calculated as the plasma mobilizing index (P.M.I). Therefore, the

definition for the P.M.I is the percentage increase in total concentration of low molar mass complexes with a specific metal ion that is caused by the ligand. Complexes which are sufficient to bind to endogenous copper(II), produce a high P.M.I value, and this value can be calculated using Equation 32 below. [7,8]

$$P.M.I = \frac{\text{Total concentration of low molecular weight metal complex species in plasma in presence of the ligand}}{\text{Total concentration of low molecular weight metal complex species in normal plasma}} \quad (32)$$

The high P.M.I value means that there is a strong, specific chelation between copper(II) and the ligand. This then indicates that the ligands can potentially be used as a treatment for rheumatoid arthritis by increasing the bioavailable pool of copper(II) from endogenous sources. However the concentration of the ligand must be biologically suitable and therefore there should be a high P.M.I value with a low concentration of ligand.

6.2 Experimental

The program ECCLES was used to model the blood plasma copper(II), nickel(II) and zinc(II) speciation with the ligands, Gly-Leu-Phe and Sar-Leu-Phe. The stability constants determined from potentiometric titrations for copper(II), nickel(II) and zinc(II) ligand complexes were placed into the ECCLES model of blood plasma, so that the plasma mobilizing indices (P.M.I) were calculated. The P.M.I of zinc(II) and nickel(II) can then be compared to the P.M.I of copper(II) in both ligands. This can be used to determine whether a complex is sufficient to bind specifically to copper(II) in the presence of free nickel(II) and zinc(II), which have a higher concentration than free copper(II*) in vivo*.

6.3 Results

Figure 6.1 and Figure 6.2 show the P.M.I curves for copper(II), zinc(II) and nickel(II) as a function of ligand concentration. The P.M.I curves in Figure 6.1 show that above a concentration of 0.01 M, zinc(II) and nickel(II) are not competitors against copper(II) in the blood plasma. At a ligand concentration of 0.1 M, Gly-Leu-Phe increases the low molecular mass metal species concentration by 63 times. The P.M.I curves in Figure 6.2 show that below the ligand concentration of 0.03 M, Sar-Leu-Phe mobilises zinc(II) over copper(II) and nickel(II).

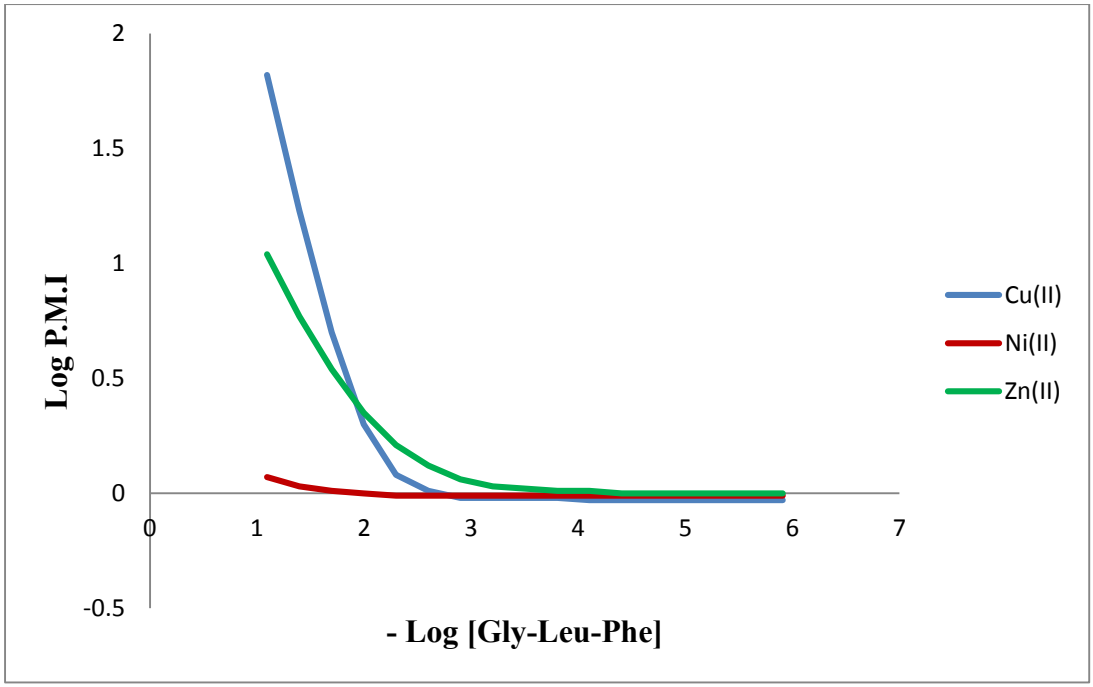

Figure 6.1: Log P.M.I curves for copper(II), nickel(II) and zinc(II) with Gly-Leu-Phe and plotted against –log[Gly-Leu-Phe].

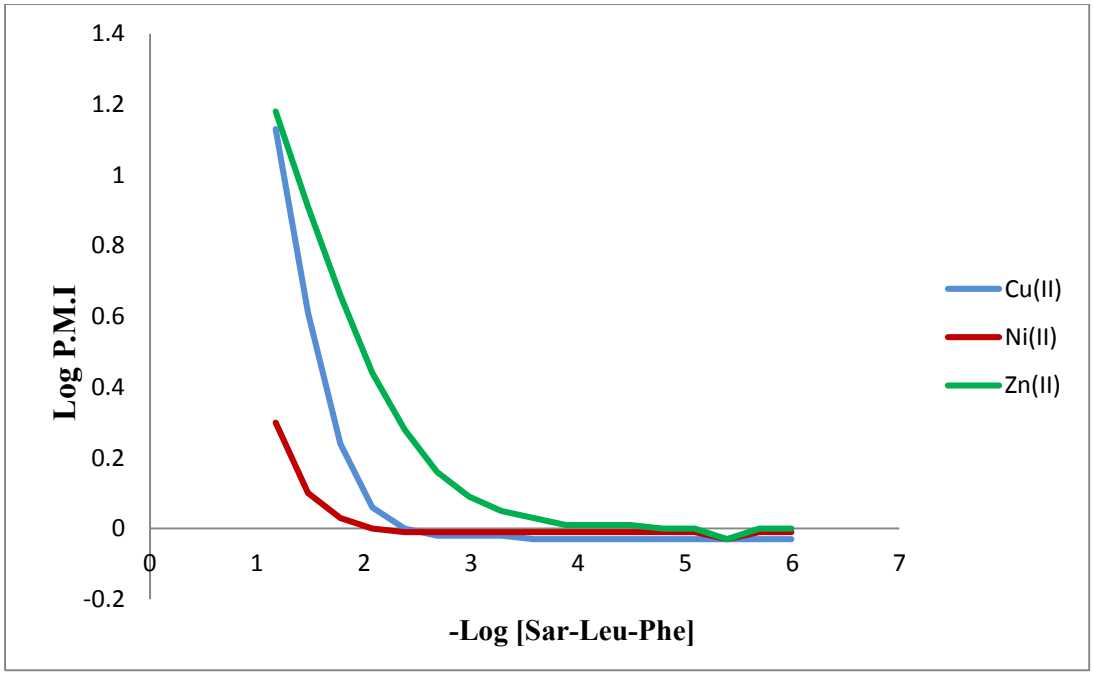

Figure 6.2: Log P.M.I curves for copper(II), nickel(II) and zinc(II) with Sar-Leu-Phe and plotted against –log[Sar-Leu-Phe].

6.4 Discussion

The Gly-Leu-Phe ligand showed that above the concentration of 0.01 M, the ligand will effectively mobilise copper(II), even though the concentration of zinc(II) and nickel(II) in the blood plasma is higher than that of copper(II). However, even though the low molecular mass metal species are substantially increased by 63 times at a ligand concentration of 0.1 M, the concentration value is too high to be realistic. At the more realistic ligand concentration of 0.001M, the ligand mobilises zinc(II) more effectively and therefore lower concentrations of the ligand cannot be used. Therefore it will not be feasible to use Gly-Leu-Phe as a potential therapeutic drug that will increase the bioavailable pool from endogenous sources. Similarly, the Sar-Leu-Phe ligand also cannot be used as a carrier for copper(II) ions, since it will preferentially bind to zinc(II) at concentrations lower than 0.03 M. This shows that since both ligands mobilise zinc(II) more readily than copper(II), they disrupt the homeostasis of zinc(II) ions. This also indicates that once *in vivo*, the copper(II) complexes will dissociate and therefore do not have an anti-inflammatory activity themselves.

Mohajane found that the dipeptides Gly-Leu and Gly-Phe had the highest mobilising capacities compared to other dipeptides in the study.[9] Therefore the combination of the amino acids, Leu and Phe, were suggested as the other possible amino acids to form the tripeptides containing the amino acid Gly or Sar.[9] The Gly-Leu and Gly-Phe dipeptides were found to be able to mobilise copper(II) at ligand concentrations from 0.001 M. However in comparison, the tripeptides Gly-Leu-Phe and Sar-Leu-Phe could not mobilise copper(II) at the same low ligand concentration of 0.001 M. Therefore the dipeptides have better copper mobilizing capacities than these tripeptides.

In comparison to other anti-inflammatory drugs which have been studied previously, Odisitse *et al*.,[5,8] and Zvimba *et al*.[9,10] all show that the ligands used in the respective studies all had better copper mobilizing capacities than the tripeptides in this study.

6.5 Conclusion

Gly-Leu-Phe can mobilise copper(II) in the blood plasma above a concentrations of 0.01 M. Below this concentration zinc(II) is mobilized over copper(II). At a concentration of 0.1 M the low molecular mass metal species are substantially increased by 63 times. However, this concentration is not realistic for the therapeutic treatment for rheumatoid arthritis. Sar-Leu-Phe mobilises zinc(II) over copper(II) from a concentration of 0.03 M and therefore also cannot be used for therapeutic treatment. When comparing these tripeptides to the dipeptides from literature, it was found that the dipeptides have a better copper(II) mobilizing capacity than these tripeptides.[9]

References

1. S. Odisitse and G. E. Jackson, *Inorg. Chim. Acta*, 2009, **362**, 125-135.
2. F. Pehourcq, M. Matoga, C. Jarry and B. Bannwarth, *J. Liq. Chrom. Rel. Technol.,* 2001, **24**, 2177-2186.
3. D. M. Templeton, F. W. Sunderman and R. F. Herber, *Sci. Total Environ*., 1994, **148**, 243-251.
4. P. M. May, P. W. Linder and D. R. Williams, J. *Chem. Soc. Dalton Trans*., 1977, 588-595.
5. S. Odisitse, G. E. Jackson, T. Govender, H. G. Kruger and A. Singh, J. *Chem. Soc. Dalton Trans*., 2007, 1140-1149.
6. E. T. Nomkoko, G. E. Jackson, B. S. Nakani and S. A. Bourne, *J. Chem. Soc. Dalton Trans*., 2004, 1789-1796.
7. J. R. Zeevaart, D. R. Jansen, M. F. Botelho, A. Abrunhosa, C. Gomes, L. Metello, Z. I. Kolar, G. C. Krijger, W. K. A. Louw and I. C. Dormehl, *J. Inorg. Biochem*., 2004, **98**, 1521-1530.
8. S. Odisitse and G. E. Jackson, *Polyhedron*, 2008, **27**, 453-464.
9. M. Mohajane, PhD Thesis, University of Cape Town, 2013.
10. J. N. Zvimba and G. E. Jackson, *J. Inorg. Biochem*., 2007, **101**, 148-158.
11. J. N. Zvimba and G. E. Jackson, *J. Inorg. Biochem*., 2007, **101**, 1120-1128.

7 General Concluding Remarks

The aim of this study was to develop a ligand that could increase the bioavailable pool of copper(II) *in vivo*. To do this, the ligand has to form a dermally absorbable, copper(II) complex that does not disrupt the homeostasis of other endogenous metal ions. An added advantage would be if it had anti-inflammatory activity itself or has sufficient mobilising capacity to release copper(II) from endogenous sources. Mohajane[1] studied dipeptides and concluded that two tripeptides, Sar-Leu-Phe and Gly-Leu-Phe would be better transporters of copper(II). The design of these tripeptides resemble the structure of Human Serum Albumin (HSA), which is the most effective copper transport protein.[2] Copper(II) binds to HSA on an amine-N and on three amide-N donors. The binding sites for the tripeptides are on an amine-N, two amide-Ns, two carbonyl-Os and a carboxyl-O.

The objective to determine how well the copper(II) complexes can undergo transdermal absorption was achieved using two methods. The first was the Flask Shake method, which gives the octanol/water partition coefficients and hence determines the lipophilicity of the copper(II) complexes. The second was the Franz cell diffusion method which gives the permeability coefficients and physically measures how well the copper(II) complexes can undergo dermal absorption. Both of these methods indicated that both Cu-Gly-Leu-Phe and Cu-Sar-Leu-Phe are successful at undergoing dermal absorption.

The octanol/water partition coefficients (log $P_{oct/aq}$) for Cu-Gly-Leu-Phe and Cu-Sar-Leu-Phe were measured as a function of pH. The species from both of these copper(II) complexes were found to have negative log $P_{oct/aq}$ values over the pH range from 2-10, which indicated that the species are relatively hydrophilic. However, even though the partition coefficient values were found to be hydrophilic, they were still relatively high for copper(II) complexes. A correlation between the charge of each species and the degree of lipophilicity was found, where the less charged a species is, the more lipophilic it is. The log $P_{oct/aq}$ values for the N-methylated group on Sar-Leu-Phe compared to Gly-Leu-Phe did not improve the lipophilicity significantly as was predicted in literature.[1] The permeability coefficients, K_p, were measured at a pH of 7.4. The K_p values of the two copper(II) tripeptides, where found to be significantly larger than the K_p value of copper(II) chloride and therefore increased the permeability of the

copper(II) ions. The N-methyl substituent also did not have an effect on the permeation rate of copper(II) ions. When the permeability of these copper(II) complexes was compared to literature values, it was found that they were between 2.1 to 8.8 times more permeable than the copper(II) complexes investigated in literature.[3,4] This shows that these copper(II) complexes are more suitable to use for increasing the bioavailable pool from external sources than the complexes studied in literature.[3,4]

Consequently this study has proved to be more successful than previous investigations, using tripeptides to determine the permeability of copper(II) complexes. The success of Gly-Leu-Phe and Sar-Leu-Phe can be attributed to the polarity of the amino acids. The only difference between the tripeptides of this study compared to the tripeptides of the other studies is that leucine and phenylalanine are used instead of histidine and lysine.[3,4] Leucine and phenylalanine are non-polar, while histidine and lysine are polar. Therefore the non-polarity of leucine and phenylalanine has been responsible for the advantageous increase in the permeability of these copper(II) complexes. Consequently, leucine and phenylalanine should be considered for future use in the development of permeable copper(II) complexes, since they have uniquely added an aspect that can improve future research.

An illustration of the increased suitability in permeability for Cu-Gly-Leu-Phe and Cu-Sar-Leu-Phe compared to the permeability found in literature[3] can be seen in Figure 7.1. A comparison between the permeability coefficient values was achieved by calculating the difference between the K_p value of the copper(II) complexes and the K_p value of copper(II) chloride from the same studies and then using the resultant ratios for the comparison.

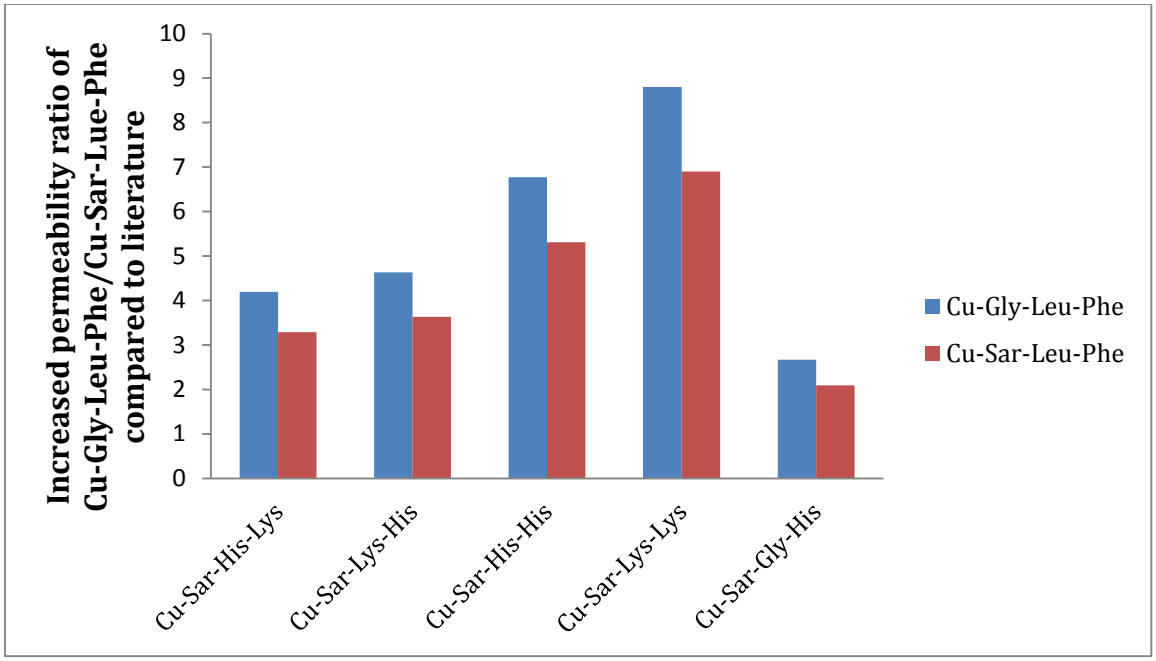

Figure 7.1: The resultant ratios of Cu-Gly-Leu-Phe and Cu-Sar-Leu-Phe with copper(II) tripeptide complexes from literature,[3] by calculating the difference in permeability coefficients of the copper(II) complex and copper(II) chloride from the same studies.

As mentioned before these copper(II) complexes undergo dermal absorption at a pH of 7.4. To see which species for each copper(II) complex is present at this particular pH, glass electrode potentiometry was used to study the thermodynamics of the copper(II) complexes at 25 °C and at a 0.15 M ionic strength (NaCl). At different pH values, different copper(II) species formed and these species were found to be the ML, MLH_{-1}, ML_2H_{-1} and MLH_{-2} species. The loss of protons caused the changes in these species. Only the species which formed at the physiological pH of 7.4 will be present when either of the tripeptides transport copper(II) *in vivo*. Therefore from the potentiometric species distribution graph, at a pH of 7.4, the ML_2H_{-1} species for both complexes is the dominant species, while the MLH_{-2} species for Cu-Gly-Leu-Phe and MLH_{-1} species for Cu-Sar-Leu-Phe are non-dominant, but still significant. Unlike the stratum corneum, the Franz cell does not have physiochemical properties to hinder membrane permeation. The ML_2H_{-1} species is a large compound that would be too large to diffuse in between the corneocytes, while the non-dominant species are small and therefore will undergo permeation. Therefore this could indicate that the permeability for these complexes could be lower than expected when conducting animal studies in future work.

Gly-Leu-Phe and Sar-Leu-Phe have to form a stable enough complex with copper(II) so that copper(II) can be transported transdermally. However, the stability of the copper(II) complexes cannot be too strong, or copper(II) will potentially be excreted instead of being released *in vivo*. The overall stability of the tripeptides were found to be lower than the dipeptides studied by Mohajane.[1] The stability of the methylated copper(II) complexes were also found to be lower than the non-methylated copper(II) complexes, unlike the dipeptides, in which the stability of the methylated and non-methylated copper(II) complexes were the same. From these results, it showed that copper(II) complexes can be formed from the two ligands, which will then be able to transport copper(II) across the skin. Unlike HSA, which forms a stable complex with copper(II), the stability of Cu-Gly-Leu-Phe and Cu-Sar-Leu-Phe is less than HSA and therefore should release copper(II) *in vivo*. This is because copper(II) can bind to O-donor groups in both Gly-Leu-Phe and Sar-Leu-Phe, which decreases the stability of the complex compared to HSA.[5] The difference in stability between the methylated and non-methylated copper(II) complexes could mean that the less stable Cu-Sar-Leu-Phe complex is more suitable for releasing copper *in vivo* than Cu-Gly-Leu-Phe.

During complexation, the exact coordination mode for each species is not known and thus a series of structure determining techniques was used. These were UV-Vis, IR, ^{1}H NMR and molecular mechanics calculations, as well as the determination of the species from the potentiometric results. A visual observation of the change in species for Cu-Gly-Leu-Phe and Cu-Sar-Leu-Phe, as the pH increased from 2-10 in increments of 1, can be seen in Figures 7.2 and 7.3 respectively.

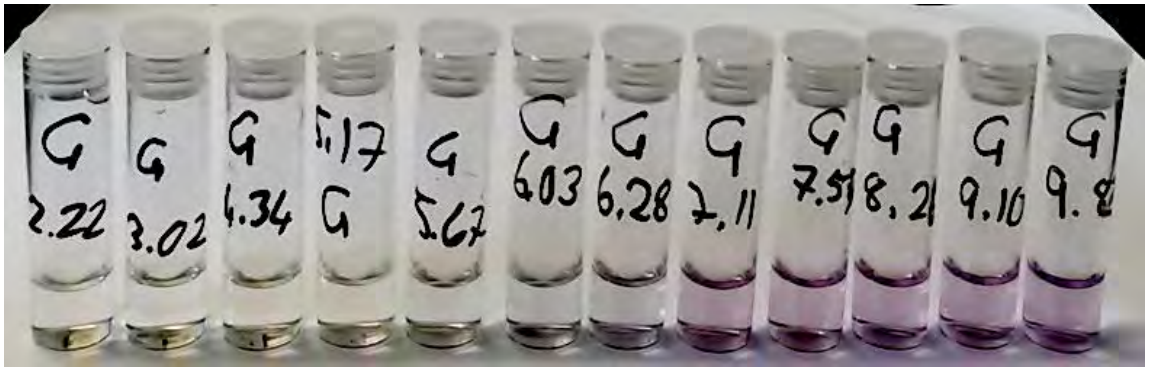

Figure 7.2: Visual observation of Cu-Gly-Leu-Phe as the pH increases in increments of 1 from left to right from a pH of 2-10.

Figure 7.3: Visual observation of Cu-Sar-Leu-Phe as the pH increases in increments of 1 from left to right from a pH of 2-10.

The progression of the violet colour shows that different species form over a changing pH. The colour, as well as the wavelengths of each species during the UV-Vis study, determined that the coordination modes tended more towards a square planar complex instead of the expected tetragonally distorted octahedral geometry. Each structure determining technique contributed information that helped to gain an overall indication of what each coordination mode for each species is. A summary of how each technique helped to determine each coordination mode can be seen in Table 7.1. The molecular modelling calculations gave a 3D visual image for each coordination mode that validated each of the other techniques. Therefore these visual representations can be viewed as the final suggestions for each coordination mode.

Table 7.1: A summary of the results from each structure determining technique that was used to determine the coordination mode of each species.

Potentiometric	UV-Vis	IR	^{1}H NMR	Molecular modelling
Cu-Gly-Leu-Phe				
ML			Amine-N, Leu-O and Gly-O	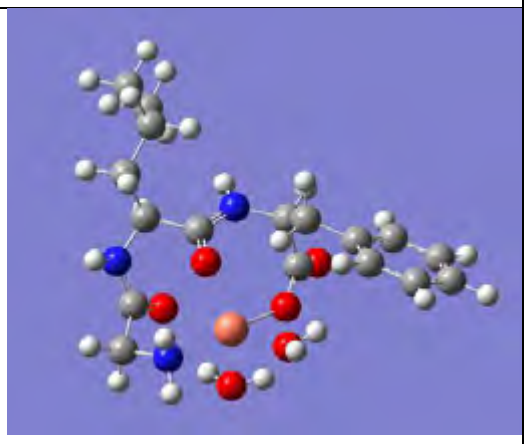
MLH_{-1}	Amide-N	Amide-N	Amine-N, Leu-N and Leu-O	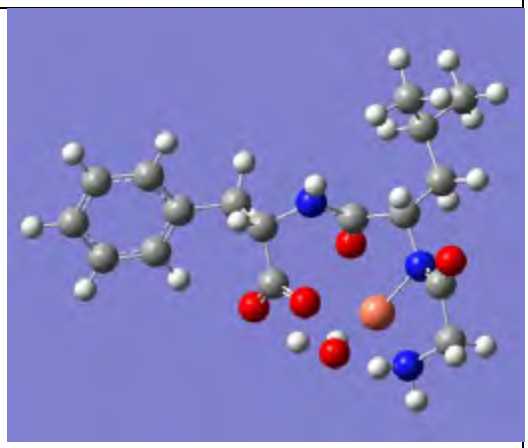
ML_2H_{-1}	Amide-N	Amide-N	Amine-N, Leu-N, Leu-O, Gly-O, Phe-N, carboxyl-O.	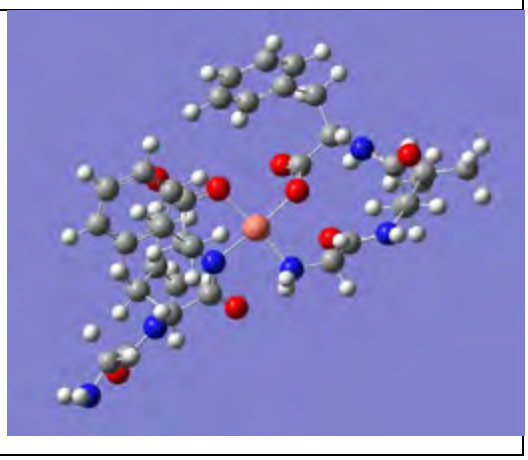

MLH_{-2}	One or two Amide-Ns	One or two Amide-Ns	Amine-N	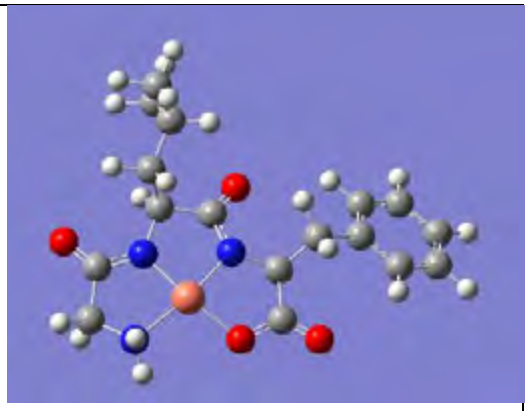
Cu-Sar-Leu-Phe				
ML		Carboxyl-O, Carbonyl-O	Amine-N, Leu-O and Gly-O.	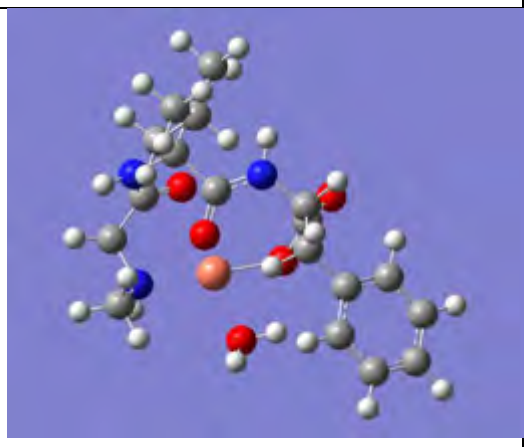
MLH_{-1}	Amide-N	Carboxyl-O, Carbonyl-O	Amine-N Leu-N, Leu-O, Gly-O, Phe-N, carboxyl-O.	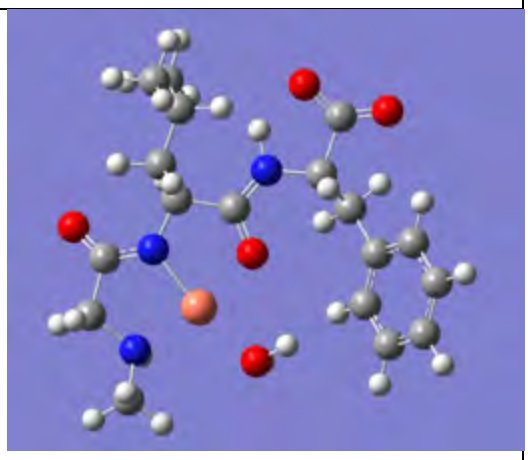
ML_2H_{-1}	Amide-N	Carboxyl-O, Carbonyl-O, One Amide-N	Amine-N	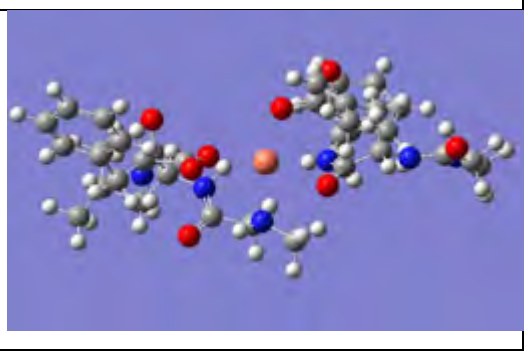

MLH_{-2}	One or two Amide-Ns	Carboxyl-O, Carbonyl-O, One or two Amide-Ns	Amine-N	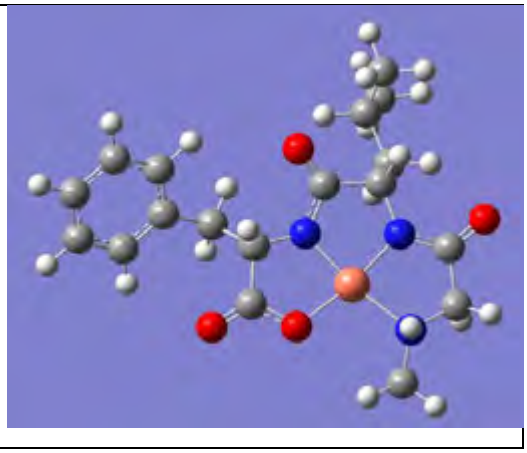

Even though these copper(II) complexes were found to be successful at undergoing dermal absorption and thus are able to increase the bioavailable pool of copper(II) *in vivo* from external sources, it would be an added advantage for them to increase the bioavailable pool from endogenous sources as well. This can be achieved if the stability of the copper(II) complexes is strong enough to mobilise copper(II) from HSA. Therefore Evaluation of Constituent Concentrations in Large Equilibrium Systems (ECCLES) was used to determine the mobility capacity of copper(II) complexes *in vivo*. The tripeptides were not able to mobilise copper(II) *in vivo*, since both ligands mobilised zinc(II) more effectively at realistic ligand concentrations. In comparison, two ligands with good mobilising capacities, N^1-(2-aminoethyl)-N^2-(pyridine-2-ylmethyl)-ethane-1,2-diamine, ([555-N]) and N-(2-(2-aminoethylamino)ethyl)picolinamide, ([H(555)N]), have been added to a graph with the Gly-Leu-Phe and Sar-Leu-Phe ligands.[6] This can be seen in Figure 7.4 below. The [555-N] and [H(555)N] ligands could cause a 10-fold increase in the copper(II) low molecular weight concentrations at a ligand concentration of 10^{-8} M and 10^{-5} M respectively.

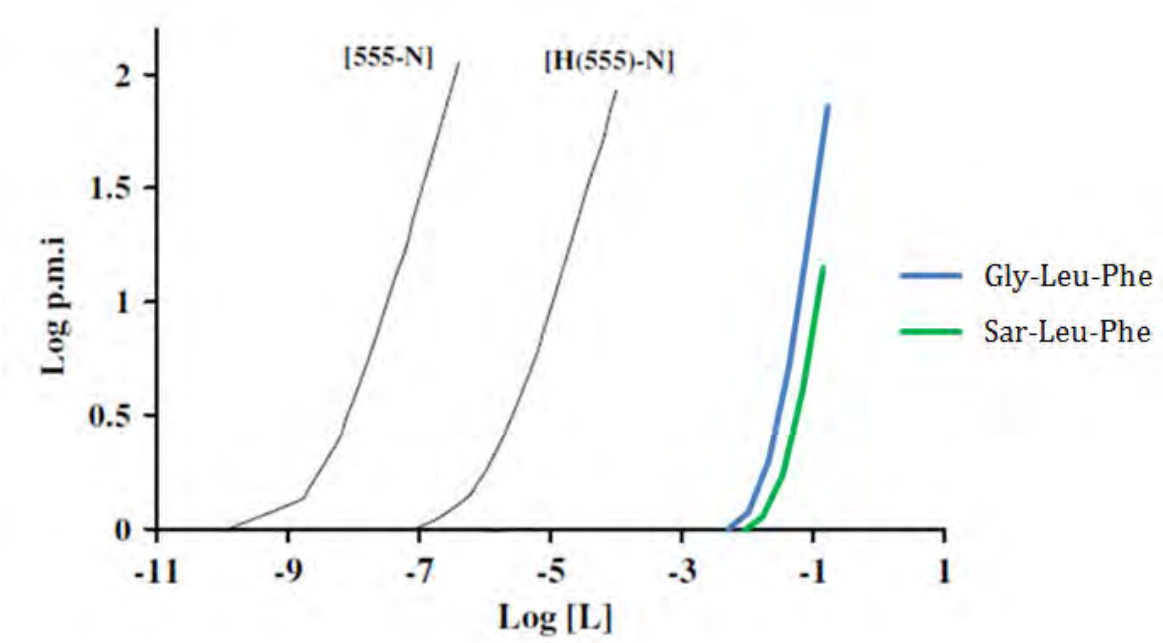

Figure 7.4: Copper(II) plasma mobilising index for, [555-N] and [H(555)-N], found in Zvimba *et al.* and Cu-Gly-Leu-Phe and Cu-Sar-Leu-Phe.[6]

This graph illustrates the difference between a study that had more positive results from ligands than the results which were obtained from Gly-Leu-Phe and Sar-Leu-Phe.[6] This shows that in comparison these tripeptides had a poor mobilising capacity for copper(II) ions *in vivo* and thus increasing the bioavailable pool of copper(II) from endogenous sources would be inefficient with these tripeptides. It also shows that since the P.M.I values are low, the complexes will dissociate *in vivo* and therefore anti-inflammatory activity due to the complexes themselves is not achievable. Both ligands also disrupted the homeostasis of zinc(II) ions and therefore once *in vivo,* patients would have to take zinc(II) supplementation for the duration of the treatment.

However, overall the Cu-Gly-Leu-Phe and Cu-Sar-Leu-Phe complexes can be considered as more preferable transporters of copper(II) than previous studies.[3,4,6] To date, this is the only study that theoretically is able to form stable complexes that dissociate to release copper(II) once they are *in vivo*, as well as undergo the highest transdermal absorption rates for tripeptides. Future work should include studies on animal testing where a topical application of radio-labelled Cu-Gly-Leu-Phe and Cu-Sar-Leu-Phe will be applied on rats/mice to determine the anti-inflammatory activity.

References

1. M. Mohajane, PhD Thesis, University of Cape Town, 2013.
2. L. Perrone, E. Mothes, M. Vignes, A. S. Mockel, C. Figueroa, M. C. Miquel, M. L. Maddelein and P. Faller, *ChemBioChem*., 2010, **11**, 110-118.
3. A.Hammouda, PhD Thesis, University of Cape Town, 2015.
4. L. Mazurowska and M. Mojski, *Talanta*, 2007, **72**, 650-654.
5. L. Perrone, E. Mothes, M. Vignes, A. S. Mockel, C. Figueroa, M. C. Miquel, M. L. Maddelein and P. Faller, *ChemBioChem.*, 2010, **11**, 110-118.
6. J. N. Zvimba and G. E. Jackson, *J. Inorg. Biochem.*, 2007, **101**, 148-158.

Appendix

1. Molecular Modelling

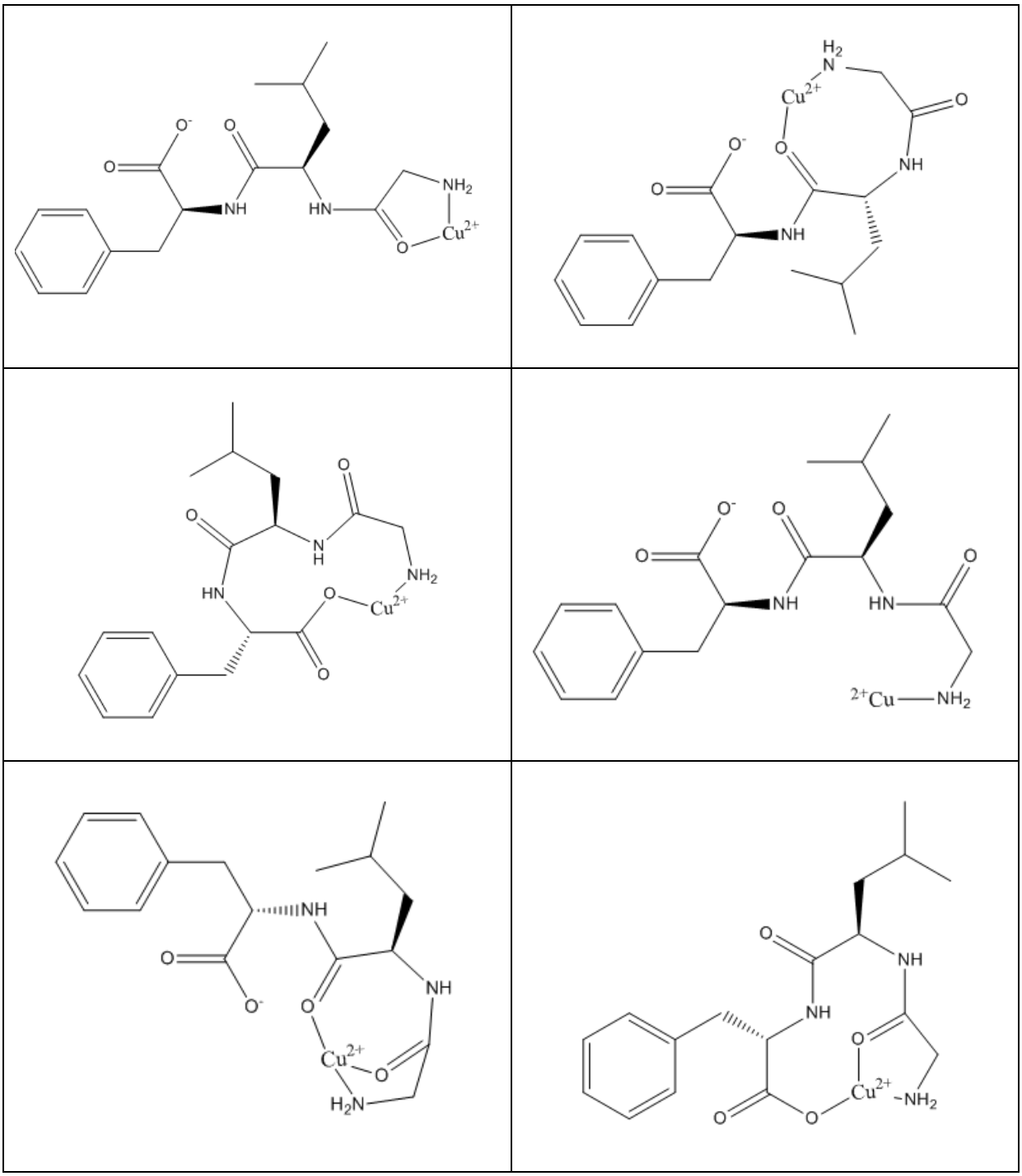

Figure 1: Coordination modes from the ML species of Cu-Gly-Leu-Phe that could not converge in Gaussian 09.

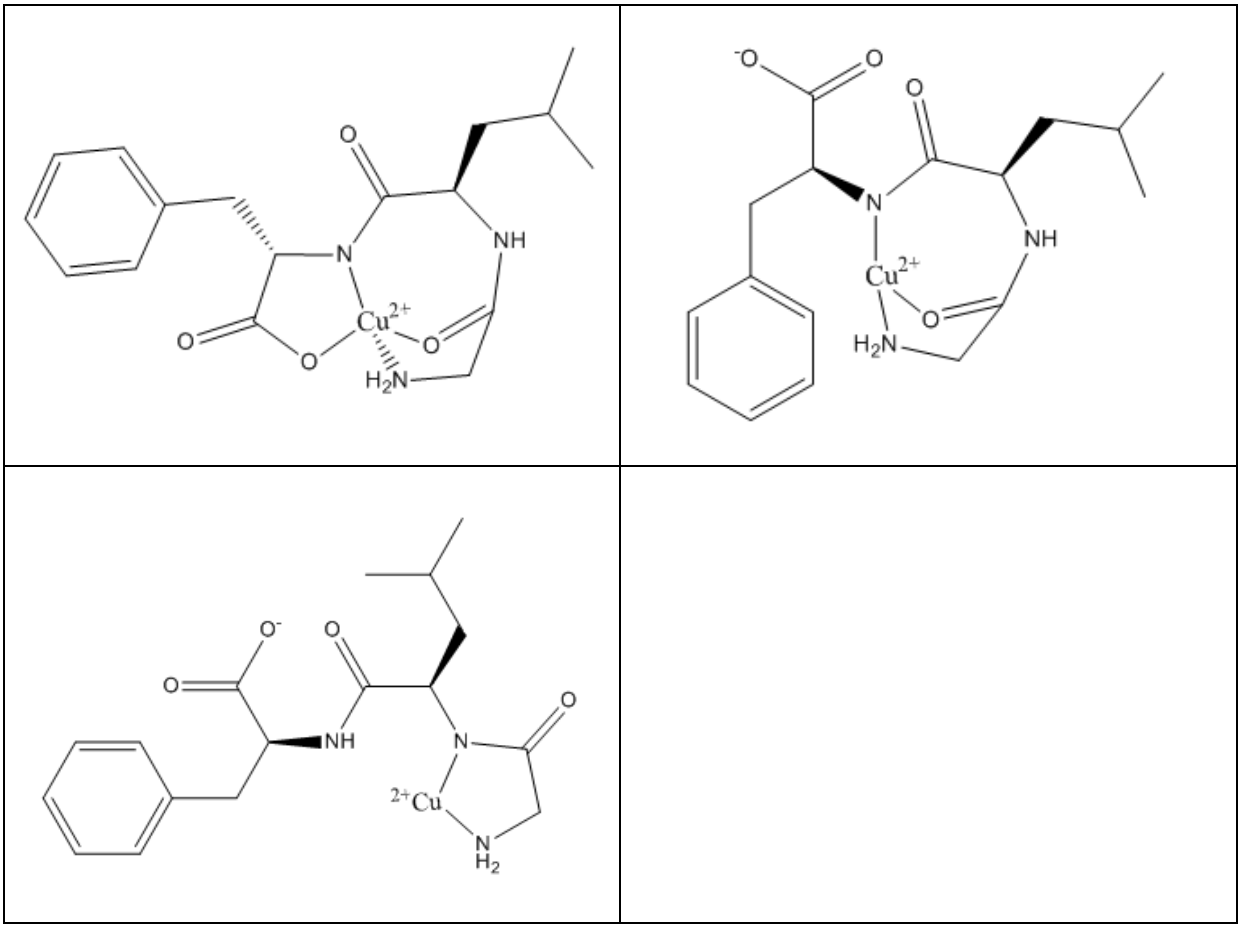

Figure 2: Coordination modes from the MLH_{-1} species of Cu-Gly-Leu-Phe that could not converge in Gaussian 09.

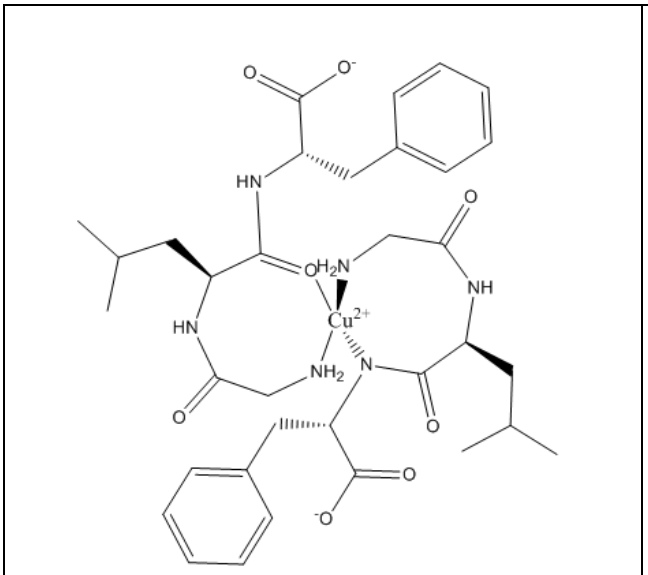

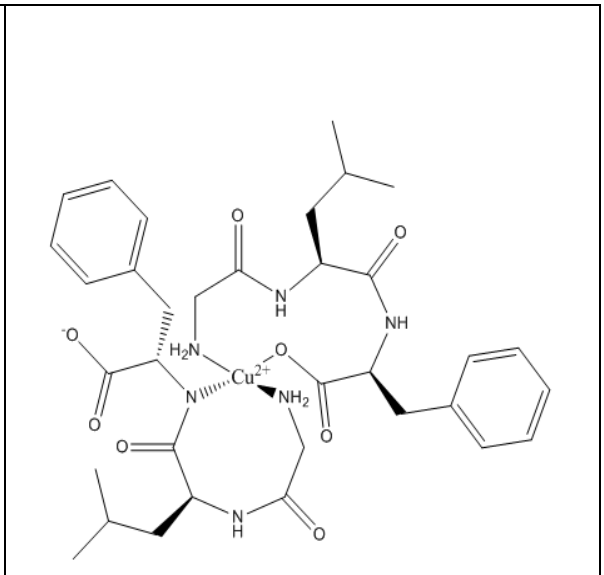

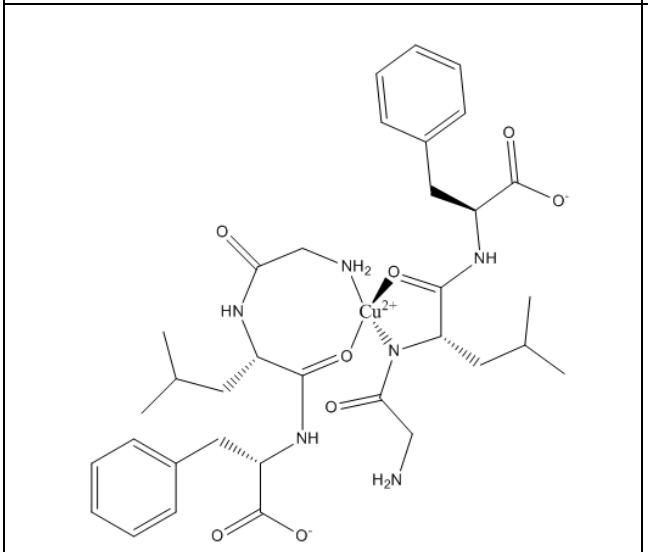

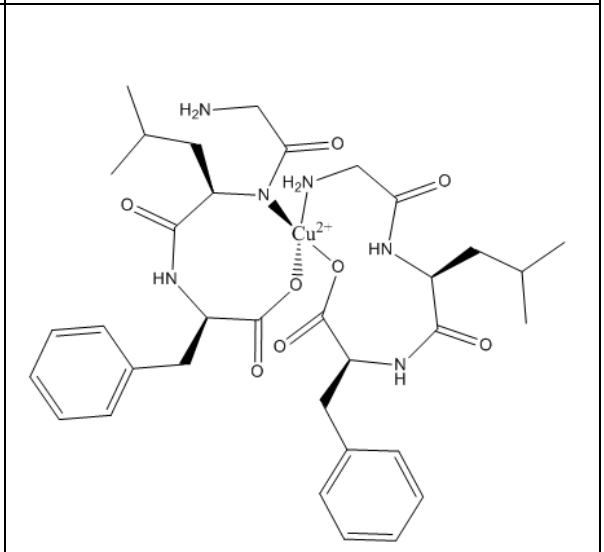

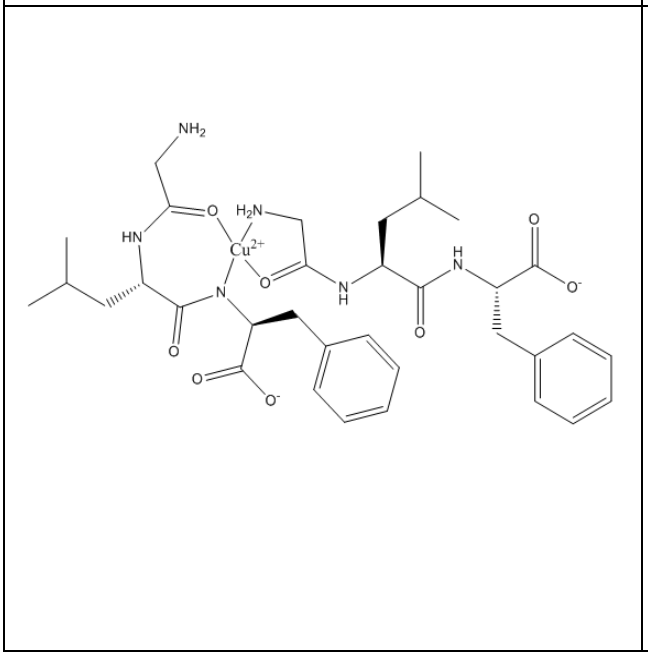

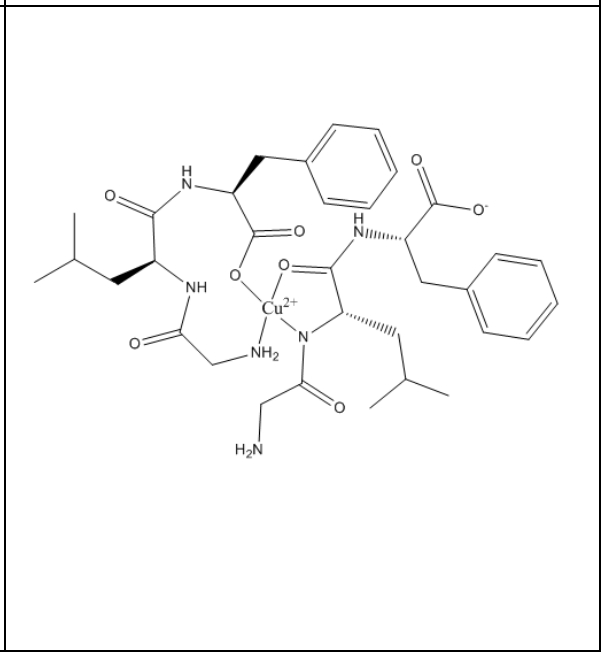

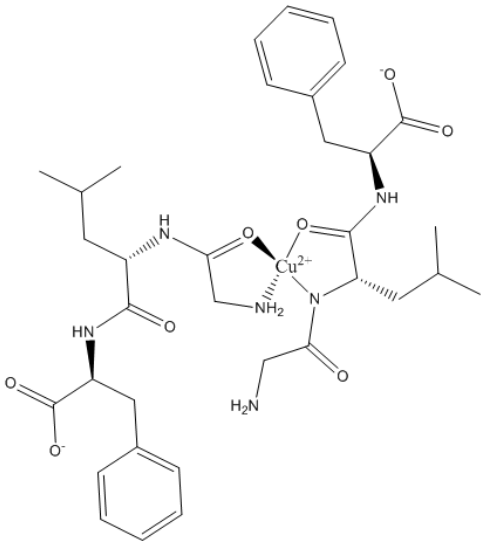

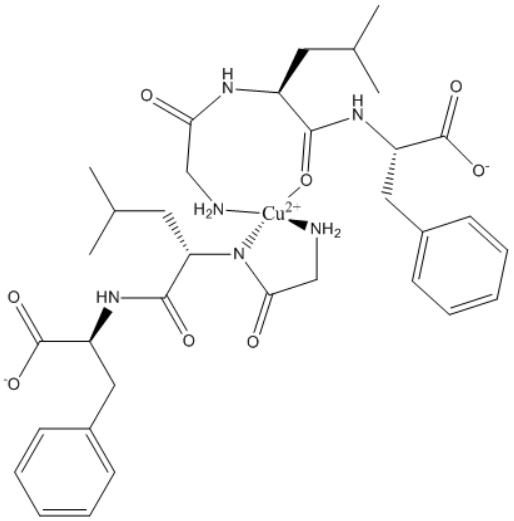

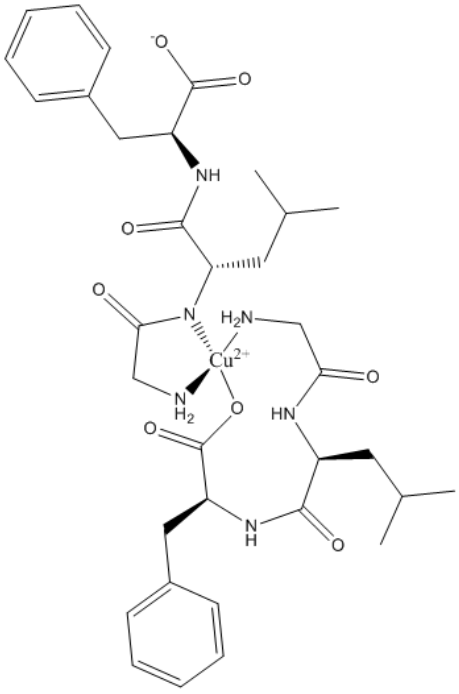

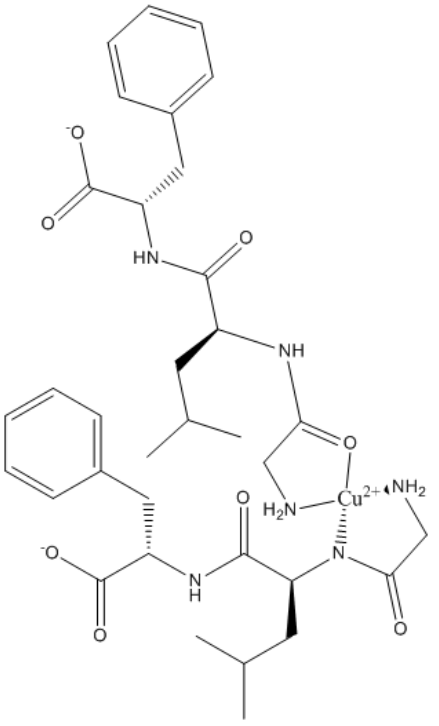

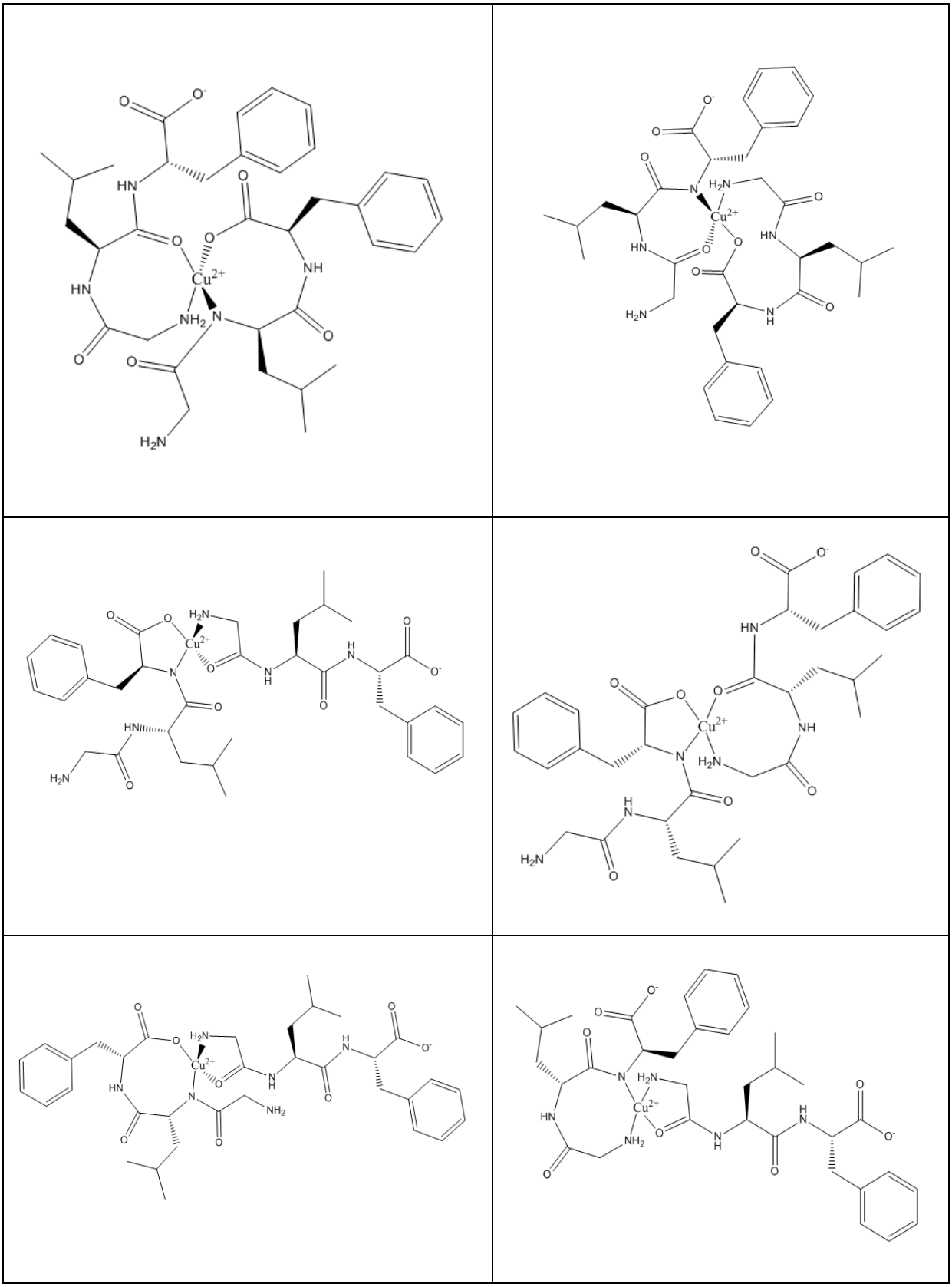

Figure 3: Coordination modes from the ML_2H_{-1} species of Cu-Gly-Leu-Phe that could not converge in Gaussian 09.

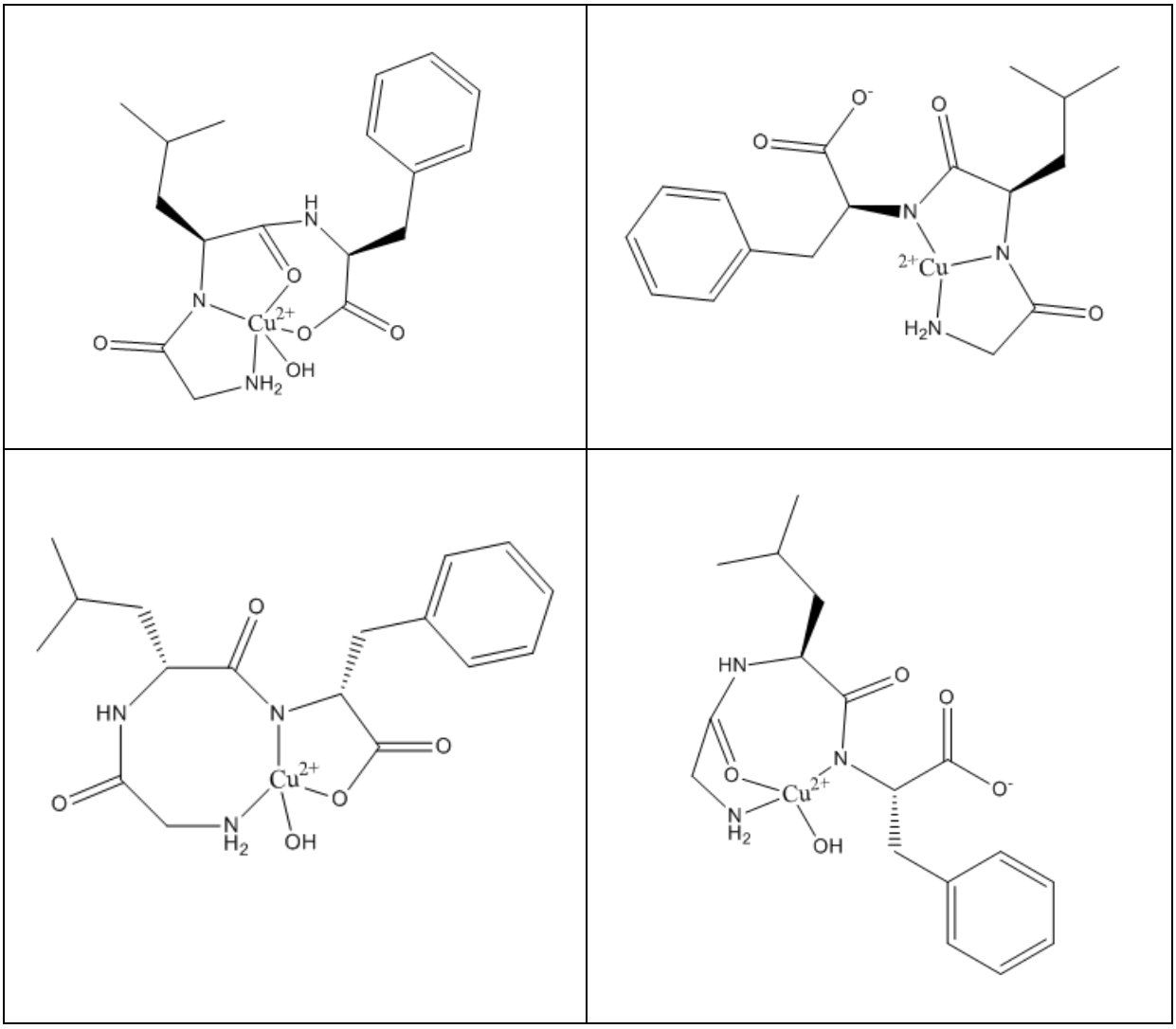

Figure 4: Coordination modes from the MLH_{-2} species of Cu-Gly-Leu-Phe that could not converge in Gaussian 09.

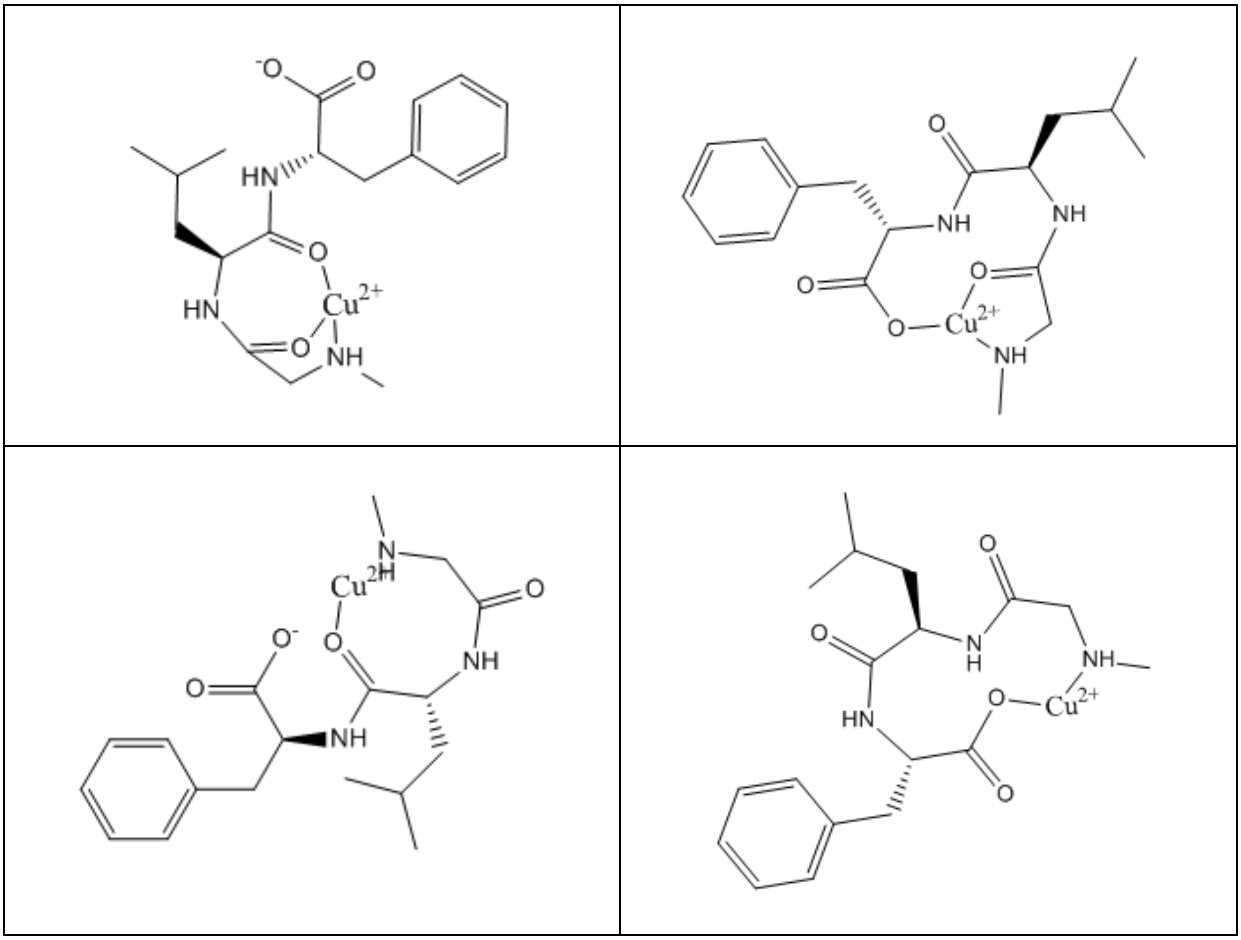

Figure 5: Coordination modes from the ML species of Cu-Sar-Leu-Phe that could not converge in Gaussian 09.

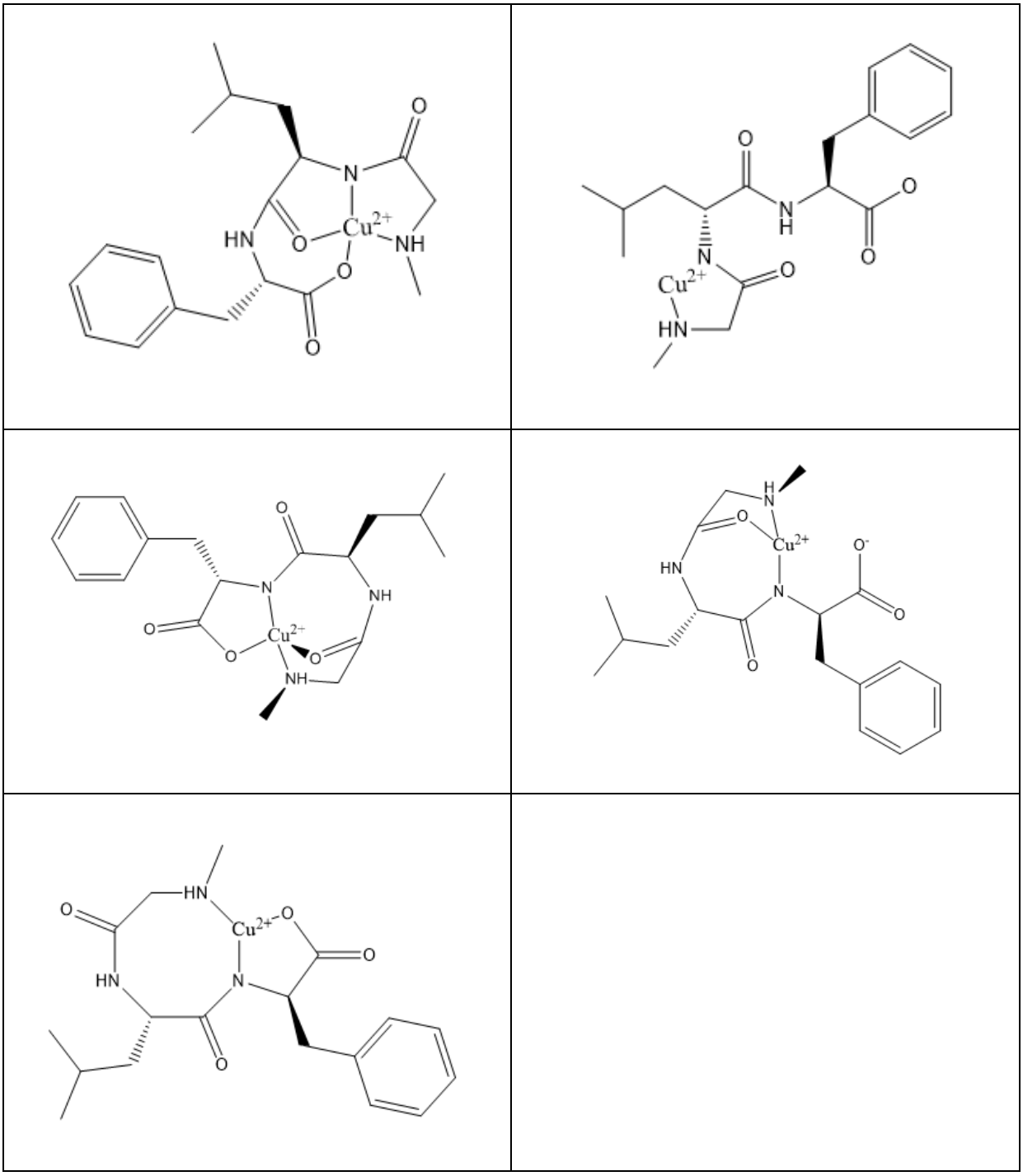

Figure 6: Coordination modes from the MLH_{-1} species of Cu-Sar-Leu-Phe that could not converge in Gaussian 09.

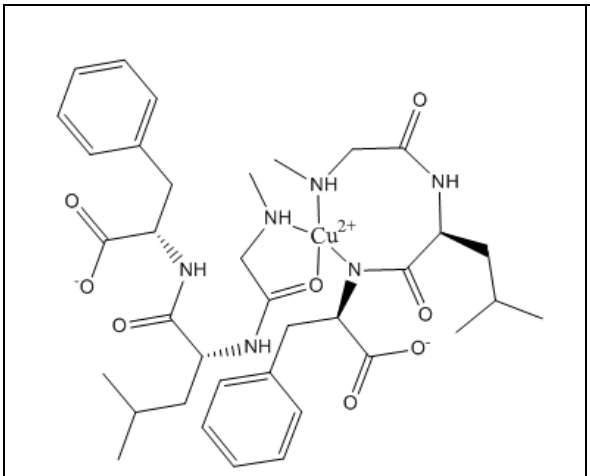

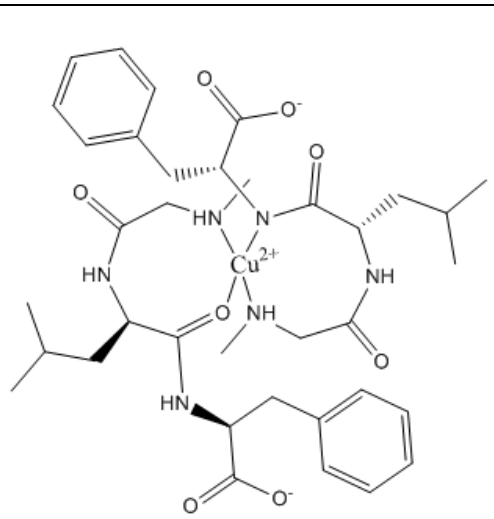

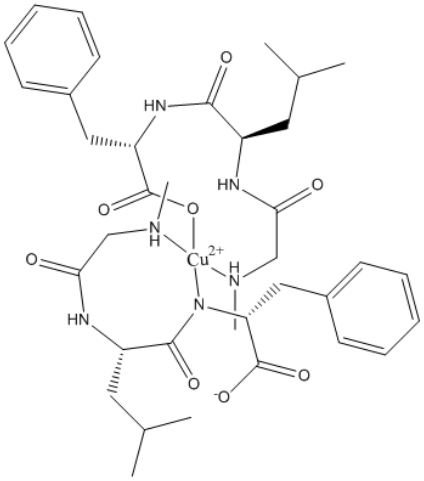

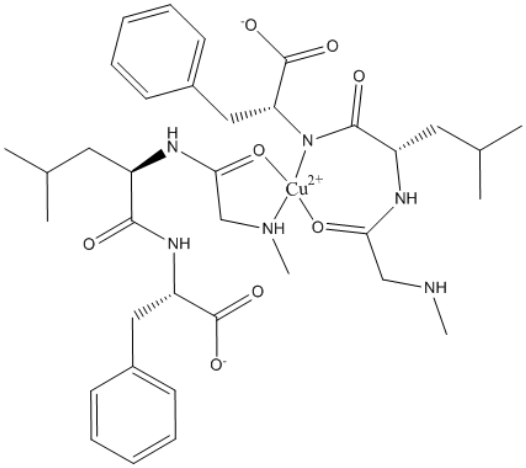

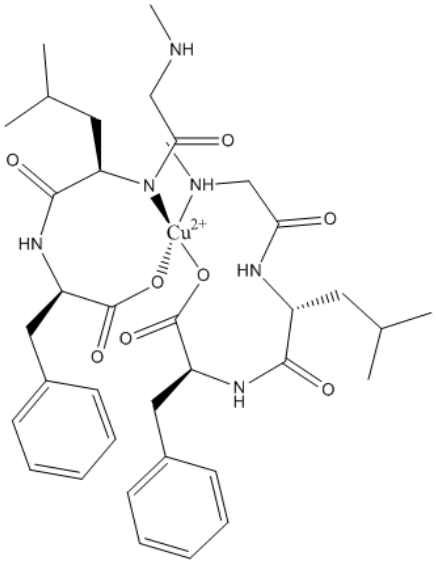

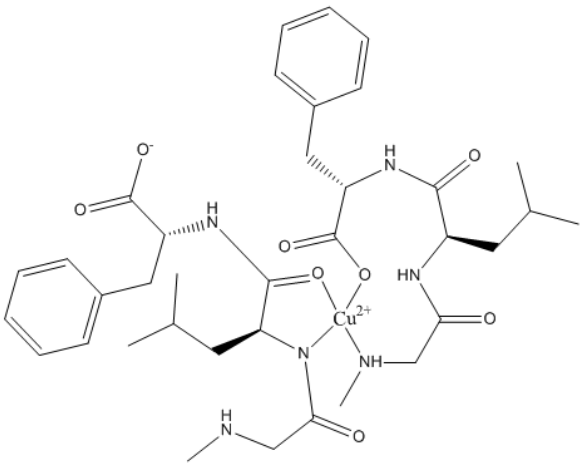

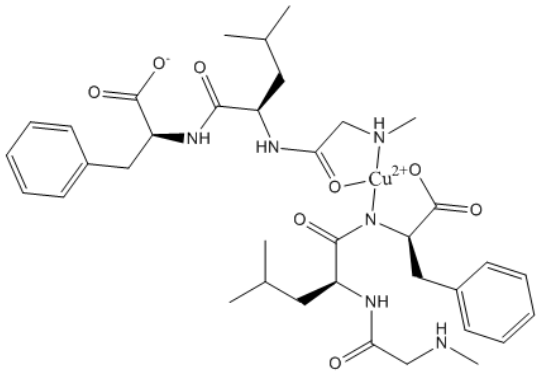

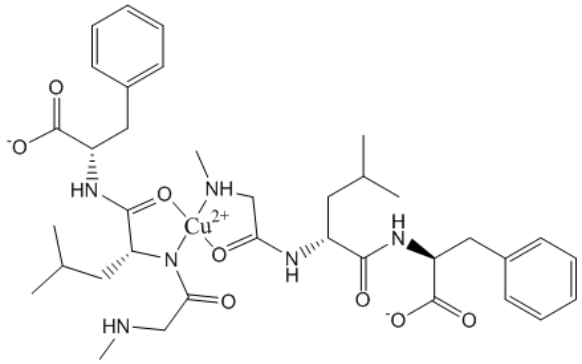

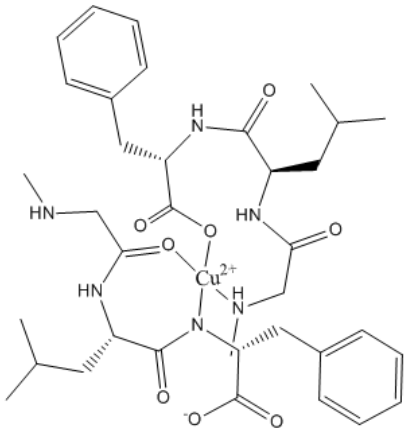

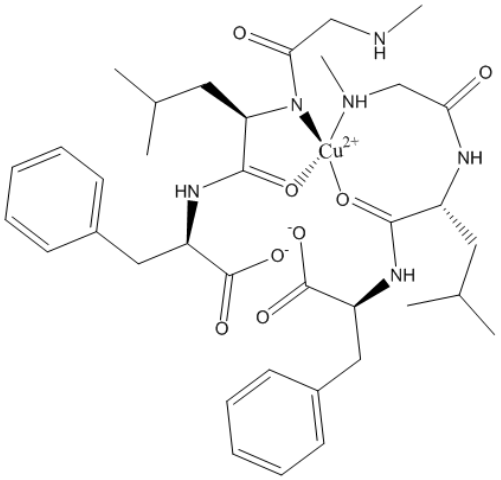

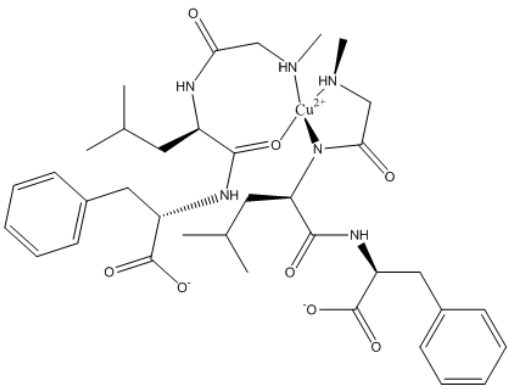

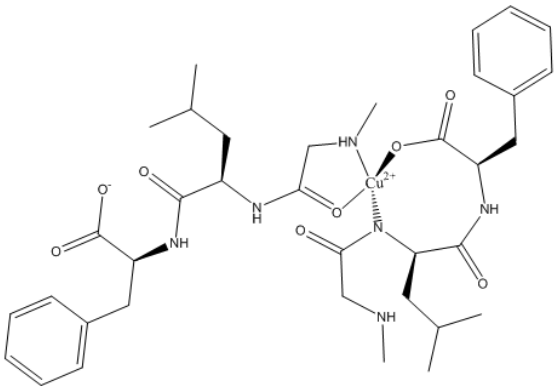

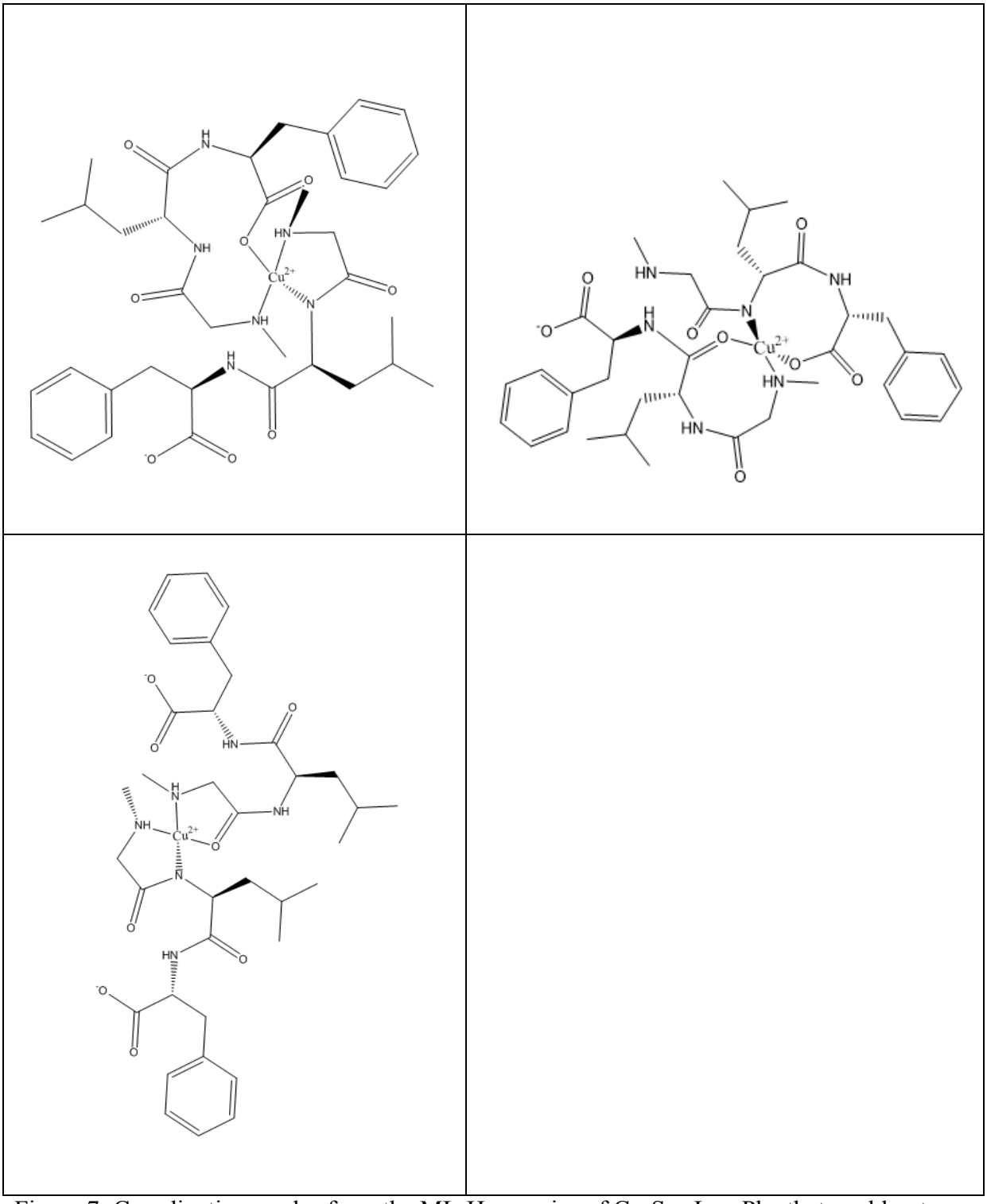

Figure 7: Coordination modes from the ML_2H_{-1} species of Cu-Sar-Leu-Phe that could not converge in Gaussian 09.

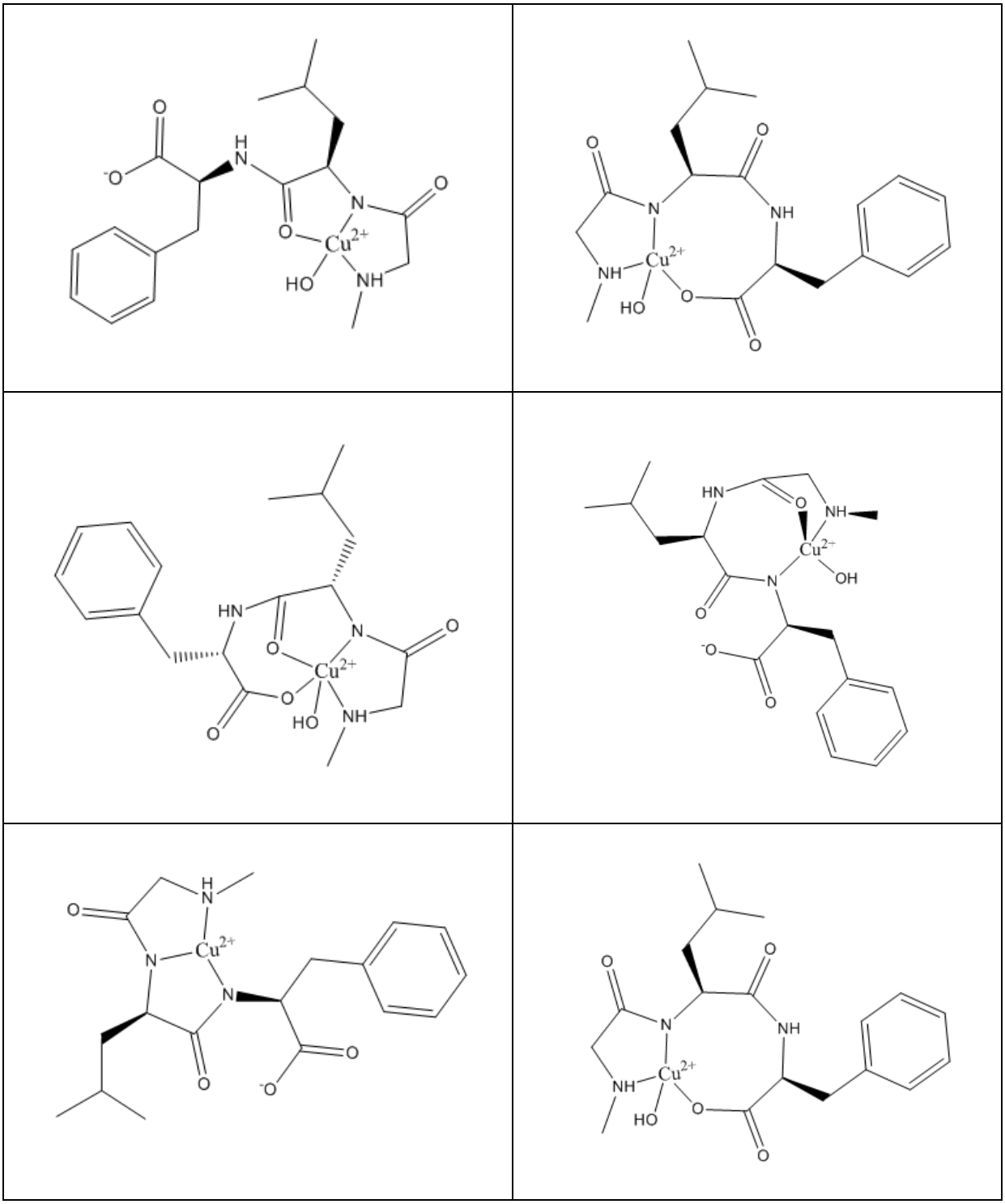

Figure 8: Coordination modes from the MLH_{-2} species of Cu-Sar-Leu-Phe that could not converge in Gaussian 09.